Author:
Gamez, Monica

Title:
Therapeutically Targeting Heparan Sulphate To Restore The Endothelial Glycocalyx In Diabetic Microvascular Disease

Author:
Gamez, Monica

Title:
Therapeutically Targeting Heparan Sulphate To Restore The Endothelial Glycocalyx In Diabetic Microvascular Disease

Therapeutically Targeting Heparan Sulphate To Restore The Endothelial Glycocalyx In Diabetic Microvascular Disease

Monica Gamez

Bristol Medical School

Translational Health Sciences

March 2020

A dissertation submitted to the University of Bristol in accordance with the requirements of the degree of PhD in Bristol Medical School

Word Count: 52,809

Abstract

Introduction: Diabetes mellitus (DM) causes life altering microvascular complications, such as diabetic nephropathy and retinopathy (DR and DN). The endothelial glycocalyx (eGlx), containing proteoglycans (core proteins with glycosaminoglycan (GAG) sidechains), lines all blood vessels and helps to maintain vascular permeability barriers. Heparan sulfate (HS) is the most abundant GAG in the eGlx. In DM, heparanase, an HS degrading enzyme, is upregulated. The aim of this PhD was to show that eGlx HS is important in glomerular and retinal microvascular barriers and that preventing its shedding, using a novel heparanase inhibitor, OVZ/HS-1638, is protective in DM.

Methods: EGlx HS was removed in mice by i.v. of heparinase III, or by an Ext1 (an HS biosynthesis enzyme) endothelial-specific conditional knock-out mouse (Ext1CKO). Type 2 diabetic mice (db/db) were treated with OVZ/HS-1638 or vehicle for two weeks, with a 9-week and 11-week old endpoint. Fluorescein angiography analysis was used as a measure of retinal apparent solute flux, and albumin staining to measure vascular leak. Mice were Ringer or Alcian blue/glutaraldehyde perfused for apparent glomerular permeability (Ps'alb) studies and electron microscopy (EM), respectively. EGlx depth and coverage was measured by EM. Urine albumin creatinine ratios (uACRs) were measured at endpoint.

Results: A reduction of eGlx, using heparinase III or in Ext1CKO mice, was associated with increased retinal solute flux and Ps'alb. Ext1CKO mice also had increased uACR when tubular absorption was blocked. In 9-week-old db/db, OVZ/HS-1638 increased retinal eGlx depth and reduced retinal albumin leak. In 11-week-old db/db mice, OVZ/HS-1638 restored glomerular eGlx depth and restored Ps'alb. uACR was no longer significantly increased.

Conclusions: Together, this work shows that eGlx HS is structurally and functionally important in two spatially and functionally distinct vessel beds and suggests that HS is amenable to therapeutic intervention in DM, using a clinically relevant heparanase inhibitor.

Dedication

For my mom, who has been my best friend and cheerleader at every stage of my life and provided me with the tools I needed to succeed. From her, I have learned what it looks like to be a strong and compassionate human, who works hard to achieve your goals.

For my dad and siblings, who have always been supportive of my dreams and encourage me to work towards reaching them.

For my husband, who has been there for me through the good and the bad, the pretty and the ugly. And for listening to all my practice talks, asking insightful questions, and providing me with valuable feedback.

For my dogs, Madison and Finley, who are always happy to see me and are a continual source of joy, even when I come home upset after a day of bad data.

For all my friends, who celebrate my successes and are always there for a chat and a glass of wine.

And to all the animals used in research, past, present, and future. Without them, our research would not be possible.

Acknowledgements

I would like to thank Dr. Becky Foster for all her invaluable guidance from start to finish of my PhD. She has been an unhindered source of support in every way, and has always made time to listen to my thoughts and questions with genuine interest. Her critic and mentorship have helped me grow as a person and academic, and I am so grateful to have had her has my supervisor.

I would also like to thank Professor Simon Satchell and Dr. Gavin Welsh for their constant support and guidance. The intellectual discussion at meetings and their critic have helped develop my own thinking skills and I am thankful to have had such a supportive group of supervisors throughout my PhD.

A thank you to our collaborator Dr. Olga Zubkova at Victoria University of Wellington for providing the compound used in this study, OVZ/HS-1638. I also thank her for her enthusiasm related to this project and willingness to provide help in any way possible.

I am thankful to all of the members of the Bristol Renal team, who are a wonderful group of colleagues and friends who are always willing to listen, provide feedback, and help where needed.

Thank you to Professor David Bates and Dr. Kenton Arkill at the University of Nottingham for collaboration and discussion on the solute flux assay used in this thesis.

Thank you to Dr. Neill Campbell and Kwan Ho Ho, MSc in the Faculty of Engineering at The University of Bristol, for their collaboration in developing the solute flux analysis software used in this thesis.

I would like to thank Dr. David Copland and Dr. Denise Atan in Bristol Ophthalmology at The University of Bristol for their training and guidance in retina related techniques and topics.

I would like to thank the Wolfson Imaging Centre at The University of Brisotl, an excellent source of knowledge and expertise who trained me in processing EM samples, and who without their guidance I would not have been able to complete this work.

I would also like to thank Dr. Nicholas Wallace, Dr. Dan Boyle, and Dr. Sherry Flemming at Kansas State University, who hosted me during a three-month placement, and provided me with mentorship.

And a big thank you to the University of Bristol and the Alumni and Friends association for seeing the potential in me as an academic and providing me with funding, giving me the opportunity to carry out this PhD.

Author’s Declaration

I declare that the work in this dissertation was carried out in accordance with the requirements of the University's *Regulations and Code of Practice for Research Degree Programmes* and that it has not been submitted for any other academic award. Except where indicated by specific reference in the text, the work is the candidate's own work. Work done in collaboration with, or with the assistance of, others, is indicated as such. Any views expressed in the dissertation are those of the author.

SIGNED: .  . DATE: 18/03/20

Dr Rebecca Foster 18th March, 2020

Primary supervisor

Table of Contents

Table of Figures

Table of Tables

Abbreviations

ACEI	angiotensin converting enzyme inhibitors
ARBs	angiotensin receptor blockers
BSA	bovine serum albumin
CCB	calcium channel blockers
CD2	cluster of differentiation 2
CD31	cluster of differentiation 31
CKO	conditional knock out
CS	chondroitin sulphate
CTCF	corrected total cell fluorescence
DME	diabetic macular oedema
DN	diabetic nephropathy
DR	diabetic retinopathy
eGlx	endothelial glycocalyx
EM	transmission electron microscopy
EMCN	endomucin
Ext1	exotosin 1
Ext2	exotosin 2
FA	sodium fluorescein angiography
GAG	glycosaminoglycan
GalNAc	D-N-acetylgalactosamine
GBM	glomerular basement membrane

GEnC	glomerular endothelial cell
GFB	glomerular filtration barrier
GlcA	D-glucuronic acid
GlcNAc	D-N-acetylglucosamine
GlcNS	D-Glucosamine-2-sulphate
GLP-1	glucagon-like-peptide-1
HA	hyaluronic acid
HbA1c	glycated hemoglobin
HPSE	heparanase
HS	heparan sulphate
HSPGs	heparan sulphate proteoglycans
i.m.	intramuscular
i.p.	intraperitoneal
i.v.	intravenous
iBRB	inner blood retina barrier
ICAM-1	intracellular adhesion molecule
LMC	litter mate control
MMPs	matrix metalloproteinases
Ndst	*N*-deacetylase-*N*-sulfotransferase
NO	nitric oxide
OCT	optical coherence tomography
PBS	phosphate buffered saline
pGlx	podocyte glycocalyx
RAAS	renin-angiotensin-aldosterone system

REnC	retinal endothelial cells
ROS	reactive oxygen species
s.c.	subcutaneous
SLGT-2	sodium glucose transporter-1
STZ	streptozotocin
T1D	type 1 diabetes
T2D	type 2 diabetes
TNF-α	tumour necrosis factor alpha
TZDs	thiazolidinediones
uACR	urine albumin creatinine ratio
UAE	urine albumin excretion
UKPDs	United Kingdom Prospective Diabetes Study
VCAM-1	vascular cell adhesion molecule
VE-cadherins	vascular endothelial cadherin
VEGF	vascular endothelial growth factor A
VEGFR2	vascular endothelial growth factor receptor 2
ZO	zonula occluden

Mathematical Symbols

$\Delta\Pi$	difference in oncotic pressure
ΔP	difference in hydrostatic pressure
Δx	distance of concentration gradient dissipation
Π	oncotic pressure
A	surface area
a	molecular radius
Ap	surface area of available pores
C	concentration
D	diffusion coefficient
D'	restricted diffusion coefficient
$\Delta I_f/\Delta t$	solute flux
Js	rate of diffuse solute flux
Jv	fluid volume filtration rate
k	filtration coefficient
Lp	hydraulic conductivity
LpA	ultrafiltration coefficient
N	Avogadro's number
n	number of pores
P	hydrostatic pressure
Ps	Solute permeability
Ps'alb	apparent permeability of albumin
r	radius

R	radius of capillary
S	surface area
x’	diffusion length (pathlength of a pore)
ΔC	solute concentration difference
ΔI_f	change in fluorescent intensity
Δt	change in time
σ	solute reflection coefficient
ϕ	partition coefficient

Chapter 1 Introduction

1.1 *The Importance of Vascular Permeability*

1.1.1 Preamble

This thesis focuses on the role of heparan sulphate within the endothelial glycocalyx in vascular permeability. I will investigate whether endothelial glycocalyx heparan sulphate can be targeted therapeutically to prevent microvascular complication in diabetes, using vessel beds in the kidney and eye as examples. As will be discussed, the endothelial glycocalyx has a role in the maintenance of permeability in microvessels and is damaged in diabetes. The principles of permeability will be introduced in order to understand the various factors that contribute to microvascular permeability and the importance it has in health and disease. With this understanding, the known microvascular and endothelial glycocalyx changes that occur in diabetes in the kidney and eye will then be discussed. Lastly, I will introduce evidence for a potential key role for heparan sulphate in the glycocalyx and development of microvascular complications and will be the focus of my investigation.

1.1.2 The Role of Vascular Permeability in the Body

The circulatory system is essential to life as it delivers oxygen and nutrients to tissues throughout the body while simultaneously removing waste products. This vital job is accomplished by two vascular groups, the macrovasculature and microvasculature. Macrovascular vessels are larger and come in the form of arteries and veins. Because of their size and vessel structure, they possess the ability to transport large volumes of blood rapidly to and from organs (1). Microvessels on the other hand are small, in the form of venules, capillaries, and arterioles. Arterioles are largely thought to regulate local blood perfusion by contractile and relaxation capabilities, made possible by the smooth muscle cells that cover them (1). As capillaries and venules typically lack smooth muscle cells, and are composed largely of endothelial cells that lack vasomotor functions, they are responsible for the blood-tissue exchange that is crucial for a healthy functioning organ (1). The exchange vessels allow water and small solutes to pass relatively freely while restricting the free passage of larger molecules. As will be discussed in detail in this thesis, the manifestation of diseases in microvessels, and consequently the breakdown of their barrier function, can be detrimental to tissues and even fatal, showing the importance of these small vessels.

1.2 *Initial Physiological Studies on Microvascular Permeability*

1.2.1 Fluid Filtration in Microvessels

Because of the essential role microvessels play in maintaining tissue homeostasis, the movement of molecules across microvessel walls has long been an area of intensive research. In 1896 a British physiologist, named Ernest H. Starling, proposed that fluid movement across the capillary wall is driven by the difference of two forces (2). The first force is hydrostatic pressure, which is generated by circulating blood fluid. The second is colloid osmotic pressure (oncotic), which comes from the plasma proteins within the lumen of the vessel (inside vessel) relative to proteins in the extravascular (interstitial) space. Later work in 1932 by an American physiologist, Eugene Landis (3), helped to confirm and establish this theory, which is now known as the Starling-Landis equation, which states:

$$\frac{J_v}{A} = L_p[(P_c - P_i) - \sigma(\prod_c - \prod_i)]$$

Equation 1-1

Here, L_p is the coefficient that describes the permeation property of the capillary wall to water, known as hydraulic conductivity (cm/s/mm Hg), J_v is the fluid volume filtration rate (mL/s), A is the surface of the endothelial cell (cm^2), P_c is the blood fluid hydrostatic pressure inside the capillary (mm Hg) as well as P_i, but in the interstitial space. Π_c is the oncotic pressure in the plasma (mm Hg) as well as Π_i but for the interstitial space. Finally, σ is the reflection coefficient, which is the molecular sieving property of the capillary wall to a specific molecule, where if σ=0, the molecule is completely permeable and if σ=1, the molecule is completely impermeable (1). Alternatively, a more simplified version takes the form:

$$\frac{J_v}{A} = L_p[\Delta P - \sigma \Delta \prod]$$

Equation 1-2

where ΔP is determined by capillary blood pressure (12-54 mmHg) and ΔΠ is the difference in concentration of plasma proteins inside and outside the vessel **(FIGURE 1-1)** (1).

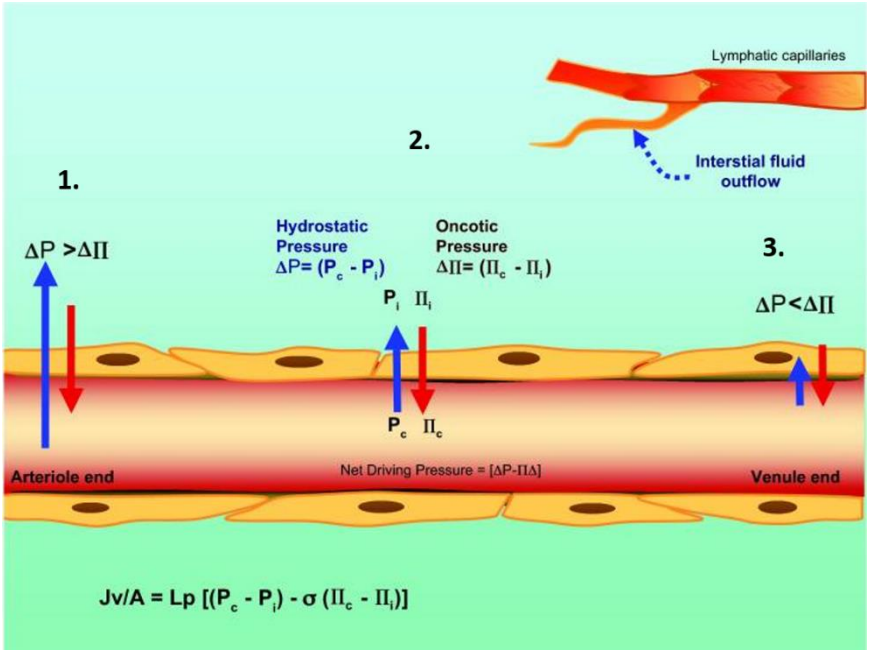

Figure 1-1 The Forces that Drive Fluid Filtration in Microvessels

1. At the arteriole end, hydrostatic pressure is higher than the oncotic pressure and drives fluid filtration out of the vessel. 2. The change in hydrostatic pressure and oncotic pressure is the difference of respective pressures inside the capillary and outside the capillary. 3. At the venule end, oncotic pressure is greater than hydrostatic pressure, believed to cause fluid absorption into the vessel. It is now known that the lymphatic vessels are responsible for fluid reabsorption. Image adapted from (Yuan and Rigor, 2010)(1).

Under normal microvasculature conditions, hydrostatic pressure is higher at the arteriolar end than at the venular end, favouring fluid filtration out of the vessel into the tissue, while the opposite is true at the venular end **(FIGURE 1-1)** (4). This was understood to be key for the proper function of microvessels. In diseased states in which there is a breakdown in the barrier, as will be discussed in later sections, naturally L_p would be increased, allowing plasma proteins to accumulate in the interstitial space (4). This would result in an increased oncotic force that promotes fluid accumulation into the tissue that prevents fluid absorption by the microvessels (1). However, we now know that there is no steady state absorption in to microvessels, as will be discussed below, and lymphatic vessels are responsible for clearing excess of fluid in the interstitial space (5), but this work has served as a solid foundation for describing the movement of molecules across a capillary wall.

1.2.1.1 The Glycocalyx and Vascular Permeability

1.2.1.1.1 Modification of Starling-Landis Equation to Account for Glycocalyx

The endothelial glycocalyx (eGlx), a mesh like layer lining the luminal side of endothelial cells, was first visualised by transmission electron microscopy (EM) in 1966 (6) and, thanks to a wealth of research, is now known to contribute to vascular permeability. As a result Curry, Levick, and Michael (4,7) proposed a modification to the original fluid filtration model **(EQUATION 1-1)** to account for the contribution of the eGlx , stating:

$$\frac{J_v}{A} = L_p\left[(P_c - P_i) - \sigma\left(\prod_c - \prod_g\right)\right]$$

Equation 1-3

The equation is almost identical to the original described in **EQUATION 1-1**, but Π_p is now Π_g, where Π_g is the oncotic pressure of the sub eGlx space. Therefore, if we go back to the simplified version in **EQUATION 1-2**, $\Delta\Pi$ is now the oncotic pressure difference across the eGlx, rather than across the endothelium **(FIGURE 1-2)**. Since the sub glycocalyx space is protein free, the glycocalyx oncotic pressure (Π_g) is lower, resulting in no steady state absorption into the vessel **(FIGURE 1-2)**, contrary to what was originally believed to occur under unrevised Starling Principles. This has been shown experimentally where albumin

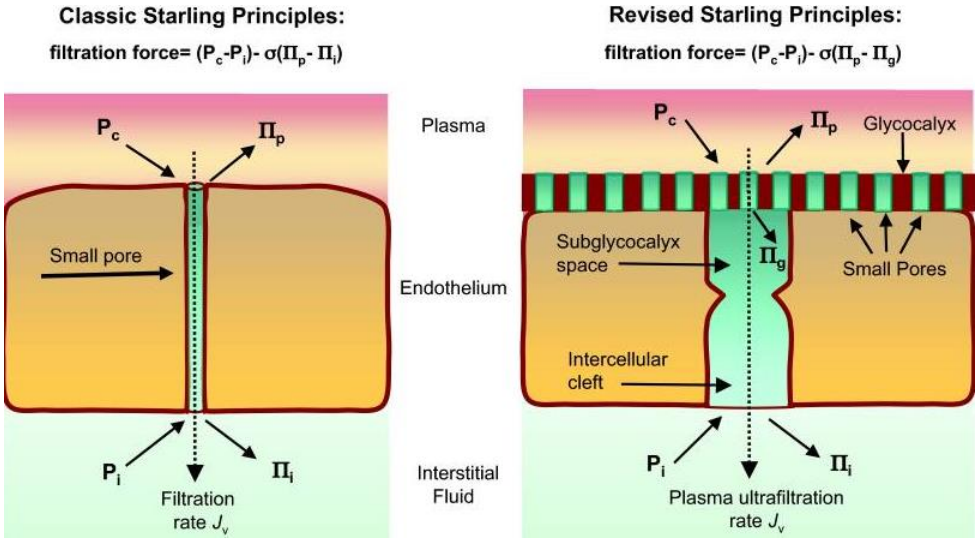

Figure 1-2 The Glycocalyx in Revised Starling Principles

Left: In the original model, the difference in oncotic pressure (∏) is determined by the oncotic pressure of the plasma in the capillary and the intestinal fluid. Right: In the revised model, the glycocalyx is a barrier that separates the lumen from the plasma protein restricted area below the glycocalyx (subglycocalyx space). As a result, the change in oncotic pressure is now contributed to by oncotic pressure in the lumen and oncotic pressure in the subglycocalyx space. Image adapted from (Yuan and Rigor, 2010)(1).

concentrations are directly changed inside and outside the vessel, and show that an increase of fluid filtration into the vessel does not occur (8).

1.2.1.1.2 The Glycocalyx: Structure and Function

Since its first visualisation it is now accepted that the eGlx lines the luminal side of virtually all endothelial cells found in the vasculature throughout the body, and serves as a selective barrier based on size and charge (9–11). The eGlx is a carbohydrate rich layer made primarily of proteoglycans and glycoproteins, which includes different families of glycosaminoglycans (GAGs); heparan sulphate (HS), chondroitin/dermatan sulphate (CS), and hyaluronic acid (HA) (6). With the exception of HA, GAGs are covalently attached to soluble and membrane bound proteoglycans, anchoring them to the cell surface (6).

HS is the most abundant GAG, representing 50-90% of the eGlx proteoglycans (12). Each GAG family is characterized by specific combinations of distinct disaccharide unit repeats, made of D-glucuronic acid (GlcA), L-iduronic acid, or D-galactose bound to either D-N-acetylglucosamine (GlcNAc) or D-N-acetylgalactosamine (GalNAc) **(FIGURE 1-3)** (6). CS is composed of GalNAc and GlcA linked by a glycosidic linkage GlcA β(1→3) GalNAc β(1→4) to form unbranched GAG chains (13). HS on the other hand is a linear polysaccharide that ranges from 50-150 disaccharide units, the most prominent being GlcA and GlcNAc with a -GlcA(1→4)GlcNAc- linkage and unique variations in number of acetyl groups and sulphation (14).

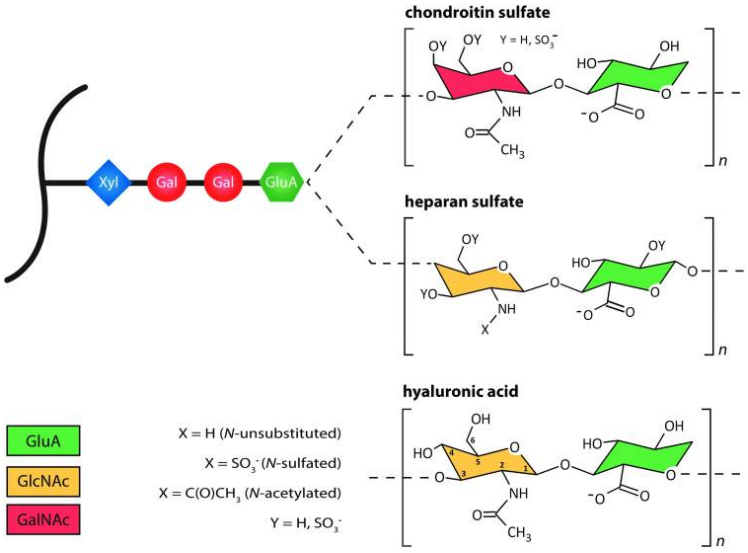

Figure 1-3 Structure and Components of Glycosaminoglycans (GAGs)

The three* main GAGs are chondroitin sulphate, heparan sulphate, and hyaluronic acid. GAGs are made *of different patterns of GluA, GlcNAc, and GalNac, with variations in sulphation and acetylation that contribute to function. Figure adapted from (van Golen et al.,2014)(39).

Additionally, each GAG chain can contain up to 50 disaccharide subunits, also with variable sulfation (13). Because changes in lengths and sulphation and/or (de)acetylation modifications heavily influences function, different tissues have predominating lengths, disaccharide variations, and modifications that meet the need of that tissue type (15). As will be discussed in more detail in **CHAPTER 3**, work on HS has been primarily focused on its role in the basement membrane and involvement in inflammatory responses, but how it contributes to eGlx structure and permeability function is not well known.

In addition to its barrier functions, the eGlx also serves as a protective layer, shielding the endothelial cell. Studies show that changes in fluid shear stress, caused by blood flow in the vessels, results in redistribution of GAG components, which may lead to a decrease in shielding of the endothelial cell membranes (11,16). It can also help regulate leukocyte adhesion, since the endothelium has leukocyte binding receptors, such as ICAM-1 and VCAM-1, which can be blocked or made accessible by the eGlx (14). It also has a role in controlling the microenvironment, acting as a reservoir for molecules like vascular endothelial growth factor-A (VEGF), chemokines, and antithrombin III, which can be released upon eGlx shedding (14). Its direct and continual interaction with flowing blood render it sensitive to changes in its local environment, including cation concentration, pH, and blood pressure, allowing this dynamic and versatile structure to adjust as required (11,14).

1.2.1.2 Solute Diffusion in Microvascular Permeability

The glycocalyx model **(EQUATION 1-2)** and the Starling-Landis model **(EQUATION 1-1)** both describe the forces responsible for driving fluid filtration in a microvessel, but do not describe the free diffusion of molecules across a semi permeable membrane. This is known as solute diffusion and is described by Fick's Law:

$$J_s = -DA\frac{\Delta C}{\Delta x}$$

Equation 1-4

Diffuse solute flux (J_s) is equal to the product of the diffusion coefficient (D), the surface area of the exchange membrane (A), and the solute concentration gradient (ΔC) divided by the distance Δx over which the concentration gradient is dissipated (1).

As D is determined by the barrier permeability (P_s) to a specific solute, which is inversely proportional to the square route of the solute's molecular mass (1), **EQUATION 1-4** can be expressed as:

$$J_s = P_S A \Delta C$$

Equation 1-5

This describes the relationship in which a molecule can diffuse freely. However, this equation does not consider other forces which may prevent free diffusion.

1.2.1.3 The Pore Theory

The pore theory was developed when similarities in permeability characteristics of capillaries from living organisms and artificial porous membranes were observed (17). The pore theory states that capillaries have many ultramicroscopic pores, which are too small to allow the passage of plasma proteins, but large enough to allow the observed passage of water and non-protein plasma molecules, when measuring permeability. Furthermore, *Pappenheimer et al.*, acknowledged that there were many indications suggesting capillaries from different regions of the body and species differed in their permeability characteristics, and therefore may be contributed to by differences in pores. The Stokes-Einstein Radius states that the size of the pores can be estimated by the amount of restriction the pores exert on a molecule as it moves through the poor (18), or:

$$D = RT/6\,\pi\eta aN$$

Equation 1-6

Where D remains the free diffusion coefficient as stated above, (R) is the gas constant, (T) the absolute temperature, (N) is Avogadro's constant, and (a) is the molecular radius of the pore. Recall that Fick's Law **(EQUATION 1-4)** gives the diffusive solute flux for free diffusion of a solute, but does not consider restrictions of diffusion. Similarly, the Stokes-Einstein Radius does not take into account that solutes moving through a narrow pore will encounter restrictions on diffusions. For example:

1. Pores may be oblique in respect to the capillary wall, and therefore the pore length (Δx') may be greater than capillary wall depth (Δx) (5).

2. The area available for diffusion (A) is confined to the area covered by the pores (A_p) which is equal to the pore area (πr_p)n_p where r_p is pore radius and n_p is number of pores (5).
3. As the radius of the solute increases, solute drag coefficient (D') between the solute and pore wall will increase (5).
4. The surface area available for diffusion is also dependant on the radius of the pore and the solute (5). For example, If the solute is spherical in nature and has an area of ''a'' and is diffusing through a pore with the radius ''r'' than the area available for diffusion is decreased to $\pi(r-a)^2$. This relationship between the total pore area and the actual area available for diffusion is described by the partition coefficient (ϕ), which can be calculated from $\phi = (r_p-a)^2/r_p^2$ (5).

This gives rise to a modified version of Fick's Law for solute flux (J_S') which now accounts for restricted diffusion in a pore:

$$J_s' = D'^{A_p}\Phi\Delta C/\Delta x'$$

Equation 1-7

Further modifications have been made to account for things like variation in pore size and distribution (19). Additionally, in modern interpretations of the pore theory, the glycocalyx is suggested to be responsible for the sieving properties which the pore theory describes (1). In this theory, the structure of the glycocalyx, which is a mesh like structure of carbohydrates, acts as a sieving system with a uniform pore size (19).

1.2.1.4 Solute Permeability

It is clear there are several factors that contribute to permeability of a given solute. But returning to Starling's original theory, ultimately it is hydraulic conductivity, the reflection coefficient of a molecule, and diffusion that will determine the permeability of a given solute.

The many years of investigation and refinement of Starling's original equation has given rise to the following:

$$P_s = J_s'/(A\Delta C)$$

Equation 1-8

As in **EQUATION 1-5**, A is surface area of the exchange membrane, ΔC is the solute concentration gradient, but J_s, which originally did not account for restricted diffusion, is replaced by J_s', which can be calculated from **EQUATION 1-7**. These refinements are all based on what is now known as Starling's Principles, and through evidence from multiple studies, this is now widely accepted as an accurate model of microvascular permeability (20).

1.3 *Microvascular Permeability in the Kidney and Eye*

1.3.1 Microvascular Permeability in the Kidney

1.3.1.1 The Glomerular Filtration Barrier

The permeability principles described, and the theory behind how the eGlx contributes to them, lays down a good foundation for discussing the importance of microvascular permeability in the kidney. The kidney has a vital functional role in the body. Kidneys are responsible for filtering blood to eliminate waste products into the urine and returning nutrients to the body. This is accomplished by the nephron, the functional unit of the kidney **(FIGURE 1-4A,B)** (21). The nephron is divided into two main components, the

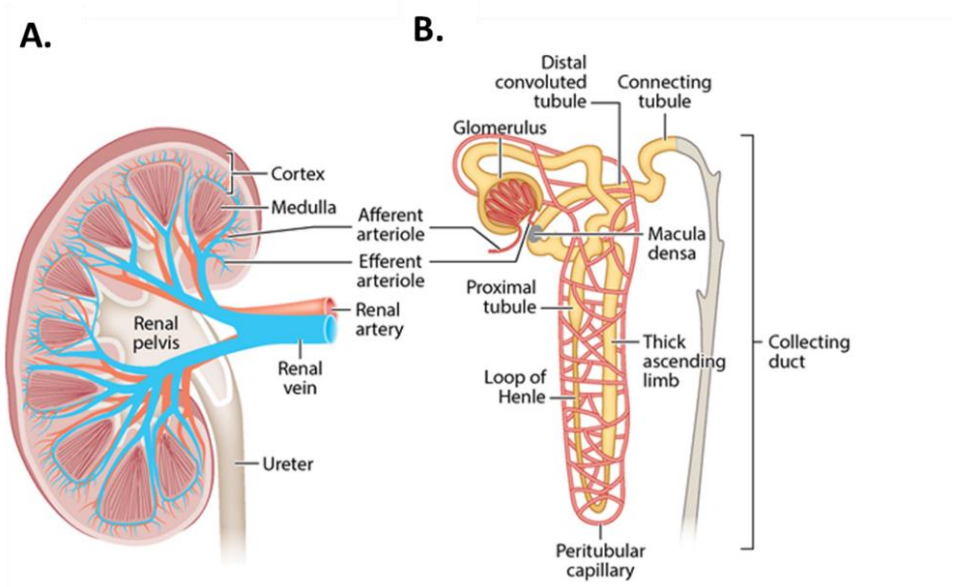

Figure 1-4 Structure of the Nephron in the Kidney

A. The renal artery feeds blood into the kidney, which is filtered, and waste products are eliminated via the ureter. The afferent and efferent arteriole feed into the glomerulus in B. B. Magnified image of the nephron shows the segments of the nephron, with a circular bundle of capillaries in the top left, labelled glomerulus. Image adapted from (Oxburgh et al., 2018)(21).

tubular epithelium and the glomerulus. The tubular epithelium is further divided into functionally distinct segments, the proximal tubule, the loop of Henle, distal convoluted tubule, and the connecting tubule **(FIGURE 1-4B)**. The tubular epithelium plays an important role in maintaining tissue homeostasis, including reabsorption of important molecules as is the case for the proximal tubules, but also water reabsorption, electrolyte balance, and urine concentration(21,22). However, the glomerulus serves as the sole filtering unit of the kidney.

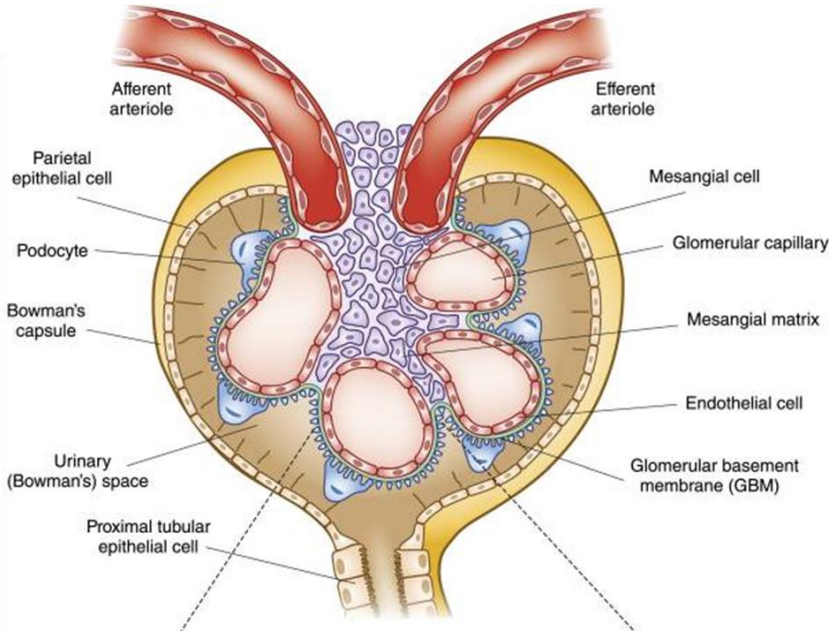

Figure 1-5 Structure of the Glomerulus

The glomerulus is the filtering unit of the kidney. Mesangial cells provide structural support to capillaries amongst other functions. Podocytes and endothelial cells in the glomerular capillaries form the glomerular filtration barrier. Image adapted from (Kitching and Hutton,2016)(23).

The glomerulus is encapsulated by the bowman's capsule, which contains the urinary space where waste products are filtrated into **(FIGURE 1-5)** (21,23). The glomerulus is a circular structure made up of a bundle of capillaries with highly specialised cells: mesangial cells, podocytes, and endothelial cells **(FIGURE 1-5)**. The mesangium, in addition to providing structural support to the glomerular capillaries, can also alter intraglomerular capillary flow, given the mesangial cell's contractile property (24). As can be seen in **FIGURE 1-5**, glomerular capillaries are atypical, as they are compromised from multiple cell types and do not have an interstitium surrounding them, instead they have the urinary space. The podocytes, glomerular basement membrane and endothelial cells

form the glomerular filtration barrier (GFB). Podocytes line the exterior surface of the glomerular capillaries, resembling an octopus like structure, with a cell body and major cytoplasmic processes. These extend outward and form interdigitating foot processes, with functional slit diaphragms, serving as a filter to passing plasma molecules **(FIGURE 1-6)**. Podocyte foot processes are covered by the glycocalyx, believed to help maintain podocyte-podocyte cytoarchitecture by promoting physical separation, due to repelling charge forces (25). The unique structure of podocytes not only provide structural support to the capillaries, but also have important cell signalling functions that allow communication with neighbouring endothelial cells, crucial for GFB function (26). The podocytes on the exterior of the capillaries and the endothelial cells on the luminal side of the GFB form a sandwich with the glomerular basement membrane (GBM) in between the middle (Figure 1-6). The GBM is an extracellular matrix made of laminin, collagen IV, proteoglycans and HS laid down by the exterior podocytes and endothelial cells that acts an important physical barrier in the GFB (27).

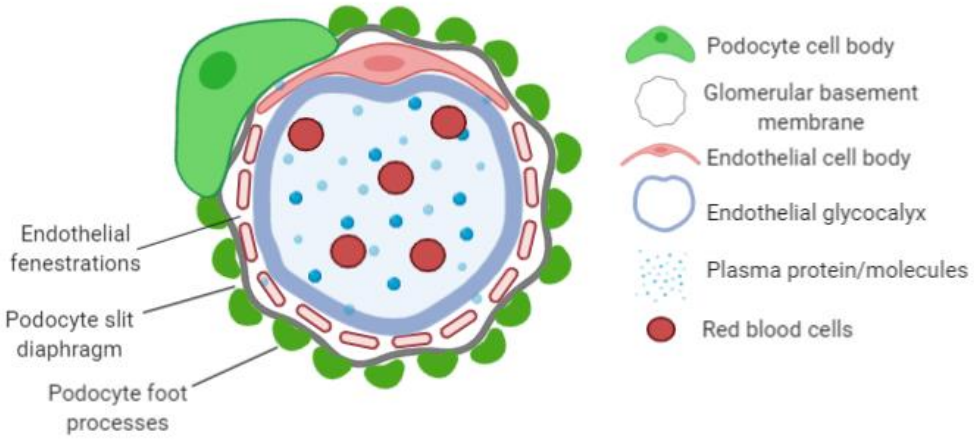

Figure 1-6 The Glomerular Filtration Barrier.

Schematic of a cross-section of a single glomerular capillary. The GFB is a trilayer. Podocytes are on the abluminal side of the capillaries and have podocyte foot processes that form part of the GFB. In between podocytes and endothelial cells sits the basement membrane. Endothelial cells sit on the luminal side of capillaries and are fenestrated. The endothelial glycocalyx is found on the surface of the luminal side of endothelial cells and prevents passive diffusion of larger plasma proteins and molecules. Image made using biorender.com

The most interior cell of the GFB is the endothelial cell, whose luminal side comes in direct contact with flowing blood and therefore plays a fundamental role in determining which molecules are filtered. The endothelial cell has unique pores all throughout its cell body, known as fenestrations **(FIGURE 1-6)**. These fenestrations are essential in the GFB, as they

allow relatively free passage of solutes and small molecules from the blood through the GFB into the urinary space. Fenestrations are 60-80nm in width (28,29) and act as a selective size barrier, preventing free passage of larger plasma proteins such as albumin. There is also evidence showing that eGlx plugs the endothelial cell fenestrations, suggesting a role for eGlx in selective permeability in the fenestrations (30). Similar to other cell types in the glomerulus which are high in metabolic activity, endothelial cell surfaces are covered with signalling receptors molecules, allowing for cross-talk between endothelial cells and podocytes, the most well studied being the VEGF/VEGF receptor 2 (VEGFR2) system, crucial for glomerular development and renal homeostasis (31). In addition to signalling molecules, endothelial cells are also covered by a layer of glycocalyx as mentioned and shown in **FIGURE 1-6**. However, unlike podocyte glycocalyx (pGlx), the eGlx is believed to have a direct functional role in vascular permeability.

1.3.1.2 The Glomerular eGlx and its Contribution to the Permeability Barrier

The closely linked, mesh-like nature of the eGlx results in a strong interplay between all of its components and changes to even one component can compromise vascular permeability, and in the glomerulus this presents as albuminuria (32). *In vitro* studies performed by our group on glomerular endothelial cells (GEnC) show that removal of HS and CS, using the specific shedding enzymes heparanase and chondroitinase, results in removal of endothelial surface HS and CS and increases albumin flux in a GEnC monolayers (10,33). However, the eGlx also contributes to the restriction of solute flux of small molecules, as was shown in cannulated frog mesenteric vessels in which pronase was used to shed eGlx, resulting in increased hydraulic conductivity without damaging tight junctions (34).

In humans, glomerular eGlx has not been well examined. *In vivo* models have been key to teasing out the functional role of eGlx in permeability. Treatment of mice with eGlx shedding enzymes heparinase III, hyaluronidase, and chondroitinase increased the frequency of close proximity intralipid droplets observed by EM (close proximity defined as 0-50nm from the GEnC), an indirect measurement of eGlx loss (35). In addition, albumin clearance measured in the urine was increased in chondroitinase treated mice, suggesting an increase in glomerular permeability (35). More recent *in vivo* studies by our group have shown that treatment of healthy mice with hyaluronidase and chondroitinase resulted in decreased glomerular eGlx measured directly by EM, using Alcian blue, an electron dense stain that allows for visualisation of the eGlx **(FIGURE 1-7, A-B)** (36). A novel technique, recently developed within our laboratory, allowing *ex vivo* measurements of

apparent albumin permeability in single capillaries (discussed in full in the methods), also demonstrated an increase in apparent glomerular albumin permeability when eGlx was shed **(FIGURE 1-7, C)** (36).

Evidence for the eGlx's contribution to permeability is further strengthened by indirect

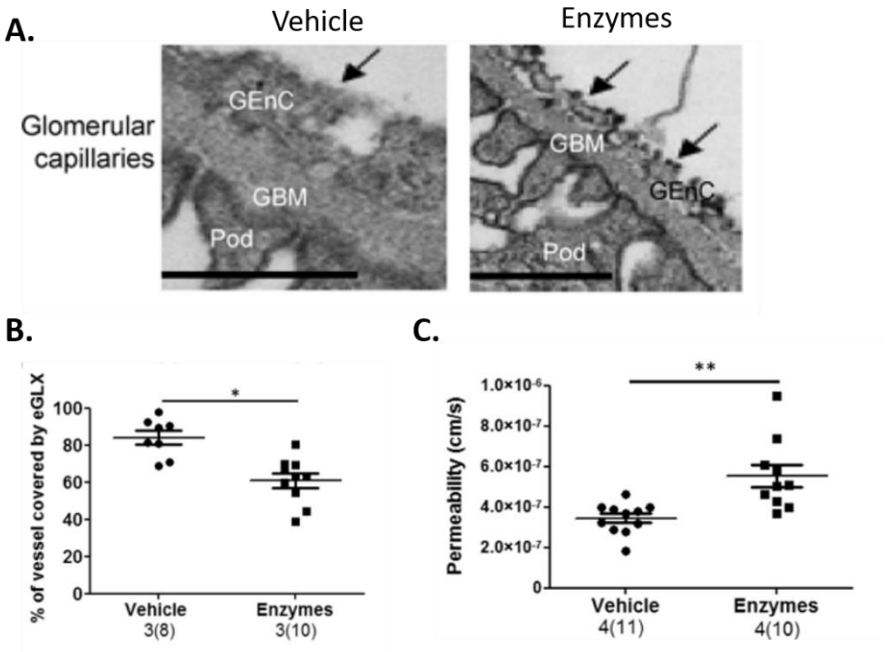

Figure 1-7 Intravenous Treatment with eGlx Shedding Enzymes Sheds eGlx and Increases Glomerular Albumin Permeability

Mice were treated with vehicle or chondroitinase and hyaluronidase to shed eGlx. A. Electron micrographs of the GFB. After treatment mice were perfused with an anionic electron dense cation called Alcian blue that allows visualisation by EM. A fuzzy electron dense layer (arrows) can be seen on the glomerular endothelial cells (GEnC). Note the reduced eGlx layer in the enzyme group. The podocyte (Pod) and glomerular basement membrane (GBM) are also visible. B. Quantification of electron micrographs showe a decrease in eGlx coverage. C. Glomerular albumin permeability was measured and increased in enzyme group. Figure modified from (Desideri et al., 2018)(36).

damage caused by less specific insults. For example, increased laminar shear stress in *in vitro* studies with GEnCs decreased the electrical resistance across the cell monolayer, indicative of increased permeability (37). Activated inflammatory cells can also release reactive oxygen species and nitrogen species (ROS/RNSs) which possess the ability to degrade not only HS, but HA and CS as well (38). Importantly, ROS causes proteinuria with no ultrastructural changes in the GFB, leaving the eGlx as the most likely culprit in observed changes (39). This result, along with the aforementioned studies have revealed the major role that the eGlx has on glomerular vascular permeability regulation (10,40–42).

1.3.2 Microvascular Permeability in the Retina

1.3.2.1 Contributing Factors to the Blood Retina Barrier

Unlike the filtration barrier in the glomerulus, the retina microvessels are continuous with no fenestrations and therefore constitutes a different type of vessel with its own mode of permeability regulation. The eye is a highly specialised organ that allows exterior visual input to ultimately come together as an image in our brain. This is only possible if all the separate components of the eye are functional. The eye can be most simply divided into three segments, the outer, middle, and inner segment which are surrounded by three transparent layers called the aqueous, lens, and vitreous **(FIGURE 1-8)** (43).The outer segment contains the cornea and sclera **(FIGURE 1-8)**, and cumulatively help maintain structure, prevent infection and damage to deeper parts of the eye, and refract and transmit light to the lens and retina **(FIGURE 1-8)** (43). The middle segment contains the iris, the ciliary body, and the choroid **(FIGURE 1-8)**. The iris determines how much light reaches the retina by controlling the pupil size, the ciliary body has roles in controlling lens shape and power and is also the site of aqueous production (43). The choroid is the

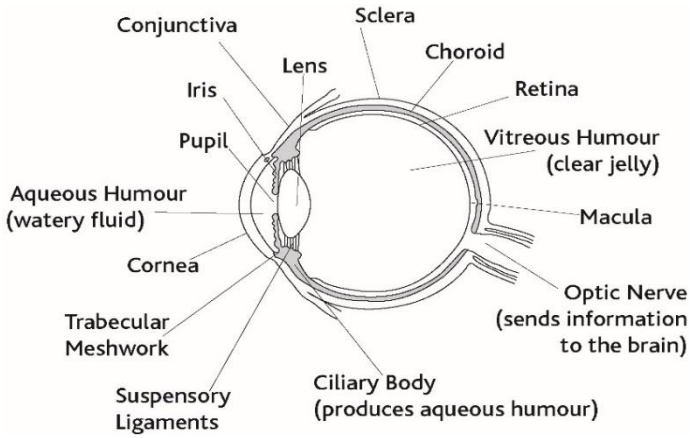

Figure 1-8 Anatomy of the Eye

Schematic of transverse cross-section of human eye. Outer segments include cornea and sclera. Middle segments include iris, ciliary body, and the choroid. Inner segment is the retina. The aqueous humour, lens, and vitreous humour are transparent layers that surround these three layers. Image adapted from (43).

vascular structure that provides nutrients and oxygen to outer retinal layers **(FIGURE 1-8)** (43). Lastly, the inner layer is the retina, the layered neuronal portion of the eye which is responsible for processing light into nerve impulses which are ultimately transmitted to the brain through the optic nerve **(FIGURE 1-8)** (43). Although all three segments are important in a healthy functioning eye, ultimately it is the retina which has one of the most important roles in fulfilling the functional role of the eye, *i.e.* sight.

Blood is supplied to the inner and outer retina by two different sources, the retinal blood vessels and the choroidal blood vessels **(FIGURE 1-9)** (44,45). Since the outer layers of the retina are avascular as depicted in **FIGURE 1-9**, nutrients are obtained through diffusion from the choroid, which, like glomerular epithelium, is fenestrated (46).

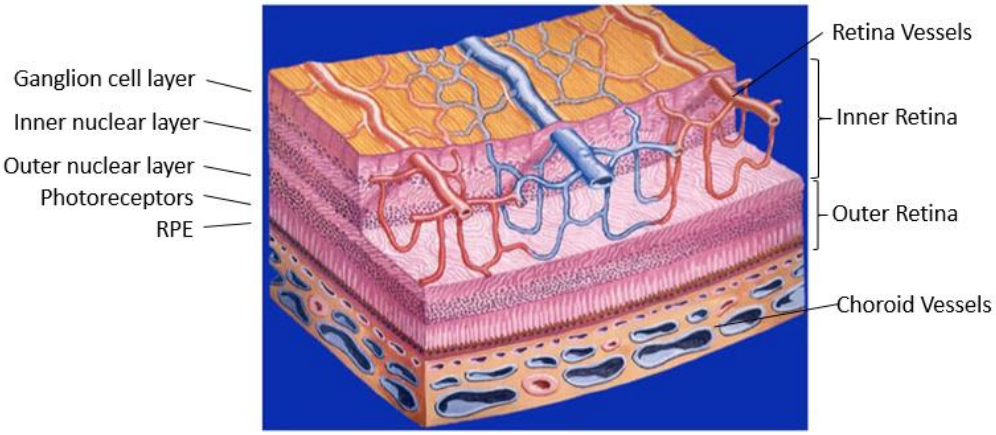

Figure 1-9 Structure of the Retina and Vasculature

The retina can be divided into several cell layers (labelled on the left) made up of specialised cells. The ganglion cell layer is the inner most layer of the retina (toward the vitreous) and the retinal pigment epithelium (RPE) is the most outer cellular layer of the retina, (toward the choroid). The inner retina gets its blood supply from the retinal vessels, while the outer retina which is avascular is supplied by the choroid. Image adapted from (theretinadoctor.com) accessed on 21/01/2020 (45).

The inner retina however is much more tightly regulated, as the vessels in the retina are continuous, with the endothelium lacking fenestrations. The inner retina vascular endothelium is surrounded by the basal lamina which is covered by pericytes, astrocyte and Müller cell processes **(FIGURE 1-10)**. The tight structure of retinal vessels, which is highly selective, is known at the inner blood retina barrier (iBRB) (47) and due to its clinical relevance in diabetic retinopathy is the focus of the retina portion of this thesis.

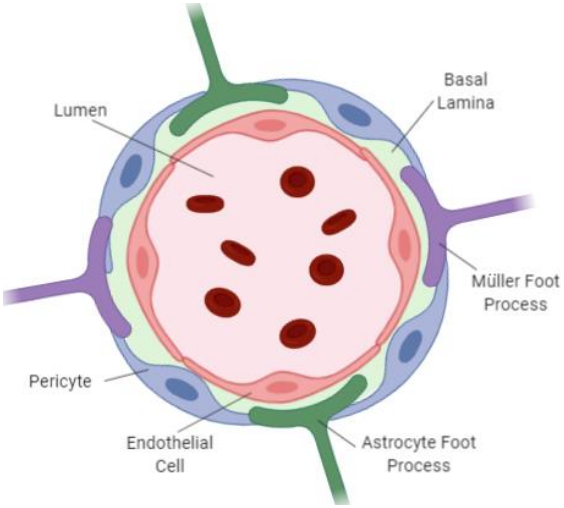

Figure 1-10 Schematic of Inner Retina Microvessel

Inner retina microvessels which form the inner blood retina barrier are continuous. Endothelial cells lack fenestrations, and are surrounded by a basal lamina, with pericytes, Müller, and astrocyte process that closely interact with each other. Image made using biorender.com

The iBRB is a physiological barrier that regulates ion, protein, and water flux in and out of the retina and is established by junctional complexes between retinal vascular endothelial cells (43,48). There are two ways in which vascular permeability is regulated, paracellular transport and transcytosis. Paracellular permeability is regulated through changes in junctional complexes which results in permeability changes around the cells **(FIGURE 1-11)** (48).

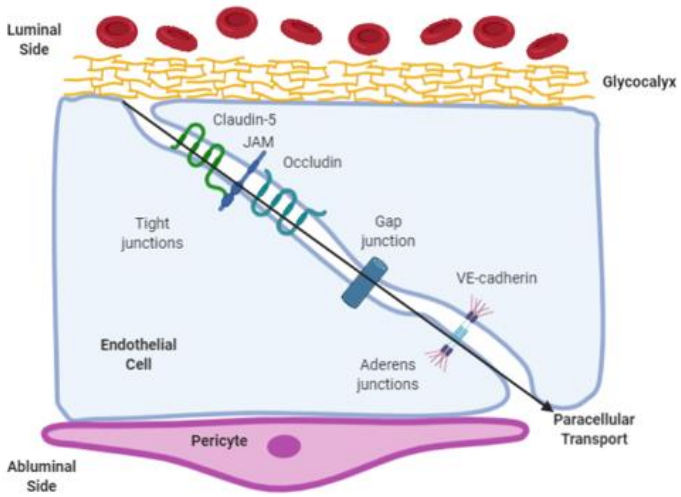

Figure 1-11 Paracellular Transport in Retinal Endothelial Cells

Examples of junctional complexes in the iBRB. Gap junctions, adherens junctions, and tight junctions which include claudins, JAM, and occludin family proteins. Junctional complexes regulate paracellular transport between two endothelial cells by junction reorganisation. Note the glycocalyx on the luminal side which may act as an additional regulation barrier in the iBRB. Image made using biorender.com.

Junctional complexes include tight junctions and adherens junctions, made up of several proteins, some well-known protein families in each junction type being zonula occludens (ZO) and vascular endothelial (VE)-cadherins, respectively. Changes to the makeup of these complexes can have dramatic effects on permeability regulation. For example, knockdown of ZO-1 in tissue culture results in failure of cells to form tight junctions, and loss of ZO-1 correlates with vascular permeability in rat retinas (49,50). Similarly, increased retina permeability in diabetic rats coincides with reduced VE-cadherin, suggesting contribution to maintenance of the iBRB through paracellular transport (51).

Transcytosis on the other hand is regulated through changes in the transport of molecules across the cell **(FIGURE 1-12)** (48). While some small lipophilic molecules have been shown to passively diffuse along the retinal endothelial membrane (52), larger or hydrophilic molecules require alternate transcytosis routes, like receptor mediated vesicular transport, non-receptor mediated pinocytosis, and pumps and transporters (48) **(FIGURE 1-12)**. By changing transport molecules on both luminal and abluminal sides, retinal endothelial cells can alter transport of molecules across the cell and therefore regulate permeability (48).

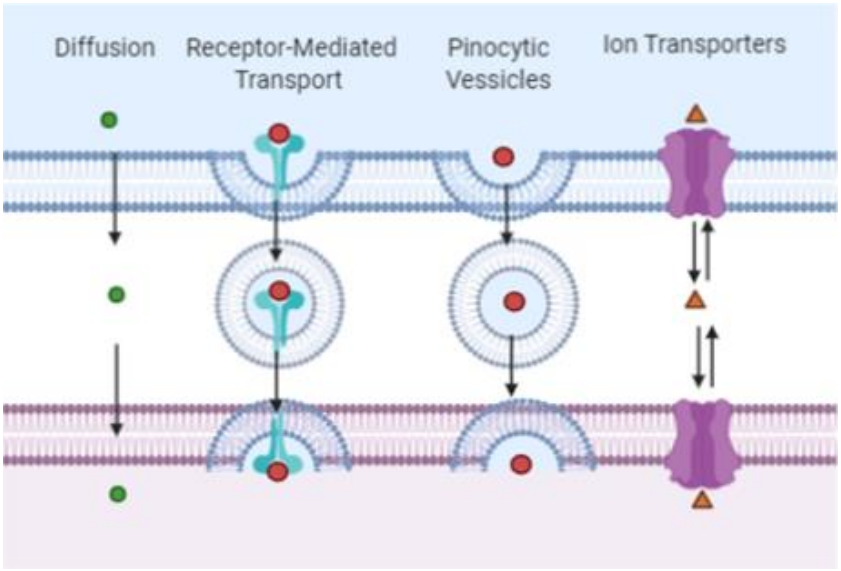

Figure 1-12 Types of Transcytosis Transport

Examples of transcytosis pathways. Diffusion of small lipophilic molecules can happen freely. For larger or hydrophilic molecules, active transcytosis is required in an adenosine triphosphate (ATP) dependant manner. This includes receptor mediated transport, pinocytosis, or through membrane channel proteins such as ion transporters. Image made using biorender.com

As in the glomerulus, retinal endothelial cells are also covered in eGlx (53). Unlike the glomerulus, the contribution of the eGlx in the iBRB has not yet been investigated in detail, but there is now some evidence that the eGlx may have a role in maintaining iBRB integrity as discussed below.

1.3.2.2 The Retinal eGlx and its Contribution to Permeability

Despite the already demonstrated importance of eGlx in other vascular beds and the eGlx's involvement in vascular diseases like diabetic nephropathy and cardiovascular disease (42,54–56) , the role of glycocalyx in retinal permeability has not been as extensively studied. Less than a hand-full of research articles have been published showing a reduction in retinal eGlx depth in disease (57–59), as will be discussed in section **1.4.3.2**, but the link between loss of eGlx in disease and permeability in the retina is lacking. Recently, *Leskova et al.* showed that treatment of healthy C57BL/6 mice with hyaluronidase, resulted in a reduction of eGlx depth in retinal arterioles and an increase in retinal vascular leak, measured using TRITC-dextran and sodium fluorescein (59). A T1D rat model also showed that restoring eGlx in diabetic rats by overexpressing endomucin (EMCN) protected iBRB permeability, measured using FITC-dextran (60). To date, these are the only published articles directly suggesting a role for eGlx in retinal vascular permeability. However, the continued study of the eGlx in this type of vascular bed is important in not only understanding similarities and differences between eGlx in the retina and other types of microvessels such as the kidney, for example, but also allows us to better understand its role in disease and how it can be potentially targeted for treatment.

1.4 *Changes in Microvascular Permeability in Diabetes*

1.4.1 Diabetes and Vascular Disease

According to GOV.UK, 2015 data from the Public Health England National Cardiovascular Intelligence Network shows an estimated 3.8 million people in England are diagnosed with Type 1 (T1D) or Type 2 (T2D) diabetes. By the year 2035, 4.9 million people are estimated to have diabetes, demonstrating the crucial need for both preventative and effective therapeutic measures (61). T1D and T2D are characterized by high blood glucose levels, *i.e.* hyperglycaemia (62). In both cases, hyperglycaemia is caused by a defect in insulin signalling. In healthy individuals, circulating insulin signals to neighbouring organs to uptake glucose. In individuals with T1D or T2D, this signalling is altered. T1D is a chronic autoimmune disorder, caused by the body's immune system attack on the β-cells located

in the islets of Langerhans in the pancreas (62). Though the exact event that leads to T1D is still under debate, numerous studies suggest a variety of genetic and environmental factors lead to its development (62,63). Because β-cells are the body's insulin producing cells, T1D results in diminished insulin production resulting in decreased glucose uptake and increased hyperglycaemia. T2D on the other hand is caused by β-cell dysfunction and/or the acquired resistance to insulin (64). A major risk factor for T2D is obesity. Because obesity causes a low but chronic level of inflammation, inflammatory molecules/processes lead to β-cell dysfunction and eventual cell death (64). In addition, continuous increased levels of glucose and fatty acids in the blood stream persistently stimulates insulin production by β-cells, and subsequent development of insulin resistance by glucose recipient organs (65). Although T1D and T2D differ in their aetiology, outcomes of uncontrolled hyperglycaemia in both types results in various pathologies including macrovasculature and microvasculature disease (66).

Macrovascular complications in diabetes stem primarily from the development of atherosclerosis, in which the arterial walls narrow, eventually leading to lipid-rich atherosclerotic lesions, which upon rupture can cause acute vascular infarction (66,67). Although there is evidence that demonstrates macrovascular and microvasculature complications are linked, the changes that occur in the microvasculature are typically one of the first observed, at times even before clinical signs of diabetes can be detected (66). Given the number of important processes microvessels are involved in, it is understandable how dysfunction of these small vessels can have large effects. Two of most common and severe microvasculature complications that occur during diabetes are diabetic nephropathy and diabetic retinopathy. As will be discussed, both involve endothelial cell dysfunction and loss of vascular permeability regulation, leading to pathology in the respective organ (68,69).

1.4.1.1 Biochemical Alterations that Contribute to Microvascular Damage in Diabetes

Hyperglycaemia in diabetes is known to cause de-regulation of a series of processes such as inflammatory mediators and growth factors, many of which contribute to microvascular damage. **TABLE 1-1** gives a brief summary of some of the known molecules and pathways to be altered in diabetes and some of the known effects which result from its alteration (38,70–81). It should be noted that this is not an exhaustive list, and many more pathways and molecules are known to be de-regulated in diabetes.

Table 1-1 Summary of Molecule and Pathway Alterations in Diabetes

Molecule or Pathway	Regulation in Diabetes	Effects	Reference
Polyol Pathway	↑	Oxidative stress	*Brownlee, (2005)*
AGEs	↑	Vascular damage	*Singh et al.,(2014)*
PKC	↑	Vascular damage	*Koya and King, (1998)*
HBP	↑	Oxidative stress and β-cell deterioration	*Kaneto et al., (2001)*
ROS	↑	Endothelial cell damage	*Busik, et al., (2008)*
RAAS	↑	Hypertension, vascular damage	*Steckelings et al., (2009)*
TNF-α	↑	Promotes insulin resistance and vascular damage	*Hotamisligil, (1999)* *Sawant et al.,(2013)*
IL-1	↑	Proinflammatory and promotes cell apoptosis	*Banerjee and Saxena, (2012)*
IL-6	↑	Promotes insulin resistance	*Rehman et al., (2017)*
Adiponectin	↓	Anti-inflammatory	*Achari and Jain, (2017)*
VEGF	↑	Angiogenesis and promotes vascular permeability	*Aiello and Wong, (2000)*
TGF-β	↑	Regulates atherosclerosis	*Gomes et al.,(2014)*

A brief summary of some of the known molecules and biological pathways which are altered in diabetes, and the effects resulting from such alterations. ↑= upregulating or activation ↓= downregulation. Advanced glycation end-products (AGEs), protein kinase C (PKC), hexosamine biosynthesis pathway (HBP), reactive oxygen species (ROS), Renin-Angiotensin-aldosterone system (RAAS), tumour necrosis factor α (TNF- α), interleukin (IL), vascular endothelial growth factor (VEGF), transforming growth factor β (TGF- β).

A major inflammatory mediator listed in **TABLE 1-1** is tumour necrosis factor α (TNF- α). TNF- α is an inflammatory cytokine produced by macrophages and monocytes, and is involved in a multitude of signalling events which result in necrosis and apoptosis (82). Elevated levels of TNF- α have been found in both T1D and T2D, which has been shown to promote insulin resistance in experimental diabetes (83,84). Additionally, TNF- α is thought to contribute to endothelial cell damage and hyperpermeability, as it is involved

in endothelial cell activation resulting in alterations of adheren junctional complexes like VE-cadherin which are required for vascular barrier integrity, and will be discussed in later sections (76). Upregulation of TNF-α also results in increases of other cell damaging agents such as ROS (76), which as mentioned earlier also results in damage to eGlx components.

Another well-known and extensively studied pathway, the renin-angiotensin-aldosterone system (RAAS), is activated in diabetes and contributes to the development of cardiovascular disease (85). RAAS is involved in a multitude of important physiological processing like maintenance of plasma sodium concentration and arterial blood pressure (85). As essentially every organ is affected by RAAS, activation of this system negatively impacts the vasculature on a systemic level. RAAS activation has been shown to result in glomerular, cerebral, and retinal vascular pathologies (86–88), and is a target of diabetes treatments as will be discussed later.

Upregulation of growth factors in diabetes also contribute to vascular damage, and one of the most well studied is VEGF, previously mentioned. VEGF is important in development, as it has a role in proliferation and angiogenesis (89). In healthy adults, it has been shown to have a role in wound healing and bone repair, as well as angiogenesis in the uterus, ovaries, and breast, during the female reproductive cycle (89). In diseases such as diabetes, upregulation of VEGFA induces vascular endothelial cell proliferation and migration, and contributes to vasopermeability in many tissue types (80), and as will be discussed in more detail below, contributes to glomerular and retinal pathologies in diabetes.

1.4.2 Microvascular Changes in the Kidney

1.4.2.1 Changes to the Glomerular Filtration Barrier in Diabetic Nephropathy

Diabetic nephropathy (DN) is characterised by increased passage of albumin into the urine, *i.e.* albuminuria. There are three categories of urine albumin excretion (UAE); normoalbuminuria (0-20ug/min), microalbuminuria (20-200ug/min), and macroalbuminuria (>200ug/min) (90,91). Increasing levels of albuminuria are generally correlated with DN progression, but not all those diagnosed with DN have albuminuria (92). This thesis focuses on early stages of DN, and therefore will focus on development of microalbuminuria and will be referred to simply as albuminuria.

The development of albuminuria is thought to result from ultrastructural changes in the GFB, though such changes can also be found in patients without it (93). That being said, DN patients do have some characteristic changes to their glomeruli depicted in **FIGURE 1-13**. One of earliest observed changes is increase in glomerular size and thickening of the glomerular basement membrane (GBM). Increase in glomerular size can be attributed to mesangial cell expansion as well as increased capillary size resulting from hemodynamic changes (90). Increased GBM thickness is thought to occur due to imbalances between synthesis and degradation of extracellular matrix components, contributed to by podocytes and endothelium (27,94,95). Other early signs include podocyte foot process effacement and therefore reduced podocyte slit diaphragm width (93), the outermost barrier in the GFB. Podocyte damage is likely caused by deregulation of crucial podocyte proteins like nephrin, podocin, and cluster of differentiation 2 (CD2) adaptor protein, amongst others (95). These proteins are crucial for maintaining the structural framework of the slit diaphragm, and genetic mutations of such proteins in mice and humans result in albuminuria, renal failure, and death (96,97). As VEGF also plays a role in regulating slit-diaphragm signalling and podocyte structure, the observed upregulation of VEGF in DN contributes to these changes (98). However, the characteristic changes seen in DN does

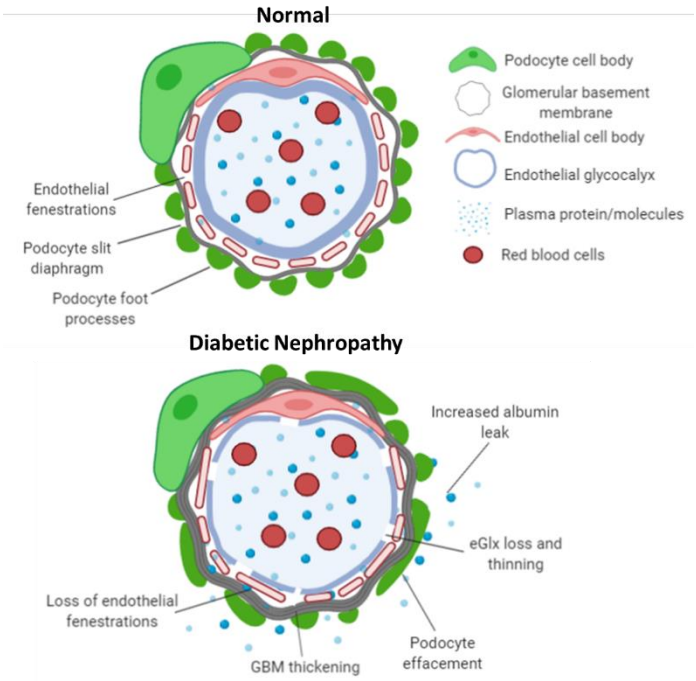

Figure 1-13 Changes to Glomerular Filtration Barrier in Diabetic Nephropathy

Early changes in the GFB during DN include thickening of the basement membrane, loss of podocyte and podocyte effacement, loss of endothelial fenestrations and eGlx thinning which all contribute to an increase in permeability to small and larger molecules such as albumin. Image made using biorender.com

not appear to be required for development of albuminuria, as is the case with approximately two thirds of type 2 diabetic (T2D) patients who have no changes in glomerular structure (99–101).

As previously mentioned, endothelial cells of the GFB are in closest contact with flowing blood. Due to the chronic exposure of endothelial cells to high glucose, which itself can cause an increase in cell damaging agents like ROS and VEGF as discussed earlier (101), it is not surprising that the endothelial cell also fall victim to structural changes during diabetes. It has been reported in T1D and T2D that loss of fenestration density occurs during diabetes **(FIGURE 1-13)** and correlates better with albuminuria than does podocyte injury (102,103), pointing to endothelial dysfunction as a potential key event in DN progression. In agreement with these findings, the protective and functional layer that covers endothelial cells, the eGlx, is also damaged during diabetes and there is accumulating evidence that loss of eGlx may be an early and key event in the development of DN.

1.4.2.2 Damage to the Glomerular Endothelial Glycocalyx

During periods of inflammation, such as diabetes, changes to the cellular environment can cause dysregulation of a multitude of pathways which can ultimately cause damage to the eGlx **(FIGURE 1-13)** (104). For example, increased ROS occurs under hyperglycemic conditions, and *in vitro* studies show that ROS causes a reduction in cell surface HS, suggesting HS is shed (38). ROS also results in increased albumin passage in glomerular endothelial cell (GEnC) monolayers (38). An increase in active eGlx shedding enzymes, known broadly as sheddases, are also upregulated in diabetes. Both *in vivo* and human studies have shown increases in circulating hyaluronidase and matrix metalloproteinases (MMPs), HA/HS and proteoglycan core protein syndecan shedding enzymes, respectively (105–108). Active heparanase-1 (HPSE), which directly targets and degrades HS, is also upregulated in diabetics with DN (109,110), and presumably is a major factor in contributing to eGlx damage, which will be discussed in section **1.5.1.4.1**.

Studies measuring shedding of eGlx components have shown an increase in the serum of patients with T1D and T2D patients. Increased sydecan-1, an eGlx proteoglycan, was shown to be increased in serum from T1D (111). HA and CS have also been shown to be increased in serum from diabetics (104,112). *In vivo* diabetic rodent models have similarly shown increased shedding of eGlx components and sheddases, such as MMPs, HPSE, and hyaluronidase (108,113–115). Diabetic rodent models have also allowed researches to

examine functional and structural changes to the eGlx. Research done in our group using EM and fluorescently conjugated lectins that bind strongly to eGlx sugar components **(FIGURE 1-14)**, show reduced glomerular eGlx in diabetic rodent models. This decrease

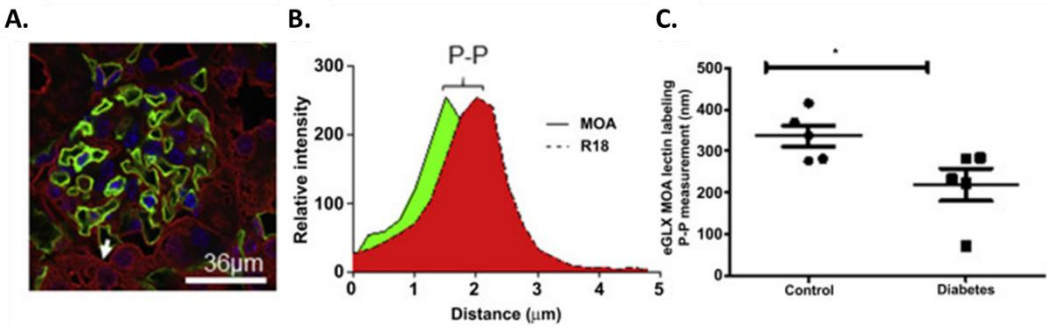

Figure 1-14 Diabetes Results in Glomerular eGlx Loss

A T1D mouse model comparing eGlx in control and diabetic mice. A. Mouse kidney section stained with Marasmim oreades agglutinin (MOA) (green), a lectin that binds sugar moieties found in eGlx components. Cell membrane is stained red and nuclei blue. B. Example of how eGlx depth was measured using lectin staining. The peak distance between the fluorescent intensity peak of the eGlx signal (green) and membrane signal (red) are measured and is representative of eGlx depth. C. A series of images were analysed and described in B. Comparison of control and diabetic mice show a significant reduction in eGlx MOA lectin labelling. Image adapted from (Ramnath et al. 2019)(108).

also coincides with increased albuminuria and glomerular albumin permeability (36,108,116), indicating a role for eGlx in maintenance of vascular permeability. Reduced eGlx in sublingual and retinal vessels has also been shown in T2D, suggesting a more global loss of eGlx damage in multiple vascular beds (58), and therefore may be a key common step in the development of microvascular diseases.

1.4.3 Microvascular Changes in the Eye

1.4.3.1 Changes to Blood Retina Barrier in Diabetes

Retinopathy is characterised by a breakdown in the iBRB which results in increased microvessel permeability. There are two defined stages of retinopathy, the early stage is non proliferative diabetic retinopathy (DR) and the more advanced stage, proliferative DR (PDR). This thesis focuses on early stages of disease in the microvessels and therefore will be focusing on the earlier stage, DR. The major criteria for diagnosis of DR, is the appearance of microvascular lesions (117). Techniques, such as ultrawide-field colour fundus photography and fluorescein angiographies, allow clinicians to non-invasively monitor changes in DR patients. During DR, evidence of vessel leakage can be observed by imaging the back of the eye, *i.e.* the retina. Early changes can be seen in the form of microaneurysms, retinal haemorrhages, intraretinal microvascular abnormalities, lipid

exudates, and cotton wool spots resulting from neuronal infarcts due to capillary non perfusion **(FIGURE 1-15)** (117).

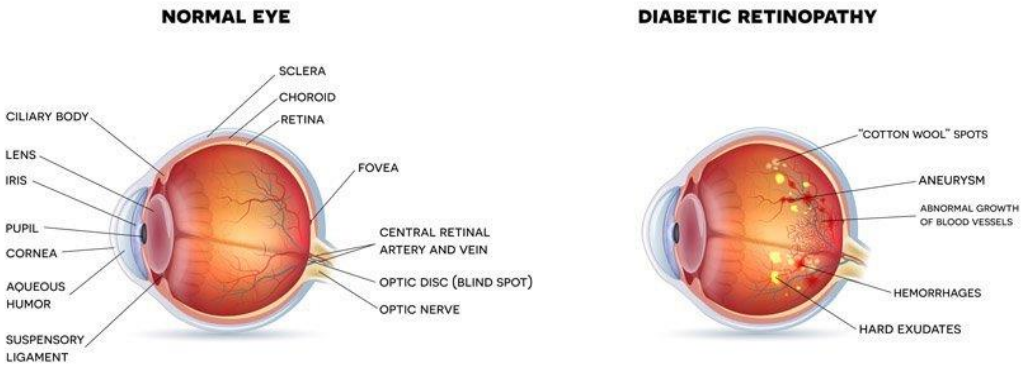

Figure 1-15 Changes to the Eye in Diabetic Retinopathy

Retinopathy causes loss of vessel integrity, leading to hemorrhages, abnormal growth of blood vessels, and hard exudates, amongst other complications. Image adapted from (eyedoctorsofsoutherntier.com) accessed 8/4/2018 (117).

The most common cause of blindness in both DR and PDR is macular oedema (DME) , caused by a breakdown in the blood retina barrier resulting in fluid and circulating protein leak into the retina (118,119). The use of optical coherence tomography (OCT) allows clinicians to measure changes in retinal thickness and has become a valuable non-invasive imaging technique used for monitoring the progression of DME.

Long term clinical studies and histology on post-mortem human eyes have shown that DR lesions are preceded/accompanied by even earlier changes in retinal vasculature (120,121). This includes loss of pericytes, thickening of vascular basement membrane, and eventual endothelial cell death (120,121). These early changes which can be seen prior to vascular lesions in humans, result in vascular integrity and loss of blood flow regulation in the retina, which is essential given the high metabolic activity of retinal neuronal cells (117).

Increased vascular permeability in DR has also been associated with changes in junctional complexes and increased transcytosis. *Frey et al.* proposed tight junctions may be disrupted by increased ROS which can result in endothelial cell dysfunction as has been seen in the kidney, and increased cytokine and growth factors production by neural retinal cells caused by hyperglycaemia (72). In a T1D rat model, increased transcytosis, measured by horse radish peroxidase staining, was observed in retinal vascular endothelial cells

(RVECs) (122). The observed increase of VEGF in diabetes is also strongly implicated in increased vascular permeability, not only in the glomerulus but also in the retina. For example, in healthy monkeys injected with VEGF into the vitreous of the eye, increased microvascular leak was observed by fluorescein angiographies, and leaky vessels were interestingly associated with increased pinocytic vesicles (123). Additionally, VEGF induces profibrotic growth factors and extracellular matrix genes *in vivo* and *in vitro* (124), and likely contributes to the basement membrane thickening observed in early stages of the disease previously mentioned. Although the effect/contribution of the eGlx was not investigated in these studies, evidence from the kidney showing the effects of ROS, cytokines, and growth factors on eGlx loss and permeability, suggest that the similar observed changes in the eye can also be linked to early changes in the eGlx.

1.4.3.2 Damage to Retinal Vascular Endothelial Glycocalyx

As mentioned, the retinal eGlx in diabetes has not been extensively studied. One study in humans showed that retinal eGlx dimensions were decreased in T2D patients (53). Diabetic rodent models have also demonstrated damage to eGlx. In T1D Wistar Kyoto rats, eGlx was reduced in retinal and choroidal vessels shown by EM (57), but eGlx staining was very patchy **(FIGURE 1-16)** even in control animals and therefore may not be reliable.

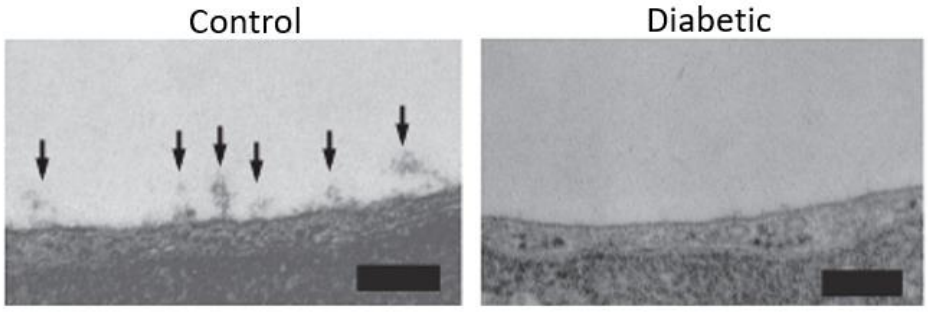

Figure 1-16 Loss of Retinal eGlx in Diabetic Rats

Electron micrographs of rats perfused with ionic colloidal iron stain. Albeit patchy, the eGlx can be visualised in nondiabetic control rats (black arrows), while diabetic rats show absence of eGlx. Image adapted from (Kumase et al, 2010)(57). Scale bar = 200nm.

A study in *Akita* mice, a T1D model, also saw a reduction in retinal eGlx by measuring the difference in vessel diameter of the fluorescent peaks using TRITC-dextran and sodium fluorescein, which the authors suggest represents eGlx depth (59). However, these authors did not report if functional changes occurred in vascular permeability. Studies on T1D rats also demonstrated a reduction in retina eGlx depth by EM and an increase in

retinal vascular permeability using FITC-Dextran (60) , though as in **(FIGURE 1-16)**, the eGlx staining was also patchy, including in the control animals. In this same study, overexpression of EMCN in T1D rats restored retina eGlx and resulted in a significant decrease in permeability, indicating that protection of retinal eGlx in diabetes prevents permeability increase (60). As in diabetic kidneys, HPSE has also been shown to be upregulated in the retinas of diabetic rats and epiretinal membranes of DR patients, but the effects on eGlx and HS were not investigated in these studies(125,126). These data, along with the noted upregulation of eGlx damaging agents like ROS and cytokines, all point to a role for eGlx in the retina. However, the evident lack of research makes it clear that there is still much work that needs to be done in characterising the exact role of HS and eGlx in health and disease of the retina, which can be applied to the development of treatment of retinopathy and microvascular complications.

1.5 *Treatments in Diabetes*

1.5.1.1 Current Diabetes Treatments and Prevention of Vascular Disease

Current treatments for T1D and T2D are aimed at maintaining blood glucose levels within the normal range, avoiding spikes or dips in glucose levels (127). For T2D, in addition to changes in diet, and physical activity aimed at weight loss, multiple treatments that increase insulin sensitivity are used in conjunction to target multiple organs (128). Treatments include metformin and thiazolidinediones (TZDs), which both act by inhibiting the increased hepatic gluconeogenesis in the liver, which causes elevated hepatic glucose production in T2D (129–131). Though this action helps in lowering blood glucose levels, the United Kingdom Prospective Diabetes Study (UKPDS) showed that over the course of fifteen years, metformin failed to provide any protective effects on β-cell function and glycaemic control, which ultimately leads to progressive diabetic complications (132). Another common class of drugs used to manage blood glucose levels are sulfonylureas. Sulfonylureas work by binding to the sulfonylurea receptor on β-cells, stimulating insulin secretion and lowering glycated hemoglobin (HbA1c), which directly correlates to blood glucose levels (131). Similarly to metformin, the UKPDS found that sulfonylurea did not help retain β-cell function after 6-12 months of treatment, and in fact led to increased HbA1c levels due to progressive β-cell loss (128). In contrast, studies have shown that TZDs do help maintain β-cell function, but these class of drugs can also increase weight gain, fluid retention, and cause heart failure (131,133,134). Because T2D patients are at an increased risk of developing cardiovascular disease and both T2D and hypertension are often seen in the same individual, patients are often put on anti-hypertensive treatments

to control blood pressure, like angiotensin converting enzyme inhibitors (ACEI), angiotensin receptor blockers (ARBs), RAAS blockers (135). Although various treatments have proven effective at preventing or slowing the process of DN and DR, the issue of blood glucose regulation remains and studies have shown, even with multiple types of treatment, target blood pressures are often not met, leaving an increased likelihood of developing cardiovascular disease (86).

Although T1D treatment aims to control blood glucose levels just as in T2D, T1D is primarily treated with exogenous insulin or insulin analogues. Because T1D individuals have decreased β-cells and therefore decreased insulin production, patients require insulin injections that allow glucose to be taken up by neighbouring organs. While exogenous insulin injections help regulate blood glucose levels, the inability of patients to physiologically respond to glucose spikes the way a healthy individual would, leads to hyperglycaemia episodes (136). These spikes contribute to complications previously mentioned, like nephropathy and retinopathy (136). In addition, exogenous insulin doses can also lead to episodes of hypoglycaemia, which has a mortality rate of 3-6% (137). Efforts have also been made using immune therapy, which aims to minimise the immune system's destruction of β-cells, slowing the progression of T1D (136,138). While this approach helps preserve patients' remaining β-cells, treatments used to accomplish this, like cyclosporine, have been shown to not only have short term effects, but also cause nephrotoxicity (136,138). In more extreme cases, whole pancreas, islet allotransplantation, and in some cases simultaneous pancreas/kidney transplantation, have been used successfully, but donor tissues are limited (139). With the added risk of required immunosuppressant to prevent tissue rejection, this is not a feasible treatment option except in the most severe cases (139). Given the increasing trend in diabetes diagnoses and the lack of fully effective treatments, most of which come with serious side effects or added complications, it has become increasingly important that a safe, effective, and accessible treatment be developed that can prevent complications associated with diabetes, like microvascular disease.

1.5.1.2 Diabetic Nephropathy Targeting Treatments

Unfortunately, there is currently no single treatment that is used to treat DN. Methods aimed at prevention and slowing progression are the main form of treatment, many of which have already been discussed in the previous section. However, treatments like ACE inhibitors may be favoured as they have shown to help lower albuminuria and blood pressure (140,141). The aldosterone antagonist Spironolactone also reduces albuminuria

in T1D and T2D by inhibiting aldosterone, which promotes fibrosis, ROS production, and endothelial cell dysfunction (142,143). The addition of calcium channel blockers (CCB) to RAAS blockers also appears to lower albuminuria in T2D (144). Treatment of T2D and chronic kidney disease patients with sodium glucose transporter-2 (SLGT-2) inhibitors, which are typically used to lower blood sugar in T2D has also shown protective renal effects that lowers albuminuria and slows progression (145). Similarly, glucagon-like-peptide-1 (GLP-1) receptor agonists, which are also used to lower blood sugar in T2D, have been shown to reduce albuminuria (146). In more progressed stages of the disease, kidney dialysis may be used to aid loss of kidney function, but unfortunately this does not reverse damage or restore function, and compared to non-diabetic counterparts, dialysis patients have a higher mortality and morbidity rate (147).

Of note, there are currently no treatments that specifically target the glomerulus therapeutically. And as discussed above, most of the current treatments have added side effects despite the benefit of lowering albuminuria, as is the case for some treatments. Therefore, an ongoing search for treatments that can safely and effectively target and prevent changes in DN is required

1.5.1.3 Diabetic Retinopathy Targeting Treatments

As with DN, DR treatments are firstly preventative with the same course of action as described above. However, DR does have some more targeted treatments to prevent DR progression. One of the most effective and widely used treatments for DR is anti-VEGF therapy. As previously discussed, VEGF is upregulated in diabetes and promotes loss of vascular integrity by promoting loss of pericytes and endothelial cell dysfunction, amongst other vascular deteriorating effects discussed above, which results in increased permeability (124). Additionally, VEGF is a pro-angiogenic protein which stimulates neovascularization. Although areas of the eye in retinopathy suffer damage due to hypoxia, VEGF actually promotes DR progression due to the uncontrolled and poor integrity of newly formed vessels, which leads to increased leak and DME (119). Anti-VEGF treatments are administered intravitreal, *i.e.* an injection directly into the vitreous of the eye. Though this treatment has proven effective in multiple studies, anti-VEGF agents have a short half-life and require DR patients to receive injections one to two times a month (119,148,149). Other treatments like anti-inflammatory corticosteroids, which target mediators of DR progression, like VEGF, TNF-α, and phosphorylation/destabilisation of tight junctions, are effective in preventing DR and reducing DME (149). These treatments have the added benefit that they are administered

into the vitreous, as with VEGF, but in a biodegradable capsule, thereby reducing the number of intravitreal injections required. Unfortunately, these treatments have increased side effects, including cataract development and elevated intraocular pressure (150,151). Non-steroidal anti-inflammatory drugs, which may have less side effects, are currently in clinical trials targeting IL-6 and integrin, one of the major proinflammatory cytokines and adhesion molecules promoting inflammation in DR patients, respectively (149). One of the older and most used therapies, second to anti-VEGF treatments, is laser photocoagulation. Panretinal photocoagulation involves creating multiple small burns in the retina, which results in reduced ischaemia, a major driving force for VEGF production in the retina, and promotes neovascularisation (152). Focal photocoagulation, another type of laser treatment, involves a strong but precise laser used to directly target and close microaneurysms, stopping vessel leak (153). The obvious draw-back to these treatments, despite advances in laser technology, is the likelihood for permanent laser damage causing loss of mild central vision and reduced night vison (154). While DR clearly has more effective and targeted therapies, they do not come without both side effects and difficulty of administration as discussed. Additionally, these targeted treatments are given once increased permeability and changes in the eye have already been detected, and do not help the wider issue of initial development and progression of microvascular disease.

1.5.1.4 Glycocalyx Targeting Treatments

The role of eGlx in maintenance of vascular permeability, along with data showing that changes in the cellular components of the GFB ultrastructure are not required for the development of microalbuminuria, suggests that an early intervention targeted at restoring the eGlx may help slow or stop the progression of microvascular complications like DN and DR.

One of the approaches that has been tested experimentally as a therapeutic to restore eGlx and mitigate the negative effects diabetes has on the vasculature is the use of growth factors known to upregulate eGlx components. Our group has shown that in tissue culture, VEGF-C treatment increased production of highly charged GAGs by GEnC (33). In agreement with this, we showed in a transgenic T1D mouse model, mice whose podocytes overexpressed VEGF-C had slowed progression of DN (116). It has also been demonstrated that in a diabetic mouse model with a systemic injection of VEGF-A_{165}b, an isoform of VEGF, protected against DN and helped restore the eGlx (155). Additionally*, Schott, U. et al.* summarized other treatments that have been shown to help restore the glycocalyx,

such as hydrocortisone and albumin (41), however these experiments were performed *in vitro*/isolated organ models and the effects this would have *in vivo* are unclear. While many of these treatments remain promising, they primarily target the eGlx through alternate pathways that lead to its restoration, and the complexity of diabetes associated vascular disease requires a multitude of available treatments.

In humans, some progress has been made in the direction of directly targeting the eGlx in diabetic patients. The eGlx is a crucial structure which contributes to 50% of the overall hydraulic resistance of the GFB (156), and likely contributes significantly to vascular barrier functions in other vessel beds as well, as has been demonstrated in cardiovascular diseases (56). Because the eGlx is a tightly bound network and HS is the most abundant GAG, it is not surprising that loss of HS may have detrimental effects on the integrity and functionality of the eGlx. To combat this, Sulodexide, a mixture of low-molecular weight heparin (80%) and dermatan sulphate (20%), has been used to treat DN and DR. Initially, several studies showed success in using Sulodexide as a therapeutic, showing an increase in sublingual and retinal glycocalyx dimensions (58), and decrease in albuminuria (157,158). Unfortunately, two larger randomized double-blinded placebo control studies later showed that treatment with Sulodexide did not reduce albuminuria when compared to placebo and had no renoprotective effects (157,159). Despite negative results however, there is still value that has come from these studies. The initial success of Sulodexide has made it a drug that continues to be studied for use in vascular diseases, with positive effects seen with long-term low-dose treatment in nephropathies and peripheral artery diseases (160,161). A one year study in patients with mild to moderate DR also showed reduction in macular hard exudates which result from lipid and protein leaking from vessels, though eGlx was not addressed in this study (53). The continual positive results, using Sulodexide, shows that treatment with a compound that has been shown to restore the eGlx has potential, and perhaps the use of a different and more potent compound with a similar end result could be successfully used to protect from microvasculature complications during diabetes.

Interestingly, an *in vitro* study by the same group who showed protection from DN in diabetic patients with Sulodexide, published a potential mechanism for DN protection (162). The group showed that Sulodexide can act as a HPSE inhibitor, exclusively due to its heparin component (162). Though not specifically addressed in this study, it is possible that Sulodexide may have a protective effect on eGlx by preventing HS shedding by inhibiting HPSE.

1.5.1.4.1 HPSE as a Potential Target for eGlx Restoration in DN and DR

Briefly mentioned in earlier sections, the HS shedding enzyme, HPSE, is elevated in diabetes. HPSE is an endo-β-D-glucuronidase and is the only known enzyme in humans that cleaves HS. Another protein, Heparanase-2 (HPSE-2), which has a similarity of 40% with HPSE, lacks enzymatic activity and actually inhibits HPSE (163). HPSE cleaves HS at specific sites, β(1,4) glycosidic linkage between GlcA and GlcNS, which generates small 5-10kDa HS fragments (164). These fragments have themselves been shown to have biological activity. For example, in melanoma studies, HPSE-cleaved HS from melanoma cells promoted cell migration and angiogenesis in rodent studies (165). *In vitro* studies also show HS fragments generated by HPSE stimulate cytokine production in peripheral blood mononuclear cells (166). Similarly, shed HS fragments from patients who underwent aortic bypass surgery also had the ability to directly activate leukocytes and platelets (167), in turn releasing more HPSE.

The investigation into HPSE in disease for the most part has been in its involvement with cancer metastasis (168). But HPSE is also upregulated in many inflammatory and proteinuric diseases like IgA nephropathy, minimal change disease, dense deposit disease, membranous glomerulopathy, and DN (169). In T2D patients, increased HPSE staining in kidney biopsies was correlated with overt DN (109). Interestingly, HPSE may also be required for the development of DN, as was shown in a recent article in which T1D HPSE knockout mice failed to develop DN, compared to T1D wild type (WT) controls (114). The same authors also demonstrated reduced albuminuria in WT T1D and T2D mice when treated with the HPSE inhibitor SST0001, but did not investigate the effect on eGlx (114).

In DR, upregulated HPSE in the vitreous of PDR patients has been observed (125). In agreement with this, high glucose was found to stimulate HPSE expression in human retinal endothelial cells, *in vitro* (126). As added evidence for a role of HPSE in DR, retina flat mounts from T1D rats had increased HPSE expression and was reduced by treatment with the HPSE inhibitor phosphomannopentaose sulphate (126). However, functional studies to determine if inhibiting HPSE reduced vascular leak, or if eGlx was impacted, were not carried out and therefore requires further investigation. Despite this, there appears to be accumulating evidence for a role of HPSE in DN and DR, and it is possible that this is mediated by shedding of HS and consequently eGlx damage.

1.6 *Hypothesis and Aims*

1.6.1 Endothelial Glycocalyx Heparan Sulphate as a Therapeutic Target in Diabetic Nephropathy and Retinopathy

Although the presence and dominating abundance of HS in the eGlx is well established, most of the work on HS has been focused on its role in the extra cellular matrix and basement membrane, but the functional and structural role it plays in the eGlx has not been looked at in detail, particularly *in vivo*. *In vivo* studies in mice glomeruli in which mice were treated with heparinase III, an HS shedding enzyme derived from *Flavobacterium*, suggested a perm-selectively role for HS in the eGlx, but the method of EM fixation did not allow for direct visualisation of eGlx (170). Heparinase III treatment of bovine aortic endothelial cells *in vitro* show that HS acts as a mechanotrasducer for fluid sheer stress, crucial to vascular endothelial cell function, but the direct effect on permeability and eGlx structure was not studied (171). Therefore, more work is required to establish the functional and structural role HS has in the eGlx.

Damage to the eGlx in disease, and most relevant to this thesis, in diabetes, has also been well established in both humans and *in vivo* laboratory experiments, albeit not in all vessel beds. However, the role of HS specifically in the eGlx and in disease has not been studied in depth. Staining on human kidney biopsies in DN patients have shown a reduction in glomerular HS staining (109), although the antibody used primarily detected GBM HS. However, loss of HS in the same glomerulus also coincided with an increase in HPSE expression (109). Given the upregulation of HPSE in both DN and DR, it may serve as a target to prevent eGlx damage and slow progression or development of DN and DR.

1.6.2 Hypothesis

The previously published studies have led me to the following hypothesis:

Heparan sulphate has a structural and functional role in the endothelial glycocalyx and is damaged in diabetes. Prevention of heparan sulphate shedding in diabetic mice will ameliorate endothelial glycocalyx damage and restore barrier function in glomerular and retinal vasculature.

1.6.3 Aims

To test my hypothesis, I have conducted experiments with the following aims in mind.

Aim 1: Demonstrate the Importance of Endothelial Glycocalyx Heparan Sulphate in Kidney and Retinal Vasculature

I will perform *in vivo* and *ex vivo* studies to test if reduced HS, by enzymatic removal or use of a transgenic mouse model, results in structural damage to the eGlx and loss of function in the glomerulus and retinal vasculature. Damage to the eGlx structure will be assessed by imaging techniques such as electron microscopy and immunofluorescence staining. Functional studies in the glomerulus will use the *ex vivo* technique developed by *Desideri et al.,* to determine changes in apparent glomerular albumin permeability (36). In the eye, sodium fluorescein angiographies will be performed and used to develop an 'apparent solute flux' assay.

Aim 2: Determine if the Endothelial Glycocalyx is Damaged in a Type 2 Diabetic Mouse Model in the Glomerulus and Retinal Vasculature

In vivo studies will be performed in a T2D mouse model using *db/db* mice. Damage to eGlx in the glomerulus and the retina will be determined using the same techniques described in Aim 1. Similarly, the same functional studies described in Aim 1 will be performed to address changes in eGlx function in the glomerulus and retina during diabetes.

Aim 3: Demonstrate That Prevention of HS Shedding by Inhibiting HPSE in a Type 2 Diabetic Mouse Model Will Restore eGlx Structure and Function

In order to prevent HS shedding and damage to the eGlx, *db/db* mice will be treated with either vehicle or a novel HPSE inhibitor OVZ/HS-1638 and restorative effects of treatment determined using the same structural and functional assays described in Aim 1 and Aim 2. Non-diabetic controls treated with vehicle will act as healthy controls.

1.6.4 Potential Outcomes

This investigation of the role of HS in the eGlx takes place in two spatially (kidney vs eye) and functionally (fenestrated vs continuous) different vascular beds. This allows a more global investigation into determining if therapeutically targeting HS eGlx in diabetes has beneficial effects on microvascular permeability. If successful in both vascular beds, the use of this novel inhibitor has the potential to be used for treatment of all early microvascular complications that occur in the progression of diabetes.

Chapter 2 Methods and Materials

These methods are not inclusive. Methods pertaining specifically to experiments in specific chapters can be found in the methods section of that chapter.

2.1 *In Vivo Work*

2.1.1 Animal Licence

I obtained a personal license (PIL No.: I167CEA42) for all work involving live animals. All animal work was performed in compliance with The University of Bristol's guidelines and the Animal (Scientific Procedure) Act 1986 on Dr. Rebecca Foster's project license (PPL No.: 30/3048 and P855B71B4), approved by UK Home Office.

2.1.2 Animals

FVB and C57BL/6 mice were ordered from Charles Rivers (Charles Rivers Laboratories, Wilmington, MA). Ext1 mouse colony is maintained in Barn 1 at the University of Bristol Animal Service Unit (Bristol, England). Five-week-old and 7-week-old BKS.Cg-+*Lepr*^{db}/+*Lepr*^{db}/OlaHsd (*db/db*) and lean littermate controls (lean) were ordered from Envigo (Envigo, Cambridgeshire, England, UK).

2.1.3 Anaesthesia

Isoflurane was used as anaesthetic for all the following procedures at 2.5%, 1.5 litre/min unless otherwise specified: retro orbital injections, tail vein injections, cardiac perfusions, and OCT/fluorescein angiographies.

2.1.4 Measurement of Mouse Weights

Electric scales were used to measure mouse weights when appropriate, or daily in diabetic studies. Scales were zeroed with weight bucket and individual mice placed in bucket and weight recorded.

2.1.5 Urine Collection for Albumin Creatinine Ratios

Unless otherwise specified, all mouse urines were collected in metabolic cages allowing separation of solid and liquid waste. Mice were provided with drinking water and enrichment. Mice were left in metabolic cages for a maximum of 6 hours.

2.1.6 Measurement of Blood Glucose in Mice

Blood was obtained weekly in diabetic studies from end of tail prick with 18G needle for blood glucose level measurements. Glucose measurements were taken using Accu-Check

standard glucometer (range 0-40mmol/L) with Accu-Check AVIVA test strips (Roche Diagnostics Limited, West Sussex, England).

2.1.7 Treatment of Mice with Heparinase III for HS Shedding

6 week old FVB (EM and glomerular permeability studies) or C57BL/6 (fluorescein angiographies) mice were given 0.1ml retro orbital injections of heparinase III from *Flaviobacterium* (H8891, Sigma-Aldrich, St. Louis, MO) reconstituted in Phosphate Buffered Saline (PBS) (137mM NaCl, 27mM KCl, 10mM Na_2HPO_4, 1.8mM KH_2PO_4) at 8.2u/kg or PBS only for vehicle. Dose required for shedding of eGlx was previously optimised following the same procedure using vehicle, 8.2, or 82u/kg of enzyme **(FIGURE 2-1).** Mice were kept under light anaesthetic for 30 min on a heating pad. To prevent drying of the eyes, drops of eye lubricant gel were put on both eyes. After 30 min, mice were prepared for cardiac perfusions or sodium fluorescein angiographies described in **2.1.10** and **2.1.11** below.

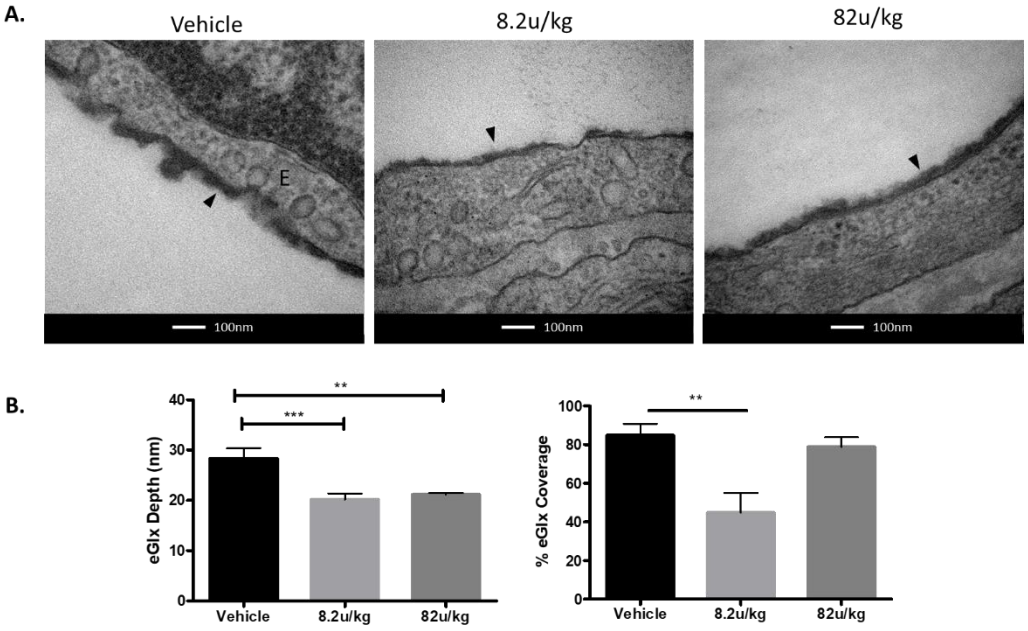

Figure 2-1 Heparinase III Pilot Experiment

A. Representative retina microvessel EM images of vehicle or enzyme treated mice perfused with Alcian blue/ glutaraldehyde. EGlx (arrowhead) is visibly thinner and patchy in 8.2u/kg treated mouse B. Quantification of eGlx depth (left) and eGlx coverage (right). Note, does not represent a real statistical difference. N=1 mouse per group, three capillaries analysed per mouse. Statistics performed on capillaries analysed for pilot experiment. One-way ANOVA, **p<0.01 ***p<0.001.

2.1.8 Administration of HPSE Inhibitor in Diabetic Studies

HPSE inhibitor OVZ/HS-1638 (Olga Zubkova, Ferrier Research Institute, Victoria University of Wellington) was reconstituted in PBS and stored at -20°C until time of use. Inhibitor was administered once daily through subcutaneous (s.c.) or intraperitoneal injection (i.p.) at 20mg/kg for 14 days starting at 7 weeks or 9 weeks of age, respectively. Vehicle mice were administered only PBS.

2.1.9 Alcian Blue Cardiac Perfusions for Electron Microscopy of Kidney and Eye Tissue

Mice were anaesthetised until no pain response was evident using tail and foot pad pinch method. Mice were cardiac perfused at 100mmHg with 30ml of Ringer's solution pH 7.4 (132mM NaCl, 4.6mM KCl, 1.27mM $MgSO_4(7H_2O)$, 2mM $CaCl_2(2H_2O)$ with 5.5mM D-glucose, 3.07mM HEPES acid, 1.9mM HEPES base), followed by 30mL of Alcian blue in fixative solution composed of 0.15M sodium cacodylate pH 7.4 (NaCa Buffer), 2.5% glutaraldehyde, and 0.01g/mL of Alcian Blue 8GX (75881-23-1, Santa Cruz Biotechnology, Dallas, TX) in water. Fixed kidney was removed, cut into small pieces and put into fixative solution until processing. Mouse eyes were enucleated and put into fix solution until processing **(SECTION 2.2).**

2.1.10 Cardiac Perfusion for Ex Vivo Glomerular Permeability Assay

Mice were anaesthetised until no pain response was evident as above and cardiac perfused with Ringer's solution as above to remove red blood cells. Renal artery was clamped with metal clip and kidney removed and placed into ice cold Ringer's solution with 4% bovine serum albumin (BSA) until permeability assay. Details provided in **SECTION 2.2.**

2.1.11 Optical Coherence Tomography (OCT) and Sodium Fluorescein Angiographies (FA)

A Micron IV imaging system (Phoenix Research Labs, Pleasanton, CA) was used for OCT and FA retinal imaging. Initial training was given by Dr. David Copland (Bristol Ophthalmology, The University of Bristol). Thirty minutes prior to imaging, mouse pupils were dilated with Tropicamide 1%w/v (Bausch and Lomb, Rochester, NY). Mice were anesthetized with isoflurane unless otherwise stated. Mouse nose cone which allows access to the eyes was used (SOMNO-0801, Kent Scientific Corporation, Torrington, CT). To prevent drying of the eye, drops of eye lubricant gel were put on both eyes for duration of imaging and recovery. Schematic of setup shown in **FIGURE 2-2.** Mice were positioned on the imaging stage for OCT imaging and images were taken averaging 30 frames per second. The following camera settings were used for FAs: Gain-10, User defined-2, exciter filter wheel- 2, barrier wheel-2. Camera settings were kept the same for duration of FA imaging for all mice, intensity and focus knobs changed as needed prior to start of video. Mice were given 50µl of 10% Sodium Fluorescein (NaF), sterile filtered with 0.22µm pore filter and diluted in water, by i.p. injection or intramuscular injection (i.m.) as specified. Recording began after NaF injection. All settings remained unchanged for all recordings. Analysis of images is described in **SECTION 2.2**. Once completed, mice were allowed to recover on a cage placed on top of a heating pad before being placed in original cage.

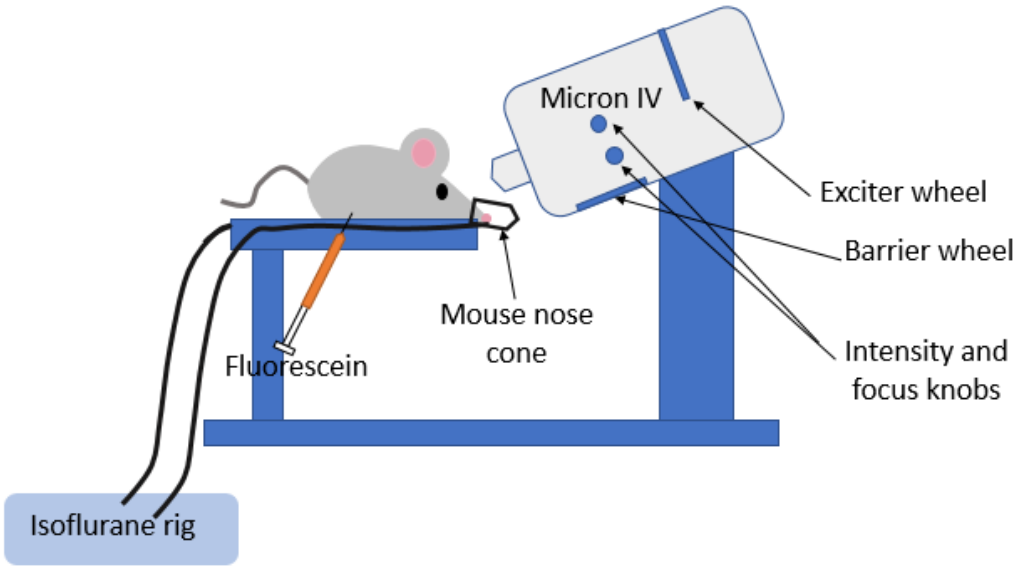

Figure 2-2 Schematic of Set Up for OCT and FA Imaging

Mouse is put onto stage where mouse nose cone lays and is connected to isoflurane rig. Mouse eye is focused with camera and OCT image is taken. Once ready, recording begins and sodium fluorescein injection is given while mouse remains in situ and under anaesthetic.

2.2 *Ex Vivo and In Vitro Work, and Analysis*

2.2.1 Immunofluorescence with anti-HS Phage Display Antibodies in Paraffin Embedded Kidney

Kidney harvested from respective mice were fixed in 4% paraformaldehyde (PFA) for minimum of 24 hours and were paraffin embedded and sectioned at 5μm at The University of Bristol Histology Lab. For immunofluorescence, slides were deparaffinized two times in Xylenes for 10 min. Slides were rehydrated by sequential 5min incubations in decreasing ethanol concentrations: 100% twice, 95%, 70%, and 50%. Slides were incubated in deionized water for 5min followed by a 15min incubation in PBS. Slides were blocked for 30min in block solution (3%BSA/0.3% Triton-X in PBS). Anti-HS phage display antibodies (gift from Jerry Turnbull, The University of Liverpool) were diluted 1:5 and incubated at 4°C overnight. The following antibodies were screened for eGlx staining (HS3A8V, HS4C3V, LKIV69V, EV3C3V, MPB49V) (172). These antibodies were previously shown to identify distinct HS epitopes in embryonic rat lung, but due to the nature of HS binding flexibility, distinct binding epitopes have not been determined (173) . Slides were washed three times for 5min in PBS. Secondary anti-VSVG (A190-131A, Bethyl Laboratories, Inc., Montgomery, TX) was added for one hour at room temperature 1:50. Slides were washed three times for 5min in PBS. Tertiary anti-rabbit 488 (A-11001, ThermoFisher Scientific, Waltham, MA) was added for 1 hour at 1:500. Slides were washed three times for 5min in PBS. Tissue was counterstained in 300nM 4',6-Diamidino-2-Phenylindole, Dihydrochloride (DAPI) (D1306, ThermoFisher Scientific) for 5min followed by 15min membrane stain with Octadecyl Rhodamine B Chloride (R18) (O246, ThermoFisher Scientific) diluted 1:1000 in PBS. Slides were washed in PBS for 5min and coverslip mounted with Pro long gold (P10144, ThermoFisher Scientific).

2.2.1.1 Confocal Imaging

Multi-Laser CLSM Leica SP5 provided by University of Bristol Wolfson Bioimaging Facility was used for confocal imaging unless otherwise specified. Slides were imaged using 100X oil immersion lens for eGlx analysis.

2.2.1.2 Analysis of Total Glomerular HS Staining in Mouse Kidney

Images were analysed on FIJI image analysis software (174). To measure total glomerular HS, the freehand selection tool was used to draw around glomeruli perimeters. The "analyse" tool was used to obtain area, mean grey values, and integrated density values for each image. Four background values were obtained similarly, and the background

mean grey value mean was calculated for each image by average the background mean grey values. To calculate Corrected Total Cell Fluorescence (CTCF) the following equation was used:

$$CTCF = IntDen - (area\ of\ region\ of\ interest\ x\ mean\ fluorscece\ of\ background\ means)$$

Equation 2-1

A minimum of three glomeruli per mouse were measured, and CTCF values for each group were averaged. Statistics performed on mouse number.

2.2.2 Urine Albumin Creatinine Ratios (uACR)

Urine ACR for each mouse was calculated by determining the amount of albumin (mg/L) and creatinine (mmol/L) in the urine. Ratio was calculated by dividing albumin concentration by creatinine concentration to obtain uACR (mg/mmol). Urine was centrifuged at 13,000rpm for 30 seconds to remove debris prior to analysis.

2.2.2.1 Mouse Urine Albumin Enzyme-Linked Immunosorbent Assay (ELISA)

Albumin levels in mouse urine were obtained using the Mouse Albumin ELISA Quantitation Set (E90-134, Bethyl Laboratories, Inc.) following manufactures instructions. If needed, urine samples were diluted in sample/conjugate diluent solution to obtain an optical density reading within the linear range of the assay **FIGURE 2-3** and actual concentration was back calculated from dilution factor.

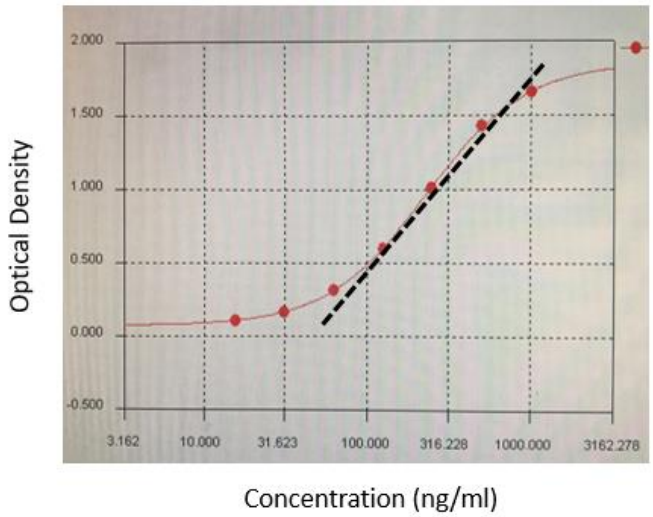

Figure 2-3 Example of Standard Curve for Albumin ELISA

Example of standard curve for ELISA albumin assays. Dotted line shows the linear range for the curve.

2.2.2.2 Urine Creatinine

Mouse urines were sent to Langford Vets Diagnostic Laboratories (The University of Bristol) for creatinine measurements using an Enzymatic Creatinine Assay (ThermoFisher Scientific).

2.2.3 Isolation of Retinas from Enucleated Mouse Eyes

Mouse retinas for retinal flat mounts and EM were isolated from enucleated eyes. Under a dissection microscope, an incision was made along the eye to separate anterior and posterior cups of eye **(FIGURE 2-4 A)**. Once separated, lens and anterior cup were discarded **(FIGURE 2-4 B,C).**

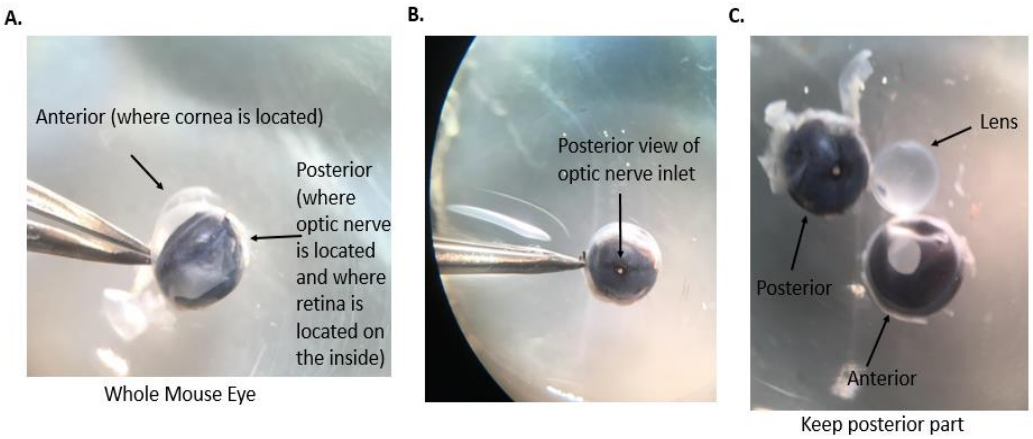

Figure 2-4 Dissection of Mouse Eye for Retinal Isolation

A. Image of enucleated eye from mouse under dissection microscope. Orientation of eye labelled. B. View of back of eye, arrow points to optic nerve entrance. C. Image of eye cut in half into posterior and anterior parts with lens removed. Posterior part is kept for retina isolation.

To remove the retina from eye cup, cup was turned over to allow visualisation of retina. Small tweezers were used to carefully separate retinal pigment epithelium and choroid layer **(FIGURE 2-5 A,B)**. This was continued until retina could be easily separated **(FIGURE 2-5 C)**. In unperfused vessels or Alcian blue perfused eyes, some faint vessels may be visible as shown in **FIGURE 2-5 D**.

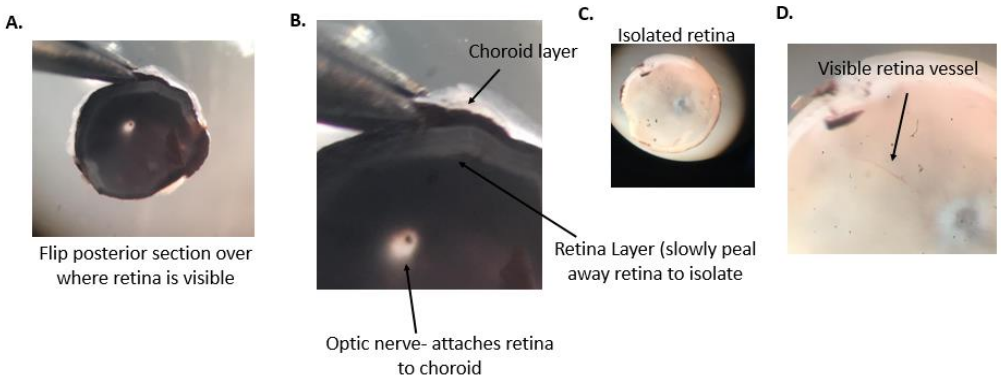

Figure 2-5 Isolation of Retina from Eye Cup

A. Image of inside of posterior part of eye. B. Enlarged image shows retina layer separating from choroid layer, as well as area where optic nerve attaches to retina. C. Image of isolated retina once choroid has been pealed from retina. D. A large vessel filled with red blood cells can be seen in isolated mouse retina.

2.2.4 Electron Microscopy Processing and Sectioning for Alcian Blue Tissue

All processing and sectioning of EM samples were completed by me. Training and processing were completed at the Wolfson Bioimaging Facility at The University of Bristol. EM samples were removed from fixative buffer and washed in 0.1M sodium cacodylate (NaCa) buffer three times for 5min. Samples were switched to 1% OsO_4 in 0.1M NaCa Buffer for 1 hour and washed in NaCa buffer again three times for 5min followed by a de-ionized water wash. Samples were incubated in 3% aqueous uranyl acetate (UA) in the dark for 30mins and washed with de-ionized water. Samples were dehydrated through a series of increasing concentration of ethanol washes (70%,80%,90%,96%,100%) followed by propylene oxide washes for 10min, three times. Samples were then incubated overnight in a 1:1 mixture of Epon and propylene oxide overnight. Samples were switched over to fresh 100% Epon and incubated overnight on a rocker. Samples were embedded in fresh Epon in silicon moulds and allowed to cure for 72 hours at 60°C. Blocks were trimmed and sectioned using the ultramicrotome Leica EM UC7 (Leica Microsystems, Milton Keynes, England, UK) first at 1000nm using homemade glass knives to confirm area of interest and then at 70nm with DiATOME diamond knife (Electron Microscopy Sciences, Hatfield, PA). Sections were mounted on copper grids and stained in UA for 10 min followed by two 5min washes in de-ionized water. Grids were stained once more with a lead stain made by mixing of 1mL Sodium citrate, 1mL lead nitrate, and 0.38mL of NaOH. Grids were incubated in stain for 10min followed by two 5min washes in de-ionized water. Grids allowed to dry before imaging.

2.2.5 Imaging and Quantitative Electron Microscopy Analysis

2.2.5.1 Electron Microscopy Imaging

EM images were taken on FEI Tecnai 12 120Kv BioTwin Spirit transmission electron microscope (ThermoFisher Scientific, Hillsboro, OR) provided by the Wolfson Bioimaging Facility. High power images (49,000x magnification) used for EM analysis.

2.2.5.2 Glomerular Filtration Barrier Measurements

A minimum of three capillaries per glomerulus were measured for each animal. Analysis was done using FIJI image processing program using the measurement tool. Examples of how measurements were taken are shown in **(FIGURE 2-6)**. GBM thickness was measured by averaging a minimum of ten measurements per image. Number of endothelial fenestrations were determined by counting the number of fenestrations per image and normalizing to total length of GBM measured. Slit diaphragm (SD) width and podocyte foot process (PFP) width was measured from relevant lipid bilayer to lipid bilayer.

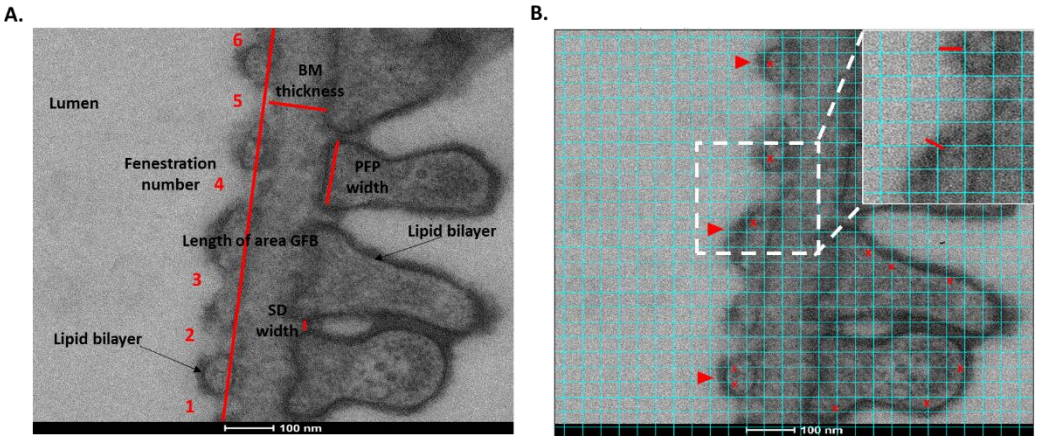

Figure 2-6 Analysis of Glomerular Filtration Barrier Ultrastructure and eGlx

A. Red lines indicate how measurements for each parameter are taken. Measurements are made from lipid bilayer to lipid bilayer of next point. Number of fenestrations are counted and divided by length of basement membrane (BM) measured. B. A grid is placed over the image to be analysed and Glx (arrow heads) measurements for endothelial cells and podocytes are made where intersecting grid marks lay on lipid bilayer (red crosses). Glx measurements are made from lipid bilayer to end of Glx layer (inset, red lines)

Glycocalyx depth and coverage was analysed only where the phospholipid bilayer was easily distinguishable, to allow for accurate measurements. To eliminate bias measurements, two steps were taken. First, all images were blinded for analysis. Second, images were covered in a grid and where intersecting grid lines also intersected lipid bilayers, glycocalyx measurements were taken **(FIGURE 2-6, B)**. Glycocalyx depth was

calculated by averaging all depth values for that capillary. Percent coverage was calculated as follows:

$$\%\ Glycocalyx\ Coverage = 1 - \left(\frac{total\ measrumentes\ less\ than\ 10nm}{total\ measurments}\right) x\ 100\%$$

2.2.5.3 Retina Microvessels Measurements

A minimum of three microvessels were measured per animal, and a minimum of five images were analysed per microvessels. Retinal basement membrane thickness was measured by averaging a minimum of ten measurements per image **FIGURE 2-7**. Glycocalyx measurements were taken as described above for glomerular filtration barrier, areas of measurement indicated in **FIGURE 2-7 B.**

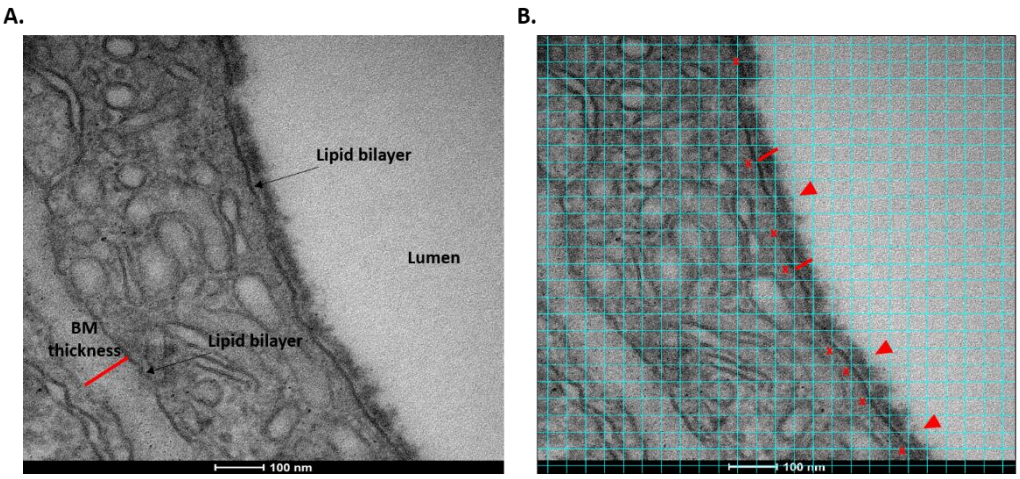

Figure 2-7 Analysis of Retina EM Images

A. Red lines indicate how measurements for basement membrane (BM) thickness are measured. Measurements are made from lipid bilayer to lipid bilayer of next point. B. A grid is placed over the image to be analysed and eGlx (red arrow heads) measurements are made where intersecting grid marks fall on lipid bilayer (red crosses). Glx is measured from endothelial lipid bilayer to end of Glx layer (red lines).

2.2.6 Glomerular Albumin Permeability Assay and Analysis

To determine changes in permeability, our lab recently developed an assay allowing us to measure fluorescently labelled albumin permeability across a single glomerular capillary wall. This assay is more sensitive and allows for direct measurement of glomerular albumin permeability in the absence of other physiological processes that contribute to variations in measurements of albuminuria. To do this, glomeruli were perfused with Ringer's solution as described above, to clear capillaries of red blood cells and other debris that could interfere with permeability measurement. Glomeruli were isolated from kidneys in 4%BSA ringer by using a series of sieves with decreasing pore size (425,180,125,100,71μm) and a 5mL plunger to push glomeruli through. Glomeruli were isolated from 75μm sieve. Glomeruli were resuspended in 1mL of 4% BSA ringer containing 36.5μg/mL R18 (O246, ThermoFisher Scientific, Waltham, MA) and incubated in the dark for 15 min on ice to label cell membranes. Glomeruli were poured onto a 40μm pore sieve and washed with 4%BSA ringer and isolated in 1mL of 4%BSA ringer containing 30μg/mL of AlexaFluor 488 BSA (BSA-488) (A13100, ThermoFisher Scientific) and allowed to incubate in the dark for 15 min on ice to allow fluorescently labelled BSA to diffuse into capillaries. Using a pulled glass capillary tube made with a magnetic pipette puller, a single glomerulus (free of Bowman's capsule) was trapped on a glass plate **(FIGURE 2-8),** fitted with plastic capillaries attached to a peristaltic pump, to allow washing of BSA-488 bath in which glomeruli were in. Nikon TI inverted confocal microscope (Nikon Instruments Inc (Nikon), Melville, NY) was focused so that the maximum number of capillaries for each glomerulus met the following criteria: capillary was on outer edge of glomerulus, had clear R18 membrane staining (under TRITC filter), interior was free of red blood cells or any other particles (bright field), BSA-488 intensity was equal both inside capillary and outside capillary in the BSA-488 bath (under FITC filter) **(FIGURE 2-8 A)**. Once correct focus was chosen, recording commenced for 3 min. During recording, pump was turned on and bath was washed with 4%BSA ringer until bath was black and free of BSA-488 **(FIGURE 2-8)**, typically around 30s.

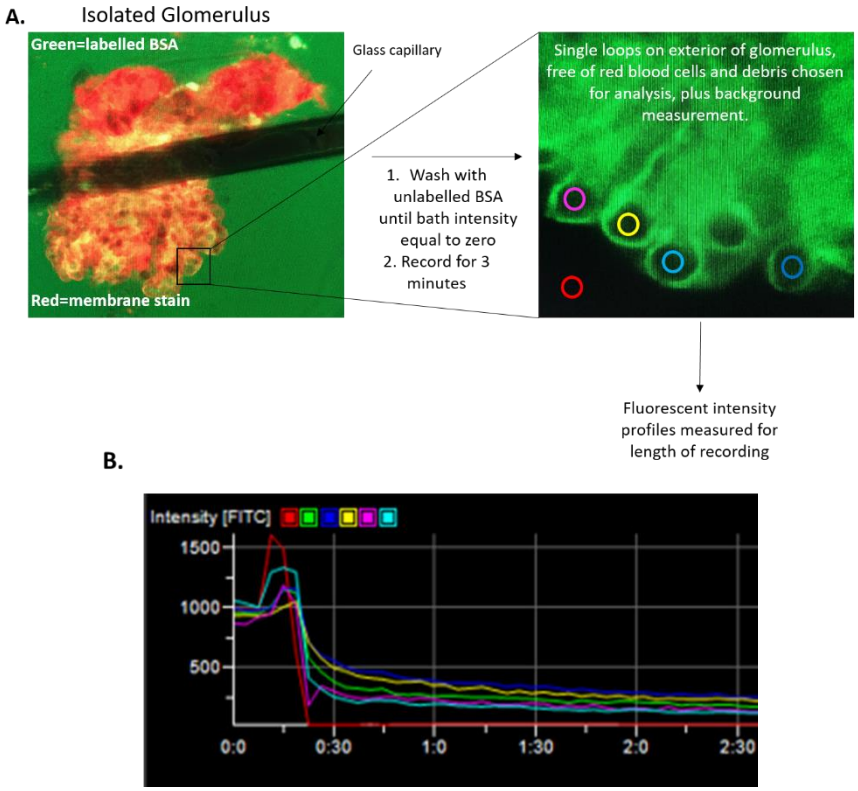

Figure 2-8 Albumin Glomerular Permeability Assay

A. An individual glomerulus labelled with R18 to define capillary loops and perfused with BSA-488 (labelled albumin) is isolated containing loops free of debris and red blood cells (left image). The bath is then washed with non-labelled BSA until bath is black (upper right image). B Immediately after, a 3-minute recording is done to obtain intensity profiles for each loop over time.

Using NIS Elements software (Nikon), loops which met criteria previously mentioned were selected as regions of interest, and fluorescent intensity profiles were measured over time **(FIGURE 2-8 A (RIGHT IMAGE) AND B)**. One minute after the wash was determined in previous studies as the most accurate window for analysis (36).

Because this is an *ex vivo* measurement which is also static (no fluid flow in the capillaries) Starlings principles cannot be accurately applied. As a result, using Fick's first law of diffusion, the following formula, whose derivation is explained further ny *Desideri et al.*, was derived to calculate apparent albumin permeability (Ps'alb):

$$Ps'alb = -kR/2$$

In this equation, k, the filtration coefficient, which is the negative slope of the relationship obtained from calculating the natural log of fluorescent intensity and time, where raw

values are obtained from fluorescent intensity profiles **(FIGURE 2-8)** (36). R is the radius of the capillary being analysed which is measured on the NIS Elements software. Using this formula allows for calculation of Ps'alb for a single capillary. A minimum of three capillaries were measured per glomerulus and values averaged per glomerulus. A minimum of three glomeruli were analysed per animal. Statistics performed on mouse number.

2.2.7 Sodium Fluorescein Angiography Analysis (Optimisation and Application)

The method of using FAs to measure apparent solute flux in the retina, was obtained from Professor David Bates at The University of Nottingham with his permission (unpublished method) as well as collaboration with Dr. Kenton Arkill at The University of Nottingham, and its application has been further optimised by myself. Analysis was first optimised using FIJI imaging processing program, and later used for the development of an automated program in collaboration with a Computer Science masters student Kwan Ho Ho, under the supervision of Dr. Neill Campbell (Faculty of Engineering, The University of Bristol), which will be discussed in **2.2.7.2**

2.2.7.1 Optimisation of Manual Analysis

Once the NaF is injected, recording began and the vessels begin to fill over time as shown in **FIGURE 2-9**.

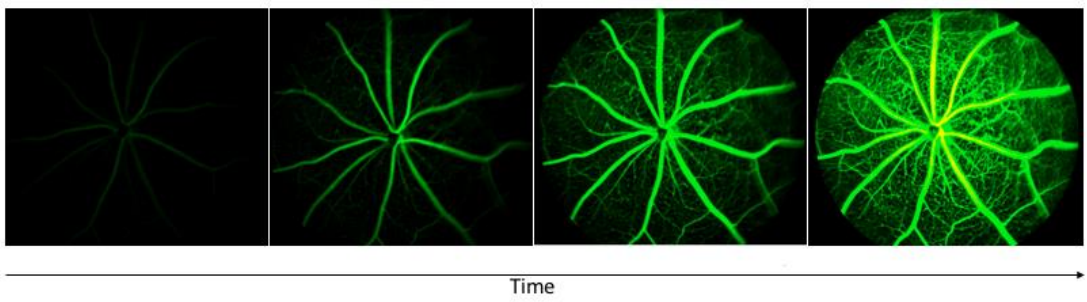

Figure 2-9 Example of Fluorescein Angiography in Mouse Retina
Shortly after injection of the mouse with sodium fluorescein, fluorescent signal appears in the main vessels. Over time, exchange vessels become visible and fluorescent intensity builds. Yellow signal in the main vessels in the far right image indicates camera saturation.

In FIJI, fluorescent intensity is measured in the main vessel (box 1) as well as in the exchange vessels (box 2) every 10 frames **(FIGURE 2-10 A,B)**, ensuring that if eye movement occurs, measurements are still within the same box, and therefore may require manual movement of boxes. A modified version of Fick's Law derived by Professor David Bates is used to calculate solute flux:

$$P = \Delta I_f / \Delta t \, / (\Delta C \; x \; A)$$

Equation 2-2

where permeability is equal to solute flux ($\Delta I_f/\Delta t$), which is the change in fluorescence intensity (ΔI_f) over the change in time (Δt), divided by the product of the change in concentration (ΔC) of solute and the area measured (A). The use of this equation in solute flux measurements makes the following assumptions:

1. Area of exchange vessels (in box 2) does not change from week to week (if multiple solute flux measurements are being taken on the same animal).
2. Solute flux is diffusive, not convective.
3. Plasma concentration does not decrease during measurements.
4. The interstitial concentration is a small fraction of plasma concentration, and therefore the slope is linear.
5. Only exchange vessels are in box 2.

To account for any potential variations in total fluorescent intensity that may be due to varied acquisition settings, the fluorescent intensity ratio between box 2:box 1 is taken for each measurement at that given time point, and then plotted against time **(FIGURE 2-10 C)**. This yields a line where the equation from a linear fit of the line, represents the relationship between ΔI_f and Δt, where the slope of the line ($\Delta I_f/\Delta t$) is solute flux, as described in **EQUATION 2-2** above. Therefore the solute flux measurement in **FIGURE 2-10 C** is 0.0014 µm/second(s) or 14 x 10^4 cm/s. It should be pointed out that measurments of solute flux using this assay is still a work in progress, and therefore we are using change in fluoescent intesnsity over time so represent solute flux (cm/s). This method of calculating solute flux and permeability will require futuer optimisation with collaboratores.

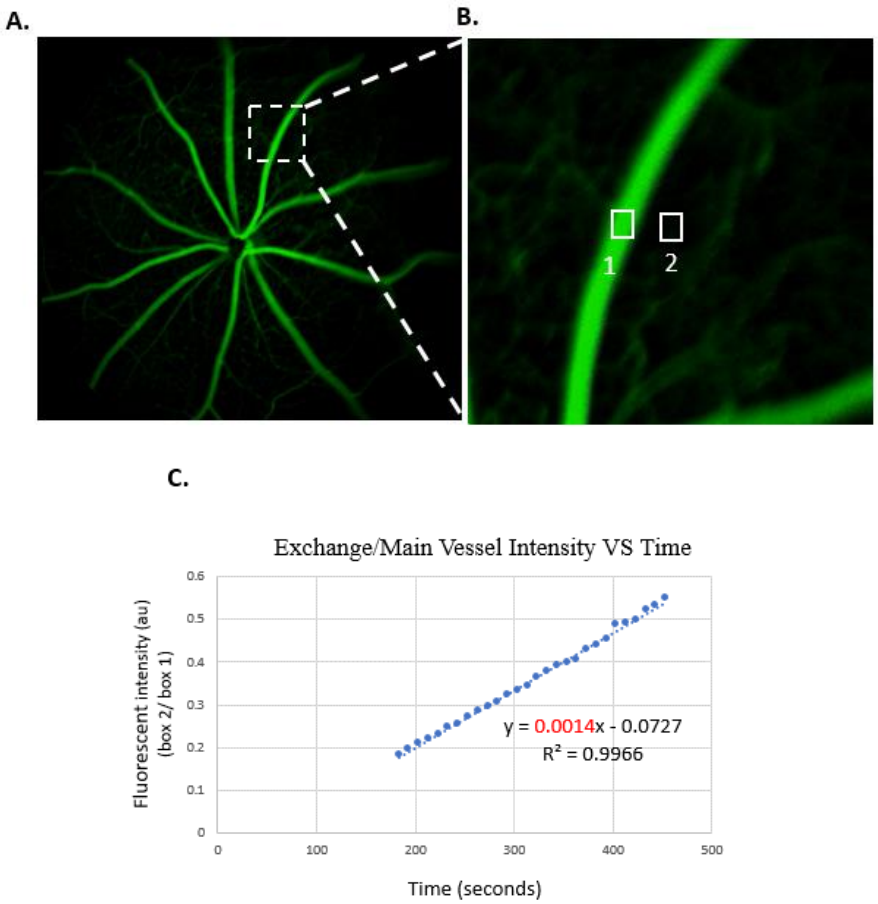

Figure 2-10 Measurement of Fluorescent Intensity from Angiography Videos

Fluorescent intensity measurements are taken over time for the length of the video. A. Snapshot of fluorescein angiography at time x. B. Enlarged image from white box in A shows area of measurements, box 1 in the main vessels and box 2 in the exchange vessels. Boxes of equal size are placed in main vessel and exchange vessels, and fluorescent intensity is measured approximately every 10 frames. C. Graph of ratio box2/box1 of exchange vessel intensity and main vessel intensity is plotted over time from determined time frame. Y axis in arbitrary unites (a.u.). A line of best fit is applied, and linear equation calculated. Slope of line (red) is representative of solute flux.

An issue that can arise when comparing one animal to another, is the variability in fluorescent profiles in the main vessel which, as mentioned, is used as a way to account for potential variations in fluorescent intensity due to difference in acquisition settings, fluorescein batch variations, etc. For example, **FIGURE 2-11** shows the fluorescent intensity profiles for the main vessel and exchange vessels for two different animals, injected either through i.m. or i.p. Both mice were healthy C57BL/6 mice litter mates with

the same age, sex, and similar weights of 26.5g and 26.2g. The main vessel profile for animal 2 shows a delayed vessel filling compared to animal 1. Therefore, use of data points at the same time frame (those between the dotted red lines) to calculate solute flux ($\Delta I_f/\Delta t$) would not be accurate in animal 2, as the main vessel is still filling and that time frame is not comparable to animal 1.

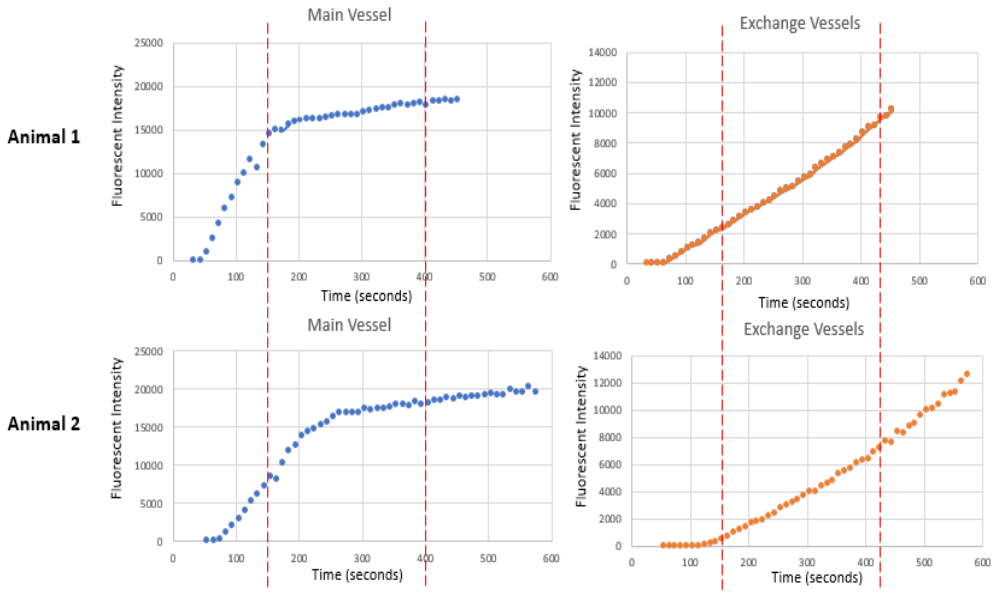

Figure 2-11 Fluorescent Intensity Profiles for Two Different Animals

Main vessel and exchange vessel intensity profiles shown for each animal. Animal 1 was injected with sodium fluorescein through i.m. whereas animal 2 was injected through i.p. Note that animal 2 has a delayed filling in the main vessel and begins to reach a steady state at a later time point. Red dotted lines indicate example of data points used if the same time frames are used for analysis for both animals.

Betteridge et al. demonstrated the fluorescent intensity profile for a single vessel located in the rat mesentery perfused with Alexa Fluor 488-labelled BSA (175). As shown in **FIGURE 2-12**, there is an initial filling of the vessel represented by ΔI_{f0}, followed by a steady linear increase in fluorescent intensity (I_f) represented by the solid horizontal line, and an eventual drop in fluorescence as the Alexa Fluor 488-labelled BSA is cleared (175). *Betteridge et al.* used this rate of fluorescent intensity change $[dI_f/dt]_0$ to represent the rate of solute flux across the vessel wall.

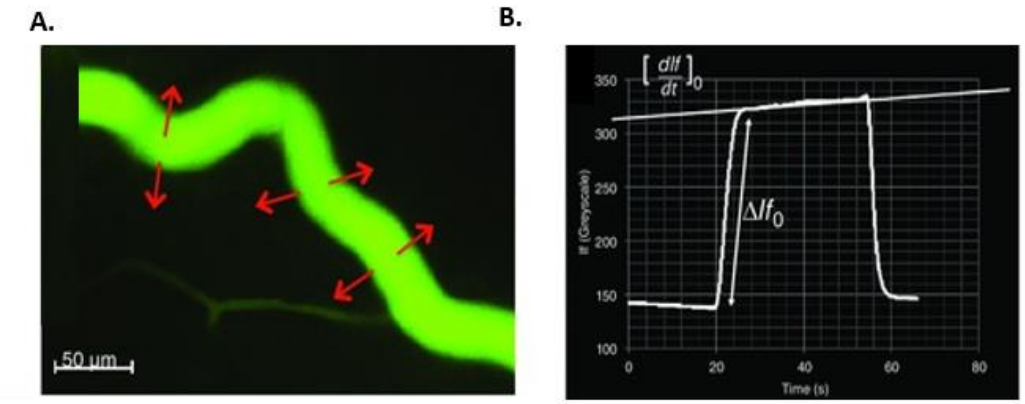

Figure 2-12 Determining Solute Flux in Rat Mesentery

A. A rat mesenteric vessel perfused with Alexa Fluor 488-labelled BSA is used to measure changes in permeability as the labelled BSA crosses the vessel (red arrows). B. The fluorescent intensity profile measured upon perfusion with labelled BSA shows a rapid increase in fluorescence followed by a steady state (horizontal line). The slope of the steady state line represents solute flux. Image adapted from (Betteridge et al, 2017)(175).

Therefore, in order to circumvent differences in rates of vessel filling between animals that may confound results, I used the steady state linear increase portion of the fluorescent intensity profile in the main vessel as the time frame to calculate solute flux for any given animal. To determine the exact point at which the main vessel reaches a linear steady state in an objective manner, I chose to fit a linear line to the main vessel profile and calculate where the R^2 value was the highest. This is demonstrated in calculation **A** vs **B** in **FIGURE 2-13** where the cut off in **B** (184 seconds) yields the highest R^2. This point would therefore be used as the cut off for where the main vessel has reached a steady state.

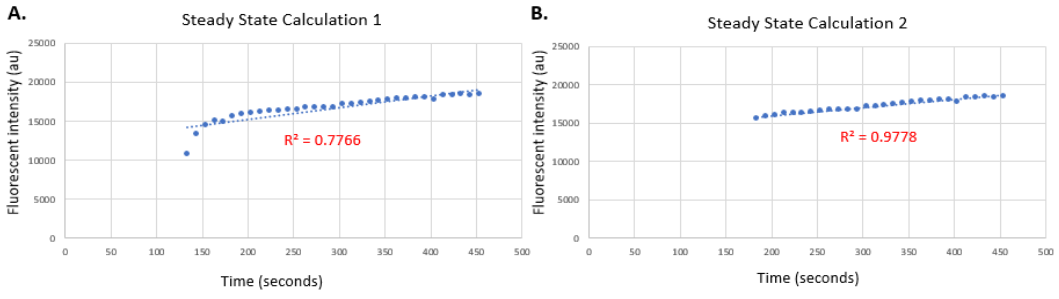

Figure 2-13 Determining Point at Which Steady State Begins for Solute Flux Measurement

Time frame used for analysis is determined based on where the main vessel intensity approaches a steady state, i.e. the most linear part of the curve determined by highest R^2 value. A. Example of R^2 value for line which still has non-linear points included. B. Removal of non-linear points yields highest R^2 value.

If we apply this method to both animal 1 and animal 2 in **FIGURE 2-13** to determine when the steady state is reached in the main vessels, and then plot the ratio of the exchange vessel and the main vessel over time to calculate solute flux as in **FIGURE 2-10 C** for both animals, we obtain the graphs in **FIGURE 2-14**. Note that slopes of the line, i.e. solute flux are both 0.0014. This is a good indication that this method of analysis is consistent as these mice would be expected to have similar solute flux measurements.

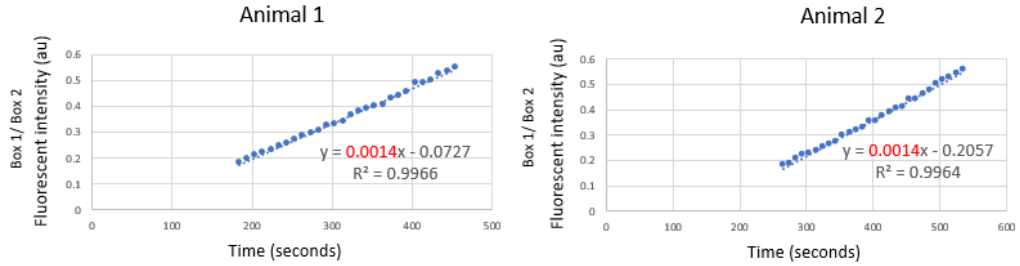

Figure 2-14 Solute Flux Comparison in Animal 1 and Animal 2

Analysis performed on two different mice with the same age and background show similar results for solute flux (slope=0.0014), confirming that the method of analysis yields consistent results.

2.2.7.2 Automated Analysis of Solute Flux

Manual analysis of these videos was very time consuming, as videos can have over a thousand frames, and great attention needs to be given during the analysis process. As these mice are under anaesthesia during the recording, rolling of the eye as well as movement due to heartbeats required changing of the position of box 1 and box 2 for fluorescent intensity measurements so that they remained in place. Additionally, movement of the eye also caused occasional frames to become out of focus **(FIGURE 2-15)**, therefore skewing the fluorescent intensity measurements.

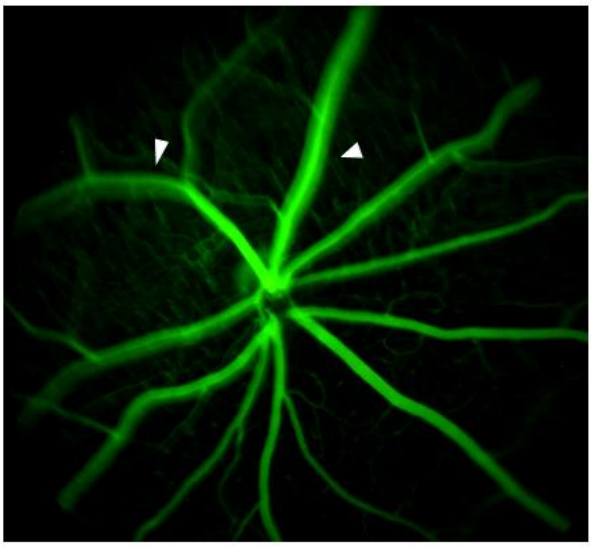

Figure 2-15 Example of Out of Focus Frame

Movement of the eye during recording can cause vessels to go in and out of focus, giving fluorescent intensity measurements that are not accurate. White arrowheads point to example of out of focus vessels.

In collaboration with a Computer Sciences MSc student, Kwan Ho Ho whom I co-supervised with Dr. Neill Campbell in the Computer Sciences, Faculty of Engineering, we developed software with a user-friendly interface which allowed for automated analysis, with the ability to exclude frames which were out of focus, from analysis. A more in-depth description of the program and the computer science techniques used to develop it can be found in Kwan Ho Ho's MSc thesis (176). I will describe how the software analyses the videos in order to calculate solute flux.

In the program, the video is loaded and a snapshot of the video opens. Here, the region of interest (ROI) for analysis is selected **(FIGURE 2-16)**.Note that the ROI is no longer a box in the main vessel and a box in the exchange vessels as in **FIGURE 2-10**. Instead, the

program was designed to distinguish between ‘bright’ and ‘dark’ pixels, and in this way measures fluorescent intensity in the main vessel and exchange vessels.

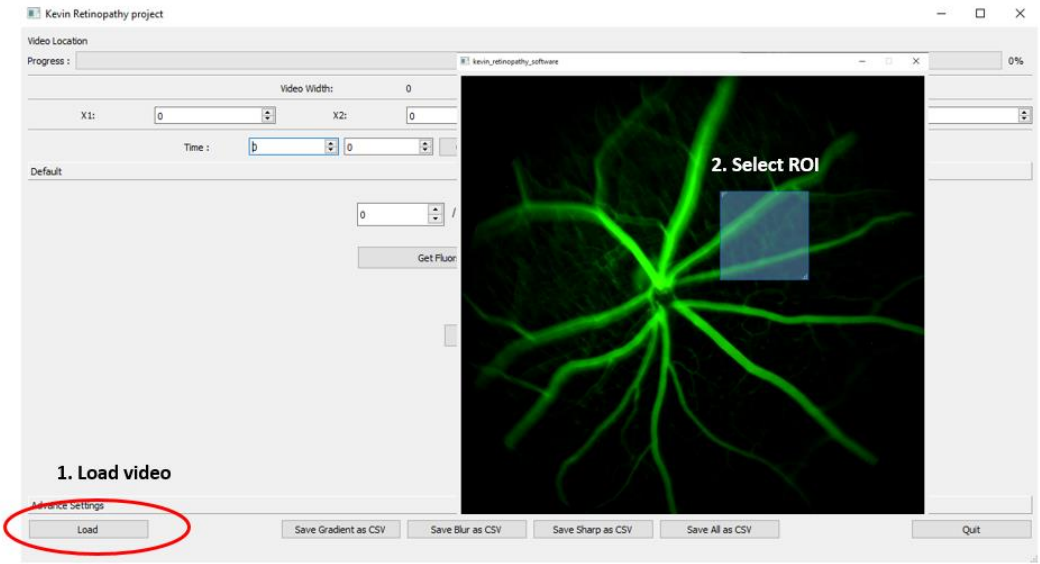

Figure 2-16 Loading and Selection of ROI in FA Analysis Program

The video to be analysed is first loaded. 2. A window with a snapshot of the video allows you to select the ROI for analysis. ROI can be moved around and changed in size.

The program can distinguish blurry frames and remove them from the data points used for analysis. **FIGURE 2-17 A** shows fluorescent intensity ratio plotted against time for the entire video, in which data points which deviate significantly from the curve are apparent (arrow). These points were confirmed to represent blurry frames in **FIGURE 2-17 C**, as blurry frames have a smaller "edgesharpness" value. **FIGURE 2-17 D** shows a graph for which values are deemed sharp, or in focus. These frames are then removed from **FIGURE 2-17 A** to give the graph in **FIGURE 2-17 B,** representing the values which can be used to calculate solute flux without data from blurry frames.

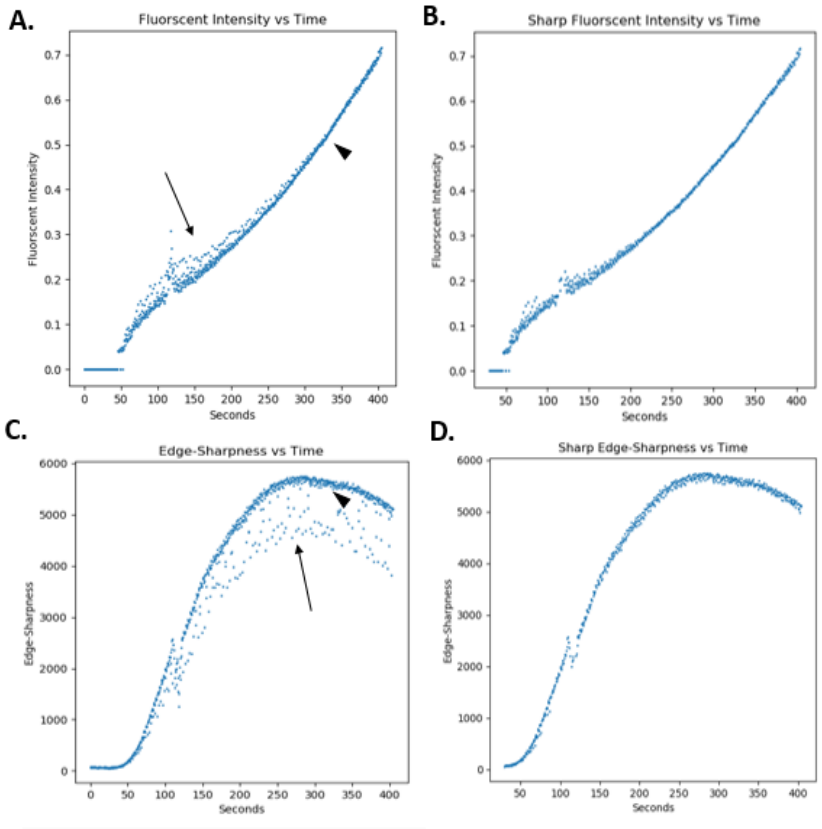

Figure 2-17 Removal of Blurry Frames from Analysis

Graphs produced from video ROI measurement. A. The fluorescent intensity ratio over time for the entire video. The arrow points to fluorescent intensity values which deviate from the curve produced from the other data points. Arrowhead points to the clustered values which appear to deviate less. B. Results from removing deviating data points, which were deemed as blurry frames, based on data from C. C. Graph of edge sharpness vs seconds indicating which frames are considered blurry, as blurry frames have lower edge sharpness values (arrow) compared to the majority (arrowhead). D. Graph representing those frames which are considered sharp (in focus) and therefore can be used for analysis.

The program then allows you to select the time frame from which data points should be used to calculate solute flux. As in **FIGURE 2-13**, the point at which the main vessel begins to reach a steady is determined and the time frame is selected on the main vessel graph **(FIGURE 2-18)**.

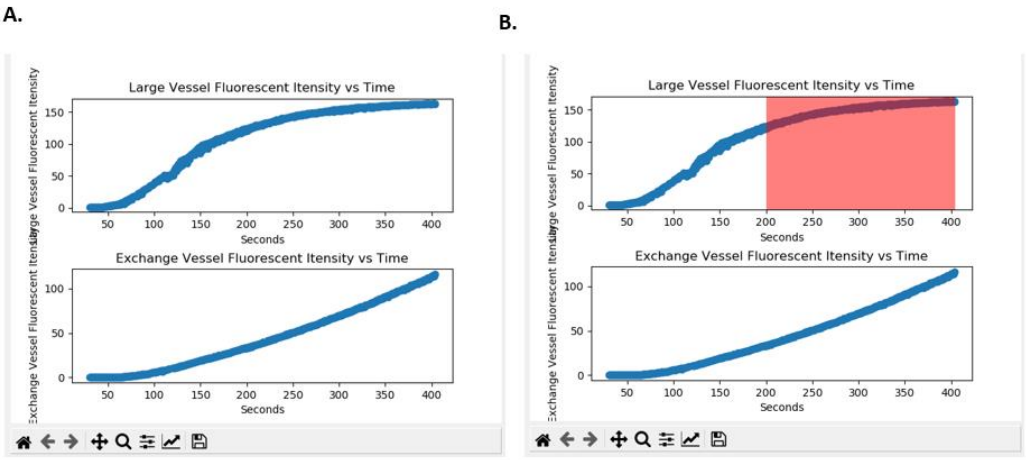

Figure 2-18 Selection of Analysis Time Frame

The program produces fluorescent intensity profiles for the main vessel (large vessel) and exchange vessels as with manual measurements. B. Once the point at which the main vessel reaches a steady state, the time frame used for analysis can be selected (red highlighting).

Once selected, the program produces a graph plotting the ratio of the exchange vessel and main vessel over time, as is done in manual analysis, and displays the calculated slope from the line **(FIGURE 2-19)**.

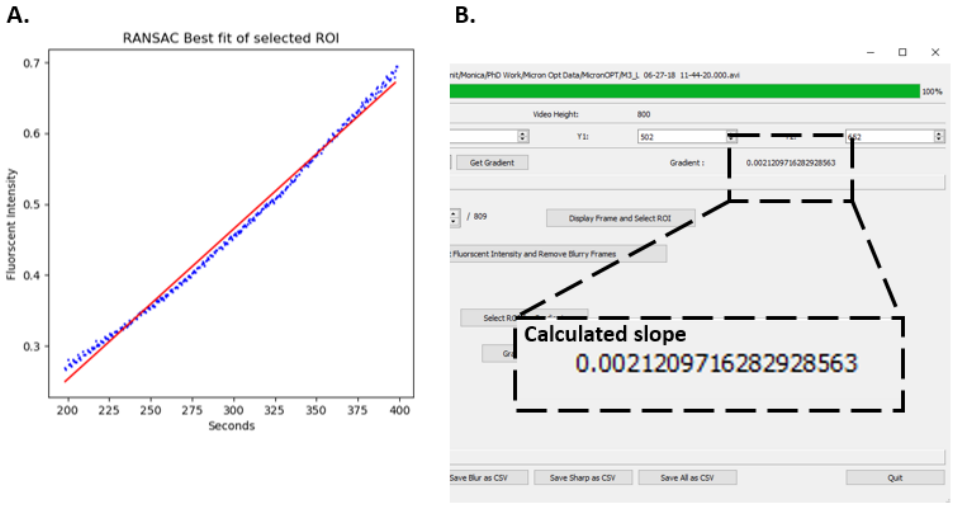

Figure 2-19 Calculation of the Slope of the Line Representing Solute Flux

The program uses the data selected as the time frame for analysis excluding blurry data points and plots a line of the ration of the exchange and main vessel fluorescent intensity vs time. B. From this line, the slope is calculated and displayed.

To confirm that the automated method of analysis yields similar results to the manual method, Kwan Ho Ho validated a series of videos from which manual analysis was done as well as automated analysis. An example of the results from the same video, manual measurements versus automated measurements are shown in **FIGURE 2-20**. As shown, the slope of the line is 0.0021 for both methods **(FIGURE 2-20)**, confirming that automated analysis is consistent with manual analysis.

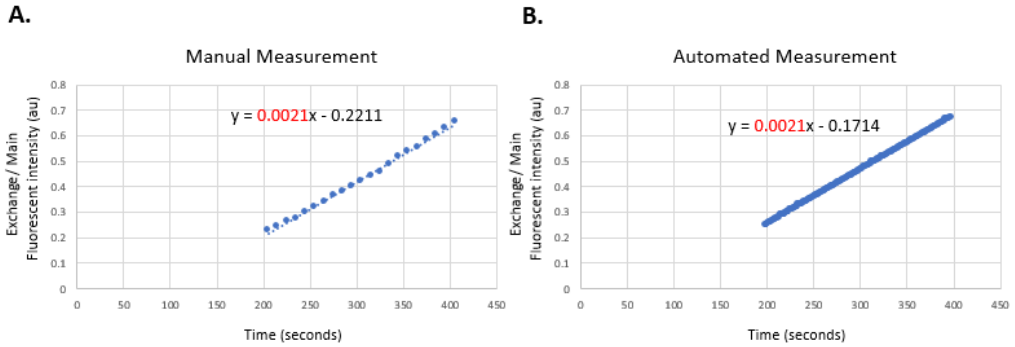

Figure 2-20 Manual Versus Automated Measurements for Solute Flux

Manual and automated measurements for the same video. A. The fluorescent intensity ratio over time for manual measurements yields a slope of 0.0021. B. The fluorescent intensity ratio over time for automated measurements also yields a slope of 0.0021.

In addition to being consistent with manual measurements, this method of analysis has added benefits. Because the area of analysis is bigger, and no longer just a very small portion of the main vessel and exchange vessel as in **FIGURE 2-10**, this method is likely a more accurate representation of solute flux in the retina rather than very local changes which would result from measuring a smaller area of the retina. Additionally, manual measurements were taken every 10 frames due to the large volume of frames in each video. These videos have an imaging rate of 2 frames per second, meaning manual measurements were taken every 5 seconds. Automated analysis takes a measurement every frame (*i.e.* every 0.5 seconds), therefore gathering more data points to which a line of best fit can be more accurately applied to calculate solute flux.

2.2.8 Statistics

GraphPad Prism version 5.00 for Windows was used for all statistical analyses (GraphPad Software, La Jolla California USA, www.graphpad.com). Statistical test for each set of data can be found in figure legends of corresponding data. For data comparing two groups for statistical differences, unpaired Student's t- test was used, or where appropriate paired t-test, as indicated in figure legends. One-way ANOVA followed by Tukey's multiple comparisons test, which is recommended when comparing a mean with every other mean, was performed for comparing more than two groups for statistical differences (177). All data are presented graphically as the mean $\pm$ standard error of the mean. If P values were ≥ 0.05 for a given set of data, the data was considered not statistically significant. For graphs, asterisks correspond to following p values: * $p \leq 0.05$, ** $p \leq 0.01$, and *** $p \leq 0.001$.

Chapter 3 Importance of Endothelial Glycocalyx Heparan Sulphate in the Kidney

3.1 *Introduction*

3.1.1 Structure and Biological Role of Hepran Sulphate in the Glomerular Filtration Barrier

Heparan sulphate (HS) belongs to a family of linear polysaccharides called glycosaminoglycans (GAGs). HS is one of the most complex GAGs, made of alternating D-glucuronic acid (GlcA) or L-iduronic acid (IdoA) and D-glucosamine (GlcNac), with variations of *N*-sulphation or *N*-acetylation (178). HS should not be confused with heparin. Although both are comprised of the same back-bone disaccharides, heparin has higher levels of *N*- and *O*-sulphation and is differentially localized with different functions (179). Although HS was originally identified in commercial preparations of heparin as low sulphation heparin, years of research have identified unique biological function for HS (178). HS is most commonly referred to in the context of HS proteoglycans (HSPGs), because HS is covalently bound to different proteoglycans, which are membrane bound on cell surfaces or in the extra cellular matrixes/ basement membrane of all tissues. Syndecans and glypicans are the two main families of membrane bound HSPGs, while perlecan is a major HSPG in basement membranes (180). HS has been shown to have roles in cell growth and differentiation, host defence and viral infections, lipid transport, inflammation, cell-cell and cell-matrix signalling, and cancer (179). Because different HSPGs are differentially distributed, HS can have different functions in each tissue type, depending on its location.

In the glomerulus, HS is widely expressed in podocytes, GBM, and the eGlx. In podocytes, expression of HS may help in adhesion and motility, demonstrated by *in vitro* experiments where podocytes which lacked HS had reduced motility and focal adhesion formations (181). In agreement with this, *in vivo* studies show that loss of podocyte HS in a mouse model resulted in podocyte effacement and reduced GBM HS (182). For years it was believed that that HS in the GBM contributed to charge selectivity, since the high levels of *N*- and *O*- sulphation make HS a highly negatively charged molecule , but a study showing that loss of some HS epitopes in the GBM, and consequently reduction of anionic charge sites, led to no structural change to GBM or large increases in albuminuria (183,184). Perlecan and another HSPG called agrin are both abundant in the GBM, but

studies have confirmed that loss of agrin and perlecan HS in the GBM has no effect on the GFB (185,186), so whether or not GBM HS has a role in charge selectivity remains under debate, but has largely been debunked. There is, however, evidence suggesting a role of GBM HS in modulating local compliment activation by recruiting and binding Factor H from the plasma, a major inhibitor of the alternative compliment pathway, and part of the innate immune system's defence against infections (187). However, the role of HS in the glomerular eGlx has not been fully elucidated.

3.1.1.1 Heparan Sulphate in the Glomerular eGlx

On GEnC, prominent HSPGs include sydecans-1,-2,-4 and glypican-1, all of which form part of the eGlx (188), but there remains to be conclusive evidence in the form of images showing HS is in fact in the glomerular eGlx. *Rops et al.* showed that immunofluorescence on mouse kidney sections using HS targeting antibodies had an endothelial cell staining pattern in the glomerulus, but the authors did not show conclusive evidence that this was eGlx staining and not just basement membrane staining (189). Functionally, there is evidence that eGlx HS acts as a mechanotransducer in glomerular capillaries, resulting in regulation of the nitric oxide (NO) response, a modulator of vasodilation (190). HS in the eGlx may also serve as a regulator of inflammatory responses. Specific 'inflammatory' *N*- and *6*-*O*-sulphated HS domains have been identified to be upregulated after GEnC activation *in vitro* and during nephritis *in vivo* (189). Furthermore, a mouse with a conditional endothelial knockdown of these inflammatory domains had increased renal function measured by plasma creatinine concentration and blood urea nitrogen concentration (189). Knockdown mice also had less glomerular injury during anti-GBM nephritis, due to reduced leukocyte infiltration (189). Therefore, variation in HS domains in the eGlx may help modulate the inflammatory response, not only by acting as a reservoir for chemokines as has been previously discussed, but also by variations in its composition. Interestingly, alteration of HS sulfation patterns does not seem to negatively impact GFB function, as mice who are deficient in the modifying enzyme *N*-deacetylase-*N*-sulfotransferase 1 and 2 (Ndst-1 and Ndst-2) do not have increased albuminuria (189,191). However, presence of eGlx HS does seem to play a role in the GFB function, as isolated perfused kidneys from mice treated with heparinase III have a significant increase in albumin clearance (35), but because these studies were performed *ex vivo* and the eGlx was not directly visualised, the effect of HS shedding on eGlx structure and function *in vivo* is not yet fully elucidated, and will be the focus of this chapter.

3.1.2 Synthesis of Hepran Sulphate in the Cell

HS is synthesised in the Golgi, where attachment of a linkage region of four monosaccharides to the core protein occurs (192). This chain is extended by addition of GlcA and GlcNac to the protein core, which is accomplished by two glycosyl transferases, exotosin 1 (Ext1) and exotosin 2 (Ext2), which form a heterodimer referred to as HS-polymerase **(FIGURE 3-1)** (192). Once the chain has been extended, though likely occurs simultaneously as well, a series of enzymes such as NDSTs, and *2-O*,*3-O* and *6-O* sulfotransferases (2OSTs,3OSTs,6OSTs) modify the nascent HS chain **(FIGURE 3-1)** (193). Upon completion of HS synthesis, membrane HSPGs are transported in cytoplasmic vesicles to the cell surface (178).

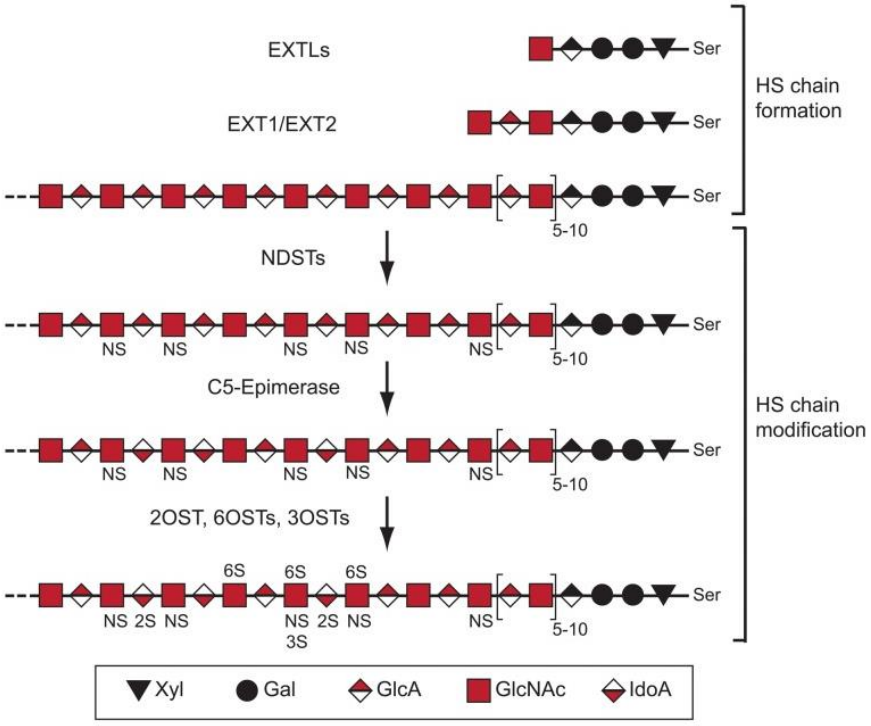

Figure 3-1 Synthesis and Modification of HS

Example of HS synthesis and chain modification. Ext1/Ext2 complex is involved in HS chain formation and elongation, adding repeating GlcA, GlcNAc, and IdoA units. HS chain modifications are then made by a series of enzymes (NDSTs, epimerase, 2OST, 6OST, 3OST). Modifications include: N-sulphated GlcN (NS), 6-O-sulphated GlcN (6S), 2-O-sulphated IdoA (2S), and 3-O-sulphated GlcN (3S). Image adapted from (Rosenberg et al., 1997)(192).

Interestingly, although Ext1 and Ext2 both have GlcA and GlcNac transferase activity, in the absence of Ext1, Ext2 does not have any significant glycosyltransferase activity (194). Additionally, mutation in either gene causes hereditary multiple exotoses (HME), a

disorder that leads to skeletal abnormalities, and in some instances osteosarcomas (195). This suggests that, despite structural homology, Ext1/Ext2 are not functionally redundant and both are required for normal HS synthesis. Importantly, this means that genetically modified mice which have a knockout of just one of these genes should be sufficient to prevent HS synthesis, which will be of use for the experiments discussed in this chapter.

3.1.3 Heparan Sulphate Degrading Enzymes

There are two groups of known HS-degrading enzymes. One group is the mammalian endoglucuronidase, HPSE, which will be discussed in detail in **CHAPTER 4**. The second is a family of bacterial lyases isolated from *Flavobacterium heparinum*. This group of enzymes have been useful in studying heparin and HS, as affinities for heparin or HS differ between members of the enzyme family. Heparinase I and II have the ability to degrade heparin and HS (196,197). Heparinase III is more specific to HS, acting on regions of low sulphation and therefore having little activity against heparin (196,197). Heparinase III primarily acts on non-sulphated GlcNac domains, while S-domains on HS which are highly sulphated remain resistant (196). Due to its specificity, Heparinase III has been used in countless studies to investigate the role of HS in biological systems, including in the eGlx (10,170,184,198,199), and is used as a tool for enzymatic removal of vascular eGlx HS in this chapter.

3.1.4 Chapter Aims and Experimental Approaches

The aim of this chapter is to show the importance of HS in the glomerular eGlx, which is accomplished in two parts.

1. Show that that HS is present in the glomerular eGlx using immunofluorescence.
2. Show that removal of HS from glomerular eGlx increases vascular permeability. I used two approaches for this aim. The first was to directly target HS by treatment with the HS shedding enzyme Heparinase III, allowing me to investigate if HS contributes structurally and functionally to the glomerular eGlx in healthy mice. The second approach was the use of a transgenic mouse model in which endothelial Ext1 was knocked out, in an inducible manner, in healthy mice. This allowed me to study the effects of reduced HS synthesis on the glomerular eGlx *in vivo.*

3.2 *Methods*

These methods are not inclusive. The methods described in this section are those that pertain specifically to this chapter or have been adapted for experiments in this chapter. All other methods are described in the **CHAPTER 2 METHODS AND MATERIALS.**

3.2.1 Generation of Ext1 Knock Down Mice

Set up of Ext1 colony and partial characterisation of this inducible Ext1 mouse model was previously done by a previous PhD student in the Bristol Renal group, Dr. Hesham E Hussien Elhegni. A more in-depth discussion on the creation of the Ext1 model and characterisation can be found in his thesis (200). Briefly, due to the embryonic mortality in homozygous Ext1 knockout mice, an inducible knockdown was created by combining the Tet-O-Cre-Loxp systems on a C57BL/6 background. Doxycycline (an analogue of tetracycline) controlled expression of reverse tetracycline trans-activator (rtTA) under the Tie2 (endothelial specific (201)) promoter (Tie2 rtTA). This drove Cre recombinase expression, the bacteriophage P1 recombinase (201), in endothelial cells. The Cre recombinase target LoxP sites were inserted in the 5' untranslated region of exon1 and the second in the intron downstream of exon1 (*Ext1*$^{flx/flx}$). Excision of Ext1 can therefore be induced by treatment of triple transgenic mice Tie2^{+}/Cre^{+}/*Ext1*$^{flx/flx}$ with doxycycline. A schematic of the system can be found in **FIGURE 3-2**.

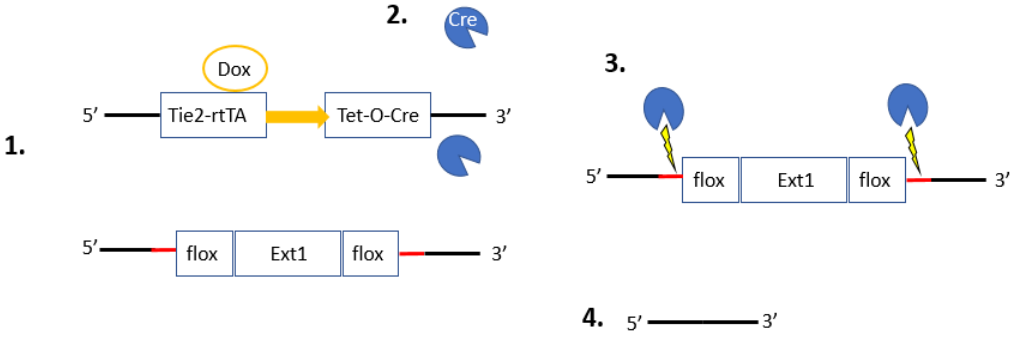

Figure 3-2 Excision of Ext1 in Ext$^{flx/flx}$ Mice

1. Treatment of mice with doxycycline (Dox) leads to Dox binding to rtTA. 2. Binding of Dox allows for Cre recombinase expression. 3. Cre recombinase target sites (flox) which are on both sides of Ext1, are cut upon Cre expression. 4. Ext1 is excised, preventing Ext1 expression.

To obtain Tie2^{+}/Cre^{+}/*Ext1*$^{flx/flx}$ Ext1 conditional knock out (*Ext1*^{CKO}) mice, breeding pairs were set up as shown in **FIGURE 3-3** in the Animal Service Unit, Barn 1, at the University of Bristol. Offspring were genotyped for the three transgenes. Ext1^{CKO} were used as experimental mice while littermate control mice (LMC) had the requirement of lacking at least one of the transgenes. For example, Tie2^{+}/Cre^{+}/Ext1$^{wt/wt}$, Tie^{+}/Cre^{-}/ Ext1$^{wt/flx}$, and Tie^{-}/Cre^{+}/ Ext1$^{flx/flx}$ would all serve as suitable littler mate controls.

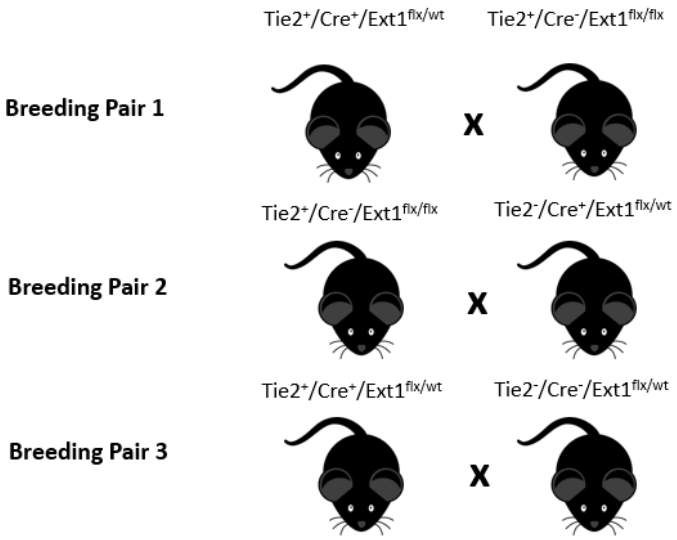

Figure 3-3 Schematic of Breeding Pair Set Up for Generation of Ext1^{CKO} Mice

Breeding pairs were set up to generate triple transgenic mice as well as litter mate control mice.

3.2.2 Animal Genotyping

Ear notches were digested in 100µl of 50mM NaOH for 1 hour at 95°C. 20µl of 1M Tris-HCl pH 8.0 was added to neutralise. For reactions, The PCRBIO HS Taq Mix (PB10.22-02, PCRBIOSYSTEMS, London, England, UK) was used following manufacture instructions. Samples were genotypes for Tie2 rtTA (Tie2), Cre, and *Ext1*$^{flx/flx}$. A list of primer sequences and program protocols can be found in **TABLE 3-1** and **TABLE 3-2** . 6X PCR loading dye (B7024S, New England BioLabs (NEB), Ipswich, MA) was added to 1X to all samples, and samples were run on a 2% Agarose gel for 1 hour and 100V with 100bp ladder (N0457S, NEB) and imaged to determine product sizes, listed in **TABLE 3-2**.

Table 3-1 Ext1 Mouse Genotyping Primers

Primer Name	Sequence	Product Size
Ext1 Forward	GTTGAAGTTGCTTTCCCCGGGCT	Flox: 420 base pairs (bp) WT: 320 bp
Ext1 Reverse	GCCATCTTCCC CCTGT	
Tie2 Forward	ATGATCCTGCAAGCCTCGTCGTCT	460 bp
Tie2 Reverse	TTTAGTTAGCTTGCTAGGGC	
Cre Forward	TGCCACGACCAAGTGACAGCAATG	370 bp
Cre Reverse	AGAGACGGAAATCCATCGCTCG	

Table 3-2 PCR Reaction Protocol

Cycle	Temp °C	Time	Notes
1	95	1:30min	
2	95	15s	Steps 2-4 40 cycles
3	x	15s	X=temp for each primer
4	72	1 min	
5	72	7 min	
6	4	hold	

x	Temp °C
EXT1	62
Cre	60
Tie2	60

3.2.3 Inducing Ext1 Knockdown with Doxycycline

Prior to the start of experiments, litter mate controls (LMC) and *Ext1*^{CKO} (6 weeks to 9 months, age matched) were given 2mg/ml doxycycline (D3447, Sigma-Aldrich) in drinking water for three weeks supplemented with 5% sucrose to encourage drinking and prevent dehydration due to bitterness of doxycycline **(FIGURE 3-4)**. Water was provided in blacked out plastic bottles to protect doxycycline water from light. Fresh doxycycline water was made up every 2 days.

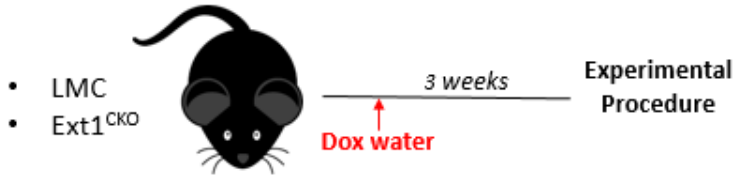

Figure 3-4 Induction of Knockdown in Ext1^{CKO} Mice Prior to Experimental Procedures

LMC and Ext1^{CKO} mice were given 2mg/ml of Doxycycline drinking water (Dox water) for 3 weeks followed by experimental procedures (urine collection, perfusions, glomeruli isolation, etc).

3.2.4 Fluorescence Activated Cell Sorting (FACS) Cytometry for CD31 Positive Cells

This work was performed by Dr. Sarah Fawaz, a member of the group. Glomeruli were isolated from 75µm pore sieve (see main methods). Glomeruli were digested with 1mg/mL collagenase I,V,and VI (Sigma-Aldrich) for 1 hour at 37°C with constant rotation. Digest was passed through 35µm mesh cell strainer (353355, BD Falcon, Thermo Fisher Scientific) to remove cell clumps. Cells were washed three times and cell pellet resuspended in HBSS with 1mM EDTA, 0.1µl/ml DNAse and 0.3% BSA. Cells were incubated with PE Rat anti-mouse CD31 (550083,BD Pharminigen, San Jose, CA) 1:50 for 1 hour at 4°C. Cells were washed again three times and FACS sorted/collected for CD31 (an endothelial cell marker) positive cells using Becton Dickinson Influx Cell Sorter (BD Biosciences, San Jose, CA) at the University of Bristol Flow Cytometry Core Facility.

3.2.5 RNA Extraction and Real-Time Quantitative Polymerase Chain Reaction (qPCR) for EXT1

This work was performed by Dr. Sarah Fawaz. RNA was extracted from isolated cells using RNeasy Mini Kit (Qiagen, Manchester, UK) following manufacturer's instructions. A total of 2µg of RNA was converted to cDNA using high-capacity RNA to cDNA conversion kit

(Applied Biosystems, Foster City, CA) following manufacturer's instructions. For qPCR , SYBR Green Master Mix was used (S-4438, Sigma-Aldrich) following manufacturer's instructions using StepOne 96-well plate real-time PCR system (Life Technologies- Applied Biosystems, Foster City, CA). Ext1 and β-Actin, primer sequences in **TABLE 3-3**. Relative fold change ($2^{-\Delta\Delta CT}$) was calculated and Ext1 values and normalised to β-Actin.

Table 3-3 qPCR Primer Sequences

Primer Name	Sequence
Ext1 Forward	GTCATCCATGCTGTGACTCC
Ext1 Reverse	GGCTTGTCACAATTCCACAG
β-Actin Forward	CTGTCCCTGTATGCCTCTG
β-Actin Reverse	ATGTCACGCACGATTTCC

3.2.6 Urine Collection for L-Lysine Experiments

All urine was collected on hydrophobic sand (LabSand, Animalab, Poznan, Poland) unless otherwise specified. To collect urine on hydrophobic sand, mice were placed in a cage with a thin layer of sand and solid waste removed immediately to prevent contamination of urine. Clean urine which was freshly voided was collected with pipette into an Eppendorf tube. Any urine that came into contact with solid waste was deemed contaminated. See main methods for uACR measurements.

3.2.7 Blocking Tubular Reabsorption with L-Lysine in FVB Mice

Upon pre-treatment urine collection, all mice receiving L-Lysine were injected via intraperitoneal (i.p.) route 2g/kg with freshly made L-Lysine (L5751, Sigma-Aldrich) dissolved in PBS, a dose previously shown to be effective in mice (202). Post treatment urine was collected over the following 2 hours in metabolic cages with enrichment to allow access to water.

3.2.8 Treatment with eGlx Shedding Enzymes Chondroitinase and Hyaluronidase

After pre-treatment urine collection, mice were anaesthetised (2.5 % isoflurane, 1.5 litre/minute) and administered 0.087mU/g Chondroitinase (C3667, Sigma-Aldrich) and 15mU/g Hyaluronidase (385931, Sigma-Aldrich) via tail vein (t.v.) injection in a volume of 100uL, a dose previously shown to shed eGlx and increase glomerular albumin

permeability (116). Mice receiving L-Lysine were administered this treatment as described above. Mice were allowed to fully recover (approximate time required - 10 minutes) before collection of post treatment urines over the following one to two hours in metabolic cages, with enrichment, to allow access to water. A schematic of the experimental design is shown in **FIGURE 3-5.**

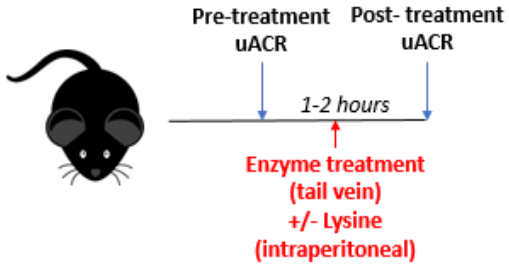

Figure 3-5 Visual Representation of Enzyme + Lysine Experimental Set Up

Pre-treatment urines were collected immediately followed by enzyme +/- L-Lysine treatment. Post-treatment urines were collected the following 1-2 hours after treatments.

3.2.9 Blocking Tubular Reabsorption in *Ext1*^{CKO} Mice

LMC and *Ext1*^{CKO} mice were given doxycycline water as described above. Pre-treatment urine was collected on hydrophobic sand and upon urine collection mice were treated with L-Lysine as previous. Mice were then placed in metabolic cages with enrichment to allow access to water, and urine collected for the following one to two hours. A schematic of experimental design is shown in **FIGURE 3-6.**

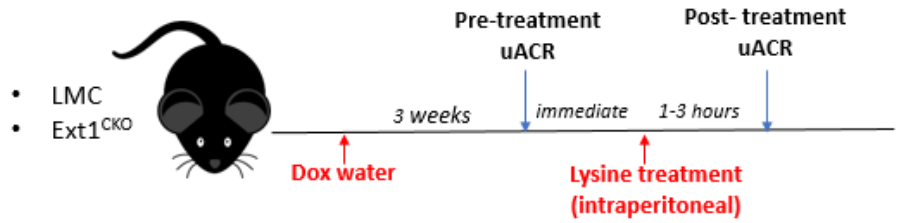

Figure 3-6 Experimental Design for Albuminuria Measurements and Tubular Reabsorption Inhibiting Treatments in Ext1^{CKO} Mice.

LMC and Ext1^{CKO} mice were given 2mg/ml of doxycycline drinking water for 3 weeks. Urine was collected after 3 weeks immediately followed by 2g/kg of L-Lysine. Post-treatment urine was collected for 1-3 hours after treatment.

3.3 *Results*

3.3.1 Presence of Heparan Sulphate in Glomerular eGlx

3.3.1.1 Heparan Sulphate is Present in the Glomerular eGlx

To show conclusively that HS is present on the eGlx of glomeruli, I used paraffin embedded BKS lean kidney tissue and performed IF staining for HS with epitope specific phage display antibody anti-HS3A8V or no primary as a control. HS staining was present throughout the kidney and glomerulus but absent in the no primary control **(FIGURE 3-7)**. Magnification of a single capillary showed that, although HS staining was present in the GBM and/or podocytes, HS staining on the luminal side of the capillary was clear indicating eGlx staining.

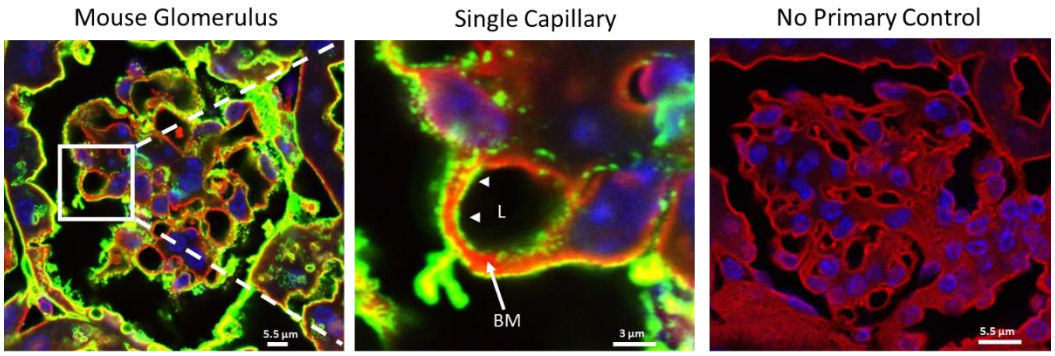

Figure 3-7 HS is Present in the Glomerular eGlx

Mouse kidney tissue stained with anti-HS HS3A8V phage display antibody (green), R18 cell membrane stain (red), and DAPI nuclear stain (blue). Left: 100x image of mouse glomerulus Middle: Zoomed in image from white box in left panel of single capillary. Basement membrane (BM) in red separates HS staining (white arrow heads) on luminal side (L) of endothelial cell. Right: No primary control indicating HS staining specificity.

3.3.2 Heparinase III Treatment Studies

3.3.2.1 Heparinase III Treatment Results in Loss of Glomerular eGlx

Having established the presence of HS in the glomerular eGlx, further investigation was required to determine if HS has a structural role in the eGlx in the glomerulus. It has been previously shown that mice treated with heparinase III have a significant reduction in kidney eGlx depth measured by the distance of intralipid droplets from the endothelial cell on EM (170), but this is an indirect measurement of eGlx. To more directly measure the effect that an HS shedding enzyme would have on the eGlx, FVB mice were treated with systemic heparinase III or heat inactivated enzyme and 30mins later were perfused with glutaraldehyde and Alcian blue, allowing for direct visualisation of eGlx by EM. Mice treated with inactive enzyme had visible eGlx on both podocyte and endothelial cells, while mice treated with active enzyme had a noticeable decrease in eGlx **(FIGURE 3-8 A)**. Quantitative EM showed a significant reduction in both eGlx depth and coverage on GEnC, indicating that treatment with HS shedding enzyme damages and causes loss of eGlx **(FIGURE 3-8 B)**. No significant differences were observed in pGlx **(FIGURE 3-8 C)**.

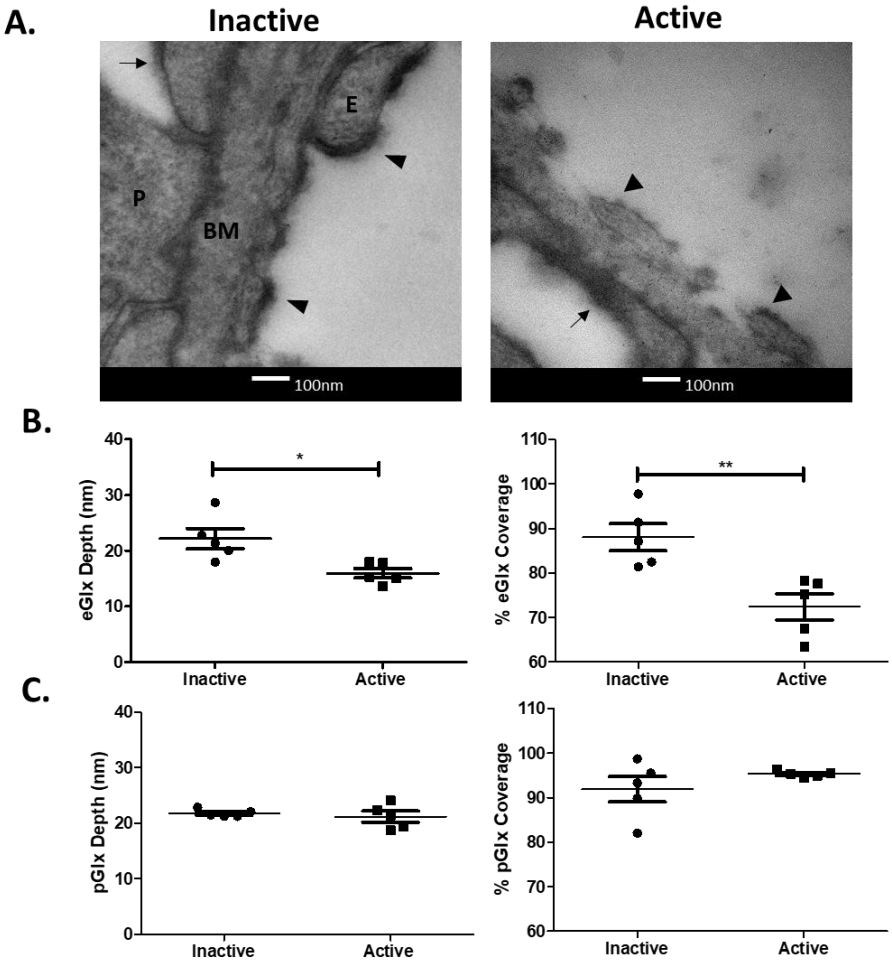

Figure 3-8 Treatment of Healthy FVB Mice with HS Shedding Enzyme Results in Loss of eGlx

A. Representative EM images of GFB from mice treated with active or inactive enzyme. Podocyte (P), basement membrane (BM), endothelial cell (E) shown. Arrow points to pGlx and arrowheads point to eGlx. B. EM images were analysed for eGlx depth (left) and eGlx coverage (right) and C. pGlx depth (left) and eGlx coverage (right), n=5 mice, unpaired Student's t-test indicated, *p≤0.05, **p≤0.01.

3.3.2.2 Heparinase III Treatment Does Not Affect GFB Structure

Changes in the GFB coincide with increases in albumin permeability. This includes some of the previously discussed characteristic changes observed in DN, such as podocyte foot process effacement, increased GBM thickness and loss of GEnC fenestrations (101).To confirm that treatment with heparinase III did not have any off-target effects that would result in permeability increases unrelated to HS shedding, quantitative EM was used to measure changes in the GFB ultrastructure. Treatment with active enzyme had no effect on podocyte foot process width or slit diaphragm width (measures of foot process effacement), fenestration density, or basement membrane thickness compared to inactive enzyme **(FIGURE 3-9 A-D)**, suggesting no off-target effects of the active enzyme.

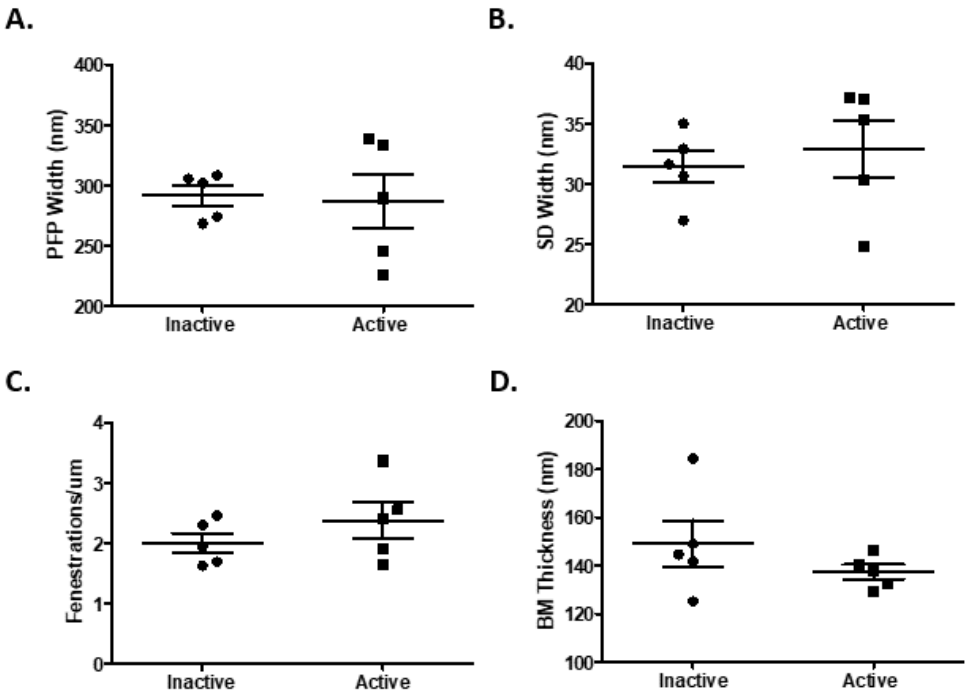

Figure 3-9 Heparinase III Treatment Does Not Affect GFB Structure

EM images were analysed for changes in: A. Podocyte foot process (PFP) width. B. Slit diaphragm (SD) width. C. Endothelial cell fenestration number. C. Basement membrane (BM) thickness. Minimum of 3 capillaries per mouse measured. N= 5 mice, unpaired Sutdent's t-test, not significant.

3.3.2.3 Heparinase III Treatment Increases Glomerular Albumin Permeability

To examine if the observed loss of eGlx resulting from heparinase III treatment also resulted in functional changes, FVB mice were treated with inactive or active enzyme as before. Thirty minutes later, mice were perfused, and glomerular albumin permeability assays performed. Treatment with active enzyme resulted in a significant increase in apparent albumin permeability (Ps'alb) **(FIGURE 3-10)** indicating that HS shedding negatively impacted GFB integrity.

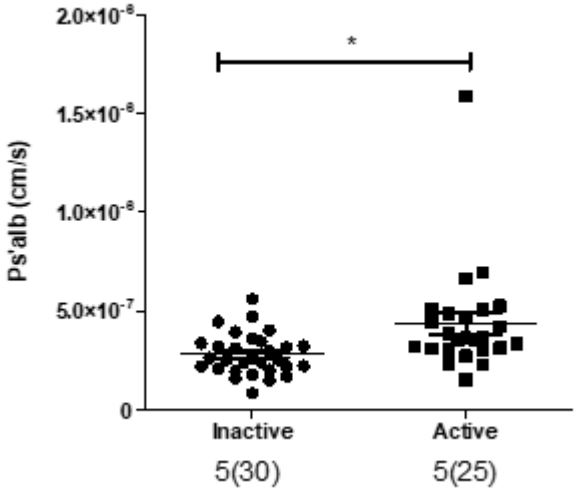

Figure 3-10 Heparinase III Treatment Increases Glomerular Albumin Permeability

Ringer perfused mice, previously treated with inactive or active Heparinase III, and glomerular albumin permeability was measured. On x-axis (mouse number (glomeruli analysed)). Stats performed on animal numbers. Unpaired Student's t-test indicated, *p≤0.05.

3.3.3 Endothelial *Ext1^{CKO}* Mouse Model

3.3.3.1 Ext1^{CKO} Mice Have Reduced Ext1 mRNA Expression

Although this mouse line was partially characterized by Dr. Elhegni, confirmation of Ext1 knock down was not performed at the time of his thesis submission, therefore confirmation was required prior to using the model in further studies. This following work was completed by Dr. Sarah Fawaz. Experimental mice *Ext1^{CKO}* and LMC mice were treated with doxycycline water to induce knockdown of Ext1. In order to confirm that Ext1 mRNA expression was reduced after doxycycline treatment, glomeruli from LMC or *Ext1^{CKO}* mice were isolated and CD31+ cells FACS sorted and collected. QPCR was performed on FACS sorted endothelial cells to confirm knockdown. As expected, *Ext1^{CKO}* mice had a significant reduction in Ext1 mRNA compared to control mice, indicating that Ext1 is reduced in experimental mice **(FIGURE 3-11)**.

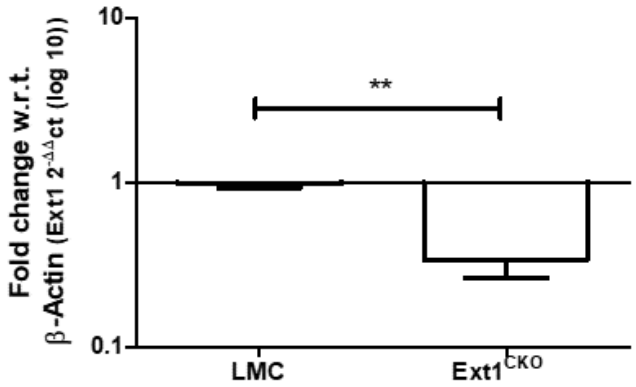

Figure 3-11 Ext1^{CKO} Mice Have Reduced Ext1 mRNA Expression

Ext1^{CKO} mRNA quantified with regard to (w.r.t.) β-Actin from FACS sorted CD31+ endothelial cells from LMC and Ext1^{CKO} mice. N=3 mice, unpaired Student's t test indicated, **p≤0.01. This figure is from work done by Dr. Sarah Fawaz.

3.3.3.2 Changes in HS Cannot Be Detected by Anti-HS Phage Display Antibody in Ext1^{CKO}

As mentioned, Ext1 is part of the HS-polymerase complex, and is required for HS chain elongation. It therefore stands to reason, that reduced Ext1 activity would result in reduction of HS expression in endothelial cells and eGlx. To determine if this was the case in *Ext1^{CKO}* mice, kidneys from LMC and *Ext1^{CKO}* mice were harvested 3wk post doxycycline treatment and I performed immunofluorescence on kidney sections using the same phage display antibody, anti-HS HS3A8V, as used previously. With this antibody, no detectable changes were observed in HS staining when comparing the two groups **(FIGURE 3-12).**

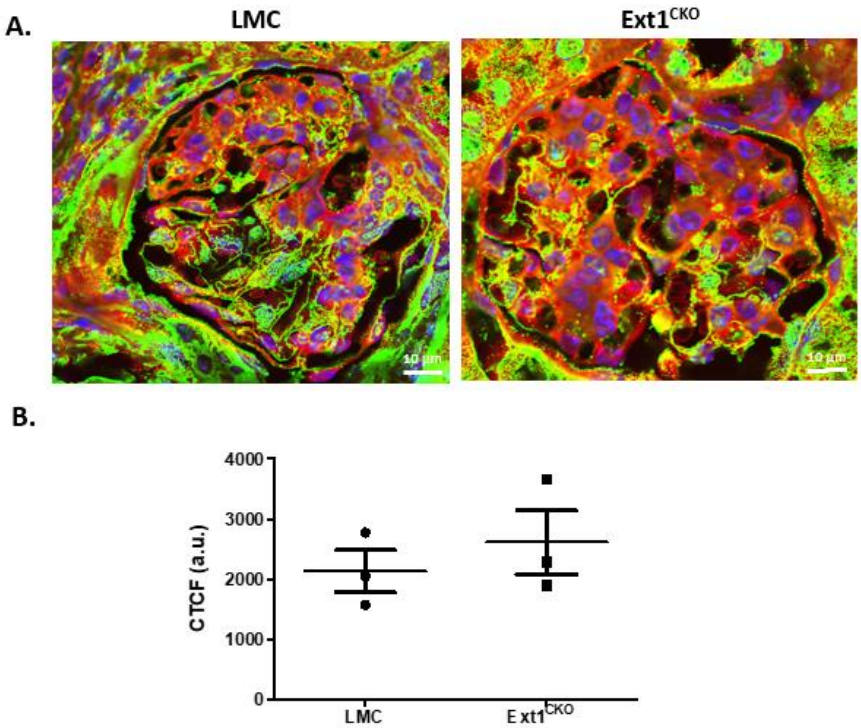

Figure 3-12 Changes in HS Cannot be Detected by anti-HS Phage Display Antibody

A. Representative images from mouse kidney section from LMC and Ext1^{CKO} mice, stained with anti-HS HS3A8V phage display antibody (green), R18 cell membrane stain (red), and DAPI nuclear stain (blue).B. CTCF analysis of total glomerular HS. N=3 mice per group, unpaired Student's t-test, not significant.

3.3.3.3 *Ext1^{CKO} Mice Have Loss of Glomerular eGlx*

Immunofluorescence on *Ext1^{CKO}* mice did not confirm knockdown of HS. To confirm that the eGlx was impacted when HS synthesis was reduced, changes to the eGlx were measured in *Ext1^{CKO}* and LMC mice using EM as previous. Perfusions and images were completed by Dr. El Hengi and analysis was done by me. LMC mice had visible glomerular eGlx and appeared more abundant compared to *Ext1^{CKO}* mice **(FIGURE 3-13 A)**. In agreement with this, quantitative EM showed a significant reduction in eGlx depth and coverage in *Ext1^{CKO}* compared to LMC mice confirming that there was reduced glomerular eGlx in *Ext1^{CKO}* mice **(FIGURE 3-13 B).** There were no changes in pGlx depth or coverage **(FIGURE 3-13 C)**.

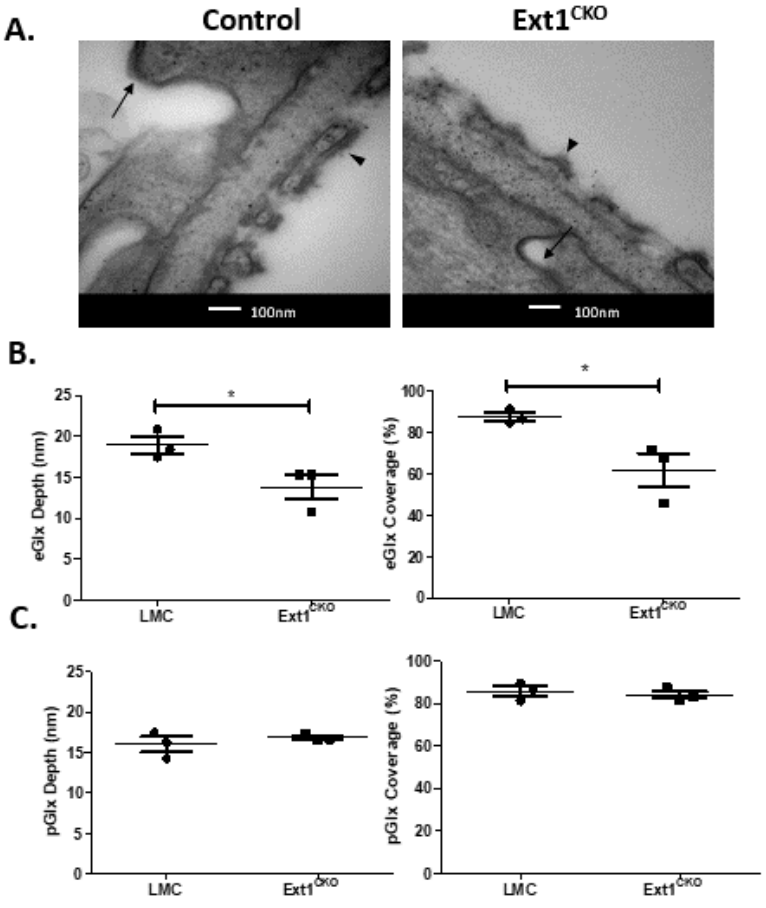

Figure 3-13 Ext1^{CKO} Mice Have Loss of Glomerular eGlx

A. Representative EM images of GFB from mice treated with active or inactive enzyme. Podocyte (P), basement membrane (BM), endothelial cell (E) shown. Arrow points to podocyte glycocalyx and arrowheads point to eGlx. B. EM images were analysed for eGlx depth (left) and eGlx coverage (right). C. pGlx depth (left) and eGlx coverage (right). N=3 mice, unpaired Student's t-test indicated, *p≤0.05. This figure is from work completed by Dr. Elhegni and me.

3.3.3.4 Ext1^{CKO} Mice Do Not Have Changes in GFB Structure

To confirm that *Ext1^{CKO}* mice did not have changes in GFB that are not specific to eGlx, quantitative EM was used to measure changes in the GFB ultrastructure. *Ext1^{CKO}* mice had no significant changes in podocyte foot process width or slit diaphragm width, fenestration density, and basement membrane thickness compared to LMC mice **(FIGURE 3-14 A-D)**, indicating knock out of endothelial Ext1 does not affect the GFB ultrastructure.

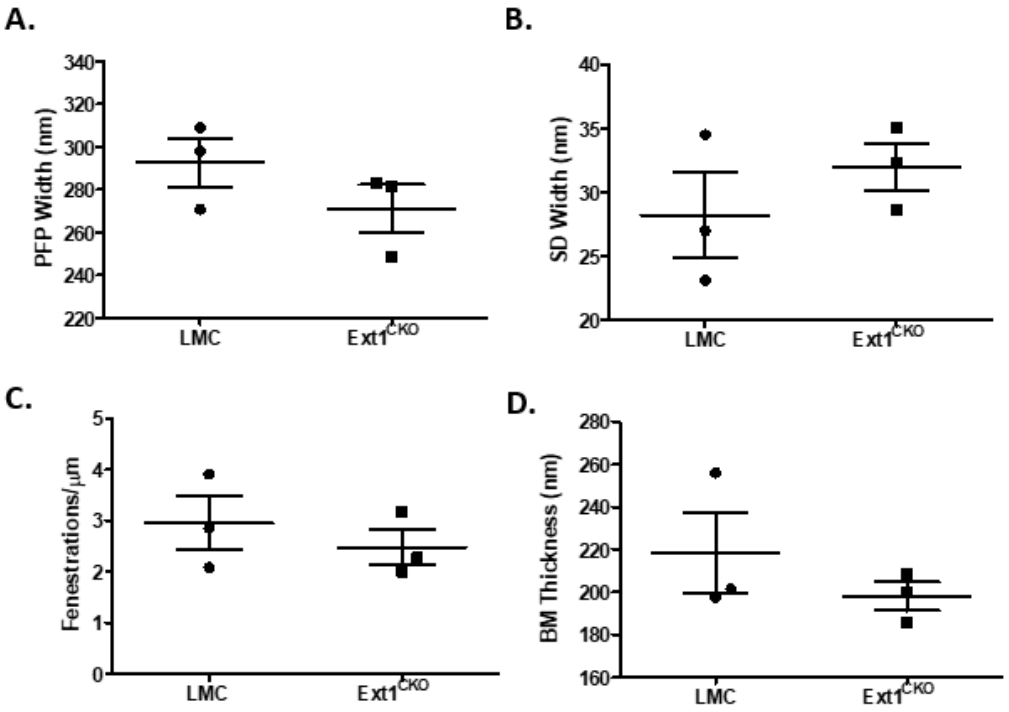

Figure 3-14 Ext1^{CKO} Mice Do Not Have Changes in GFB Structure

EM images were analysed for changes in: A. Podocyte foot process (PFP) width. B. Slit diaphragm (SD) width. C. Endothelial cell fenestration number. C. Basement membrane (BM) thickness. Minimum of 3 capillaries per mouse measured. N= 5 mice, unpaired Sutdent's t-test, not significant.

3.3.3.5 *Ext1^{CKO} Mice Have Increased Glomerular Albumin Permeability Compared to Control Mice*

Previous results show that loss of HS by treatment with heparinase III results in reduced eGlx and increased glomerular permeability. To test if reduced HS synthesis in *Ext1^{CKO}* similarly resulted in increased glomerular albumin permeability, mice were perfused, and permeability assays were performed on LMC and *Ext1^{CKO}* after doxycycline treatment. This work was completed by Dr. El Hegni, Dr. Sara Fawaz, and contributed to by me. Comparison of the two groups showed that *Ext1^{CKO}* mice had a significant increase in Ps'alb **(FIGURE 3-15)** indicating that reduced HS synthesis negatively impacted GFB integrity.

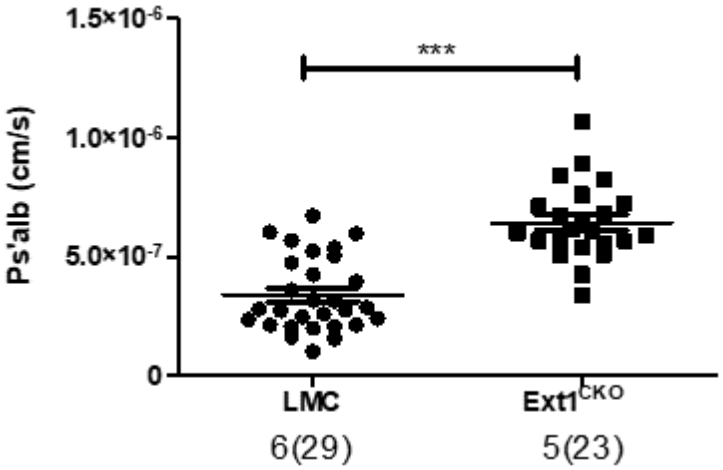

Figure 3-15 Ext1 Knockdown Mice Have Increased Glomerular Albumin Permeability

Glomeruli were isolated from Ringer perfused control and Ext1^{CKO} mice and glomerular albumin permeability was measured. On x-axis (mouse number (glomeruli analysed)). Unpaired Student's t-test indicated, ***p≤0.001.

3.3.3.6 Ext1^{CKO} Mice Do Not Have Increased Albuminuria Compared to Control Mice

To confirm that *Ext1^{CKO}* had increased albuminuria, uACR was measured in LMC and *Ext1^{CKO}* mice after doxycycline treatment. Surprisingly, *Ext1^{CKO}* did not have a significant increase in albuminuria compared to control mice as expected **(FIGURE 3-16)**, despite the previously observed increase in Ps'alb.

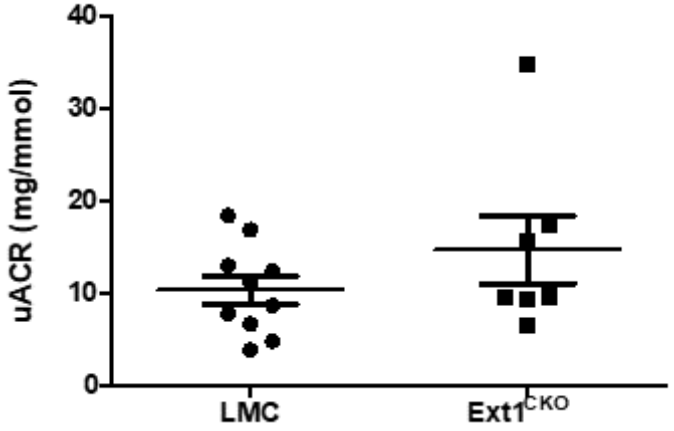

Figure 3-16 Ext1^{CKO} Mice Do Not Have Increased Albuminuria

Control and Ext1^{CKO} mice were given doxycycline for 3 weeks and albuminuria was measured. N= 7-10 mice, unpaired Student's t-test, not significant.

3.3.3.7 Optimisation of the Tubular Reabsorption Inhibitor, L-Lysine, In Vivo

The contradicting results observed in *Ext1*^{CKO} showing increased Ps'alb, but no increase in albuminuria, were not expected. Under normal conditions, the GFB regularly leaks out small amounts of protein but is almost completely reabsorbed by the proximal tubules (203). Only when the system is overwhelmed with a heavy albumin load, such as in DN, is an increase in albuminuria is observed (203). I therefore examined whether blocking tubular reabsorption would have any effect on control and *Ext1*^{CKO} mice. L-Lysine has been used as a potent tubular reabsorption inhibitor in humans and rodent models, and therefore I optimised this for use in these experiments (202,204). I first examined the effect of L-Lysine on FVB mice to determine if blocking tubular reabsorption in normal mice had any effect. Baseline urines were collected and immediately followed by L-Lysine injection given i.p., followed by a post L-Lysine urine collection. A significant increase in albuminuria was observed in post L-Lysine treated urines, suggested tubular reabsorption was blocked **(FIGURE 3-17)**.

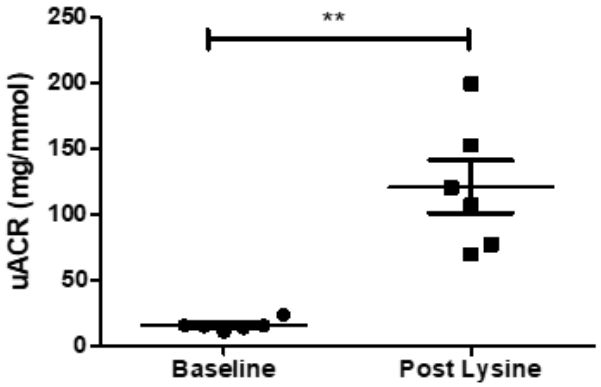

Figure 3-17 L-Lysine Blocks Tubular Reabsorption in Normal Mice

Baseline and post L-Lysine uACR measurements were taken in healthy FVB mice. N=6 mice, paired t test indicated, **p≤0.01

Previous work by a member of our group, Dr. Kai Betteridge, showed that a long term treatment of mice with chondroitinase and hyaluronidase using implanted minipumps did not result in increased albuminuria (unpublished data), but mice did have significantly increased Ps'alb (116), similar to *Ext1*^{CKO} mice. I therefore wanted to determine if lack of albuminuria in these studies was due to tubular reabsorption. To do this, I examined if treatment with eGlx shedding enzymes would result in increased albuminuria after tubular reabsorption was blocked. This would also serve as a proof of concept experiment for blocking tubular reabsorption in *Ext1*^{CKO}, as treatment with chondroitinase and hyaluronidase are known to increase glomerular permeability. If blocking tubular reabsorption is responsible for lack of albuminuria, I would expect to see an increase in albuminuria after L-Lysine treatment. To this end, baseline urines were collected from eight mice. Mice were then evenly and randomly assigned to enzyme only group or enzyme + L-Lysine group, briefly anesthetized and given chondroitinase and hyaluronidase via t.v. injection. Additionally, enzyme + L-Lysine group received an L-Lysine injection i.p. after enzyme treatment. Post treatment urines were then collected. One mouse from the enzyme only group was excluded due to a high baseline uACR. Although a modest increase in uACR was observed in the enzyme only group, it was not significant. However, mice treated with enzyme and L-Lysine had a significant increase in uACR **(FIGURE 3-18)**. This indicates that L-Lysine successfully blocks tubular reabsorption and allows measurements of permeability changes which can only be observed with when tubular reabsorption is not active, such as in glomerular albumin permeability assays.

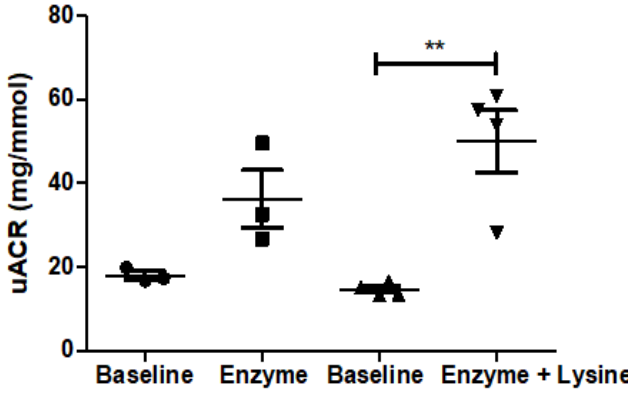

Figure 3-18 Blocking Tubular Reabsorption in eGlx Shedding Enzyme Treated Mice Increases Albuminuria

Baseline and post treatment uACR measurements were taken before and after treatment with chondroitinase/hyaluronidase with or without L-Lysine. One-way ANOVA, Tukey's multiple comparison test indicated, **p≤0.01

3.3.3.8 *Ext1^{CKO} Mice Have Increased Albuminuria When Tubular Reabsorption is Blocked*

To investigate if tubular reabsorption of albumin masked increased albuminuria in *Ext1^{CKO}*, LMC and *Ext1^{CKO}* were treated with doxycycline as before. Pre-L-Lysine treatment urines were collected, followed by L-Lysine injection, i.p. Post treatment urines were then collected. As expected, a modest increase in uACR was observed in control mice after L-Lysine treatment, though not significant **(FIGURE 3-19)**. However, *Ext1^{CKO}* mice had a significant increase in uACR after L-Lysine treatment **(FIGURE 3-19),** indicating that tubular reabsorption masked moderate uACR changes in *Ext1^{CKO}* mice.

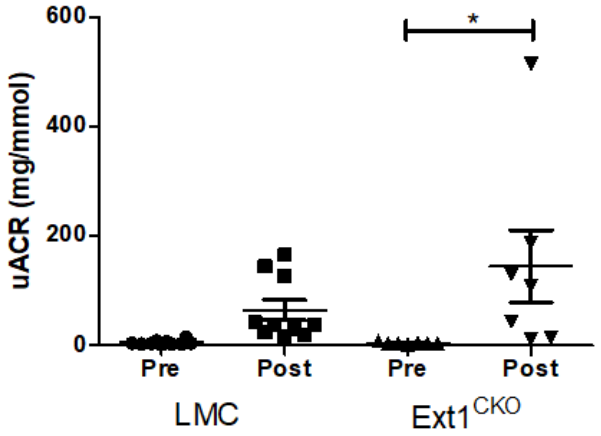

Figure 3-19 Ext1^{CKO} Mice Have Increased Albuminuria When Tubular Reabsorption is Blocked.

Albuminuria was measured in LMC mice and Ext1^{CKO} mice before treatment (pre) and after treatment (post) with L-Lysine. One-way ANOVA, Tukey's multiple comparison test indicated, *p≤0.05.

3.4 *Discussion*

3.4.1 Heparan Sulphate is Present in Glomerular eGlx

It is well established that HS plays an important role in many biological functions ranging from angiogenesis to modulator of inflammatory responses. However, the structural and functional role that HS plays in glomerular eGlx in health has not been addressed. Our group has shown that in tissue culture, GEnC expression of HS is present on the surface of cells shown by immunofluorescence (10). This signal is decreased when cells are treated with heparinase III (10), suggesting that HS is present in GEnCs surface, but whether this translated into tissue was not known. I therefore confirmed the presence of HS in glomerular eGlx in mouse kidney sections using immunofluorescence with a phage display anti-HS specific antibody. Staining showed a clear HS signal on the luminal side of endothelial cells in glomerular capillaries, confirming the presence of HS. While HS staining in glomeruli has been shown a number of times (109,186), to my knowledge, this is the first time that conclusive evidence of HS on the glomerular eGlx has been shown and is an important first step in investigating the role of HS in the eGlx.

3.4.2 Loss of HS Reduces Glomerular eGlx and Increases Permeability

3.4.2.1 Removal of Heparan Sulphate by Heparinase III

Once the presence of HS was established in the glomerular eGlx, confirmation of the functional and structural role that HS has was required to determine if HS contributed to the eGlx's barrier properties in vascular permeability. I found that mice treated with heparinase III had a significant reduction in eGlx depth and coverage, but no changes in pGlx. This damage suggests that HS plays a structural role in the eGlx. Furthermore, heparinase III treated mice had a significant increase in glomerular Ps'alb compared to the inactive enzyme treated group, indicating that loss of HS in the eGlx results in loss of glomerular barrier function. These results are in agreement with previously mentioned work showing that isolated kidneys from mice treated with heparinase III have a significant increase in albumin clearance (35). However, the glomerular albumin permeability assays and eGlx measurements by quantitative EM presented in this thesis are a more direct measurement of definitive eGlx loss and glomerular permeability changes. Loss of eGlx HS contributes to loss of barrier function in other organs as well, as was demonstrated in isolated perfused heart models, showing that loss of eGlx with heparinase III resulted in reduced endothelial barrier function (205,206). It is likely that this can be applied more widely in multiple vessel beds in which increased permeability

can be observed either experimentally or in disease, such as the retina. Changes in GFB ultrastructure that may contribute to the observed increase in permeability, such as podocyte effacement, fenestration density, or basement membrane thickening were also measured and no significant changes were observed with active enzyme, confirming that the observed changes in permeability can be attributed to loss of HS. It should be noted that as potential changes in HS expression in the GBM were not measured, I cannot conclude that that loss of HS after heparinase III treatment occurs only in the glomerular eGlx. However, since there is evidence suggesting that HS does not contribute to GBM filtration properties (183–185), and the data presented show no changes in GBM structure along with damage to eGlx, it is reasonable that glomerular permeability can be attributed to loss of glomerular eGlx HS. This suggests that HS not only plays a structural role in the eGlx, but also a functional role, establishing the importance of HS in the eGlx.

3.4.2.2 Reduction of HS Synthesis in Ext1 Mouse Model

As a second method of investigating the importance of HS in the eGlx as well as a way to dismiss potential off target effects by enzyme treatment, an inducible transgenic mouse model, in which HS synthesis in endothelial cells can be knocked out by targeting Ext1, was used. A similar mouse model has been previously used, in which Ext1 was knocked out in podocytes, with Cre expression driven by the podocin promoter, a podocyte specific promoter (182,207). Although reduced HS staining was observed in the glomerular capillary wall, the researchers did not observe changes in albuminuria (182). I investigated if reduced endothelial HS synthesis had any effect on barrier function. Previous work by Dr. Sarah Fawaz showed that Ext1 mRNA was significantly reduced in the *Ext1*^{CKO} mice after treatment with doxycycline, evidence of a working model. Surprisingly, immunofluorescence staining for HS in *Ext1*^{CKO} mice did not show an obvious decrease in HS signal in Ext1^{CKO} compared to LMCs. The reasons for these results are not clear, however there are some explanations as to why this may be the case. Firstly, the Ext1 enzyme is involved in chain elongation, as mentioned earlier. The HS3A8V antibody was originally raised against bovine kidney HS (173), but since the exact HS epitope that this antibody recognises in mouse tissue is not known, it's possible that the antibody is detecting segments of HS that are still expressed, such as the GlcNac residues which are present prior to elongation by Ext1 (208). Therefore, in *Ext1*^{CKO} mice, this pre-elongation segment may be recognised by the antibody. Perhaps a more broad HS staining antibody, such as the antibody clones JM403 and 10E4, which recognize common epitopes on HS (209,210), would reveal changes in HS between control and *Ext1*^{CKO} mice. It may also be

that this method of HS detection simply is not sensitive enough to detect changes, as this is a conditional knockout, and therefore HS is still likely present in a population of endothelial cells. In addition, other glomerular cells such as podocytes and mesangial cells still have the capacity to synthesise HS, which may prevent changes in HS expression from being easily observed. Lastly, it is possible that HS synthesis is not reduced, but the structural and functional results that followed suggest that this is likely not the case.

EM results showed that *Ext1*^{CKO} mice had a significant reduction in glomerular eGlx depth and coverage but not pGlx, suggesting a structural role for HS in the eGlx and is in agreement with heparinase III treatment studies. Additionally, *Ext1*^{CKO} had no changes in GFB unstructured, indicating that knockout of Ext1 did not negatively impact the GFB ultrastructure. *Ext1*^{CKO} mice also had a significant increase in glomerular Ps'alb, again agreeing with the heparinase III studies and the indication that HS contributes to glomerular eGlx barrier function.

Interestingly, when albuminuria was measured in *Ext1*^{CKO}, there was no significant increase compared to LMC. Because an increase in permeability was observed in the *ex vivo* glomerular permeability assays in *Ext1*^{CKO} mice, we argued that changes in albuminuria were masked by tubular reabsorption and therefore confounded results. In line with this thought, the previously mentioned heparinase III whole perfused mouse kidney studies in which increased albumin clearance was observed, kidneys were kept at 8°C to inhibit tubular function (170). Similarly, the same authors observed increased albumin clearance in mice treated with hyaluronidase and chondroitinase using the same technique, but unpublished work by our group showed long term exposure of mice to these enzymes did not yield changes in albuminuria. These two contradicting results may be due to the fact that our studies were performed under conditions in which tubular function was normal, and no treatment was given to inhibit tubular reabsorption, whereas in the perfused mouse kidney study, tubular function was inhibited by cooling the kidney.

To test this theory, I first optimised treatment with L-Lysine in normal FVB mice. Although several studies have used L-Lysine and it is acknowledged as a potent tubular reabsorption inhibitor (204,211,212), the exact mechanism remains unknown. There is some evidence suggesting that L-Lysine acts by binding to negative sites on the tubular cell surface (213). This may inhibit the proposed initial event required for tubular reabsorption, in which a positive amino- or guanidino- group from proteins binds to the negative sites on tubular cell surfaces (213). In other words, L-Lysine masks the protein binding surface for proteins

to be absorbed. In FVB mice, I confirmed that treatment with L-Lysine successfully blocked tubular reabsorption, as an observed increase in albuminuria was seen after L-Lysine treatment. I also treated FVB mice with eGlx shedding enzymes to investigate potential changes in albuminuria when tubular reabsorption was blocked, and indeed observed that mice treated with enzyme + L-Lysine had a significant increase in albuminuria compared to baselines, while the enzyme only treated group did not, suggesting that tubular reabsorption masked increases in albuminuria in the previous enzyme treatment work by our group. Of note, mice treated with L-Lysine and enzymes were treated with L-Lysine while still under anaesthesia, therefore results from the initial FVB and L-Lysine only treated mice discussed above cannot be directly compared. It would be beneficial to this study to have an additional L-Lysine only treatment group in which mice are treated under the same conditions.

In the Ext1 model, *Ext1*^{CKO} mice treated with L-Lysine had a significant increase in albuminuria compared to pre-treatment urines, while LMC mice did not. This may explain why in the absence of tubular reabsorption, as is the case with the *ex vivo* glomerular permeability assays, *Ext1*^{CKO} mice did show an increase in albumin permeability. However *in vivo*, where tubular reabsorption is active, this data suggest that increased levels of albuminuria are sufficiently reabsorbed by the proximal tubules to mask an observable increase in the urine but can be revealed by blocking tubular reabsorption. Together, these data serves as evidence for a structural and functional role of HS in the glomerular eGlx and demonstrates that loss of HS can have detrimental effects on glomerular barrier function.

3.4.3 Conclusions and Significance

The work presented in this chapter establishes an important role for HS in the glomerular eGlx which was previously not known. This work shows for the first time, that HS is present in the glomerular eGlx. Additionally, the structural and functional studies looking at the effects of the loss of HS, both by enzymatic removal and by use of a transgenic mouse model, demonstrate that loss of HS is detrimental to the eGlx and GFB integrity, resulting in increased permeability. This work lays a foundation for investigating the role of HS in vascular diseases in the kidney, such as diabetic nephropathy, where damage to the eGlx and increase vascular permeability is also observed.

Chapter 4 Loss and Restoration of Glomerular Endothelial Glycocalyx Heparan Sulphate in a Type 2 Diabetic Mouse Model

4.1 *Introduction*

4.1.1 Mouse Models of Diabetic Nephropathy

4.1.1.1 Motivations for Choice of Diabetic Mouse Model

As stated in **CHAPTER 1**, the goal of this thesis is to determine if preventing HS degradation in diabetes prevents the development of associated microvascular diseases such as DN and DR. As the ultimate goal is to find a therapeutic treatment that can be used for all microvascular complications in diabetes in the same patient, it was important to choose a mouse model which recapitulated aspects of both DR and DN seen in humans. Since the focus of this thesis is the role of HS in eGlx permeability barrier, increased permeability in the respective vessel beds was a major focus for choosing a mouse model in which both microvascular diseases can be studied. Therefore, although there exist good models for studying DN and DR individually, I chose a model in which the hope was that both diseases could successfully be investigated in parallel.

4.1.1.2 Common Mouse Models of Diabetic Nephropathy

While tissue culture techniques are valuable and necessary in studying cellular responses to stimuli, mouse models have become an invaluable tool in many research fields, allowing researchers to investigate the complexity of various disease in a living organism and the development of novel treatments. In diabetes research, inducible and genetic models of diabetes are used to study the development and treatment of this disease. This section will cover mouse models of DN, however it should be noted that there are many models that are used in diabetes research and these are only a few of the common models used in DN research.

One of the most common inducible models used to study diabetes is streptozotocin (STZ) induced diabetes. This involves injecting rodents with STZ, a chemical that leads to the destruction of β-cells. In humans, T1D is a chronic autoimmune disorder, caused by the body's immune system attack on the β-cells located in the islets of Langerhans in the pancreas (62). Because β-cells are the body's insulin producing cells, T1D results in diminished insulin production resulting in decreased glucose uptake and increased

hyperglycaemia. The STZ model therefore serves as a classic model for T1D. Importantly, the mouse background chosen for this model has a substantial effect on the phenotype observed. For example, the DBA/2 strain of mice are widely used for DN, and exhibit albuminuria 5 weeks after of induction of diabetes with STZ, and continue to progress, showing more marked albuminuria by 25 weeks (214). This model also exhibits classic pathological features associated with DN in humans, including GBM thickening, severe mesangial expansion, and glomerulosclerosis by 25 weeks of diabetes (215). STZ DBA/2 mice also have a high mortality rate of 40% after 25 weeks (215). The common laboratory mouse strain, C57BL/6, on the other hand is largely resistant to DN and renal injury, developing only mild to moderate albuminuria 6 months after development of diabetes (216). Pathological features such as glomerular hypertrophy, GBM thickening, and mild to moderate mesangial expansion are observed more than 6 months after diabetes is induced and mice can live for more than 45 weeks after the onset of hyperglycaemia (214), making it a less severe model of DN. However, one drawback to the STZ model is the non-specific kidney toxicity that can occur 6 to 48 hours after STZ injections (217). Researches have combatted this by giving multiple low dose injections of STZ rather than one large dose, and while this does seem to mitigate some of the toxicity observed in the high dose model, adjustments for individual strains have to be made as susceptibility to β-cell injury and non-specific toxicity can vary (218,219)

A common genetic model for T1D is the Insulin-2 *Akita* mouse (*Ins2*^{Akita}). This model has a mutation in the Insulin-2 gene, resulting in misfolding of insulin-2, which consequently causes β cell-selective proteotoxicity (220). Mice with homozygous mutations die within 1 to 2 months, but heterozygous mice develop hyperglycaemia and polyuria at 3-4 weeks of age (217). As with the STZ model, the background on which the Ins2^{Akita} mutation is used determines the susceptibility to DN. On a C57BL/6 background, mice are mildly resistant to DN and the associated glomerular changes that are seen in humans, with only mild development of albuminuria (221). Alternatively, on a DBA/2 or FVB/NJ background, mice develop substantial albuminuria, with some changes to renal structure in the FVB/NJ mouse such as mesangial expansion, but not in DBA/2 mice (222).

LepR^{db} */LepR*^{db} mice (*db/db*) are another genetic model of diabetes, where mice homozygous for the leptin receptor point mutation results in susceptibility to obesity and insulin resistance (223). In humans, major risk factor for T2D is obesity. Because obesity causes a low but chronic level of inflammation, inflammatory molecules/processes lead to β-cell dysfunction and eventual cell death (64). In addition, continuous increased levels

of glucose in the blood stream persistently stimulates insulin production by β-cells, and subsequent development of insulin resistance by glucose recipient organs (64,65). *Db/db* mice are therefore a model of T2D. *Db/db* mice develop many of the phenotypes observed in T2D, including hyperglycaemia, hyperinsulinemia, and morbid obesity by 4-8 weeks of age (224). Again as with previous mentioned models, severity of disease and phenotype vary from strain to strain and can also be dependent on sex, in part due to differences in estrogen levels which plays a role in insulin sensitivity (225), with male mice exhibiting more robust diabetic phenotypes (217). Male mice on a C57BLKS/J (BKS) background develop symptoms of early stages of DN such as moderate albuminuria by 8 weeks of age, while C57BL/6 mice have minimal changes (215,226). However, unlike other more severe models of DN such as the DBA/2 T1D model, *db/db* mice on a BKS do not have a consistent increase in albuminuria, as levels remain similar from 8-25 weeks (227,228). Additionally, BKS *db/db* (*db/db*) mice have a 20-30% increase in glomerular size by 2 to 4 months of age. As in humans, this is likely due to early changes in glomerular hemodynamics that coincide with hyperfiltration and mesangial expansion (90,229). Loss of podocytes and GBM thickening have also been reported in this model by 12 weeks 16 weeks, respectively and (230,231) , serving as further indications of changes in the GFB. These mice, however, fail to develop any of the more advanced features of DN such as mesangiolysis, nodular mesangial sclerosis, and tubulointerstitial fibrosis, which therefore makes *db/db* mice a good model for early changes in DN. Importantly for this thesis, in which the goal is to show protection from early changes in microvascular disease in different vessel beds, *db/db* mice also develop some early signs of DR, which will be discussed in detail in **CHAPTER 6**. In addition, T2D is now considered a global epidemic affecting all parts of the world, and is also major economic burden, costing the NHS £8.8 billion a year, alone (61,232). It is therefore crucial to find both preventative and effective therapeutic treatments for T2D, with the aim that treatment can be translated to T1D. Therefore, given the evidence for T2D *db/db* mice serving as a good model for early DN as well as DR, I chose to use this model for my investigations. Because I am interested in early changes in the microvasculature, I used two times points of 9 weeks and 11 weeks of age to investigate loss and restoration of eGlx, as the literature suggest mice at these ages develop early signs of DN with moderate albuminuria and some structural changes associated with DN, described above.

4.1.2 Heparanase and Its Role in Health and Disease

4.1.2.1 Heparanase Synthesis

As mentioned in **CHAPTER 1**, heparanase (HPSE) is the only known mammalian endoglycosidase that directly targets HS for degradation. HPSE is encoded by the gene HPSE1,and is synthesised as an enzymatically inactive 68kDa pre-proHPSE, which is targeted to the endoplasmic reticulum through its N-terminal signal peptide (25). Here, it is cleaved to produce the 65kDa proHPSE, which still lacks enzymatic activity. ProHPSE is then shuttled to the Golgi apparatus and secreted (233). Secreted proHPSE is capable of binding to extracellular components such as HSPGs and mannose-6-phosphate receptors, causing it to be internalized into the cell into latent endosomes and lysosomes (234). It is in the lysosomes where the active enzyme HPSE is activated by lysosomal cathepsin L, which excises a 6kDa linker peptide on proHPSE, forming a noncovalent heterodimer (8kDa and 50kDa) (235). Studies show that the 8kDa peptide is required for enzymatic activity, as the 50kDa chain is not active on its own (236). HPSE is then largely retained in intracellular compartments in fibroblasts and neutrophils, where it can be released upon internal or external signals either in health or disease.

4.1.2.2 Heparanase in Health

In normal conditions, active HPSE is expressed in few tissues and does not seem to have any essential roles. ProHPSE has a role in angiogenesis, cell proliferation, and tumorigenesis, through its binding of receptors on the cell surface which can lead to Akt, p38, and Src activation (237). Active HPSE however is largely restricted to placental and skin tissue (238,239). In placental tissue HPSE plays an important role in angiogenesis, embryo implantation, and placentation (239). It is also active in blood-borne cells such as platelets, neutrophils, monocytes, and mast cells, where it is stored in granules and is implicated in diapedesis and extravasation of immune cells (164,240–242). Because of its HS degradation activity, HPSE expression and activity is tightly regulated, as degradation of HS in extracellular matrixes and eGlx can release a pool of cytokines, growth factors, and enzymes which can affect cell and tissue function (187,240). HPSE expression and activation is also largely modulated by pathophysiological conditions, such as pH. In neutral conditions, HPSE is essentially inactive (243). However, under acidic conditions such as those found in inflammatory states, enzymatic activity is increased, with pH 5-6 being optimal for enzymatic activity (243). Because of its restricted expression and lack of activity in normal conditions, the focus of HPSE research has primarily been in its role in disease.

4.1.2.3 Heparanase in Diabetic Nephropathy

A large part of HPSE research has focused on its role in cancer progression, and upregulation of HPSE has been shown in a number of cancers, associated with increased metastasis (244). However, HPSE is now known to be upregulated in several diseases and, as previously mentioned, includes inflammatory and proteinuric diseases such as IgA nephropathy, membranous glomerulopathy, and DN (169). HPSE is now known to be upregulated in diabetes and increased levels have been found in urine and plasma from T1D and T2D (110,245,246). It is also upregulated in renal biopsies from DN patients in glomeruli and proximal tubules and increased HPSE activity was found in podocytes from T1D patients (109,247). Furthermore, reduced GBM HS is associated with increased HPSE expression in DN (248), but the effect on the eGlx HS has not been investigated. In laboratory studies, HPSE is increased in T1D and T2D DN rodent models (114,249,250). A previously mentioned study in **CHAPTER 1** showed that HPSE knock out mice did not develop DN when diabetes was induced with STZ, and had reduced albuminuria (114). Additionally, pre-treatment with Hyperoside, an active flavone glycoside, in T1D mice prevented progression of DN, showing reduced albuminuria and inhibition of increased HPSE expression in podocytes (249). As with humans, HPSE expression is associated with reduced glomerular HS in rodent models, but no work has been published looking at its effect on eGlx (109,249). Together, this data is strong evidence for the role of HPSE in DN and its contribution to the development of increase glomerular permeability. However, the focus of these studies has been largely on GBM HS, and the effect of HPSE on eGlx in diabetes, which is known to contribute to vascular permeability, has yet to be elucidated.

4.1.3 Use of Heparnase Inhibitors in Disease

4.1.3.1 Use of Currently Available Heparanase Inhibitors in Disease

HPSE inhibitors are currently a popular topic in the treatment of malignant and metastatic tumours. Two major events that occur during metastasis are the breakdown of the ECM and the development of new blood vessels, *i.e* angiogenesis, that nourish the tumour and allow it to survive and grow (251). HPSE is involved in both processes and is upregulated in many types of cancers such as myelomas, gliomas, and breast cancers, and is associated with poor prognosis (252–254). In fact, HPSE expressing tumour cells show an increase in metastatic potential (251,255). Importantly, because HPSE is not typically expressed in the majority of non-diseased tissue, treatment with inhibitors have so far shown to have minimal side effects (168,256). Indeed, transgenic C57BL/6 mice that have HPSE knocked out appear to be entirely normal, and mice are fertile, exhibit a normal life span, and have

no prominent pathological alterations (257), suggesting HPSE may be a good target in disease.

Use of the HPSE inhibitor SST0001 has shown to slow tumour progression in myeloma studies, both in *in vivo* laboratory models as well as *in vitro* (258) . The same inhibitor was also shown to have antitumor effects in a lymphoma and paediatric sarcoma mouse models (259). Similarly, PG545, PI-88, and M104 have all been used in *in vitro* or *in vivo* laboratory studies and shown antitumor effects (260–262).

Although the upregulation of HPSE in diabetes is also well established, there are fewer studies which have investigated the benefits of HPSE inhibitor treatment for DN. SST0001 has been used in T1D and T2D DN models showing reduced albuminuria in inhibitor treated animals (114). PI-88 was also used in a non-obese diabetic (NOD) T1D model and showed that treatment reduced the incidence of diabetes by 50% (263). Sulodexide, a therapeutic drug made from a mixture of heparin and dermatan sulphate, has also been used to treat T1D rats, resulting in reduced urine protein excretion as well as a decrease in pathological changes due to DN, compared to untreated rats (264). Although Sulodexide is not classified as a HPSE inhibitor, it does appear to possess some enzymatic inhibition properties due to its heparin component (162). However, none of these studies have specifically addressed the impact of HPSE inhibitor treatment on the GFB eGlx and HS.

4.1.3.2 Structure of Currently Available Heparanase Inhibitors

Most of the available HPSE inhibitors are modified natural heparin molecules or semi synthetic compounds which have been designed to closely resemble heparin's structure, a linear polysaccharide, while removing its anticoagulant activity (265). For example, the HPSE inhibitor PI-88 is isolated from yeast, which is comprised of a mixture of chemically highly sulfonated mannan oligiosaccharides (262,266,267). PI-88 has shown antiangiogenic and antimetastatic activity, and has gone through several phase I and phase II trials (256). SST0001 and M402 are modified natural heparin molecules, which have been altered to remove most of the anticoagulant activity and have also undergone clinical trials showing antimetastatic and antitumor effects (168,256). PG545 is regarded as the most potent inhibitor, likely attributed to the two sites on HPSE to which it can bind and inhibit HPSE enzymatic activity (268). Though so far proven effective, currently available HPSE inhibitors still have some major pitfalls. PG545 and M402 still retain significant anticoagulant activity (269,270). SST0001 and M402 are also made of complex

mixtures, and methods required to characterise batch-to-batch variation for FDA approval are costly (271) . These factors have led the development of new and improved HPSE inhibitors with unique structures that allow for more uniform and cost-effective production while retaining potency.

4.1.3.3 New Dendrimer Heparanase Inhibitors

The development of dendrimers for drug delivery has gained interest as they are versatile in drug delivery with high functionality (272). Unlike linear polysaccharides, dendrimers are known for their defined structures (272) **(FIGURE 4-1)**(273), which lend themselves to not only function as will be discussed, but also ease of characterisation for batch-to-batch variation.

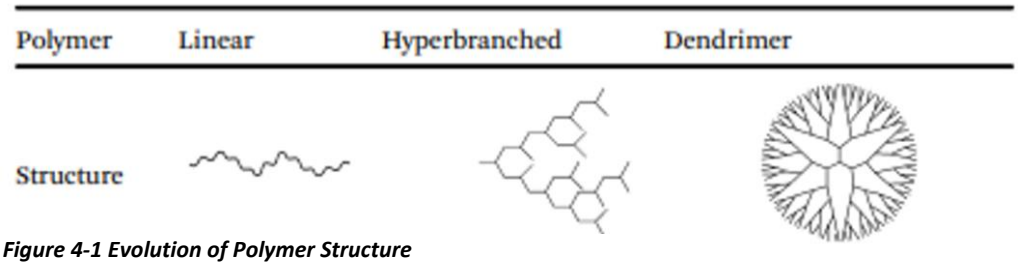

Figure 4-1 Evolution of Polymer Structure

Linear and hyperbranched polymers have disorganized structures, whereas dendrimers have highly defined organized structures. Image adapted from (Zheng et al. 2015)(273).

Dendrimers are highly branched ''globular'' structures, which have layers between each cascade point known as ''generations'' **(FIGURE 4-2)** (272). With each generation, the size

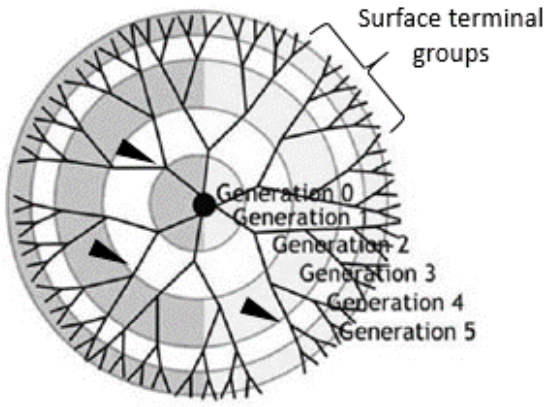

Figure 4-2 Structure of Dendrimer Molecules

The highly branched dendrimer structure has layers referred to as generations, between each cascade point (arrowheads). Each generation increases the number of surface terminal groups where the target molecule interacts. Image adapted from (Madaan et al, 2014)(272).

of the molecule and terminal surface group is increased, allowing for multiple points of interaction with the target molecule (272,274).

Our collaborator, Dr. Olga Zubkova at Victoria University of Wellington, has developed a dendrimer, OVZ/HS-1638, in which the dendrimer itself has HPSE inhibitory properties, without acting as a drug delivery system. The inhibitor is made of single-entity HS glycomimetic clusters, capped with sulphated saccharides, glucose, and maltose **(FIGURE 4-3)** (271). Importantly, this inhibitor was shown to have similar potency as PG545, with IC_{50} values of 11nM and 8nM respectively, and with a significant lack of anticoagulant activity compared to other inhibitors such as PG545 and M410 (271). It was also tested *in vivo* in an aggressive myeloma mouse model and resulted in a significant reduction in tumour spread (271). Given the role of HPSE in DN and the initial success/ apparent superior properties of this inhibitor, we investigated if use of this novel inhibitor would prevent eGlx damage and associated increase in microvascular permeability by preventing HS degradation. Additionally, if proven effective, the work on other HPSE inhibitors already in clinical trials has paved the way for the use if this type of therapy in humans, making this inhibitor clinically relevant.

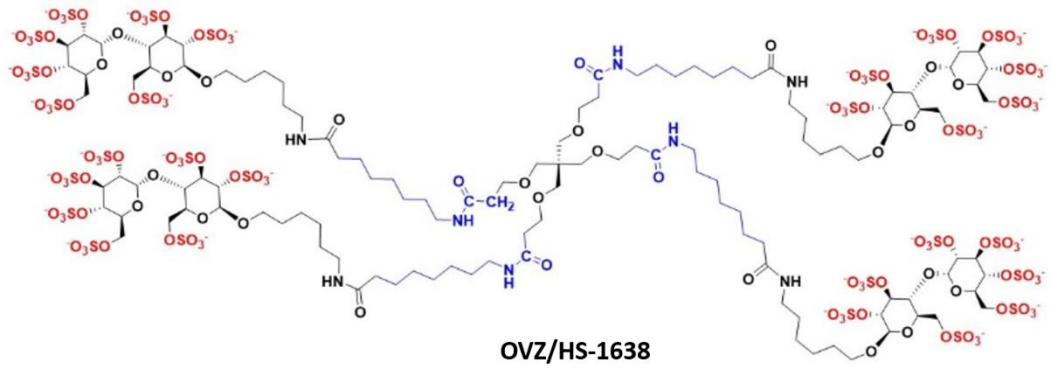

Figure 4-3 Structure of OVZ/HS-1638

OVZ/HS-1638 is a dendrimer heparanase inhibitor. This compound is highly branched, allowing for multiple interaction points. The compound is capped with sulphated groups which contribute to its potency. Image adapted from (Zubkova et al., 2018)(271).

4.1.4 Chapter Aims and Experimental Approaches

The aim of this chapter is to show that loss of HS, and consequently damage to eGlx due to upregulated levels of HPSE in DN, can be prevented by treatment with a novel HPSE inhibitor, OVZ/HS-1638. The aims to accomplish this were as follows:

1. Show that glomerular eGlx is damaged in a T2D mouse model which results in loss of eGlx function and associated increased glomerular permeability. This was done at two different timepoints, 9 weeks of age and 11 weeks of age.
2. Show that damage to the glomerular eGlx can be restored by preventing HS degradation through treatment with OVZ/HS-1638, resulting in restored eGlx function and decreased glomerular permeability. This was done at two different timepoints, 9 weeks of age and 11 weeks of age.

4.2 *Methods*

These methods are not inclusive. The methods described in this section are those that pertain specifically to this chapter or have been adapted for experiments in this chapter. All other methods are described in the **CHAPTER 2 METHODS AND MATERIALS**.

4.2.1 Study Design Nine-Week-Old Time Point

At 7 weeks of age, lean control and *db/db* control mice were administered vehicle treatment (PBS), daily for two weeks subcutaneously (s.c.). Similarly, OVZ/HS-1638 group received daily injections for two weeks of OVZ/HS-1638 dissolved in PBS at 20mg/kg, s.c. Blood glucose was measured weekly and urine was collected at end point for uACR measurements as described in **CHAPTER 2**. Mice were anesthetised and perfused as described in **CHAPTER 2** for glomerular permeability studies and EM imaging. A schematic of the experimental design is shown in **FIGURE 4-4**.

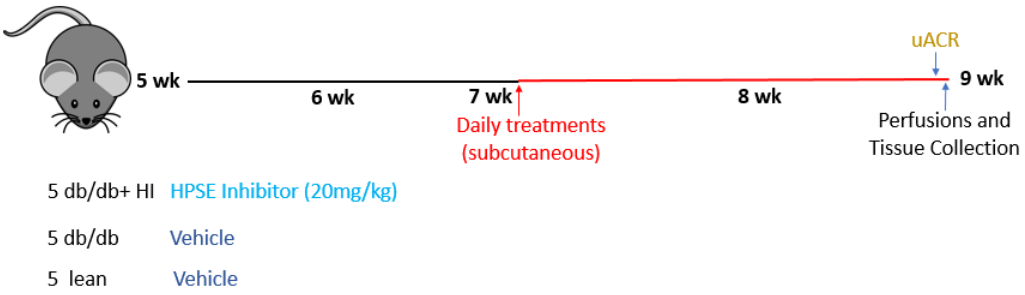

Figure 4-4 Study Design for Nine-Week-Old Time Point

At 7 weeks five lean and five db/db mice were treated with vehicle s.c. Five db/db mice were treated with 20mg/kg OVZ/HS16-38 heparanase inhibitor (HI) in vehicle, also by s.c. At 9 weeks mice were cardiac perfused and tissue collected as in methods.

4.2.2 Study Design for Eleven-Week-Old Time Point

At 9 weeks of age, lean control and *db/db* control mice were administered PBS vehicle treatment daily for two weeks i.p. Similarly, OVZ/HS-1638 group received daily injections for two weeks of OVZ/HS-1638 dissolved in PBS at 20mg/kg by i.p. Blood glucose was measured weekly and urine was collected at end point for uACR measurements as described in **CHAPTER 2**. Mice were anesthetised and perfused as described in **CHAPTER 2** for glomerular permeability studies and EM imaging. A schematic of the experimental design is shown in **FIGURE 4-5**.

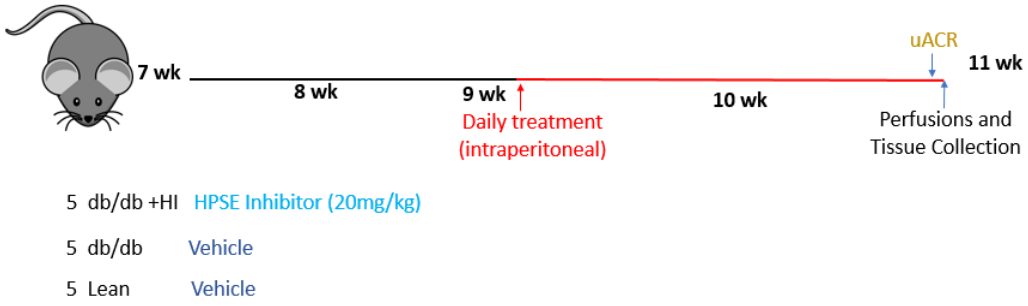

Figure 4-6 Study Design for Eleven-Week-Old Time Point

At 9 weeks five lean and five db/db mice were treated with vehicle by i.p. injection. Five db/db mice were treated with 20mg/kg OVZ/HS16-38 in vehicle, also by i.p. At 11 weeks mice were cardiac perfused and tissue collected as in methods.

4.2.3 Immunofluorescence for HPSE in Mouse Kidney

Kidneys were flash frozen in liquid nitrogen, embedded in O.C.T. Compound (23-730-571, Fisher Scientific), and sectioned at 5µm on cryostat and mounted onto superfrost slides for staining. Slides were airdried for 15 minutes and fixed in 4% PFA for 15min and washed in PBS, three times for 5min. Sections were blocked in 3%BSA/0.3% Triton-X for an hour. Primary antibody anti-HPSE Rabbit 1:100 (16673-1-AP, Proteintech) and matched rabbit IgG control was added in block solution at 4°C overnight. Slides were washed in PBS, three times for 5min. Secondary goat anti-rabbit Alexa Fluor 594 (A-11037, ThermoFisher) was applied for 1 hour at 1:200 at room temperature. Slides were washed in PBS, three times for 5min and counterstained with DAPI as described in main methods. Slides were washed two times for 5min and coverslips were mounted with Vectashield (H-1400, Vector Laboratories).

4.2.3.1 Imaging and Analysis of Total HPSE in Mouse Kidney

Images were taken on Leica DM2000 microscope (Leica Microsystems) using 20X objective, using TRICT filter (HPSE staining) and DAPI filter (nuclear staining). Images were analysed on FIJI. On DAPI images, the entire image was measured for area, mean gray value, and integrated density (IntDen) using a rectangular selection tool. Four background measurements were taken as well. CTCF was calculated as described in **CHAPTER 2**. The same measurements were taken for corresponding TRITC images and CTCF calculated for HPSE as previous with DAPI. To calculate total kidney HPSE, CTCF values for HPSE were normalised to DAPI. CTCF values were averaged for each group. A minimum of three field of view were taken for each animal.

4.2.4 Periodic Acid-Schiff Staining on Mouse Kidney

Kidney was fixed in 4% PFA for minimum of 24 hours, paraffin embedded, and sectioned at 5μm at The University of Bristol Histology Lab. For immunofluorescence, slides were deparaffinized two times in Xylenes for 10 minutes. Slides were rehydrated by sequential 5min incubations in decreasing ethanol concentrations: 100% twice, 95%, 70%, and 50%. Slides were incubated in deionized water for 5min. Periodic Acid-Schiff (PAS) kit (395b-1KT, Sigma-Aldrich) was used to stain slides following manufacturer's instructions. Slides were coverslip mounted in DPX Mountant (06522-100ML, Sigma-Aldrich).

4.2.4.1 PAS Slide Imaging and Analysis

Bright field images were taken on Leica DM2000 microscope (Leica Microsystems) with 40X objective. Images were quantified with FIJI using the H-PAS colour deconvolution plugin. Pink images were inverted and converted to 8-bit images. Using the Freehand selection tool, glomeruli perimeters were traced and the Analyse tool was used to obtain area, mean gray value, and integrated density value for each image. Four background values were obtained similarly, and the background mean grey value was calculated for each image. CTCF values were calculated as previous. Minimum of six glomeruli were analysed per mouse, and mean CTCF values were calculated for each mouse.

4.2.5 Heparan Sulphate Depth Measurements on Heparan Sulphate Stained Mouse Kidney

The technique described has been previously used and validated against EM to measure changes in eGlx depth with lectin staining (108). Briefly, confocal images were taken using the Multi-Laser CLSM Leica SP5 provided by University of Bristol Wolfson Bioimaging Facility. Slides were imaged using 100X oil immersion objective, with camera resolution

set to 2048x2048. Images were analysed using FIJI and a macro developed by a PhD student in the lab, Dr. Colin Down, M.D. with technical support from University of Bristol Wolfson Bioimaging Facility. FITC filter images (HS staining) and TRITC filter images (R18, cell membrane staining) were opened on FIJI. Using the macro, the centre of the capillary was marked by measuring the longest and shortest diameter of the capillary **(FIGURE 4-8 A)**. The macro then took 200 measurements (number set by user) of peak intensity profiles for the R18 and HS staining around the entire capillary **(FIGURE 4-8 B)**. The distance of the two peaks were then calculated and is representative of eGlx depth, or in this case, HS depth **(FIGURE 4-8 C)**.

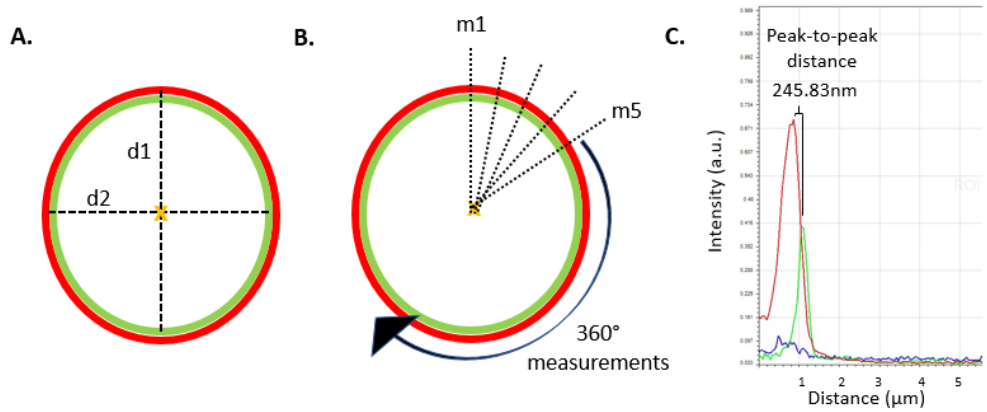

Figure 4-7 Analysis of HS Depth from HS Immunofluorescence.

A. The longest diameter (d1) and shortest diameter (d2) is set by user, which results in a marking of the centre of the capillary (yellow x). B. The macro takes 200 measurements (m1, m5) of peak intensity in at increments of equal distance around the entire capillary. C. Example of peak intensity profiles for green signal (HS) and red signal (cell membrane). The distance between the two peaks represents HS depth.

4.2.6 Diabetic Mice at Nine Weeks of Age

4.2.6.1 Db/db Mice Have Increased Weight which is Not Affected by OVZ/HS-1638

To ensure that diabetic mice were progressing as expected, mouse weights were taken daily from the time of treatment. As expected, *db/db* mouse weights were higher compared to lean controls **(FIGURE 4-9)**. Additionally, treatment with OVZ/HS-1638 did not affect mouse weights in *db/db* mice compared to db/db mice treated with vehicle **(FIGURE 4-9)**.

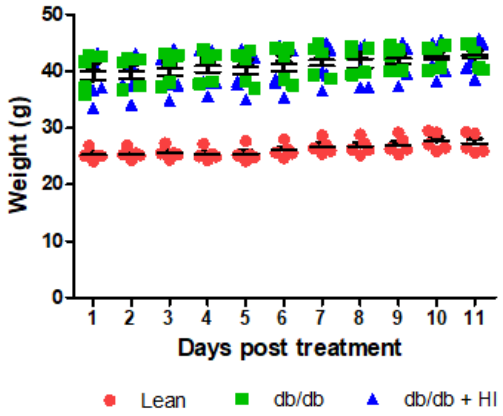

Figure 4-9 Db/db Mice Have Increased Body Weight and is Not Affected by HPSE Inhibitor Treatment

Mouse weights taken daily from 7 to 9 weeks of age in non-diabetic(lean), diabetic (db/db) mice, and db/db mice treated with OVZ/HS-1638 HPSE inhibitor (db/db+HI).

4.2.6.2 *Db/db Mice Have Increased Blood Glucose which is Not Affected by OVZ/HS-1638 Treatment*

To determine whether *db/db* mice had become hyperglycaemic and confirm that treatment with OVZ/HS-1638 did not affect it, blood glucose levels were taken weekly for all mice. As shown in **FIGURE 4-10**, *db/db* mice had a significant increase in blood glucose levels and was not affected by OVZ/HS-1638 treatment.

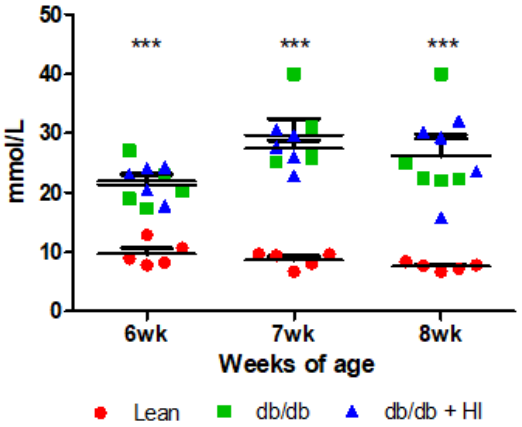

Figure 4-10 Db/db Mice are Hyperglycemic which is Not Affected by HPSE Inhibitor Treatment

Blood glucose levels were measured weekly in non-diabetic (lean), diabetic (db/db) mice, and db/db mice treated with OVZ/HS-1638 HPSE inhibitor (db/db+HI) to ensure all db/db mice were hyperglycaemic compared to lean controls. N=5 mice, two-way ANOVA, Bonferroni post-test indicated, ***p≤0.001.

4.2.6.3 Nine-Week-Old Db/db Mice Show No Changes in GFB Ultrastructure

To determine whether *db/db* mice had developed changes in GFB ultrastructure associated with DN, EM images from glutaraldehyde/Alcian blue perfused mice were taken and analysed. *Db/db* mice did not have any changes in podocyte foot process width, slit diaphragm width, fenestration density, or basement membrane thickness **(FIGURE 4-11)**, indicating that mice had not yet developed characteristic signs of DN.

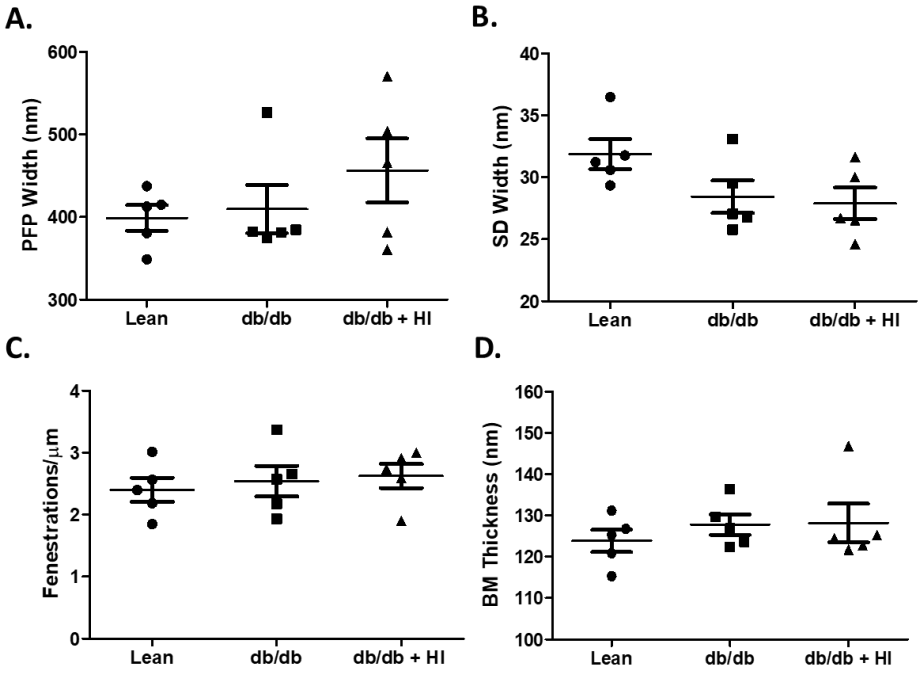

Figure 4-12 Nine-Week-Old Db/db Mice Do Not Show Changes in GFB Consistent With Diabetic

Non-diabetic (lean), diabetic (db/db) mice, and db/db mice treated with OVZ/HS-1638 HPSE inhibitor (db/db+HI) EM images were analysed for changes in: A. Podocyte foot process (PFP) width B. Slit diaphragm (SD) width. C. Endothelial cell fenestration number. D. Basement membrane (BM) thickness. Minimum of 3 capillaries per mouse measured. N= 5 mice, one-way ANOVA, Tukey's multiple comparison test, not significant.

4.2.6.1 Db/db Mice Do Not Have Reduced Glomerular eGlx at 9 Weeks of Age

To determine whether *db/db* mice had changes to the glomerular eGlx at 9 weeks of age, eGlx depth and coverage was measured using quantitative EM images from glutaraldehyde/Alcian blue perfused mice. Contrary to what was expected, vehicle and OVZ/HS-1638 treated *db/db* mice had no changes glomerular eGlx depth or coverage compared to lean **(FIGURE 1-9A,B)**. Furthermore, treatment with OVZ/HS-1638 had no significant effect on eGlx depth or coverage. Similarly, there were no significant changes in pGlx depth or coverage between groups **(FIGURE 4-13 C).**

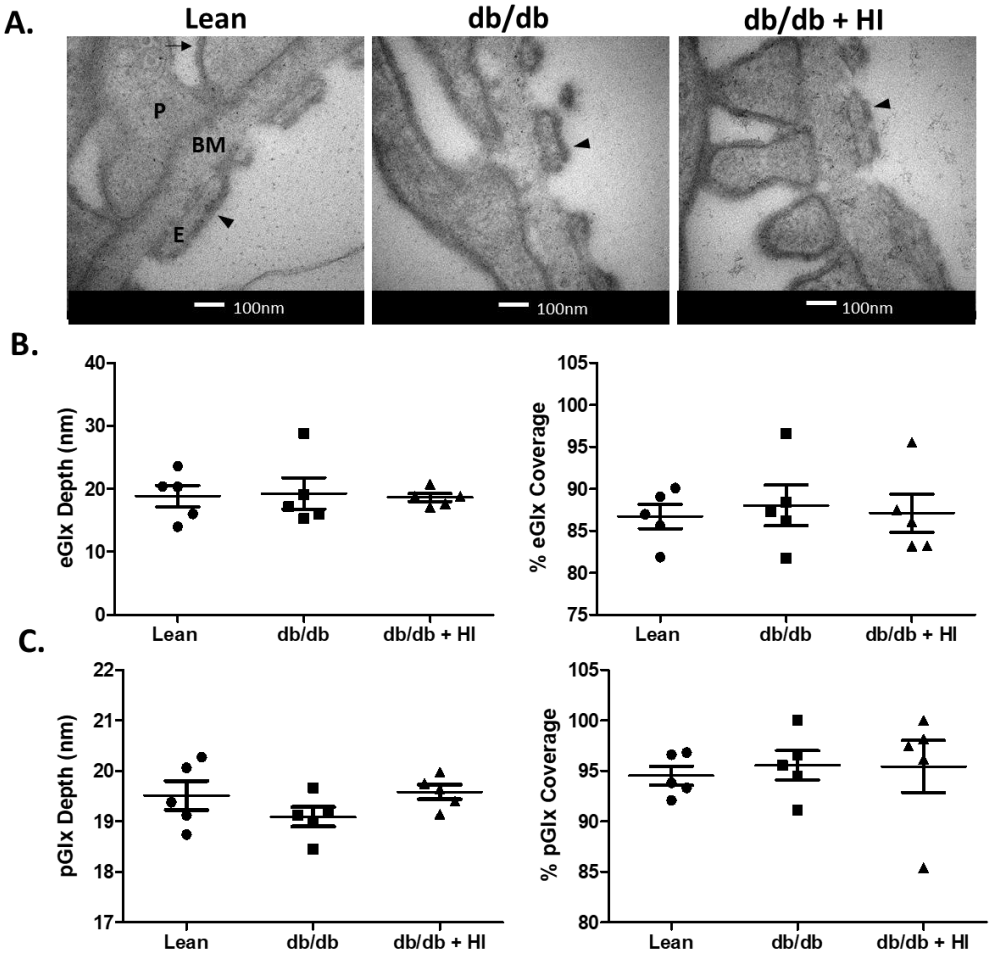

Figure 4-13 Nine-Week-Old Db/db Mice Have No Changes in eGlx or pGlx

A. Representative EM images of GFB from non-diabetic (lean), diabetic (db/db) mice, and db/db mice treated with OVZ/HS-1638 HPSE inhibitor (db/db+HI). Podocyte (P), basement membrane (BM), endothelial cell (E) shown. Arrow points to podocyte glycocalyx and arrowheads point to eGlx. B. EM images were analysed for eGlx depth (left) and eGlx coverage (right). C. EM images were analysed for pGlx depth (left) and pGlx coverage (right). Minimum of three capillaries measured per animal. Minimum of 50 measurements per capillary. N= 5 mice, one-way ANOVA, Tukey's multiple comparison test, not significant.

4.2.6.2 *Nine-Week-Old Db/db Mice Have Increased Albuminuria, which is Not Affected by OVZ/HS-1638 Treatment*

Ultrastructural measurements by EM showed no changes that were suggestive of early signs of DN, as would have otherwise been expected. To determine whether *db/db* mice had any changes to GFB function, albuminuria was measured at end point at 9 weeks of age. Vehicle and OVZ/HS-1638 treated *db/db* mice had a significant increase in albuminuria compared to lean controls, and no significant changes were observed between vehicle and OVZ/HS-1638 treated mice **(FIGURE 4-14)**. This data indicates that *db/db* mice do have changes in GFB function, despite no changes in GFB ultrastructure, but treatment with OVZ/HS-1638 has no affect at this time point.

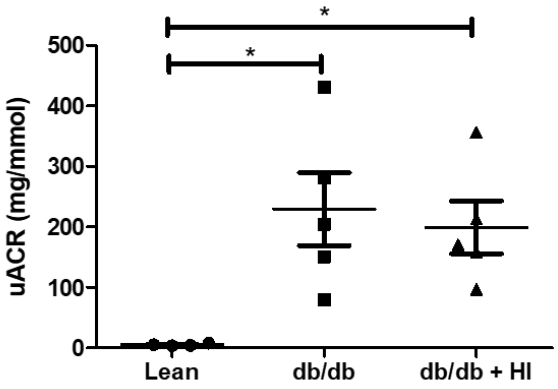

Figure 4-14 Nine-Week-Old Db/db Mice Have Increased Albuminuria which is Not Affected by OVZ/HS-1638 Treatment

Endpoint albuminuria was measured for non-diabetic (lean), diabetic (db/db) mice, and db/db mice treated with OVZ/HS-1638 HPSE inhibitor (db/db+HI) . N= 5 mice, one-way ANOVA, Tukey's multiple comparison test indicated, *p≤0.05.

4.2.6.3 *Vehicle Treated Db/db Mice but Not OVZ/HS-1638 Treated Mice Have Increased Glomerular Albumin Permeability*

As *db/db* mice had increased albuminuria, it would be expected that an increase in glomerular albumin permeability would be observed. To further investigate, glomerular permeability assays, which are more sensitive than uACR measurements, were performed on Ringer perfused isolated glomeruli from lean and *db/db* mice treated with vehicle or OVZ/HS-1638. In agreement with albuminuria data, vehicle treated *db/db* mice had a significant increase in Ps'alb compared to lean controls **(FIGURE 4-15)**. Surprisingly, *db/db* OVZ/HS-1638 treated mice did not have a significant increase in Ps'alb, though a modest increase was observed compared to lean mice **(FIGURE 4-15)**. Treatment with OVZ/HS-1638, however, did not significantly reduce Ps'alb in *db/db* mice at 9 weeks of age.

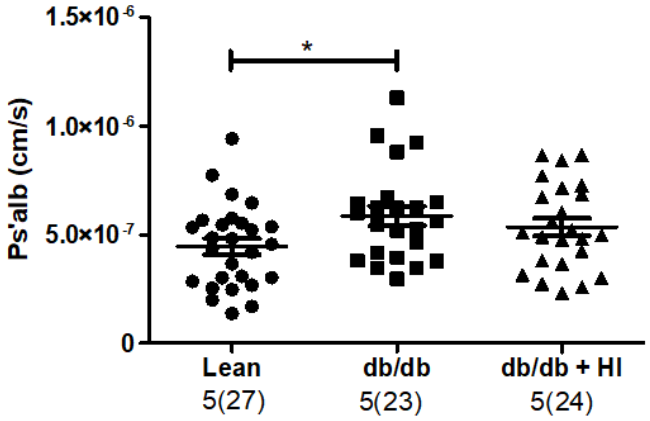

Figure 4-15 Vehicle Treated Db/db Mice but Not OVZ/HS-1638 Treated Mice Have Increased Glomerular Albumin Permeability

Glomeruli were isolated from ringer perfused non-diabetic (lean), diabetic (db/db) mice, and db/db mice treated with HPSE inhibitor (db/db+HI) and glomerular albumin permeability was measured. On x-axis (mouse number (glomeruli analysed)). One- way ANOVA, Tukey's multiple comparison test indicated, *p≤0.05.

4.2.7 Diabetic Mice at Eleven Weeks of Age

4.2.7.1 Db/db Mice Have Increased Weight which is Not Affected by OVZ/HS-1638 Treatment

Data from the 9-week-old cohort suggested that mice had not developed DN to the stage that allowed for detection of eGlx changes. I therefore decided to conduct a similar experiment using a later time point, where *db/db* mice were treated from 9-11 weeks of age. As with the earlier 9-week-old cohort of mice, weights were measured daily from the start of OVZ/HS-1638 treatment to confirm that *db/db* mice were progressing as expected and determine whether OVZ/HS-1638 treatment had any effect on weight gain. As before, both vehicle and OVZ/HS-1638 treated *db/db* mice had increased body weight compared to lean controls **(FIGURE 4-16)**. OVZ/HS-1638 treatment also had no effect on weight gain in *db/db* mice **(FIGURE 4-16)**.

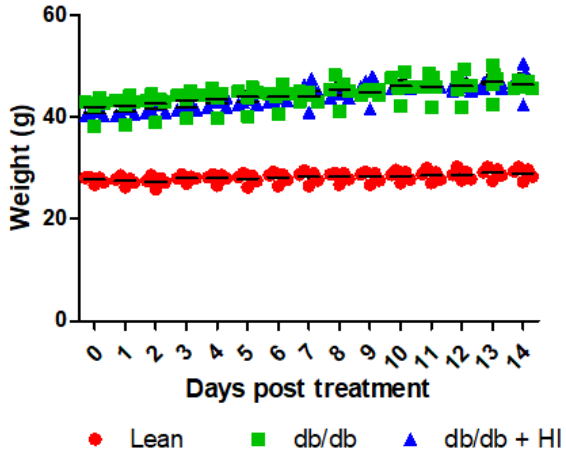

Figure 4-16 Db/db Mice Have Increased Body Weight, which is Not Affected by OVZ/HS-1638 Treatment

Weights were taken daily post treatment (age) to monitor growth progression in non-diabetic (lean), diabetic (db/db) mice, and db/db mice treated with OVZ/HS-1638 HPSE inhibitor (db/db+HI).

4.2.7.2 *Db/db Mice Have Increased Blood Glucose which is Not Affected by OVZ/HS-1638*

To confirm that *db/db* mice were hyperglycaemic and remained so for the duration of the experiment, weekly blood glucose was taken at the start of treatment. As with the 9-week-old cohort, all *db/db* mice had elevated blood glucose which remained elevated for the duration of the experiment with and without OVZ/HS-1638 treatment, compared to lean controls **(FIGURE 4-17)**.

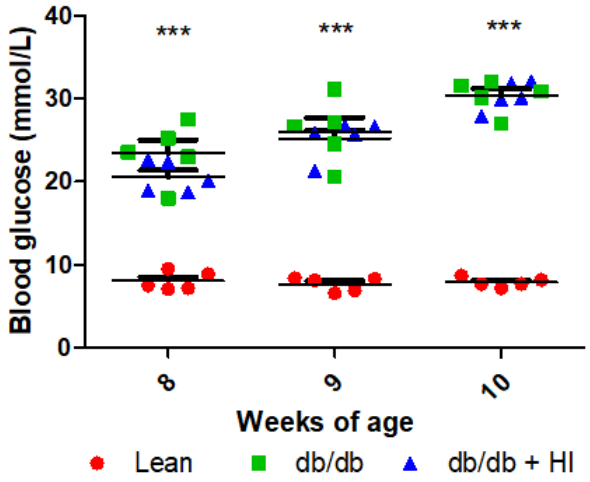

Figure 4-17 Db/db Mice are Hyperglycaemic which is Not Affected by OVZ/HS-1638 Treatment

Blood glucose levels were measured weekly for non-diabetic (lean), diabetic (db/db) mice, and db/db mice treated with OVZ/HS-1638 HPSE inhibitor (db/db+HI) to ensure all db/db were hyperglycaemic. N=5 mice, two-way ANOVA, Bonferroni post-test indicated, ***$p \leq 0.001$.

4.2.7.3 Eleven-Week-Old Db/db Mice Have Increased HPSE Expression in Kidney Tissue

It is well established that HPSE expression is upregulated in diabetes. To confirm that HPSE was elevated in this mouse model at this time point, I performed immunofluorescence staining for HPSE in kidney sections from lean and all *db/db* mice. Staining confirmed that HPSE levels were increased in *db/db* mice compared to lean controls, while *db/db* mice treated with OVZ/HS-1638 had only a modest increase **(FIGURE 4-18 A)**. Images were quantified by measuring CTCF. As shown in **FIGURE 4-18 B**, and in agreement with representative images, *db/db* mice treated with vehicle had a significant increase in HPSE signal compared to lean controls. Interestingly, OVZ/HS-1638 treated mice did not have a significant increase in HPSE signal compared to leans, but was not significantly reduced compared to vehicle treated *db/db* mice **(FIGURE 4-18 B)**.

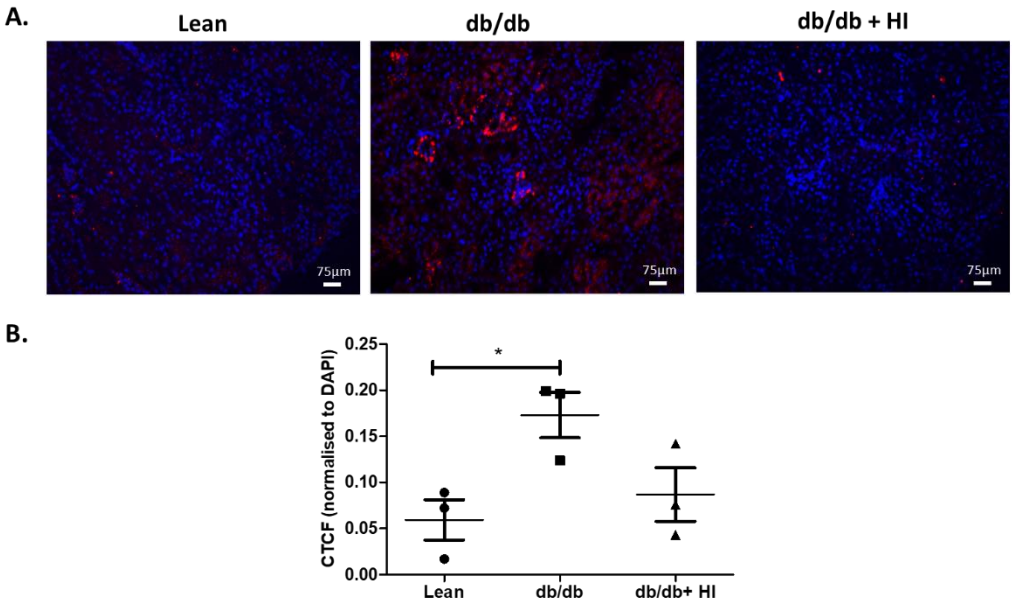

Figure 4-18 Eleven Week Old Db/db Mice Have Increased HPSE Levels in Kidney Tissue

A. Representative immunofluorescent images of HPSE (red) and DAPI nuclear stain (red) in kidneys from non-diabetic (lean), diabetic (db/db) mice, and db/db mice treated with OVZ/HS-1638 HPSE inhibitor (db/db+HI) . B. Total HPSE CTCF was measured and normalised to DAPI. Minimum of three fields of view per mouse analysed. N=3 mice, one-way ANOVA, Tukey's multiple comparison test indicated, *p≤0.05.

4.2.7.4 Eleven-Week-Old Db/Db Mice Have Ultrastructural Changes Consistent with Early Diabetic Nephropathy

To determine whether *db/db* mice had characteristic ultrastructural changes in the GFB at 11 weeks, and therefore an indication that mice had developed DN, podocyte foot process width, slit diaphragm width, fenestration density, and GBM thickness were measured as before using quantitative EM. *Db/db* mice treated with vehicle had a significant increase in podocyte foot process width and decrease in slit diaphragm width, a sign of podocyte effacement **(FIGURE 4-19 A,B)**. While *db/db* mice treated with OVZ/HS-1638 did not have a significant increase in podocyte foot process width, mice did have a modest increase, and had a significant decrease in slit diaphragm width **(FIGURE 4-19 A,B)**. There were no significant changes measured between any groups in fenestration density and GBM thickness.

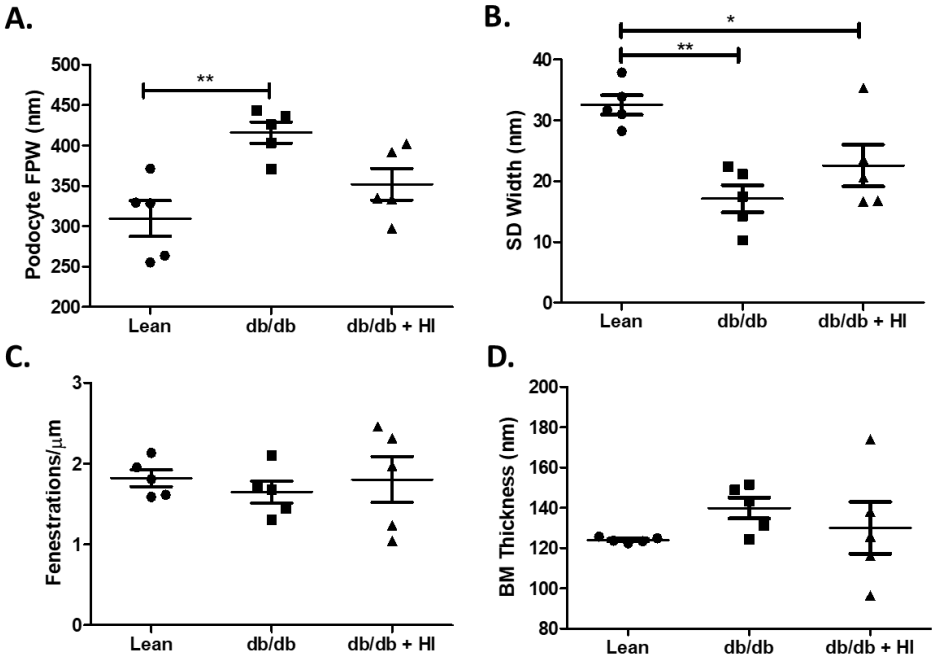

Figure 4-19 Eleven-Week-Old Db/db Mice Show Changes Consistent with Diabetic Nephropathy

Non-diabetic (lean), diabetic (db/db) mice, and db/db mice treated with OVZ/HS-1638 HPSE inhibitor (db/db+HI) EM images were analysed for changes in: A. podocyte foot process (PFP) width B. Slit diaphragm (SD) width C. Endothelial cell fenestration number D. Basement membrane (BM) thickness. Minimum of 3 capillaries per mouse measured. N= 5 mice, one-way ANOVA, Tukey's multiple comparison test indicated, *p<0.05 **p<0.01.

4.2.7.5 Db/db Mice Have Reduced Glomerular eGlx, which is Restored by OVZ/HS-1638 Treatment

Nine-week-old *db/db* mice did not show changes in eGlx depth or coverage, but also showed no ultrastructural changes suggestive of DN. The data so far for 11 week-old-mice suggest a more progressed level of DN compared to the 9-week-old mice. I therefore measured eGlx depth and coverage in 11-week-old mice using quantitative EM as before. As shown in **FIGURE 4-20 A**, *db/db* mice had reduced eGlx compared to lean, with eGlx appearing thinner and more patchy. This was confirmed by quantitative EM, with a significant reduction in depth and coverage **FIGURE 4-20 B**. OVZ/HS-1638 treated mice appeared to have thicker and more evenly spread eGlx, more similar to lean mice. In agreement with this, quantified images showed no significant decrease in eGlx depth or coverage compared to leans, and in fact had a significant increase in eGlx measurements compared to *db/db* mice treated with vehicle **(FIGURE 4-20 B)** . There were no significant changes in pGlx depth or coverage between any groups **(FIGURE 4-20 C)**.

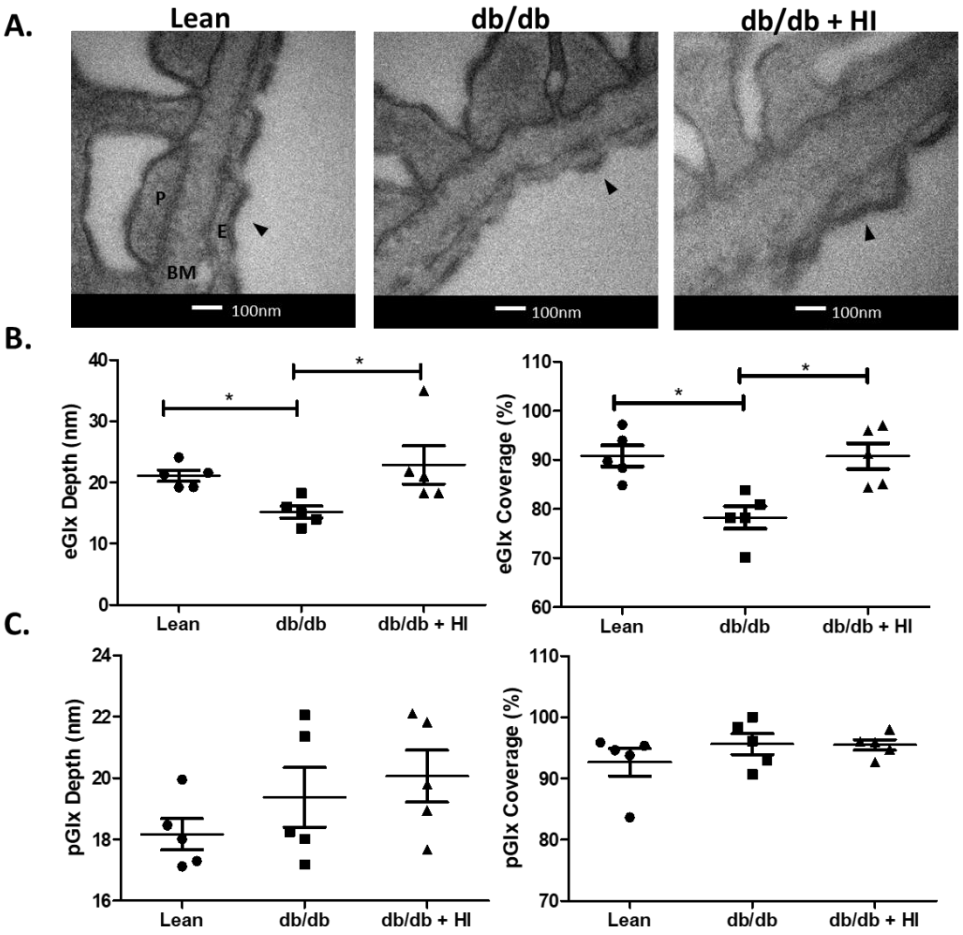

Figure 4-20 Db/Db Mice Have Decreased Glomerular eGlx depth and coverage, which is Restored by OVZ/HS-1638 Treatment

A. Representative EM images of GFB from non-diabetic (lean), diabetic (db/db) mice, and db/db mice treated with OVZ/HS-1638 HPSE inhibitor (db/db+HI) . Podocyte (P), basement membrane (BM), endothelial cell (E) shown. Arrow points to podocyte glycocalyx and arrowheads point to eGlx. B. EM images were analysed for eGlx depth (left) and eGlx coverage (right). C. EM images were analysed for pGlx depth (left) and pGlx coverage (right). Minimum of three capillaries measured per animal. Minimum of 50 measurements per capillary. N= 5 mice, one-way ANOVA, Tukey's multiple comparison test indicated, *p<0.05.

4.2.7.6 *Changes in Heparan Sulphate Cannot be Detected by HS Phage Display Antibody in Db/db Mice*

As HPSE is increased in 11-week-old db/db mice and was associated with decreased eGlx, I investigated whether mice also had reduced HS in glomerular eGlx. To do this, kidney sections were immunostained with anti-HS3A8V, previously determined to stain eGlx HS (**CHAPTER 2**). There were no visible changes between lean, *db/db*, and *db/db* treated with OVZ/HS-1638 mice **(FIGURE 4-21 A)**. As a way to quantify eGlx HS depth, fluorescent peak-to-peak measurements were taken for eGlx HS, a technique which has been previously used by our group to quantify changes in eGlx using lectins and was validated with EM (108). There were no detectable changes in eGlx HS depth, nor in total glomerular HS expression **(FIGURE 4-21 B,C)**.

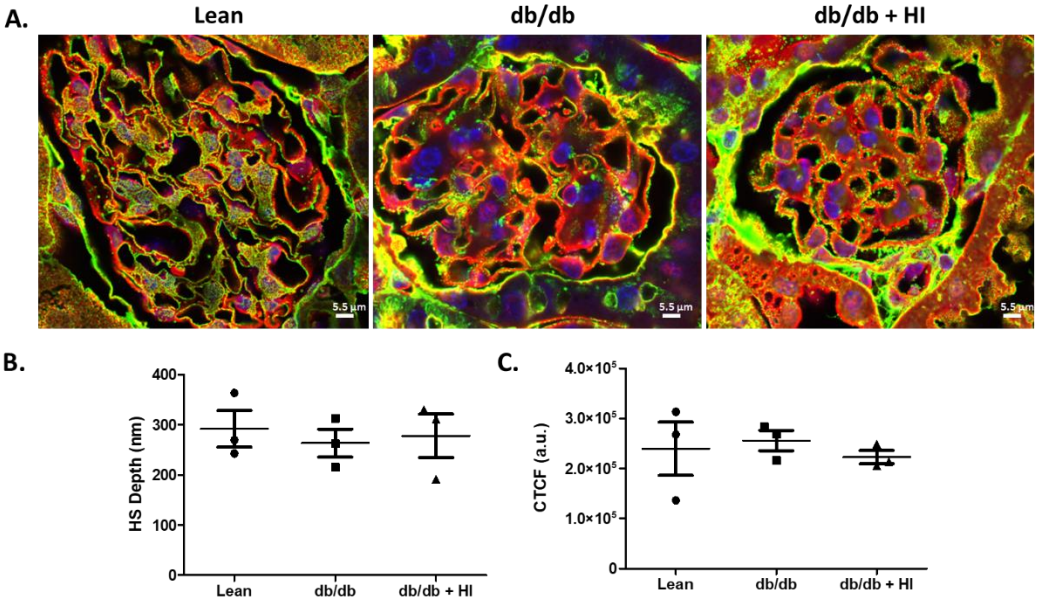

Figure 4-21 Changes in HS Cannot be Detected by Anti-HS Phage Display Antibody in Db/db Mice

A. Representative images of mouse kidney tissue from non-diabetic (lean), diabetic (db/db) mice, and db/db mice treated with OVZ/HS-1638 HPSE inhibitor (db/db+HI) stained with anti-HS HS3A8V phage display antibody (green), R18 cell membrane stain (red), and DAPI nuclear stain (blue). B. eGlx HS depth measurements taken for individual capillaries. Minimum of 3 glomeruli (3 capillaries each) measured per mouse. N=3 mice, one-way ANOVA, Tukey's multiple comparison test, not significant. C. CTCF was calculated for total glomerular HS. Minimum of 3 glomerular measured per mouse. N=3 mice, One-way ANOVA, Tukey's multiple comparison test, not significant.

4.2.7.7 *Eleven-Week-Old Db/Db Mice Have a Significant Increase in Albuminuria, which is Prevented by OVZ/HS-1638 Treatment*

The results presented so far indicate development of DN in *db/db* mice. Furthermore, reduced glomerular eGlx, as was seen in *db/db* mice, is associated with increased albuminuria (36,108,116). To determine whether *db/db* mice had changes in GFB function and examine whether treatment with OVZ/HS-1638 had any effect on this, uACR measurements were taken at end point for all mice. *Db/db* mice had a significant increase in albuminuria compared to lean mice **(FIGURE 4-22)**. OVZ/HS-1638 treated mice did not have a significant increase in albuminuria, and had a modest but not significant decrease in albuminuria compared to *db/db* mice treated with vehicle **(FIGURE 4-22)**. It should be noted that one urine sample from *db/db* and one urine sample from *db/db* treated with inhibitor were excluded due to bacterial contamination.

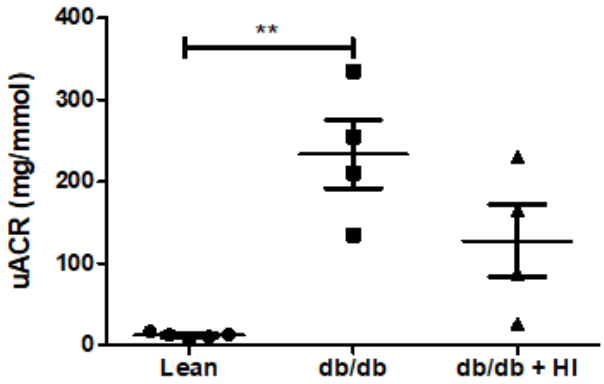

Figure 4-22 ***Eleven-Week-Old Db/db Mice Have Increased Albuminuria and is Prevented by OVZ/HS-1638 Treatment***

Endpoint albuminuria was measured for non-diabetic (lean), diabetic (db/db) mice, and db/db mice treated with OVZ/HS-1638 HPSE inhibitor (db/db+HI) . N= 4-5 mice, one-way ANOVA, Tukey's multiple comparison test indicated, **p≤0.01.

4.2.7.8 *Db/db Mice Have Increased Glomerular Albumin Permeability, which is Reduced by OVZ/HS-1638 Treatment*

Albuminuria and eGlx data for 11-week-old mice showed an increase in uACR and decreased in eGlx depth and coverage, suggesting loss of GFB function. To further confirm this data, glomerular albumin permeability assays, with greater statistical power and sensitivity than uACR, were performed to determine whether glomeruli isolated from *db/db* mice had increased albumin permeability and determine whether treatment with OVZ/HS-1638 had any therapeutic effect. As expected, *db/db* mice had a significant increase in Ps'alb compared to lean mice, as was observed in 9-week-old *db/db* mice **(FIGURE 4-23)**. Additionally, OVZ/HS-1638 treated mice had no significant increase in Ps'alb, yet had a significant decrease compared to *db/db* mice treated with vehicle **(FIGURE 4-23)**.

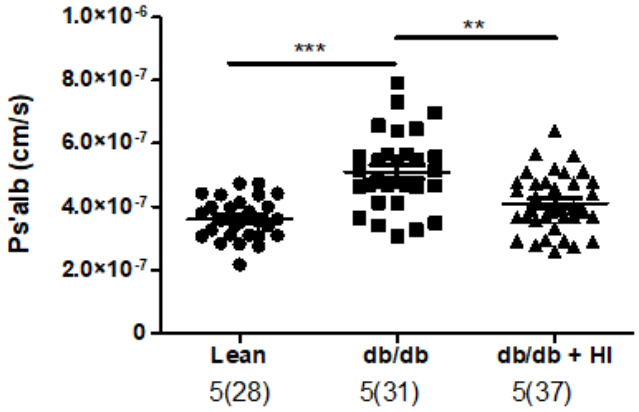

Figure 4-23 Eleven Week Old Db/db Mice Have Increased Glomerular Albumin Permeability which is Reduced by OVZ/HS-1638 Treatment

Glomeruli were isolated from non-diabetic (lean), diabetic (db/db) mice, and db/db mice treated with OVZ/HS-1638 HPSE inhibitor (db/db+HI) ringer perfused mice and glomerular albumin permeability was measured. On x-axis (mouse number (glomerular analysed)). Statistics performed on mouse number, One-way ANOVA, Tukey's multiple comparison test indicated, **p≤0.01, ***p≤0.001.

4.2.7.9 Glomerular Permeability Negatively Correlates with eGlx Depth and Coverage

To determine whether eGlx was correlated with permeability, and therefore suggestive of a causal relationship, I plotted eGlx depth and coverage against permeability and performed correlation studies. As shown in **FIGURE 4-24**, both eGlx depth and coverage was significantly correlated with glomerular permeability, with increasing eGlx negatively correlating with reduced permeability. This indicates a potential causal relationship between eGlx and permeability.

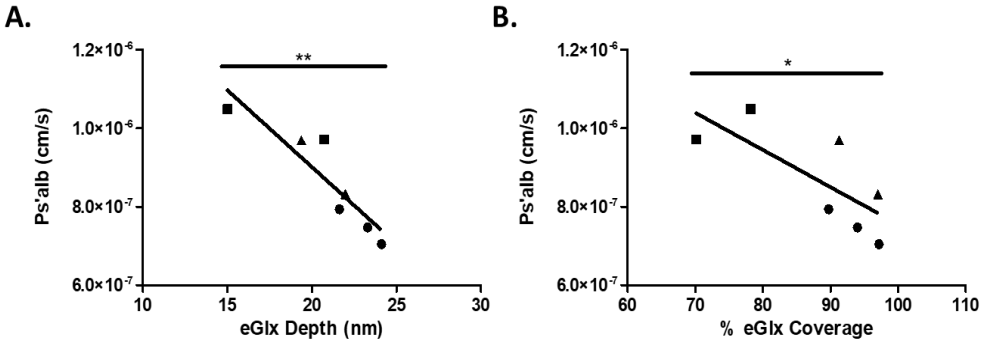

Figure 4-24 Glomerular Permeability Negatively Correlated with eGlx Depth and Coverage

A. Relationship between permeability and eGlx depth. B. Relationship between eGlx coverage and permeability. Two-tailed correlation indicated, *p≤0.05, **p≤0.01.

4.2.7.10 Glomerular Fibrosis is Increased in Db/db Mice, which is Reduced by OVZ/HS-1638 Treatment

Because *db/db* mice exhibited changes in GFB ultrastructure and function, I investigated whether *db/db* mice had developed other signs associated with DN, such as glomerular fibrosis. Additionally, I wanted to determine whether the protective effects of OVZ/HS-1638 on eGlx structure and GFB function extended further than the GFB. To do this, I used the histological stain PAS, a stain which detects deposition of glycogen, glycoproteins, glycolipids, and mucins in tissue (275). *Db/db* mice treated with vehicle had increased PAS intensity staining compared to lean mice, which appeared decreased in OVZ/HS-1638 treated mice **(FIGURE 4-25 A)**. In agreement with this, quantification of CTCF in PAS stained kidney showed that *db/db* mice had a significant increase in fibrosis staining which was significantly reduced in OVZ/HS-1638 treated mice **(FIGURE 4-25)**.

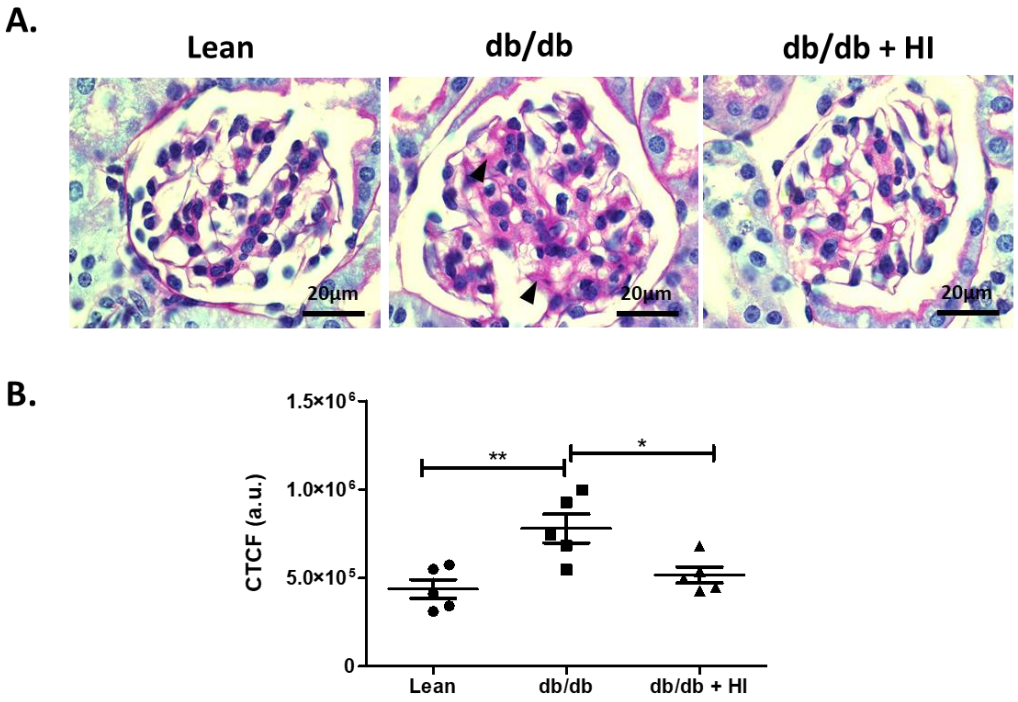

Figure 4-25 Glomerular Fibrosis is Increased in Db/db Mice which is Reduced in by OVZ/HS-1638

A. Representative bright field images of PAS stained kidney from non-diabetic (lean), diabetic (db/db) mice, and db/db mice treated with OVZ/HS-1638 HPSE inhibitor (db/db+HI). Arrowheads point to fibrosis staining in pink. B. Total glomerular CTCF was measured. Minimum of six glomeruli measured per animal. N= 5 mice, one-way ANOVA, Tukey's multiple comparison test indicated, *p<0.05, **p<0.01.

4.3 *Discussion*

4.3.1 Nine-Week-Old Diabetic Mice Do Not Show Signs of eGlx Damage in Early Stages of Diabetic Nephropathy

The aim for this chapter was to show that eGlx is damaged in a T2D mouse model using *db/db* mice, and to show that microvascular changes that occur in early DN could be prevented by treatment with a novel HPSE inhibitor, OVZ/HS-1638. I therefore used an early time point of 7-9 weeks of age, at which time *db/db* mice are recognized to be hyperglycaemic and have increased albuminuria. In agreement with previous reports using this model, *db/db* mice treated with vehicle had increased weight and blood glucose levels by 7 weeks of age compared to lean controls treated with vehicle, and remained elevated for the duration of the experiment. This suggested that the mouse model was progressing as would be expected for a T2D model, resembling aspects of the disease in humans. Treatment with OVZ/HS-1638 also had no effects on weight or blood glucose levels, indicating that the inhibitor itself was not having any off-target effects that changed metabolic processes. Interestingly, T1D models have shown that HS is highly expressed in mouse islets, and is essential for β-cell survival (276), suggesting preventing HS loss in mouse islets may help prevent T1D diabetes. Indeed, T1D mice treated with the heparanase inhibitor PI-88, had a delayed development of diabetes by 10 weeks (276). However, as this is a T2D mouse model in which tissues become insulin resistant, any protective affects which OVZ/HS-1638 may have on β-cell survival, may not impact blood glucose in the same way. This may explain why no differences are observed in blood glucose levels when comparing vehicle and OVZ/HS-1638 treated *db/db* mice. Examining changes in GFB ultrastructure, all *db/db* mice showed no significant changes that would have been expected if mice had developed early changes associated with DN. But it is likely that this was too early of a time point to observe such changes as previous reports of podocyte effacement and GBM thickening for example, did not occur until 12 and 16 weeks of age, respectively (230,277). Measurements of eGlx depth and coverage were also unchanged in *db/db* mice compared to lean controls, further evidence that this was too early of a time point to detect changes in eGlx structure. Surprisingly, *db/db* mice did have a significant increase in albuminuria at 9 weeks of age. Although this is in line with the literature, which reports a moderate increase in albuminuria by 8 weeks of age (217,277), I expected this to be associated with changes in eGlx. It is possible that small changes in eGlx did occur, but with moderate changes, a larger sample size is required to see significant differences. Staining by Alcian blue can also vary slightly from perfusion-

to-perfusion and depth can be further affected by EM processing due to dehydration and rehydration steps (10). Bigger changes however are more evident despite slight variations in perfusions and EM processing. It is of course also possible that there are simply no changes in eGlx at this time point. However, glomerular albumin permeability assays also showed a significant increase in permeability in *db/db* mice, which our group has shown is associated with loss of eGlx in other diabetic models such as STZ mice and rats (36,108). Increased permeability is further evidence that mice have changes in their GFB function, despite the lack of ultrastructural changes. Additionally, although Ps'alb was not significantly reduced by OVZ/HS-1638 treatment at 9wk compared to vehicle treated *db/db* mice, it was not significantly increased compared to lean controls. This contradicts the albuminuria results showing that both sets of *db/db* mice had increased albuminuria. However, the glomerular permeability assay is a more sensitive and direct measurement of glomerular permeability, therefore it is possible that it is able to distinguish smaller changes in glomerular permeability that are not detectable by the ELISAs used to measure albumin in the urine.

As there were no changes in eGlx depth or coverage, it cannot be concluded wheather or not treatment with OVZ/HS-1638 is protective at this time point. Albuminuria data suggest that functionally, OVZ/HS-1638 treatment is not protective. However, there are several factors that can affect albuminuria. First, as discussed in **CHAPTER 3**, tubular reabsorption plays a major role in reabsorbing low levels of albumin that is leaked out by the glomerulus. Although these mice were all treated the same, slight differences in kidney physiology in individual mice could affect albuminuria. Indeed, a study performed on diabetic children showed that diabetic subjects had a significant increase in tubular reabsorption of sodium, glucose, and calcium, compared to non-diabetic children (278). Additionally, an STZ rat model showed that rats in early stages of diabetes had reduced tubular reabsorption of albumin (279), which may explain the large variability observed in all *db/db* mice. Additionally, time and methods of urine collection has been shown to have effects on albuminuria results. Human studies report that the first morning void is better for investigating changes in albuminuria in patients, versus the 24-hour collection or spot collection method (280). Unfortunately, the nature of these experiments did not allow for collection of urines at a specific time for each mouse, which may also contribute to variabilities in albuminuria that could be masking protective effects of the inhibitor. It should also be noted that the route of injection for OVZ/HS-1638 in this study was subcutaneous, based on personal communications with one of our collaborators

Professor Jerry Turnbull at University of Liverpool, who had positive results using this route of injection with OVZ/HS-1638 in myeloma studies. However, efficacy may vary depending on the model and disease being investigated, and it is possible a different route of injection would increase efficacy. Ultimately, an end point of 9 weeks of age in *db/db* mice did not provide conclusive evidence that glomerular eGlx structure and function is deteriorated, and therefore potential protective effects with OVZ/HS-1638 treatment could not be established.

4.3.2 Loss of eGlx Structure and Function in Eleven-Week-Old Mice is Restored by Treatment with OVZ/HS-1638

As the 9-week timepoint did not yield conclusive evidence, likely due to a small sample size and too early of a time point. Based on ultrastructural data, I decided to use a later time point in hopes that changes in *db/db* mice would be more robust and therefore more easily measurable. I also changed the OVZ/HS-1638 administration to i.p., in hopes this would be a more effective route for HPSE inhibition. For this later timepoint, experiments began at 9 weeks of age with vehicle or OVZ/HS-1638 treatments for two weeks and an endpoint of 11 weeks. As before, weights and blood glucose were measured in *db/db* mice, showing that diabetic mice were progressing as expected, and treatment with the OVZ/HS-1638 had no effects on either parameter.

Although an increase in circulating HPSE and expression in diabetic kidneys is well established and has been shown in a number of animal and human studies (109,247,250,281), including *db/db* mice (114), I wanted to confirm our cohort of *db/db* mice at 11 weeks had increased HPSE expression. Using immunofluorescence on mouse kidney sections, I confirmed that HPSE expression was significantly increased in *db/db* mice as measured by CTCF. Of note, HPSE staining was primarily tubular in the kidneys of *db/db* mice. Although unexpected, this is in agreement with HPSE staining in human studies, which showed a significant reduction in glomerular HS, despite HPSE signal being primarily in the tubules (109). It is possible that loss of glomerular HS occurs due to circulating active HPSE, which may not be directly sourced from glomerular cells. Indeed, as mentioned previously, leukocytes and platelets have been shown to be sources of active HPSE (84). Surprisingly, OVZ/HS-1638 treated mice had a decrease in HPSE expression in their kidneys, though not significant. The supposed mechanism of action for this inhibitor is inhibition by binding to HPSE in a way that prevents catalytic cleavage of HS molecules (271). However, it has been shown that HS shed from eGlx can activate leukocytes and platelets to release more active HPSE (167), which as mentioned earlier,

is stored in granules and can be released upon intracellular or extracellular signals. This may explain why mice treated with the inhibitor have reduced HPSE expression, as presumably eGlx HS shedding is inhibited, preventing inflammatory cell activation and HPSE release.

In agreement with the literature for this mouse model which showed reduced podocytes by 12 weeks (230), *db/db* mice had a significant increase in podocyte foot process width and decrease in slit diaphragm width, consistent with podocyte effacement, an early sign of DN seen in both humans and mice. A significant increase in GBM thickening was not observed, however there was a modest increase in *db/db* mice compared to lean controls, and possibly would become significant were it not for the greater variation observed in diabetic mice. No changes were observed in fenestration density, however this becomes more prevalent in slightly later stages of DN (103), and therefore may not be apparent at 11 weeks. Inhibitor treated mice also had a significant increase in podocyte foot process width suggesting podocyte effacement, though no changes were observed in slit diaphragm width. Additionally, no changes were observed in pGlx between any groups. This has been observed by our group in many diabetic studies (116,155). Though it is not entirely clear why, it is likely due to the fact that the pGlx is not the first point of contact with flowing blood containing the highest concentrations Glx damaging agents.

In contrast to the 9-week model, measurement of eGlx in *db/db* mice did showed a significant decrease in depth and coverage at 11 weeks of age. Notably, treatment with OVZ/HS-1638 prevented eGlx damage and was significantly increased compared to *db/db* mice treated with vehicle. This suggests that the OVZ/HS-1638 is having protective effects on eGlx structure by preventing HS degradation. To confirm this, I performed immunofluorescence on kidney sections from these mice staining for HS using the same antibody described in **CHAPTER 3**. Unfortunately, there were no detectable changes in eGlx HS depth, measured using the validated and published method which uses lectin staining to determine the distance between fluorescent profile peaks (peak-to-peak) by confocal microscopy imaging to measure changes in eGlx depth (108). Additionally, total glomerular HS measured by CTCF also showed no changes. With regard to the peak-to-peak analysis, in retrospect it is likely that this method of analysis is not appropriate for the type of staining obtained using this antibody. The reason is that lectin staining of eGlx generally gives a very uniform signal around the capillary and was originally used to optimise the macro for analysis. However, this HS antibody gives very punctate staining and also stains the GBM, which can skew profile peak intensity measurements resulting

in inaccurate eGlx HS depth measurements. However, as total glomerular HS is also not reduced in *db/db* mice it is likely that this antibody is not suitable for detecting eGlx HS changes and faces the same issues in this model as in *Ext1*^{CKO} mice discussed in **CHAPTER 3**. Indeed, a study performed on human kidney tissue showed that staining with different antibodies yielded different results in terms of loss of HS in glomeruli. For example, staining with the HS antibodies JM403, HS4C3, and EW3D10 which target specific N-unsubstituted glucosamine residues or sulphated heparan sulphate domains, all showed a significant decrease of HS in glomeruli from DN tissue (282). However, the antibody K5, which recognises unmodified heparan sulphate domains with *N*-acetylglucosamine-glucuronic acid residues (the HS precursor domains) did not show differences in glomerular HS between control and DN tissue (282). The authors suggest that this may be due to remaining HS remnants or that non-modified HS side chains were still present (282). Therefore, applying this knowledge to these experiments, more work is required to determine whether HS is lost in glomerular eGlx in *db/db* mice and if treatment with OVZ/HS-1638 restores it. However, the observed increase in HPSE expression in these mice which coincided with a loss of eGlx measured by EM, strongly suggest that HS is likely degraded. Recall that **CHAPTER 3** showed that treatment of healthy mice with heparinase III caused a loss of eGlx, supporting the theory that increased HPSE expression in diabetes would also cause eGlx damage. Despite the further work needed to confirm loss and restoration of HS specifically, this is the first time that restoration of glomerular eGlx with a HPSE inhibitor has been demonstrated. Protection of eGlx appears to be not only structural but also functional, as *db/db* mice had a significant increase in albuminuria compared to lean mice, which was prevented by OVZ/HS-1638 treatment. This is in line with previous work by *Gil et al.,* who showed that treatment of *db/db* mice with the HPSE inhibitor SST001 significantly reduced albuminuria from 10 to 18 weeks of age, compared to vehicle treated *db/db mice* (114). The same was shown for STZ T1D mice at 12 weeks of age (114). These studies suggest that HPSE has a role in the development of albuminuria and can be prevented by treatment with a HPSE inhibitor, but eGlx was not examined in either of these models.

Following the albuminuria data presented in this chapter, *db/db* mice also had a significant increase in glomerular albumin permeability, which was significantly reduced by treatment with the OVZ/HS-1638. These data suggest that OVZ/HS-1638 restores GFB function by restoring glomerular eGlx, most likely by preventing eGlx HS degradation. Additionally, correlation studies on the relationship between eGlx depth/ eGlx coverage

and permeability, revealed that there was a significant negative correlation between the two. Of course, this does not prove a causal relationship between eGlx and permeability but does serve as a good indication that damage to the eGlx results in increase permeability.

To see whether the protective effect on eGlx and GFB function more widely impacted glomerular health, I performed PAS staining to observe changes in glomerular fibrosis. Glomerular fibrosis results from an accumulation of extracellular matrix proteins such as collagen and fibronectin, resulting from increased synthesis by mesangial cells in response to pro-fibrotic signals from cytokines and growth factors derived from podocytes, endothelial cells, leukocytes, and mesangial cells themselves (283,284). This results in mesangial cell expansion, and early sign of DN which has a clear link with progression to diabetic kidney disease (284). Quantification of PAS stained kidney sections showed that *db/db* mice had a significant increase in PAS staining, evidence of glomerular fibrosis. *Db/db* mice treated with OVZ/HS-1638, however, did not have a significant increase in staining, and had significantly reduced fibrosis staining compared to *db/db* mice treated with vehicle. We have seen similar results in T1D model in which VEGFC overexpression was used to therapeutically targeting eGlx. VEGFC overexpressing diabetic mice had reduced PAS staining compared to control diabetics, which may be due to reduced tubular toxicity as a result of reduced albumin filtration (116). This suggests that restoration of eGlx structure and function not only has beneficial effects on the GFB, but also has a wider effect on glomerular health, as fibrosis is prevented with treatment.

4.3.3 Conclusions and Significance

The work presented in this chapter reveals a novel HPSE inhibitor as a potential treatment to therapeutically target HS during DN. Though loss of HS in the eGlx specifically could not be established, increase HPSE coincided with a loss of eGlx, increased glomerular albumin permeability, and glomerular fibrosis. These changes were prevented by treatment with OVZ/HS-1638 that is not only clinically relevant, but also has the added benefit of having similar potency to the most potent HPSE inhibitor currently available, as well as reduced anticoagulant activity, a major hurdle for HPSE inhibitors in clinical use. This work also shows for the first time that glomerular eGlx damage can be prevented by treatment with OVZ/HS-1638, and ameliorates associated microvascular changes in DN, with the potential to be applied to other vascular beds such as the retina.

Chapter 5 The Importance of Endothelial Glycocalyx Heparan Sulphate in the Inner Blood Retina Barrier

5.1 *Introduction*

5.1.1 Biological Role of Heparan Sulphate in the Retina

The structure and synthesis of HS was discussed in detail in **CHAPTER 3** and applies to the eye as well. **CHAPTER 3** also provided discussion and evidence for the role of HS in the glomerulus, HS however is ubiquitously expressed throughout the body and plays an important role in the retina. HS and heparan sulphate proteoglycans (HSPG) are present throughout all layers of the retina and much of the work exploring their role in the retina has been on the development of the neuronal retina (285). Studies in rats showed that syndecan HSPG were spatiotemporally expressed during retinal development, which the authors suggested means that syndecan may play a role in the formation of neural networks (286). In zebrafish, knockdown of the HSPG agrin, results in microphthalmia, a condition in which the eye is abnormally small and fails to develop properly (287). In fact, agrin mRNA was found at various stages of retinal development such as retinal ganglion cell differentiation and stages in which laminated retina is formed and synaptic connections are established not only in zebrafish, but also rats, mice, and chickens (287–289). Retinal lamination is the process in vertebrates in which neuronal cell bodies are organised into distinct layers based on function, giving the retina its layered appearance, and disturbance of this process results in impaired function (290). HS and other GAGs also have a role in angiogenesis in development of the retina, as UDP-glucose-5-dehydrogenase (*Ugdh*) knock down mice have defects in astrocyte and endothelial cell migration, which is required for vessel formation (291). *Ugdh* is involved in production of UDP-GlcA, which is a precursor for the synthesis of GAG chains (292). Therefore, the absence of *Ugdh* results in loss of GAG synthesis, including HS. In adults, *Ugdh* knock down mice had increased glial fibrillary acidic protein (GFAP) staining in astrocytes and Müller cells, a marker of cell activation, and contributed to extensive retinal degeneration (291).

In the retinal microvasculature, HS has been shown to be present, but staining was attributed to the basement membrane, and has not been described in the retinal eGlx (293). HS may have a role in maintenance of tight junctions, which, as discussed in **CHAPTER 1**, are important in maintaining the inner blood retina barrier (iBRB) and

permeability. In tissue culture, high glucose induced shedding of HS on human retinal endothelial cells (hRECs) coincided with loss of tight junction proteins, occludin and ZO-1 (294). It is possible that the eGlx and HS act as an initial and extra barrier in tight junctions, and damage to it results in a loss of regulation of tight junction proteins. This may result in increased permeability of lipids and proteins, resulting in some characteristic lesions seen in DR such as hard exudates (295). Interestingly, and related to this thesis, high glucose also increases HPSE expression in hRECs (294). Additionally, *in vivo* studies in a T1D mouse model showed that up-regulated HPSE expression by retinal endothelial cells was accompanied by loss of the same tight junction proteins in diabetic mice, suggesting a role for HS in maintenance of tight junctions and vascular permeability (294). However, the authors of this article attributed this observation to loss of HS in the basement membrane, yet provided no evidence for this. It is therefore possible that in fact eGlx HS also has a role in maintaining the iBRB, as it is in direct contact with flowing blood, and has been shown in other microvasculature vessel beds to act as a protective shield for endothelial cells (55). Though there is minimal research on the role of eGlx in the retina, there is some evidence in diabetic humans and in experimental rodent studies showing that loss of eGlx results in increased permeability in the retina (57,59,60), though HS was not examined in these studies. These studies will be discussed in more depth in the next chapter as they relate to changes in diabetes. In this chapter I will focus on investigating the importance of HS in the eGlx of retinal microvasculature. As **CHAPTER 3** and **4** have shown, HS plays an important role in maintenance of glomerular permeability, and the work in this chapter will provide evidence for a more global role for eGlx HS in different vessel beds such as the retina.

5.1.2 Chapter Aims and Experimental Approaches

The aim of this chapter is to establish a role for HS in the retinal eGlx. This is accomplished in two parts.

1. Show that HS is present in the retinal eGlx using immunofluorescence.
2. Show that removal of HS from retinal eGlx increases vascular permeability. This was accomplished in two ways. The first was by enzymatic removal of HS in the retina of healthy mice with heparinase III. This allowed me to investigate whether loss of HS had any effect on eGlx structure and function. The second was using the transgenic mouse model used in **CHAPTER 3** (*Ext1*^{CKO}), which allowed me to study the effects of reduced HS synthesis in retinal eGlx *in vivo*.

5.2 *Methods*

These methods are not inclusive. The methods described in this section are those that pertain specifically to this chapter or have been adapted for experiments in this chapter. All other methods are described in the **CHAPTER 2** Methods and Materials.

5.2.1 Heparan Sulphate Staining on Retina Whole Mounts and Imaging

Mouse eyes were enucleated from fresh C57BL/6 mouse carcasses (provided by Dr. Sherry Flemming, Kansas State University) and put into 2% PFA/2% glutaraldehyde for 24 hours. After fixation, retinas were isolated under a dissection microscope as described in **CHAPTER 2**.

Retinas were mounted onto glass slides followed by 10min incubation in 0.1% Triton-X. Retinas were blocked in 5% BSA for 1 hour. Anti-HS phage display antibodies RB4Ea12V, HS3A8V, HS4C3V, LKIV69V, EV3C3V, MPB49V (gift from Jerry Turnbull, The University of Liverpool) were diluted 1:5 in block solution and incubated at 4°C overnight. Secondary mouse anti-VSVG (sc-365019, Santa Cruz Biotechnology, Dallas, TX) was added for two hours at 1:50. Retinas were washed in PBS three times for 5min. Tertiary anti-mouse Alexa Fluor 488 (A-11001, ThermoFisher Scientific) was added for 1 hour at 1:200. Retinas were washed as before and counterstained with DAPI (D1306, ThermoFisher Scientific) for 5min and coverslip mounted with Pro long gold (P10144, Thermo-Fisher). Carl Zeiss 700 confocal microscope was used for retina imaging provided by Kansas State University Confocal Core to determine antibodies that bind to eGlx HS . EGlx was determined based on location of staining, where luminal staining on surface of endothelial cells was deemed eGlx HS **(FIGURE 5-1)**.

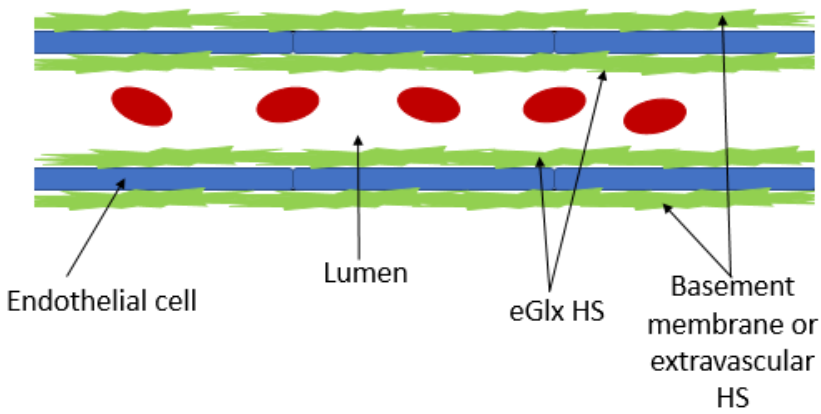

Figure 5-1 Schematic of HS Staining in Retinal Vasculature

Location of eGlx staining in the retina. Staining deemed as eGlx if located on the luminal side of the endothelial cell.

5.2.2 Sodium Fluorescein Angiographies (FAs)

5.2.2.1 Heparinase III Treated Mice

Baseline FAs were performed on C57BL/6 mice as described in **CHAPTER 2** at day 0. Two days later, mice were given heparinase III treatment as described in **CHAPTER 2**. Thirty minutes later, FAs were performed, and data analysed for solute flux as described in **CHAPTER 2**. **FIGURE 5-2** shows a schematic of experimental timeline.

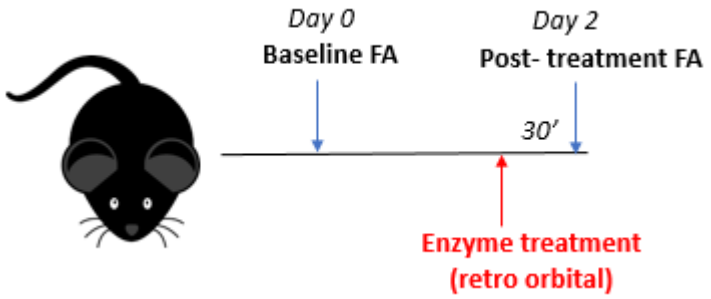

Figure 5-2 Treatment with Heparinase III for Solute Flux Measurements

C57BL/6 mice were given baseline angiography on day zero. Two days later mice were treated with 8.2u/kg of Heparinase III. Thirty minutes later post treatment angiography performed.

5.2.2.2 Endothelial Ext1^{CKO} Mouse Model

Ext1^{CKO} and LMC mice were given 2mg/ml of doxycycline supplemented with 5% sucrose as described in **CHAPTER 3** for 2 weeks to induce Ext1 knock out. After 2 weeks, FAs were performed on mice and analysis for solute flux done as described in **CHAPTER 2**. **FIGURE 5-3** shows a schematic of the experimental timeline.

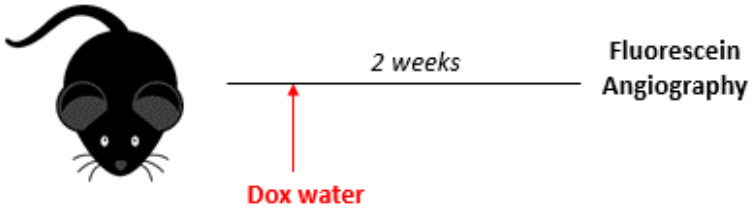

Figure 5-3 Induction of Knock Out in Ext1^{CKO} Mice for Solute Flux Measurements

Control and Ext1^{CKO} mice were given 2mg/ml of Doxycycline drinking water for 2 weeks followed by fluorescein angiography for solute flux measurements.

5.3 *Results*

5.3.1 Presence of Heparan Sulphate in Retinal eGlx

5.3.1.1 Retinal Vessels Are Coated in eGlx

Although it is well accepted that the eGlx can be found in all of the body's vasculature, a literature search of eGlx images in the retinal vessels yielded minimal results. *Broekhuizen et al.* demonstrated eGlx in rat retinas with EM, but eGlx was very sparse and patchy in nature when compared to EM images of other capillary beds, such as heart and kidney, which is typically more continuous in nature (36,296). To determine the coverage of eGlx in mouse retina, eyes from AB cardiac perfused mice were imaged by EM. **FIGURE 5-4A** shows a low powered image of a mouse microvessel in the retina, showing the different components of the vessel, including surrounding pericyte, basal lamina, and basement membrane of the endothelial cell with an intercellular cleft and tight junction. The closed capillary endothelial structure can be observed, in contrast to capillaries located in the glomerullus, which are fenestrated. A higher magnification image shows clear eGlx covering the luminal side of the endothelial cell **(FIGURE 5-4B).** This eGlx appears more continuous than what was described in *Broekhuizen et al*. and its presence suggests eGlx likely serves a similar function in retinal vasculature as elsewhere.

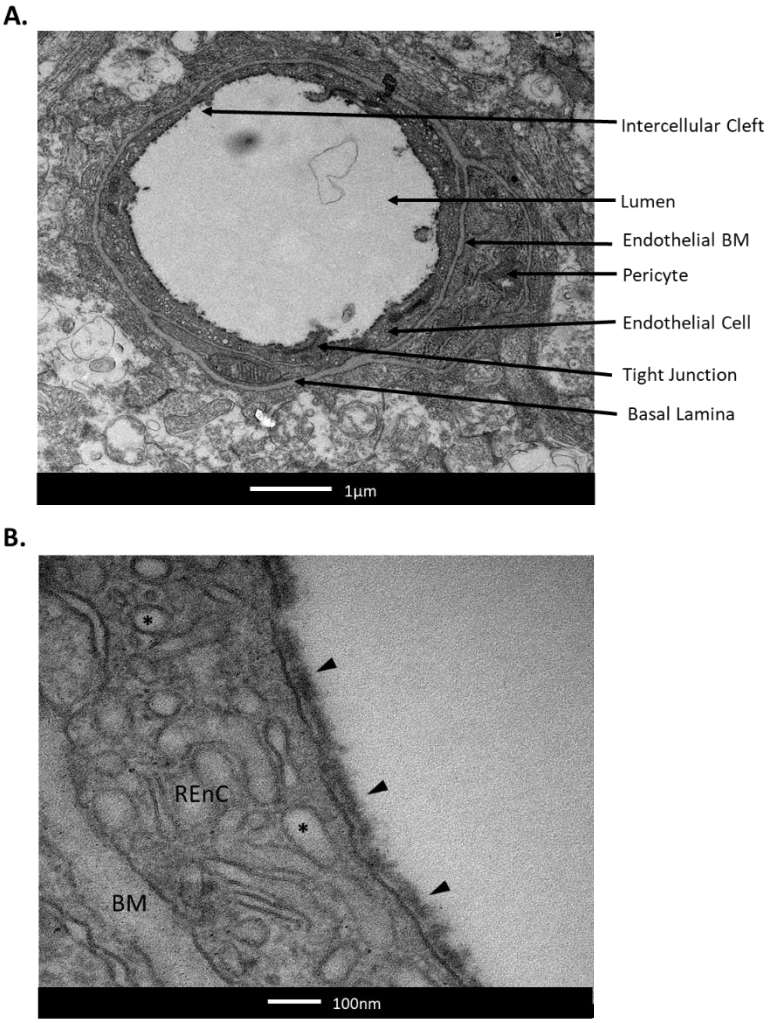

Figure 5-5 Retinal Vessels Have eGlx

Representative EM images of retinal vascular from mice cardiac perfused with Alcian blue and glutaraldehyde. A. Low magnification image, retinal structures labelled. B. High magnification image showing eGlx staining on luminal side of retinal endothelial cell (REnC) (arrow heads). Basement membrane (BM) shown along with vesicles * in REnC.

5.3.1.2 Heparan Sulphate is Present in Retinal eGlx

Although it has been well documented that HS is widely distributed in tissues, including the retina, it has not been well characterized in the retina vasculature. To determine if HS is present in the retina eGlx, I performed immunofluorescence on mouse retina whole mounts using six different phage display antibodies in order to find one which recognized eGlx HS epitopes, presenting as HS staining on the luminal side of endothelial cells in the retinal vasculature. As shown in **FIGURE 5-6** , there were variations in eGlx in HS staining patterns between the antibodies, and little to no staining with the LKIV69V and EV3C3V antibodies. HS3A8V and MPB49V appeared to stain primarily extravascular or basement membrane HS, while RB4Ea12V had luminal staining.

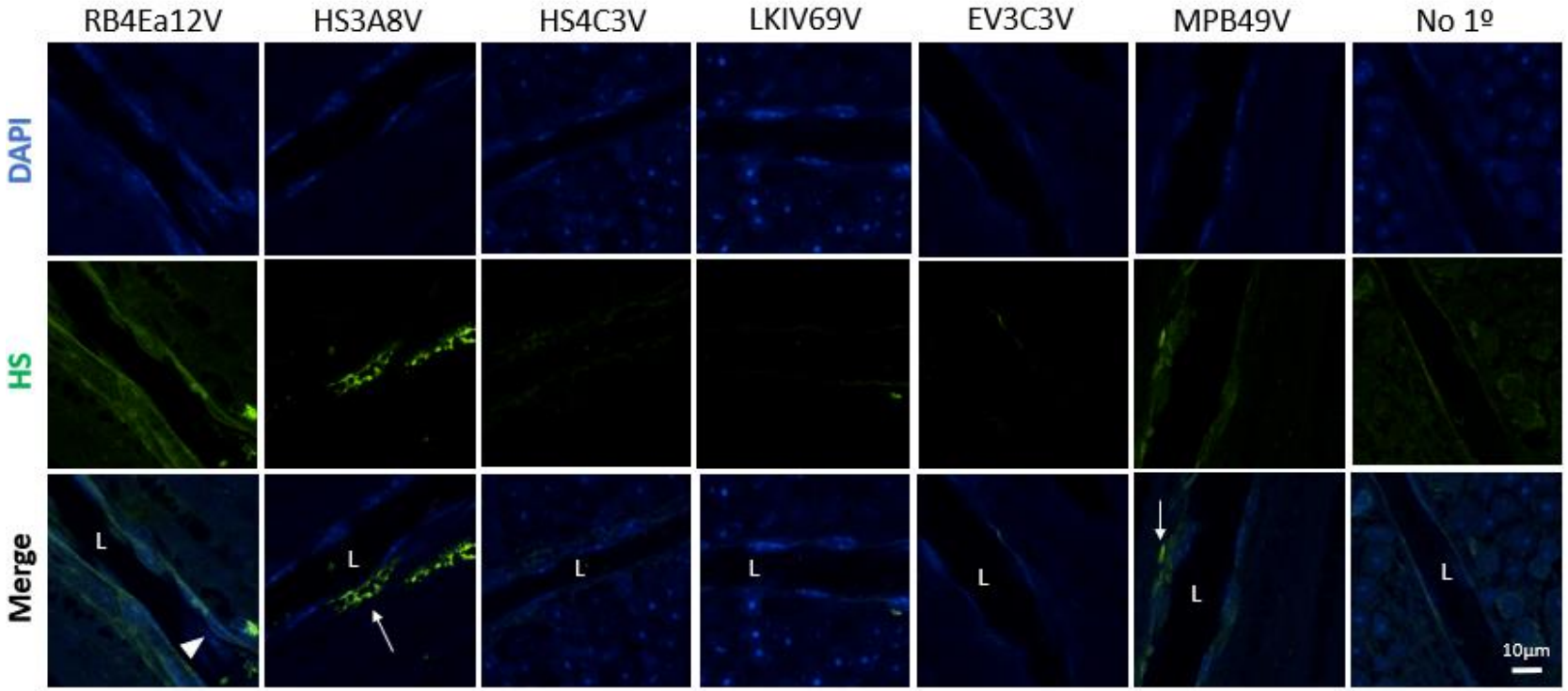

Figure 5-6 Anti-Phase Display HS Antibody Panel Optimisation

A panel of 6 anti-HS phage display antibodies were used to determine best antibody suitable for eGlx staining in mouse retinal flat mounts. Basement membrane staining (arrows) and eGlx staining (arrowhead). Lumen (L) of each vessel is marked. Scale bar applies to all images.

A magnified image of RB4Ea12V staining is shown in **FIGURE 5-7**. HS staining in the eGlx is evident by the signal found on top of the endothelial cell nucleus on the luminal side of the vessel as described in methods. This confirmed that HS is present in the eGlx of the retina. This antibody also appeared to recognized basement membrane HS. Though there was some non-specific staining in the no primary control, there was no staining resembling eGlx as in anti-HS probed tissue, indicating antibody staining was specific.

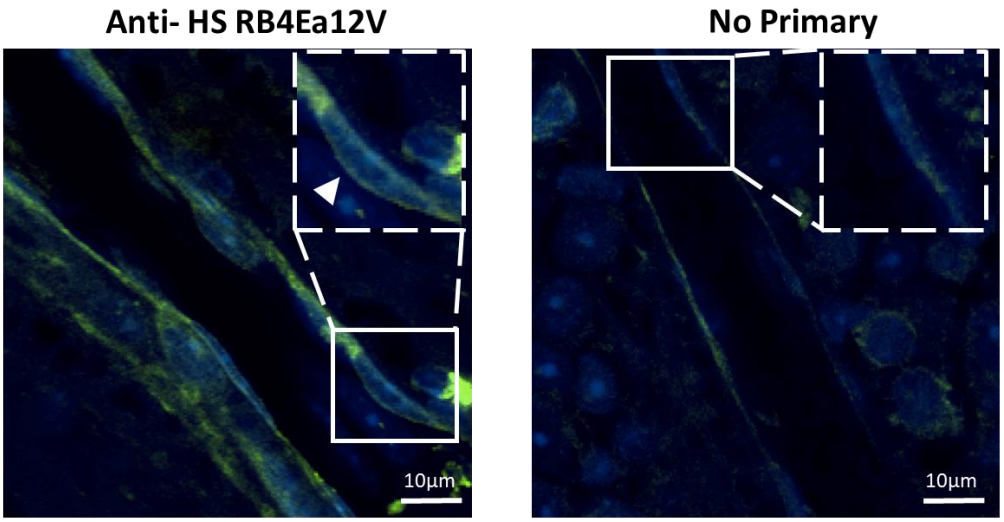

Figure 5-7 HS is Present in Retinal eGlx

Mouse retina tissue stained with anti-HS RB4Ea12V phage display antibody (green) and DAPI nuclear stain (blue). Left: Image of vessel from retina flat mount. Inset shows magnified image of HS staining (arrowhead) over endothelial cell nucleus. Right: No primary control show lack of HS staining over nucleus.

5.3.2 Heparinase III Treatment Studies

5.3.2.1 Heparinase III Treatment Results in Loss of Retinal eGlx

Although the role of HS has been investigated in other aspects of retinal physiology as described above, the role of HS in the eGlx had not yet been determined. To examine the role HS plays in the eGlx, retinal microvasculature EM images were taken from Alcian blue and glutaraldehyde perfused mice which had previously been treated i.v. with inactive or active heparinase III as in previous experiments. As shown in **FIGURE 5-8 A**, active enzyme treated mice had reduced eGlx which was patchy in nature. Quantitative EM confirmed that eGlx coverage was significantly reduced in active enzyme treated mice **(FIGURE 5-8 B)**. Although there was not a significant reduction in eGlx depth, there was a strong trend **(FIGURE 5-8 B)**, and together with the coverage data, indicates the HS is important for eGlx structure.

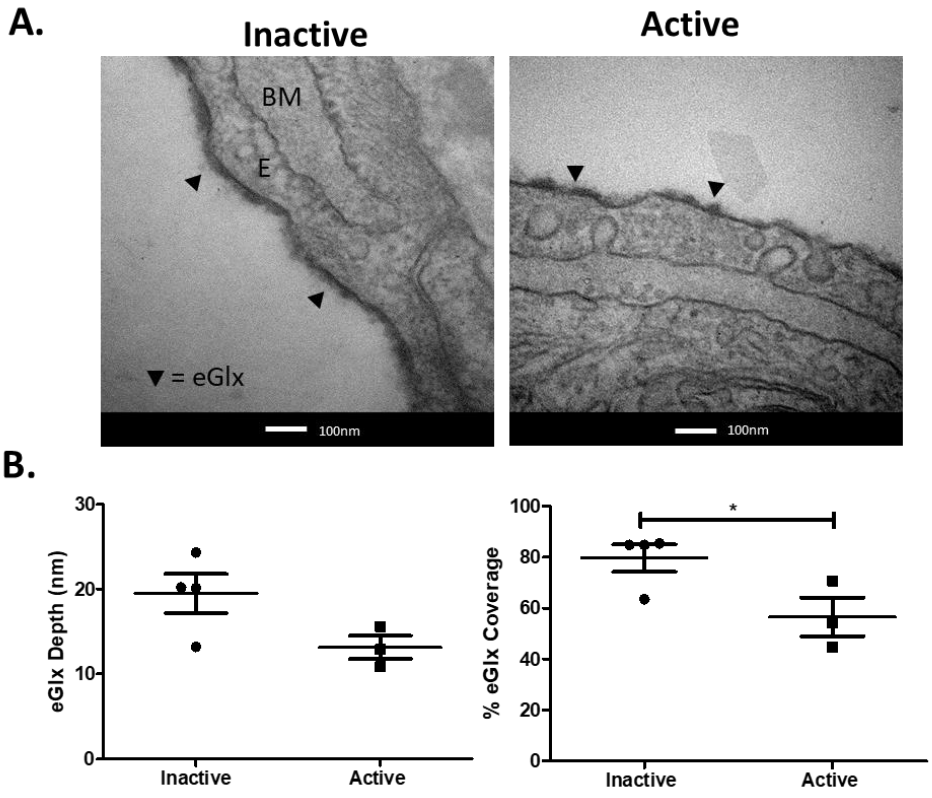

Figure 5-8 Heparinase III Treatment Results in Loss of Retinal eGlx

A. Representative high magnification EM images of retinal vessel from mice treated with inactive or active heparinase III. Basement membrane (BM) and endothelial cell (E) shown. Arrow heads points to eGlx. B. EM images were analysed for changes in eGlx depth (left) and eGlx coverage (right). N=3 mice, unpaired Student's t-test indicated, *p≤0.05.

5.3.2.2 *Heparinase III Treatment Does Not Affect the Basement Membrane in the Inner Blood Retina Barrier*

As with basement membranes located in other microvasculature such as the glomerulus, the retinal basement membrane is abundant in HSPGs and loss of it may impact blood vessel integrity (297). To determine whether treatment with heparinase III treatment had any effects on the basement membrane structure, basement membrane thickness was measured from EM images. While there did seem to be a trend toward a decrease in thickness in active enzyme-treated mice, the results were not significant compared to inactive enzyme-treated mice **(FIGURE 5-9)**, suggesting that heparinase III treatment does not significantly impact the basement membrane.

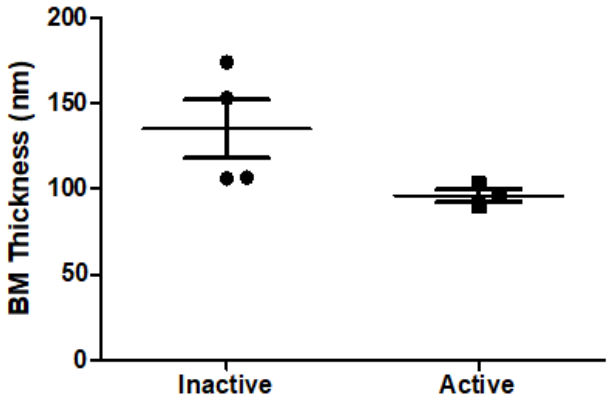

Figure 5-9 Heparinase III Treatment Does Not Affect the Basement Membrane in Blood Retina Barrier

Basement membrane (BM) thickness of retina microvessels was measured in inactive and active enzyme treated groups. N=4-5 mice, unpaired Student's t-test, not significant.

5.3.2.3 Heparinase III Treatment Increases Retinal Solute Flux

To determine whether removal of eGlx HS with heparinase III resulted in increased solute flux, solute flux measurements were taken in inactive and active enzyme treated mice using sodium fluorescein angiography imaging described in **CHAPTER 2**. To confirm that baselines were similar for both groups, solute flux measurements were taken two days prior to enzyme treatment. As shown in **FIGURE 5-10 A**, solute measurements were similar for both groups of mice. However, treatment with active enzyme resulted in a significant increase in solute flux compared to inactive mice **FIGURE 5-10 B**, indicating that loss of HS negatively impacts iBRB integrity.

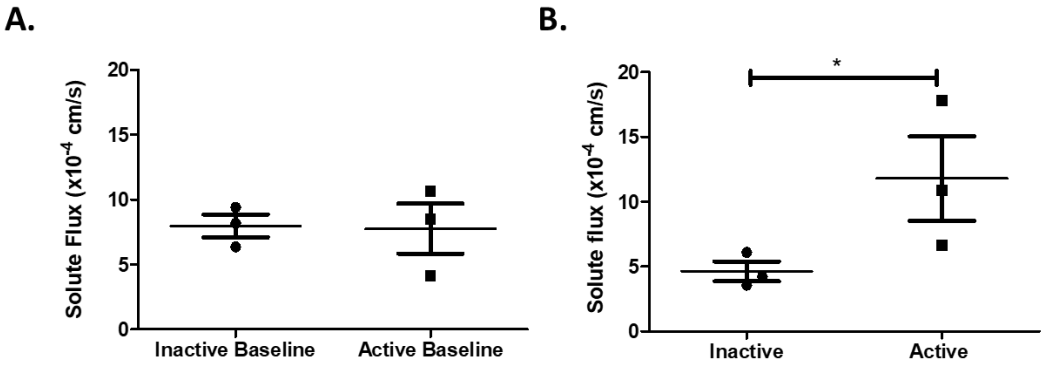

Figure 5-10 Heparinase III Treatment Increases Retinal Solute Flux

Solute flux measurements were taken for mice treated with active or inactive Heparinase III. A. Baseline solute flux measurements taken two days prior to treatment. B. Post treatment solute flux measurements taken thirty minutes after treatment. N=3 mice, unpaired Student's t-test indicated, *$p \leq 0.05$

5.3.3 Endothelial *Ext1*^{CKO} Mouse Model

5.3.3.1 Ext1^{CKO} *Mice Have Increased Retina Solute Flux*

Enzymatic removal of HS by heparinase III negatively impacted retinal eGlx and increased solute flux in active enzyme treated mice. As a second method of validating the role of HS in the eGlx of the retina, I used *Ext1*^{CKO} to determine whether endothelial specific reduction of HS synthesis resulted in loss of eGlx barrier function. To do this, I performed sodium fluorescein angiographies as previous, on LMC or *Ext1*^{CKO} mice after inducing Ext1 knockout. Solute flux measurements showed that *Ext1*^{CKO} had a significant increase in solute flux compared to control mice **(FIGURE 5-11)**, indicating that reduced endothelial cell HS synthesis results in loss of iBRB integrity.

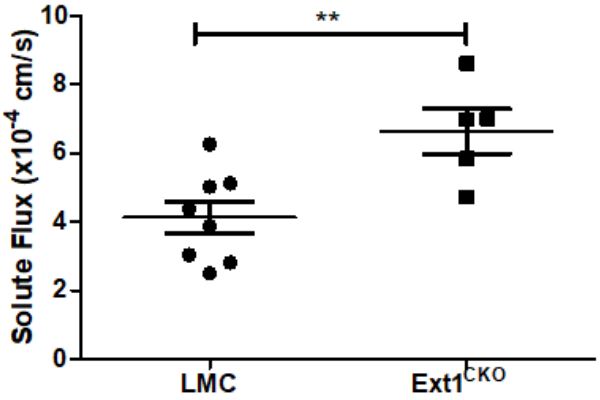

Figure 5-11 Ext1*^{CKO} *Mice Have Increased Retina Solute Flux

Solute flux measurements were taken for LMC and Ext1*^{CKO} *mice. N=5-8 mice, unpaired Student's t-test indicated, **p≤0.01

5.4 *Discussion*

5.4.1 Heparan Sulphate is Present in Retinal eGlx

To date, there has been minimal research focused on the eGlx in the retina. HS has been shown to be abundant all throughout the retina, including in the microvasculature basement membrane (293). While it is presumed that HS is a component of all eGlx throughout the body, the presence of HS specifically in the retinal eGlx had not been shown. Moreover, published EM images of retina eGlx did not appear to resemble the eGlx in other vessel beds such as in the kidney and heart tissue. However, we know eGlx is present as studies in T2D patients have shown that retina eGlx can be measured with darkfield side stream imaging, a technique that allows for eGlx measurements *in vivo* (58). Using retina tissue from healthy Alcian blue and glutaraldehyde perfused mice, I was able to visualise the eGlx in the retina. As in other tissues, and in contrast to published EM images, eGlx in the retina was present in a relatively uniform manner. To confirm that HS was present in the retinal eGlx, I performed immunofluorescence on retina flat mounts. HS varies greatly in structural diversity due to variation in length, sulfation and acetylation patterns, and domain structure, which also varies in tissue type and species (173). I therefore used a panel of antibodies previously reported to recognize distinct, but not yet specifically defined epitopes of HS in rat, mouse, and human tissue (172,173,298), to determine whether any of them recognized HS present in the retinal eGlx in mice. One antibody of the six tested, RB4Ea12V, recognized HS in the eGlx, evident by staining on the luminal side of the endothelial cell. This is confirmation that HS is present in the retinal eGlx, and to my knowledge is the first time that this has been conclusively shown. The presence of eGlx and HS in the retina microvasculature suggests it may play a functional role in permeability, as it has been shown to do in the glomerulus in **CHAPTER 3**. However, further studies were required to determine whether the role of HS and eGlx in permeability can be applied more broadly to other vessel beds such as the retina.

5.4.2 Loss of Heparan Sulphate Reduced Retinal eGlx and Increases Solute Flux in the Eye

5.4.2.1 Removal of Heparan Sulphate by Heparinase III

To date, the only published work looking at the importance of eGlx components in the retina is one article which focuses on the role of HA, as previously discussed in **CHAPTER 1** (59). In this study, mice were treated with hyaluronidase and eGlx depth was decreased and microvascular leakage increased, measured with fluorescent tracers (59). The authors

did note that hyaluronidase can also shed chondroitin sulphate, another GAG found in the eGlx, so the affects observed may not be specific to HA shedding. This study suggests a role for eGlx in vascular permeability, however the method used to measure eGlx was indirect. In this study, TRITC -dextran (155kDa) and sodium fluorescein were injected into mice, and the diameter of the retinal vessel was measured on ImageJ with each tracer using fluorescent intensity profile peaks at each side of the vessel. The idea behind this method is that sodium fluorescein is a small solute that can easily diffuse through the glycocalyx (*i.e.* diameter observed represents the entire width of the vessel), while dextran is a large molecule which would be excluded by the eGlx (*i.e.* diameter observed represents the area where eGlx is not present). Therefore, taking the difference between the two measurements and dividing it by two, to account for each side of the vessel, represents eGlx depth. While this technique resembles the peak-to-peak method for eGlx measurements used by our group using live and fixed tissue with lectin staining (108,175), the resolution on the videos used to measure vessel diameter with fluorescent tracers is likely not good enough to accurately detect changes in the eGlx, and also does not allow for direct visualisation. Additionally, the study was focused on HA, so the role of HS was not determined. To investigate if HS contributes to eGlx structure and function in the retina, I treated mice with heparinase III. EM images showed that mice treated with active enzyme had a significant reduction in eGlx coverage and a strong trend toward a decrease in eGlx depth, suggesting HS is structurally important in retinal eGlx. Additionally, mice treated with active enzyme had a significant increase in solute flux compared to mice treated with inactive enzyme, suggesting a functional role for not only the eGlx, but also HS eGlx, in the retina. However, it should be noted that the sample size was small for this study (n=3 mice per group) and it would be useful to increase sample size to further corroborate these results. Despite the small sample size for functional studies, these results show for the first time that eGlx HS is structurally and functionally important in the retina, suggesting its loss in disease may be detrimental to microvascular permeability.

5.4.2.2 Reduction of HS Synthesis in Ext1 Mouse Model

Treatment with heparinase III is a systemic treatment and therefore potential effects on other areas besides the eGlx HS cannot be completely dismissed. I therefore used *Ext1*^{CKO} *mice* to determine what affect, if any, an endothelial specific reduction of HS synthesis would have on solute flux in the retina. Solute flux measurements in *Ext1*^{CKO} mice were significantly increased compared to LMC mice, this strengthens the increased solute flux observed in heparinase III treated mice, and strongly suggesting that eGlx HS is important

for iBRB integrity. However, as in **CHAPTER 4**, it would be useful to confirm reduced HS by immunofluorescence in the retinas of these mice, and future studies should focus on finding a suitable antibody to detect these differences.

5.4.2.3 Future Work

Interestingly, comparing baseline measurements of C57BL/6 mice in heparinase III studies to those of LMC in Ext1 knockout studies, shows an average solute flux measurement of 8 cm/s and 4 cm/s, respectively. However, mice in Ext1 studies had been treated with doxycycline for 2 weeks. As the impact of doxycycline on retinal solute flux is not known, it may potentially account for solute flux differences observed between control mice from each study. To address this question, it would be useful to conduct solute flux experiments on age and sex matched LMCs from the Ext1 breeding line, comparing mice given doxycycline in their drinking water, to mice given normal drinking water. This would allow me to determine if the observed differences in the two studies are simply a result of doxycycline treatment. Alternatively, as these mice do not have the exact same genetic background, it is possible that different genetics result in variations in solute flux. However, as both heparinase III and *Ext1*^{CKO} mice had the appropriate controls, the increased solute flux observed in each study individually is still evidence of HS contribution to the iBRB integrity.

Unfortunately, due to time constraints during my PhD, analysis on eGlx depth and coverage in *Ext1*^{CKO} mice in the retina was not completed. However, work with this model is ongoing in our group and will be available for further studies. Additionally, it would be useful to confirm Ext1 knockdown in retina tissue. However, we have previously shown Ext1 knockdown in GEnC **(CHAPTER 3)** and this should reflect all endothelial beds equally. It would also be helpful to specifically confirm reduced HS synthesis by immunofluorescence in the retinas of *Ext1*^{CKO} as mentioned above. However, despite the further needed work to confirm changes to the retina eGlx in these mice, this study shows that mice with reduced HS biosynthesis enzyme Ext1 and there reduced HS, results in loss of iBRB function and is in agreement with heparinase III treatment studies in which HS shedding and loss of eGlx coincided with increased solute flux.

5.4.3 Conclusions and Significance

The work presented in this chapter establishes a role for HS in the eGlx of the retina. To my knowledge, I have shown for the first time that HS is present in the eGlx of the retina, and enzymatic loss of HS results in reduced eGlx and increased solute flux. The importance

of HS was further confirmed by an Ext1 knockout model, showing that *Ext1*^{CKO} mice had an increase in solute flux, suggesting that retinal eGlx HS is important for iBRB integrity. These studies will serve as the groundwork for investigating the role of HS in vascular disease in the retina, such as diabetic retinopathy **(CHAPTER 6)**, where there is evidence of eGlx loss and increased permeability, which can result in loss of sight if not treated.

Chapter 6 Loss and Restoration of Retinal Endothelial Glycocalyx Heparan Sulphate in a Type 2 Diabetic Mouse Model

6.1 *Introduction*

6.1.1 Mouse Models of Diabetic Retinopathy

Currently there is no individual *in vivo* model that develops all of the vascular and neural complications that occur at all stages of diabetic retinopathy (DR), but a number of models have been developed that replicate many of the aspects of the disease at different time points of DR observed in humans. As with DN, DR models are either inducible or genetic.

The most common inducible model for DR is STZ, and is often used on a C57BL/6 background or the F1 hybrid, a cross between FVB/N and C57BL/6J mice (299). STZ mouse models develop early signs of DR, such as loss of astrocyte number and activation of retinal glia by 4-5 weeks after the onset of hyperglycaemia (300,301). In humans, changes in retinal glia have been shown to precede vascular damage (302). By six weeks, loss of retinal ganglion cells (RGC) can be observed, followed by retinal layer thinning of the inner nuclear and outer nuclear layer at 10 weeks (303). Loss of RGC have been shown in T2D patients with no DR, and is progressive in moderate and severe DR (304), making it an early sign of DR. Similarly, thinning of the inner and out nuclear layers have been observed in diabetics without clinical evidence of DR using optical coherence tomography (OCT) imaging, and is caused by ischaemia and retina tissue injury (305). OCT imaging uses interferometry to create a cross sectional image of the retina *in vivo*, and is of standard use in diabetic patients to monitor retinal health and diagnosis of DR (306). Basement membrane thickening, which is often observed in DR, was not found to occur on a C57BL/6J background up to 15 months after diabetes was induced (307). However, increased leak in the retina can be detected with fluorescent tracers like FITC-dextran in this model on a C57BL/6 background, although a marked increased does not occur until 6 months after the induction of diabetes (308). Though this model may be a good one for studying DR in isolation, mice on a C57BL/6 background are a poor model of DN as discussed in **CHAPTER 4**, and therefore not a good choice for studying both microvascular complication in the same animal.

The *Ins2*^{Akita} mouse line, previously mentioned in **CHAPTER 4**, is a genetic model for studying DR. These mice develop some signs of vascular changes associated with DR, an important factor for the studies in this thesis. On a C57BL/6J background, mice developed signs of glial activation by 8 weeks after the commencement of hyperglycaemia, and retinal thinning after 22 weeks (309). After 12 weeks of hyperglycaemia, diabetic mice injected with BSA-FITC had increased retinal vascular leak (309). Mice also had a loss of the tight junction protein occludin in their retinal vessels, which likely contributes to increased permeability (309). This model is now regarded as a useful tool for studying early signs of DR (310), but unfortunately is incompatible with studying early signs of DN in the same mouse, as mice on this background develop only mild albuminuria and do not show robust changes indicative of DN (217).

The genetic T2D model *db/db* on a C57BLKS/J background have also been used to study the development of DR. *Db/db* mice have loss of RGC at 8 weeks of age (311). Mice also have inner and out nuclear layer and total retinal thinning at 8 weeks of age (311), a feature of neurodegeneration in DR also found in humans (312). Pericyte loss, which is a hallmark of DR in humans (313), occurs by 18 weeks of age in *db/db* mice, along with the presence of active glia (300). Pericytes have been shown to play important roles in the retina including vascular remodelling and stabilization and maintenance of the iBRB (314). Additionally, an increase in FITC-dextran leak was reported at 20 weeks of age as well as an increase in albumin accumulation in the retina parenchyma, suggesting a breakdown in the iBRB (315). At 22 weeks, retinal vascular basement membrane thickening can be observed (316). These data suggest that *db/db* mice may serve as a good model to study early vascular changes in DR, and have the added benefit of being a suitable models for DN with increased albuminuria from 8-25 weeks of age (227,228). Although *db/db* mice may not be the best model for studying each diabetic complication individually, their susceptibility to DR and DN to levels that are suitable for this study led me to choose *db/db* mice as a T2D model to investigate my hypotheses. As mentioned in **CHAPTER 4**, I am interested in early changes in the microvasculature. As a result, I used two time points of 9 weeks and 11 weeks of age to investigate loss and restoration of eGlx, as the literature suggest there are retinal change associated with DR by 8 weeks of age. Importantly, these timepoints were also chosen to allow for a parallel investigation of changes in DN and DR.

6.1.2 Heparanase in Diabetic Retinopathy

As discussed in **CHAPTER 1**, diabetic rodent models have provided evidence for a loss of eGlx in diabetic retinas by EM (57). Additionally, human studies have also shown a

decrease in glycocalyx dimensions in T2D patients (57). However, what the cause of eGlx damage in diabetic retinas has not been examined. HPSE is found to be upregulated in the plasma of T1D and T2D patients as previously discussed (245,317,318). Though not much research has been done on the role of HPSE in DR, the presence of active HPSE in the plasma suggest that HPSE ultimately becomes systemic, with the possibility of affecting multiple vascular beds, including the retina. Epithelial, endothelial cells, leukocytes, granulocytes, and mast cells, have all been shown to be sources of HPSE (263,319). Human vitreous samples from DR patients have elevated HPSE levels (125). In addition, epiretinal membranes from DR patients also show increased HPSE, with evidence of vascular endothelial cells and leukocytes as the source of HPSE (125). In agreement with this, immunohistochemistry staining of retinas from T1D rats also have increased HPSE expression, with increased vascular endothelium staining **(FIGURE 6-1)** (125).

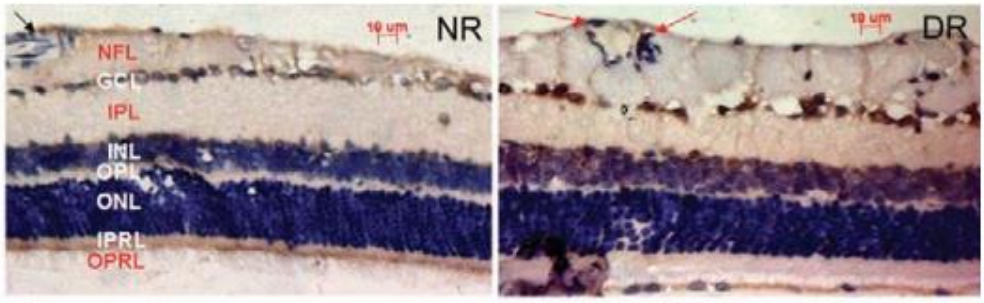

Figure 6-1 HPSE Expression in Diabetic Retinopathy

A. IHC on STZ-induced diabetic rats (DR) shows HPSE is increased when compared to non-diabetic rats (NR). Red arrows point to HPSE signal in endothelium of retinal vessel of DR, whereas NR has minimal staining (black arrows). Staining was also increased in ganglion cell layer (GCL), inner nuclear layer (INL), and outer nuclear layer (ONL). Image adapted from (Ma, et al. 2010)(125). Scale bar not published.

Briefly mentioned in **CHAPTER 5**, a study on T1D mice showed upregulated HPSE expression in STZ treated C57BL/6 mouse retinas, which the authors claim coincided with loss of HS and TJ proteins (294). Although *in vitro* studies in human retinal endothelial cells did provide evidence for high glucose-inducing HPSE expression and loss HS, the author's *in vivo* studies provided no evidence for loss of HS (294). They did however show reduced tight junction proteins and an increase in HPSE expression *in vivo* (294). Although the authors conclude that there is a loss of basement membrane HS, their *in vitro* data investigating loss of HS was obtained by western blot, so it cannot be assumed these

results pertain to basement membrane HS as suggested in the article. Since loss of HS was also not verified *in vivo*, more work needs to be done to confirm the loss of eGlx HS in the retina during diabetes. Despite this, these data support the idea that HPSE plays a role in diabetic retinopathy and preventing loss of HS may help prevent damage to the iBRB and associated increased microvascular permeability.

6.1.3 Chapter Aims and Experimental Approaches

The aim of this chapter is to show there is loss of retinal eGlx HS in diabetes, which results in increased vascular permeability. And that this is HPSE-dependent. To do so, I took the following two approaches.

1. Show that retinal eGlx is damaged in a T2D model and results in loss of eGlx function and increase retinal permeability. This was done at two different timepoints, 9 weeks of age and 11 weeks of age.
2. Show that damage to the eGlx can be prevented by treatment with a novel HPSE inhibitor, and results in reduced retinal permeability in diabetes. This was done at two different timepoints, 9 weeks of age and 11 weeks of age.

6.2 *Methods*

These methods are not inclusive. The methods described in this section are those that pertain specifically to this chapter or have been adapted for experiments in this chapter. All other methods are described in the **CHAPTER 2 METHODS AND MATERIALS**.

6.2.1 Study Design for Nine-Week-Old Time Point

At 7 weeks of age, lean control and *db/db* control mice were administered vehicle treatment (PBS), daily for two weeks s.c. Similarly, OVZ/HS-1638 group received daily injections for two weeks of OVZ/HS-1638 dissolved in PBS at 20mg/kg, subcutaneously. OCT imaging and sodium fluorescein angiographies were performed at 9 weeks as described in **CHAPTER 2** except for sodium fluorescein injection, which was given intramuscularly (i.m) in this cohort. At end point, mice were anesthetised and perfused as described in **CHAPTER 2** for tissue collection and EM imaging. A schematic of the experimental design in shown in **FIGURE 6-2**.

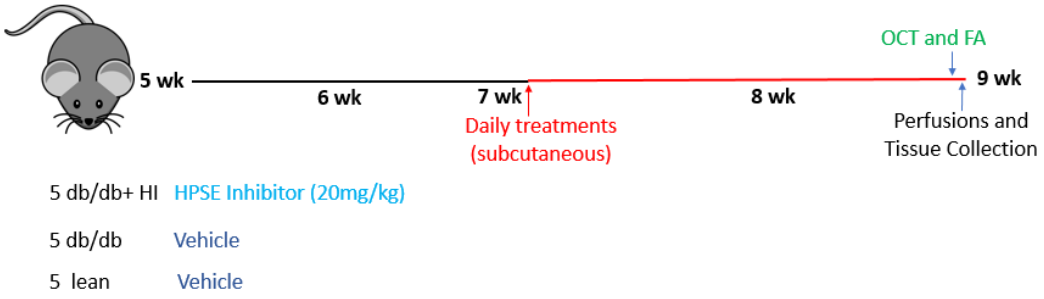

Figure 6-2 Study Design for Nine-Week-Old Time Point

At 7 weeks, five lean and five db/db mice were treated with vehicle subcutaneously (s.c.). Five db/db mice were treated with 20mg/kg OVZ/HS-1638 HPSE inhibitor in vehicle, also by s.c. At 9 weeks OCT and sodium fluorescein angiographies (FA) were performed. Mice were cardiac perfused and tissue collected as in methods.

6.2.2 Study Design for Eleven-Week-Old Time Point

At 9 weeks of age, lean control and *db/db* control mice were administered vehicle treatment (PBS), daily for two weeks by i.p. Similarly, OVZ/HS-1638 group received daily injections for two weeks of OVZ/HS-1638 dissolved in PBS at 20mg/kg, i.p. OCT imaging and sodium fluorescein angiographies were performed at 9 weeks as described in **CHAPTER 2** with the exception of anaesthesia for this procedure. For Micron IV imaging, mice were anaesthetised by intraperitoneal injection of 90µL/10g body weight of a solution containing 6 mg/mL ketamine (Ketavet; Zoetis Ireland Ltd., Dublin, Ireland) and 2 mg/mL Xylazine (Rompun; Bayer plc, Newbury, UK) mixed with sterile water. This differs from the method used in the 9-week old cohort, as specialised mask required for anaesthesia was not available. At endpoint, mice were anesthetised and perfused as described in **CHAPTER 2** for tissue collection and EM imaging. A schematic of the experimental design in shown in **FIGURE 6-3**.

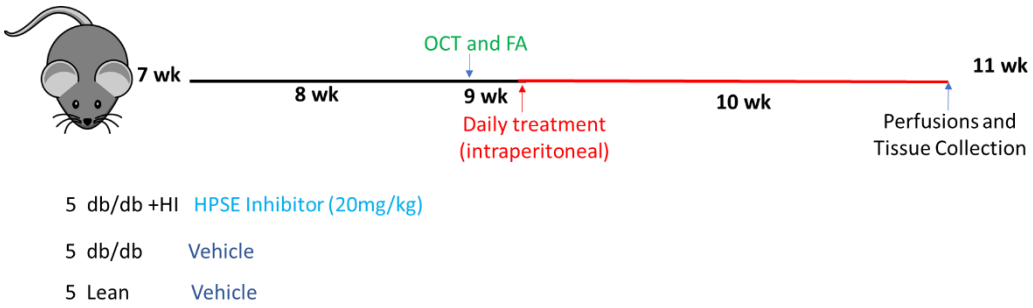

Figure 6-3 Study Design for Eleven-Week-Old Time Point

At 9 weeks of age, before treatment, OCT and sodium fluorescein angiographies (FA) were performed At 9 weeks five lean and five db/db mice were treated with vehicle i.p. Five db/db mice were treated with 20mg/kg OVZ/HS-1638 HPSE inhibitor in vehicle, also by i.p. At 11 weeks, mice were cardiac perfused, and tissue collected as in methods.

6.2.3 Optical Coherence Tomography (OCT) Images and Analysis

6.2.3.1 OCT Images

Mice were prepared for imaging as described in **CHAPTER 2**. OCT images were obtained on the Micron IV imaging system (Phoenix Research Labs). Scan area was chosen by selecting circular tool, using the optic nerve as a reference point, where the optic nerve was at the centre of the circle. It should be noted that the area selected for scanning must be consistent throughout animals in order to directly compare retinal thickness. This is due to the natural thinning of the retina, moving from the optic nerve to the outer edge of the retina.

6.2.3.2 OCT Image Analysis: Retinal Thickness

OCT images were taken using the Micron IV imaging system described above. To measure total retina thickness, a line from the top of the retina to the bottom of the retina (from ganglion cell layer to retinal pigment epithelium) **(FIGURE 6-4)** was drawn on FIJI and length measured. Choroid was excluded from retina thickness measurements as shown in **(FIGURE 6-4)**. A minimum of 10 measurements were taken per mouse per timepoint measured. Average of measurements were then calculated for total retina thickness.

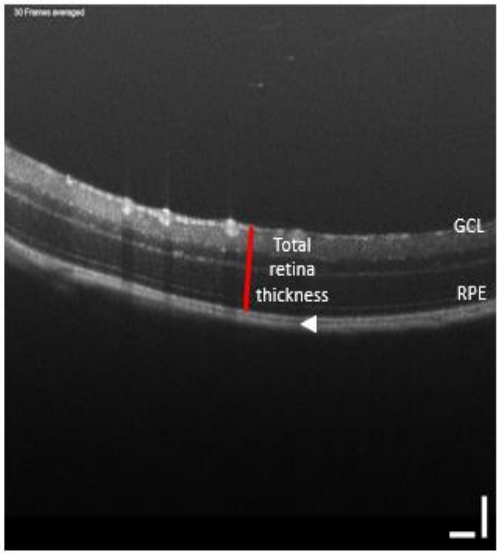

Figure 6-4 Analysis of Total Retina Thickness from OCT Images

Red line indicates where measurements are taken for total retinal thickness, from ganglion cell layer (GCL) to retinal pigment epithelium (RPE). Arrowhead points to choroid which is excluded from retina measurement. Vertical scale bar = 100µm.

6.2.4 Albumin Staining, Imaging, and Analysis on Mouse Retinas

6.2.4.1 Albumin Staining in Paraffin Embedded Retina

Eyes from 9-week-old lean and *db/db* mice were enucleated and put into 4% PFA. Paraffin embedded eyes were sectioned longitudinally in 5µM sections at the University of Bristol Histology facility. For staining, sections were deparaffinised in Xylenes for 10min, twice. Sections were then rehydrated by running through a decreasing percentage series of ethanol for 5min each (100%, 95% 70%, 50, deionised water). Sections were then incubated in PBS for 5min. Tissue was permeabilised and blocked with 0.3% Triton-X, 3% BSA in PBS solution for 30min. Goat anti-mouse albumin (A90-134A-17, Bethyl Laboratories) was then incubated at 1:200 in blocking buffer overnight at 4°C in a humidity chamber. The following day, sections were washed three times for 5min in 0.3% Triton-X in PBS. Donkey anti-goat Alexa Fluor 594 (A-11058, ThermoFisher Scientific) was then incubated at 1:200 in blocking buffer for 1 hour at room temperature. Sections were washed as described above, followed by a 5min incubation in DAPI as previously described. Sections were washed twice in PBS for 5min and coverslip mounted as previous.

6.2.4.2 Imaging and Analysis

Sections were imaged on Nikon TI inverted confocal microscope (Nikon Instruments Inc). Exposure settings were kept constant for all sections. A minimum of four fields of view were taken per animal on 20x objective.

To analyse extravascular albumin staining, brightfield images were used to trace around the retina in order to exclude choroidal and vitreous staining using FIJI **(FIGURE 6-5 A)**. On the red channel, area and Intergraded density (IntDen) measurements were taken for total retina albumin measurement **(FIGURE 6-5 B)**. Four background mean fluorescent measurements were taken as well to calculate CTCF. As these eyes were not perfused, vascular staining, which appears as bright circular staining (cross section of vessel) or long tube like staining (longitudinal section of vessel) in the retina was traced around and area and IntDen measurements were taken **(FIGURE 6-5 B,C)**. Total retina albumin CTCF was calculated using the same CTCF equation as previous and shown below.

$$CTCF = IntDen - (area\ of\ region\ of\ interest\ x\ mean\ fluorscece\ of\ background\ means)$$

Equation 6-1

The same calculation was done for vascular albumin staining by adding together the sum of the vascular area and sum of the vascular albumin IntDen measurements using these totals to calculate CTCF. Subtracting vascular albumin CTCF from total retina albumin CTCF yields extravascular albumin staining CTCF, or:

$$Extravascular\ Albumin\ CTCF = Total\ Retina\ Albumin\ CTCF - Total\ Intravascular\ Albumin\ CTCF$$

Equation 6-2

CTCF for each fields of view were averaged for each mouse and the means of each group were used to determine statistical significance.

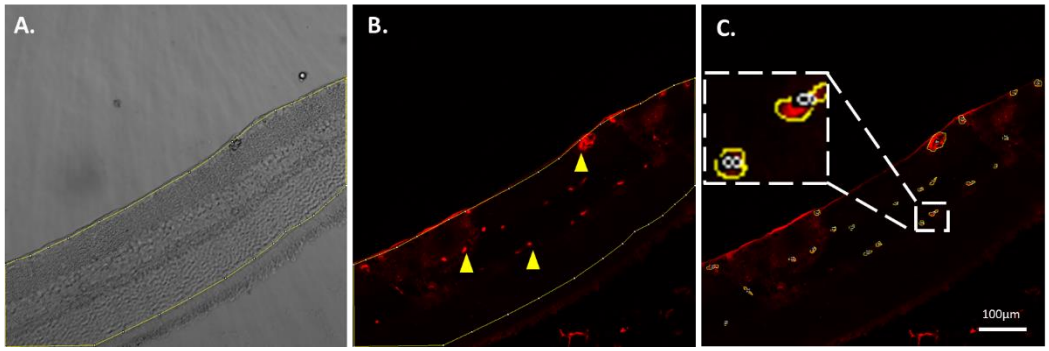

Figure 6-5 Analysis of Albumin Leak in Mouse Retina

Mouse retinal sections are stained with anti-albumin and amount of extravascular albumin is quantified. A. The region of interest is outlined shown in yellow using bright field images ensuring that choroid is excluded. B. Channel is switched to albumin staining (red) and CTCF is measured for the entire retina. Vascular albumin staining appears as bright red punctate signal, indicated by arrow heads C. Total vascular albumin staining is traced around and CTCF is measured. Inset shows zoomed in area to demonstrate tracing. This value is then subtracted CTCF calculated in B to yield extravascular CTCF.

6.3 *Results*

6.3.1 Diabetic Mice at Nine Weeks of Age

6.3.1.1 Nine-Week-Old Db/db Mice Have Retina Thinning which is Not Affected by OVZ/HS-1638 Treatment

To assess if *db/db* mice had developed signs of neurodegeneration, which can be observed in early stages of DR, OCT images were used to measure changes in retinal thickness. **FIGURE 6-6 A** shows representative OCT images for lean, *db/db*, and *db/db* mice treated with OVZ/HS-1638. Although small changes are not visible by eye, measurements of thickness show that all db/db mice have a significant reduction in retinal thickness, which is not affected by OVZ/HS-1638 treatment **FIGURE 6-6 B**.

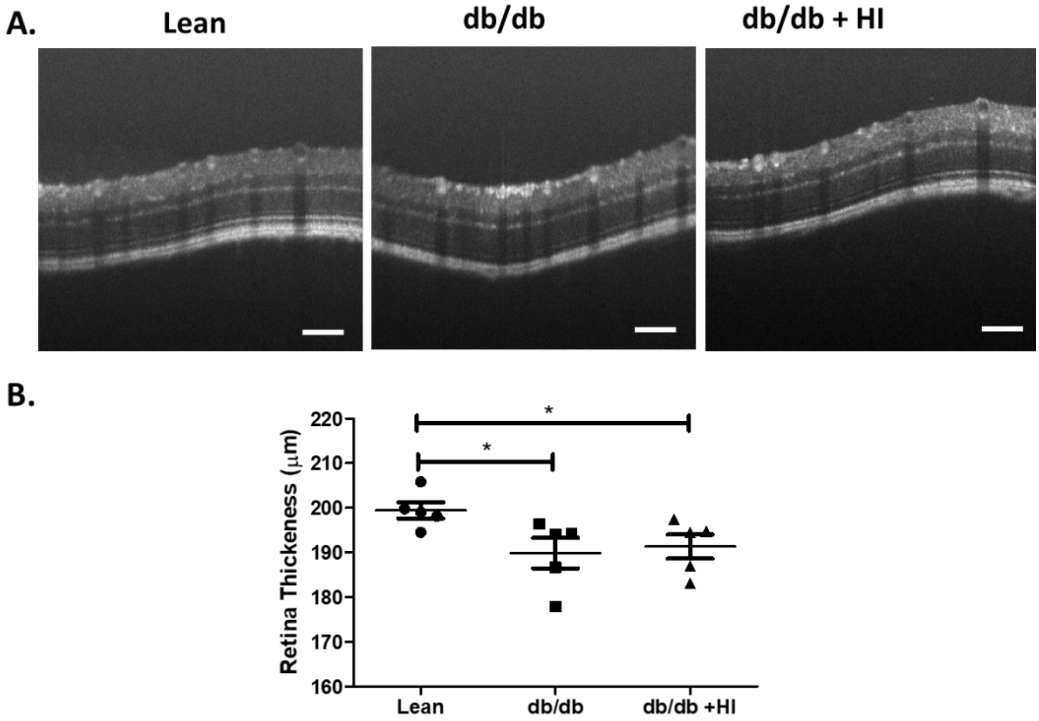

Figure 6-6 Nine-Week-Old Db/db Mice Have Retinal Thinning which is Not Affected by OVZ/HS-1638 Treatment

A. Representative OCT images for non-diabetic (lean), diabetic (db/db), and db/db mice treated with OVZ/HS-1638 HPSE inhibitor (db/db+HI) Vertical scale bar = 100μm. B. Total retinal thickness was measured on OCT images. Minimum of 10 measurements per mouse. N=5 mice, one-way ANOVA, Tukey's multiple comparison test indicated, *p<0.05.

6.3.1.2 *Nine-Week-Old Db/db Mice Have No Changes in Microvascular Basement Membrane Thickness*

Basement membrane thickening is a common feature of DR, and is associated with loss of integrity of the iBRB (320). To determine whether *db/db* mice had changes in microvascular basement membrane and whether OVZ/HS-1638 treatment had any effect on it, EM images were used to measure changes in basement membrane thickness between groups. At 9 weeks old, there were no significant changes in basement membrane thickness between groups, though there was a slight trend toward an increase in all *db/db* mice **FIGURE 6-7**.

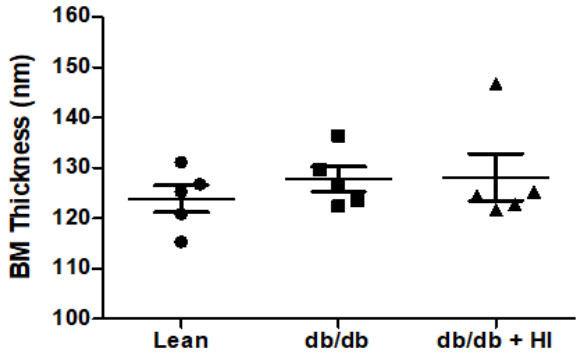

Figure 6-7 Nine-Week-Old Db/db Mice Have No Changes in Basement Membrane

EM images of non-diabetic (lean), diabetic (db/db), and db/db mice treated with OVZ/HS-1638 HPSE inhibitor (db/db+HI) were analysed for changes in basement membrane (BM) thickness. Minimum of three capillaries were measured per mouse. N=5 mice, one-way ANOVA, Tukey's multiple comparison test, not significant.

6.3.1.3 *Treatment with OVZ/HS-1638 Increases Retinal eGlx in Nine-Week-Old Db/db Mice*

There is some evidence in the literature suggesting that eGlx is reduced in the retina during diabetes. To determine if these mice had any changes in their eGlx, EM images of retinal microvessels from mice perfused with Alcian blue and glutaraldehyde were taken and analysed. Representative images of eGlx in these mice show that both lean and *db/db* mice treated with OVZ/HS-1638 had thick eGlx. *Db/db* mice treated with vehicle however appeared to have thinner and patchier eGlx compared to the other two groups, indicating damage to the eGlx **(FIGURE 6-8 A)**. Surprisingly, quantification of EM images showed there were no significant changes in eGlx depth between groups, however there was a strong trend toward a decrease in *db/db* mice and an increase in *db/db* mice treated with OVZ/HS-1638 **(FIGURE 6-8 B)**. Similarly, there was a strong trend toward a decrease in eGlx coverage in *db/db* mice. However, there was a significant increase in eGlx coverage which OVZ/HS-1638 was given **(FIGURE 6-8 B)**, indicating a restoration of eGlx.

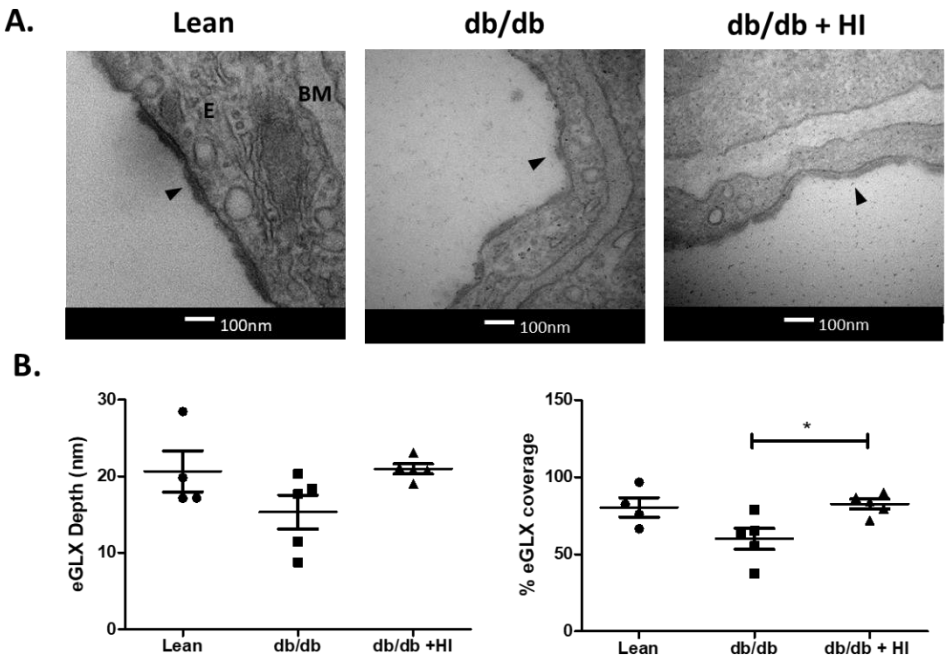

Figure 6-8 Treatment with HPSE Inhibitor Increases Retinal eGlx in Nine-Week-Old Db/db Mice

A. Representative EM images of retina from non-diabetic (lean), diabetic (db/db), and db/db mice treated with OVZ/HS-1638 HPSE inhibitor (db/db+HI). Basement membrane (BM) and endothelial cell (E) shown. Arrowheads point to eGlx. B. EM images were analysed for eGlx depth (left) and eGlx coverage (right). N= 5 mice, one-way ANOVA, Tukey's multiple comparison test indicated, *p<0.05.

6.3.1.4 Db/db Mice Have No Changes in Solute Flux at Nine Weeks of Age

Previous functional studies in **CHAPTER 5** showed that eGlx plays a role in maintaining the iBRB, as healthy mice with loss of eGlx HS had increased solute flux. Although eGlx loss was not significant in *db/db* mice, there was a decrease. I therefore performed sodium fluorescein angiographies to determine if there were any changes in solute flux. At nine weeks of age, there did not appear to be any significant changes in solute flux **FIGURE 6-9**.

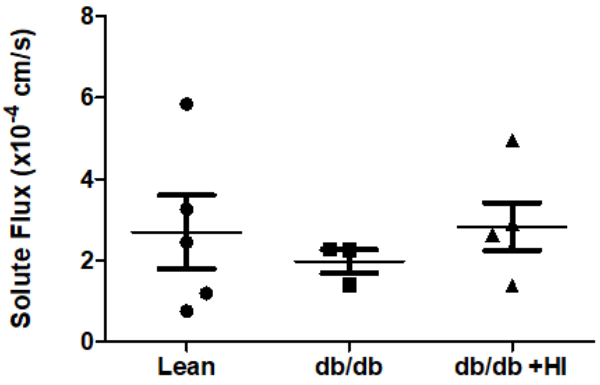

Figure 6-9 Db/db Mice Have No Changes in Solute Flux at Nine Weeks of Age

Solute flux measurements for non-diabetic (lean), diabetic (db/db), and db/db mice treated with OVZ/HS-1638 HPSE inhibitor (db/db+HI) were taken at 9 weeks of age. N=3-5 mice per group. One-way ANOVA, Tukey's multiple comparison test, not significant.

6.3.1.5 Db/db Mice Have Increased Albumin Leak at Nine Weeks of Age which is Prevented by OVZ/HS-1638 Treatment

As a second method of determining if *db/db* mice had a breakdown in the iBRB, despite no observed changes in solute flux, I stained for albumin in the retinas from nine-week-old mice. Albumin staining on *db/db* retinas revealed staining in the retinal parenchyma space, indicating albumin leak, which was absent in lean mice and visibly reduced in mice treated with OVZ/HS-1638 **(FIGURE 6-10 A)**. Quantification of images measuring extravascular albumin CTCF values showed that *db/db* mice had a significant increase in extravascular albumin compared to lean mice **(FIGURE 6-10 B)**. Furthermore, this was significantly reduced when mice were treated with OVZ/HS-1638, indicating a protective effect of the inhibitor on the iBRB in *db/db* mice **(FIGURE 6-10 B)**.

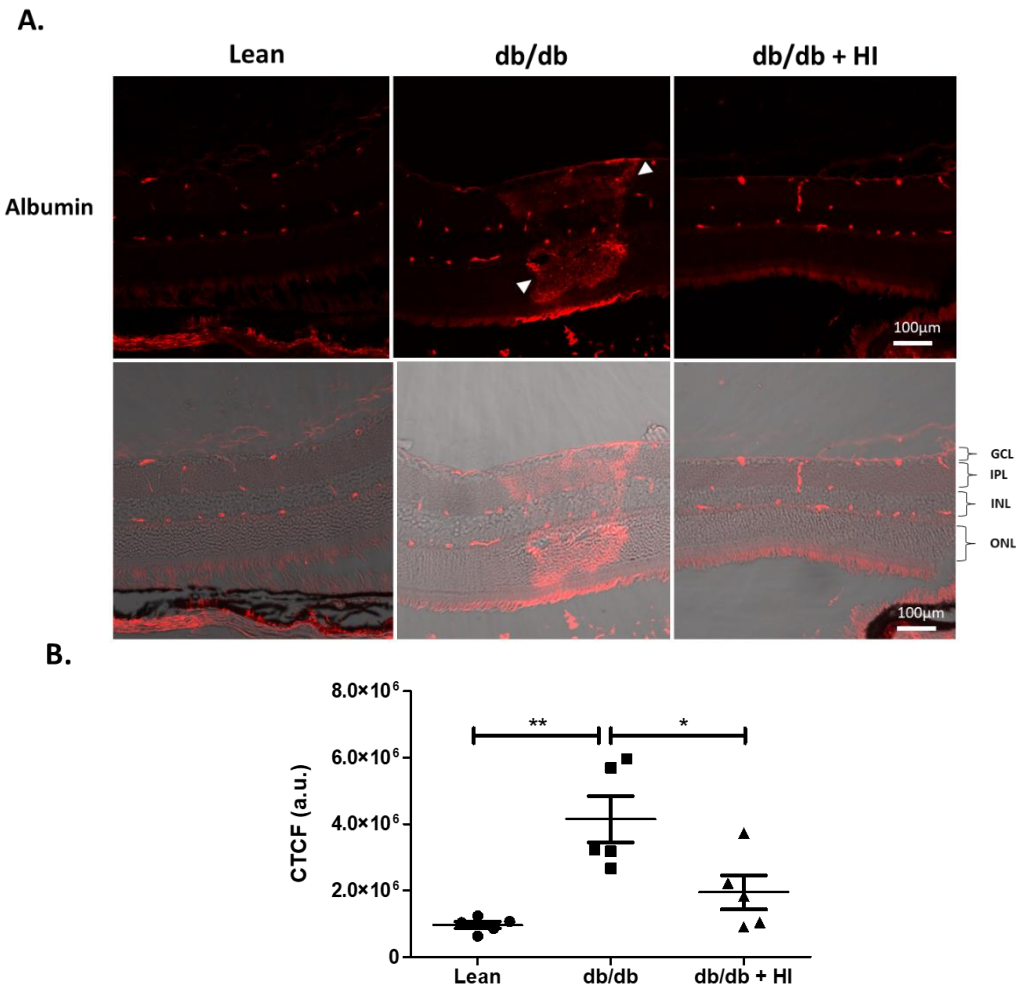

Figure 6-10 Db/db Mice Have Increased Albumin Leak at Nine Weeks of Age, which is Prevented by OVZ/HS-1638 Treatment

*A. Representative immunofluorescence images of anti-albumin stained retina from non-diabetic (lean), diabetic (db/db), and db/db mice treated with OVZ/HS-1638 HPSE inhibitor (db/db+HI). Top panel: albumin and bottom panel: brightfield merge. Layers of retina indicated, ganglion cell (GCL), inner plexiform (IPL), inner nuclear (INL), and outer nuclear (ONL) B. Extravascular albumin CTCF was measured (white arrow heads) arbitrary units (a.u.), minimum of three field of view analysed. N= 5 mice, one-way ANOVA, Tukey's multiple comparison test indicated, *p<0.05 **p<0.01.*

6.3.2 Diabetic Mice at Eleven Weeks of Age

6.3.2.1 Db/db Retina Thickness Could Not be Assessed in Eleven-Week-Old Cohort

Unfortunately, due to technical difficulties involving the use of the Micron IV Imaging system used for OCT imaging, I was not able to obtain OCT images for mice at 11 weeks of age. An incomplete set of images was obtained at 9 weeks of age. The images that were obtained show that *db/db* mice have a decrease in retinal thickness at 9 weeks **(FIGURE 6-11)**, however statistical analysis could not be performed due to insufficient sample size.

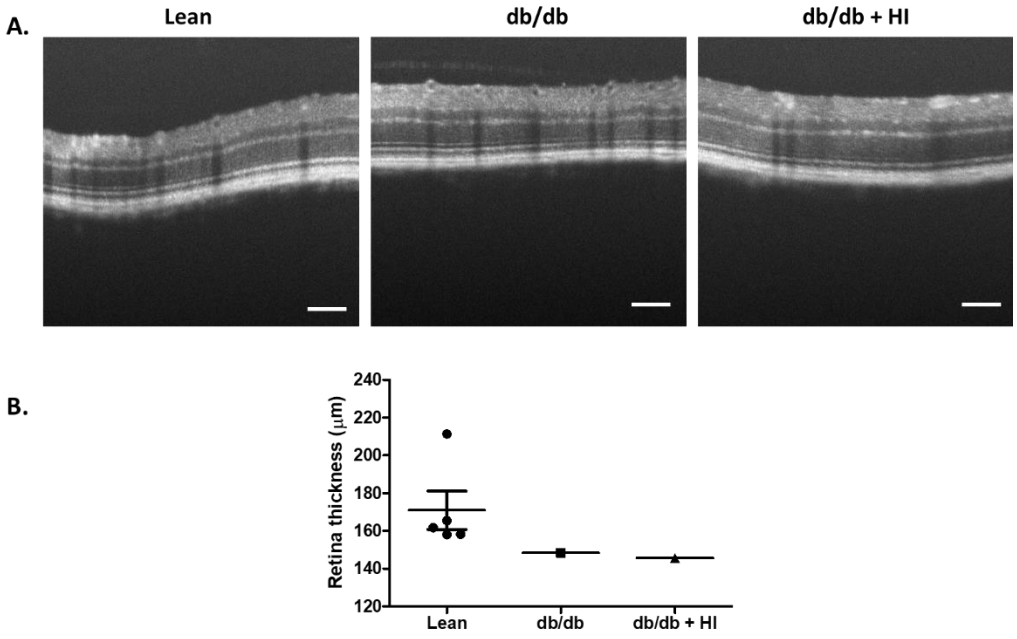

Figure 6-11 Db/db Retinal Thickness Could Not be Assessed in Eleven Week Old Cohort

Retinal thickness measurements from OCT images were taken for non-diabetic (lean), diabetic (db/db), and db/db mice treated with OVZ/HS-1638 HPSE inhibitor (db/db+HI). Minimum of 10 measurements were taken per mouse. N=5-1 mouse per group.

6.3.2.2 *Db/db Mice Do Not Have Changes in Basement Membrane Thickness at Eleven Weeks of Age*

As in the 9-week-old cohort, I wanted to determine if mice at 11 weeks of age had any changes in basement membrane thickness, a characteristic change in DR. Basement membrane measurements using EM images showed no significant differences between any groups **(FIGURE 6-12)**.

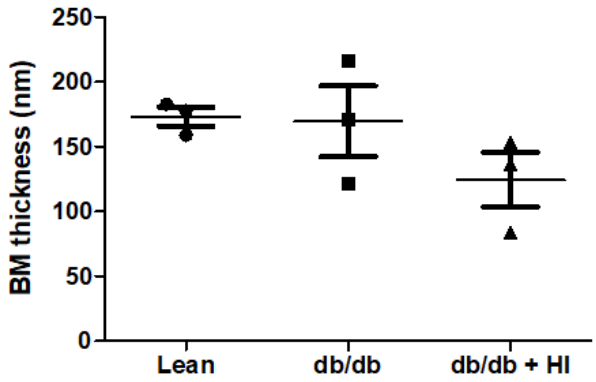

Figure 6-12 Db/db Mice Do Not Have Changes in Basement Membrane Thickness at Eleven Weeks of Age

EM images of non-diabetic (lean), diabetic (db/db), and db/db mice treated with OVZ/HS-1638 HPSE inhibitor (db/db+HI) were analysed for changes in basement membrane (BM) thickness. Minimum of three capillaries were measured per mouse. N=3 mice, one-way ANOVA, Tukey's multiple comparison test, not significant.

6.3.2.3 Changes in eGlx Could Not Be Reliably Assessed in Eleven-Week-Old Cohort

As previous, loss and restoration of eGlx in *db/db* and *db/db* mice treated with OVZ/HS-1638 was assessed using quantitative EM on images from mice perfused with Alcian blue and glutaraldehyde. **FIGURE 6-13 A** shows representative EM images from each group, where eGlx can be observed, albeit patchy and thinner than previously observed in all groups. Quantification of images showed no apparent changes in eGlx **(FIGURE 6-13 B)**. Unfortunately, perfusion in this cohort did not seem to properly reach the eye and one animal in the OVZ/HS-1638 group did not perfuse at all, therefore statistical significance could not be determined for this cohort and results were inconclusive **(FIGURE 6-13 B)**.

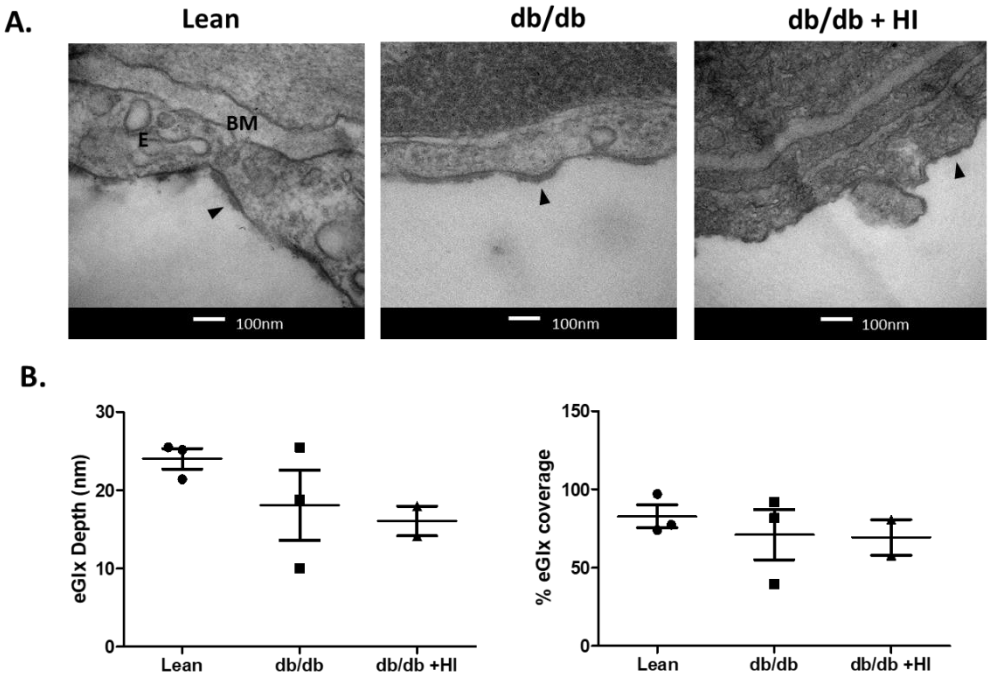

Figure 6-13 Changes in eGlx Could Not Be Reliably Assessed in Eleven Week Old Cohort

A. Representative EM images of retina from non-diabetic (lean), diabetic (db/db), and db/db mice treated with OVZ/HS-1638 HPSE inhibitor (db/db+HI). Basement membrane (BM) and endothelial cell (E) shown. Arrowheads point to eGlx. B. EM images were analysed for eGlx depth (left) and eGlx coverage (right). N= 2-3 mice.

Poor perfusion is further evident in low power images of the retinal microvessels, showing that vessel structure is collapsed **(FIGURE 6-14)**, indicating that the vessels did not perfused well and eGlx changes cannot be reliably assessed.

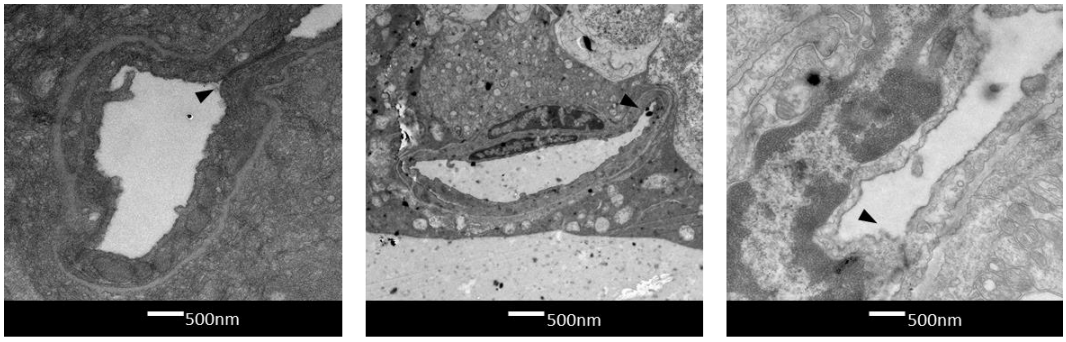

Figure 6-14 Collapsed Vessel Structure Due to Poor Perfusion

Example of low magnification EM images of perfused mouse retinal vessels used for eGlx analysis. Arrowheads point to collapsed vessel structure.

6.3.2.4 *Changes in Solute Flux Could Not Be Reliably Assessed in Eleven-Week-Old Cohort*

To examine if db/db mice had reduced function of iBRB, sodium fluorescein angiographies were performed to determine if 11-week *db/db* mice had changes in solute flux. Unfortunately, as with the OCT images, technical difficulties prevented me from obtaining videos for analysis at 11 weeks of age. An incomplete set was obtained at 9 weeks of age, prior to the start of treatment. Solute flux measurements show a potential decrease in *db/db* mice, contrary to what would be expected if a break down in the iBRB had occurred **(FIGURE 6-15)**. However, the small sample size does not allow for a statistical test to be performed and therefore no conclusions can be made.

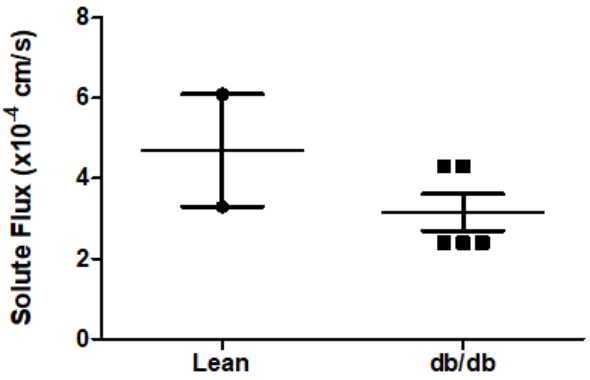

Figure 6-15 Changes in Solute Flux Could Not Be Reliability Assessed in Eleven Week Old Cohort

Solute flux measurements were obtained for non-diabetic (lean) and diabetic (db/db) prior to the start of treatment. N=2-5 mice per group.

6.3.3 Assessment of Model Suitability for Angiography Studies

6.3.3.1 Aged Db/db Mice Do Not Show Changes in Solute Flux

Although the 11-week-old cohort did not have a complete set of sodium fluorescein angiography videos for solute flux analysis, the 9-week-old cohort showed no changes in solute flux in *db/db* mice, which was contradicted by the retinal albumin staining in these mice. Albumin staining showed a clear increase in albumin leak and reduction by OVZ/HS-1638 treatment. Furthermore, solute flux results in heparinase III and *Ext1*^{CKO} studies in **CHAPTER 5** suggest that this method of measuring solute flux is sensitive enough to measure changes in solute flux. I therefore conducted a pilot experiment to determine if this technique is suitable for *db/db* mice and whether it was possible to detect changes in solute flux in more progressed DR. To do this, I performed solute flux measurements on *db/db* or lean mice every two weeks, from 6 to 14 weeks of age. Unfortunately, one *db/db* mouse died at 7 weeks of age due to natural causes, and therefore the sample size for *db/db* mice was n=2 for the duration of the experiment. As shown in **FIGURE 6-16**, there are no clear differences in solute flux between lean and *db/db* mice. **FIGURE 6-16 B** also demonstrates that there is no progression of solute flux increase as would be expected if DR was progressing in this model.

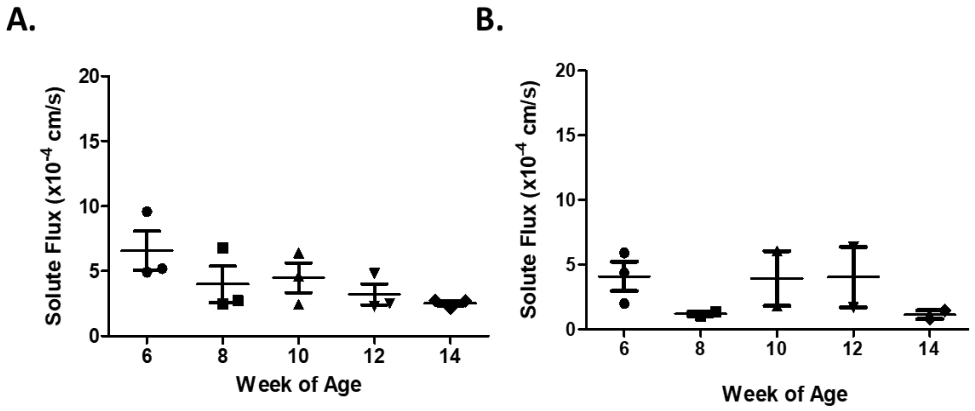

Figure 6-16 Aged Db/db Mice Do Not Show Changes in Solute Flux

Solute flux measurements were taken every two weeks for non-diabetic (lean) and diabetic (db/db) mice from 6-14 weeks of age. A. Solute flux measurements for lean mice, n=3 mice. B. Solute flux measurements for db/db mice, n=2 from 8-14 weeks.

6.3.3.2 *Sodium Fluorescein Absorption Rate is Delayed in Db/db Mice*

During acquisition of sodium fluorescein angiographies, it became apparent that there were differences in appearance of fluorescent signal between lean and *db/db* mice. As shown in **FIGURE 6-17**, at 9 minutes and 24 seconds, the angiography image for the lean mouse was significantly brighter compared to that of a *db/db* mouse. Saturation of sodium fluorescein is apparent in the main vessels, especially near the optic nerve where the central retinal artery and vein are located and feed into the retinal microvasculature **(FIGURE 6-17 A)** (321). The angiography in the *db/db* mouse however does not show similar intensity **(FIGURE 6-17 B)**.

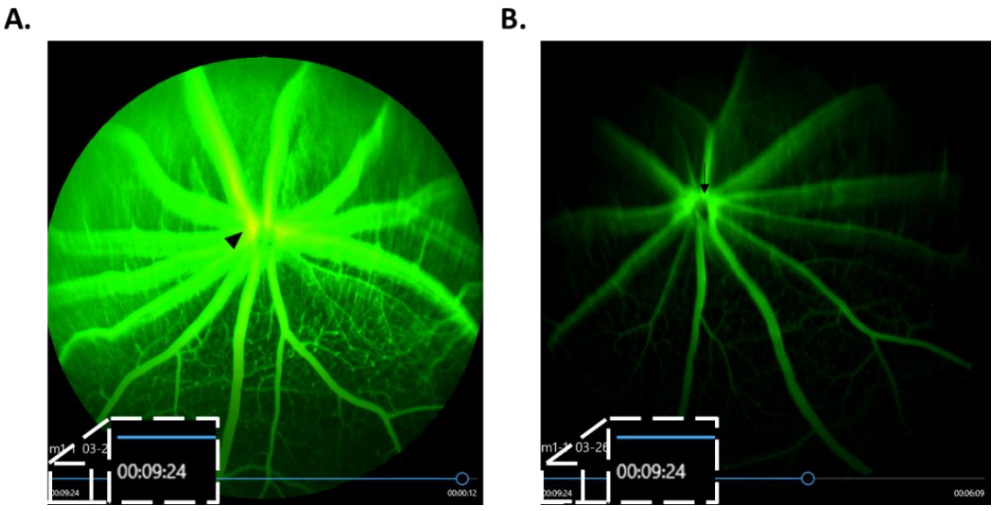

Figure 6-17 Comparison of Sodium Fluorescein Intensity in Lean and Db/db Mice

A. Sodium fluorescein angiography for a lean mouse at time 9:24 minutes. Saturation is evident by yellow signal (arrowhead). B. Sodium fluorescein angiography for db/db mouse at time 9:24minutes. No saturation is present including near the optic nerve (arrow).

Measurements of fluorescent intensity in large vessels in lean and db/db mouse are shown in **FIGURE 6-18 A,B**. Measurements for the lean mouse show that intensity starts to plateau near 50 seconds, with an intensity measurement nearing 140a.u. Fluorescent intensity in the *db/db* mouse however is steadily increasing through the entire duration of the video, and has an intensity value around 30a.u., at 40 seconds of recording. Similarly, in the exchange vessels, at 50 seconds, an intensity value of 20a.u. had been reached in the lean mouse, whereas at 50 seconds in the db/db mouse, the intensity value was approximately 3a.u. This indicates that there is a substantial difference in absorption rate of the sodium fluorescein between lean and *db/db* mice, which results in difficulty comparing lean and *db/db* mice solute flux measurements.

A.

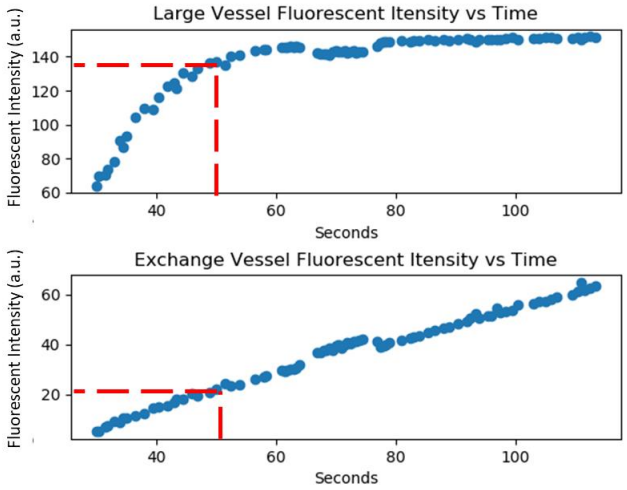

B.

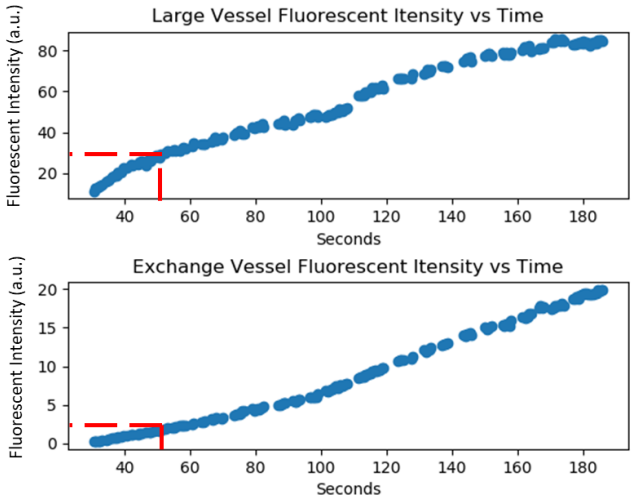

Figure 6-18 Fluorescent Intensity Curves for Main Vessels and Exchange Vessels in Lean and Db/db

Fluorescent intensity profiles for main vessel (top graphs in A. and B.) and exchange vessels (bottom graphs in A. and B.) for lean mouse and db/db mouse. Red lines indicate measurements at 50 seconds A. Lean mouse main vessels plateaus near 50s, at which point intensity values are near 140a.u. Exchange vessel at 50s are near 20a.u. for intensity readings. B. Db/db mouse main vessels had a steady increase throughout recording, with an intensity value of 30a.u. at 50s. Exchange vessel at 50s had an intensity value near 3a.u. Note difference in curve shape between top graphs of A and B.

6.4 *Discussion*

6.4.1 Treatment with OVZ/HS-1638 Has Restorative Effects on Retinal eGlx Structure and Function in Nine-Week-Old Diabetic Mice

The aim for this chapter was to show that eGlx is damaged during diabetes in a T2D model using *db/db* mice, and that treatment with a novel HPSE inhibitor can prevent eGlx damage and associated microvascular changes in permeability that occur in early DR. In agreement with the literature, which shows retinal thinning in *db/db* mice by 8 weeks of age, 9-week-old *db/db* mice had a significant reduction in retinal thickness compared to lean controls but was not affected by OVZ/HS-1638 treatment. In humans, signs of neurodegeneration can be observed by OCT in diabetic patients even before early clinical signs associated with DR can be observed, such as microaneurysms and small haemorrhages (322). Apoptosis of retinal cells, including photoreceptors, ganglion cells, and astrocytes, result in a reduction of retinal thickness and has been observed in diabetic human samples and experimental models of DR (323). The reasons for increased apoptosis is not well defined, but early changes are unlikely to be due to ischaemic necrosis, as apoptosis can be detected in STZ rats only one month after the onset of diabetes, before any vascular occlusions are apparent (323). It is however possible that increased vascular leak could contribute to increased apoptosis. In experimental diabetes in rats, increased vascular permeability can be observed after one month of diabetes measured by FITC-BSA (324), a similar time frame as when apoptosis is observed. Another factor that may contribute is microglial activation which occurs at early stages of the disease and results in a proinflammatory (M1) and anti-inflammatory (M2) phase (325). To explain, in early DR, the M1 and M2 phases occur at the same time, but progression of DR shifts toward a decrease in the M2 phase, resulting in classical proinflammatory signals like NFκB (325), involved in expression of proinflammatory cytokines, chemokines, and adhesion molecules (326), resulting in increased apoptosis. However, it is unclear if treatment with a HPSE inhibitor would be expected to prevent retinal thinning, as HPSE has been shown to have both pro- and anti-apoptotic effects (327,328) and would need to be investigated in more detail to determine the effects of HPSE inhibition on neurodegeneration. However, retinal thinning in *db/db* mice confirm that mice have developed early signs of DR.

Basement membrane thickening is considered a histological hallmark of DR, resulting from accumulation of basement membrane components like fibronectin, type IV collagen, and laminin (320). Experimental diabetes has shown that thickening of the vascular

basement membrane can be detected before other lesions associated with DR, and may even contribute to vascular lesions, pericyte loss, and acellular capillaries (329). To assess changes in microvascular ultrastructure in these mice, basement membrane thickness was measured in EM images from mice retinas at 9 weeks. Results showed there was no significant increase in basement membrane thickness in 9-week-old mice *db/db* or OVZ/HS-1638 treated *db/db* compared to lean mice. Though there was a slight trend toward an increase in diabetic mice, *db/db* mice do not typically develop significant basement membrane thickening until 22 weeks (316), therefore 9 weeks is likely too early of a time point to observe these changes. Changes to the eGlx were also measured with EM, and *db/db* mice showed a strong trend toward a decrease in eGlx depth and coverage compared to lean mice, though not significant. On the other hand, *db/db* mice treated with OVZ/HS-1638 had a strong trend toward an increase in eGlx depth and had a significant increase in eGlx coverage compared to *db/db* mice treated with vehicle. This study may lack power, and it is possible a larger sample size would show significant differences. Additionally, as this is an early time point, small but significant changes in eGlx may be not be as apparent with a small sample size. Although no conclusive remarks can be made due to the lack of significant decrease of eGlx in *db/db* mice, this data suggest that there is some loss of eGlx at 9 weeks of age in *db/db* mice, and that treatment with OVZ/HS-1638 has restorative effects on eGlx, especially eGlx coverage.

As increased vascular permeability is a serious issue that occurs in DR and is an early indication of DR progression, I investigated if *db/db* mice had any changes in solute flux and whether treatment with OVZ/HS-1638 had any effects. **CHAPTER 5** results showed that loss of eGlx HS was associated with increased solute flux in the eyes, and therefore expected to see changes in solute flux in *db/db* mice. Surprisingly, there were no changes in solute flux between any of the groups. Furthermore, there was a substantial amount of variation in solute flux in lean and *db/db* mice treated with OVZ/HS-1638, which made it difficult to determine if there was any trend. One explanation for these results is that it is too early to detect changes in solute flux, as other studies saw that increased permeability using FITC-dextran was not detected in *db/db* mice until 20 weeks (315). However, as data presented in this chapter demonstrates, and as will be discussed in a later section, there may also be issues of incompatibility of *db/db* mice with this method of measuring solute flux.

As mice had no changes in solute flux, I used an alternative method to determine if mice had increased vascular leakage. To this end, mouse retinal sections were stained with an

anti-albumin antibody to examine if there was an increase in extravascular leak. In contradiction with solute flux results, *db/db* mice had a significant increase in extravascular albumin compared to lean mice. Importantly, albumin leak was also prevented by treatment with OVZ/HS-1638 in *db/db* mice. One explanation for the discrepancy observed between solute flux and albumin leak, is that solute flux is measuring the changes that occur at a specific timepoint, *i.e.* at the time of solute flux measurement. Albumin staining however is detecting albumin accumulation. It is therefore likely that, although increased solute flux was not detected, 9-week-old mice do have areas of increased vascular leak, as shown by immunofluorescence, and is prevented by treatment with OVZ/HS-1638. Together with the eGlx data, this suggest that protection of HS degradation, likely in the eGlx evident by EM data, has restorative effects on the iBRB and maintenance of permeability. This is the first time that restorative effects have been shown in the eGlx by a HPSE inhibitor treatment in diabetes, and suggests that HS has a role in the iBRB, which can be protected in diabetes by preventing its degradation. However, because HS staining was not performed on these sections, it cannot be conclusively stated that OVZ/HS-1638 acts directly on the eGlx HS. In future studies, HS staining should be done on retinal tissue to determine if HS is reduced in the eGlx of *db/db* mice and determine if HS levels in the eGlx are restored by treatment with OVZ/HS-1638. Of note, data in **CHAPTER 5**, in which healthy mice were treated with heparinase III and had loss of eGlx, suggest that circulating HS shedding enzymes such as HPSE in diabetes, may also result in eGlx HS loss in the retina. Indeed, there did seem to be a decrease in eGlx in *db/db* mice, albeit not significant and possibly due to small sample size. It is possible that a later time point would also allow for a greater and more significant extent of eGlx damage, in which restorative effects can also be demonstrated.

6.4.2 Effects of OVZ/HS-1638 Treatment Were Not Reliably Assessed in Eleven-Week-Old *Db/Db* Mice

Unfortunately, there were technical issues that resulted in the 11-week-old cohort to yield inconclusive data. To begin, issues with the use of the Micron IV for acquiring OCT images for measurements of retinal thickness occurred due to lack of the required equipment. At the time of these angiographies, the specialised mask required for anaesthesia during angiography imaging was not available and therefore the injectable anaesthetics ketamine and Xylazine were used as described in the methods of this chapter, and have been successfully used by members of the University of Bristol Ophthalmology group. For reasons not known, *db/db* mice were particularly resistant to this form of anaesthetics,

possibly due to the large amounts of adipose tissue which can absorb the anaesthetic (330), delaying the effect of the drug and therefore increasing the likely hood of overdose if too much is administered. As a result, the majority of the mice could not be anesthetised long enough to acquire images. The incomplete set of OCT images acquired at 9 weeks of age showed that as in the 9 week old cohort previously described above, *db/db* mice did have a decrease in retinal thickness compared to lean mice, however statistical significance could not be determined due to sample size.

Measurements of basement membrane thickness by EM at 11 weeks showed no significant changes between groups. But as mentioned previously, basement membrane thickening may not occur until later stages of DR in these mice, as it has been observed at 22 weeks of age in the literature. However, accurate measurements of basement membrane thickness may have been affected by poor perfusion, as was evident by eGlx staining. As noted in **CHAPTER 2**, mice were cardiac perfused with ringer solution to clear the system of red blood cells, followed by perfusion with Alcian blue and glutaraldehyde, which simultaneously fixes the tissue for EM while also staining the eGlx. Careful measures are taken to ensure perfusion conditions are optimal, including filtering the Alcian blue solution to avoid precipitate which may hinder perfusion. However, there are occasionally instances in which perfusions are not optimal, and either do not fully perfuse some organs or fail to reach certain parts of the body. In this cohort, it was apparent that the perfusions did not properly perfuse the eyes, as eGlx staining was visibly patchier and thinner than previously observed, even in lean controls. Vessel structure was also collapsed, suggesting improper fixation of microvessels. Attempts to measure eGlx changes in these mice were still made, but retinal eGlx measurements showed no apparent differences in eGlx. Additionally, because the eyes of one animal failed to perfuse completely, statistical significance could not be determined for this cohort due to insufficient numbers. Therefore, no conclusions on changes in eGlx can be reliably drawn from this study.

As the Micron IV imaging system was also used for sodium fluorescein angiographies, and previously mentioned issues were encountered, a complete set for solute flux measurements were not obtained for this study. As a result, solute flux measured at 9 weeks of age in this cohort could not be tested for statistical significance. However, the solute flux measurements which were taken show no trend of increased solute flux in 9-week-old *db/db* mice, consistent with the 9-week-old cohort.

Although this cohort did not yield any eye data which directly contributes to the hypothesis of this thesis, changes in retinal thickness agreed with the previous 9-week-old cohort. Additionally, it was learned that the use of ketamine/Xylazine for this strain of mice is not suitable and should be avoided in any future studies. Furthermore, the solute flux measurements taken in this study gave evidence that solute flux measurements using this technique in *db/db* mice may not be suitable as they show contradicting results with albumin staining in the retina. This lead me to further investigate the use of this technique in this model discussed below.

6.4.3 Db/db Mice May Not Be Compatible with Solute Flux Assay

As the results in 9-week-old mice showed that mice had increased albumin leak, with no observable increase in solute flux, I investigated if the *db/db* mice were a good model for measuring changes in solute flux. By aging *db/db* mice from 6-14 weeks of age and performing solute flux measurements every two weeks, I was able to determine if there were any differences between lean and *db/db* mice as DR progressed. It was surprising to see that there was no observable increase in solute flux in *db/db* mice. In fact, solute flux measurements appeared to be less on average at 14 weeks in *db/db* mice than at 6 weeks. One noticeable feature when performing sodium fluorescein angiography in lean and *db/db* mice, was that the sodium fluorescein signal seemed to take longer to saturate in the main vessel compared to lean. Indeed, looking at a video snap-shot for a lean mouse after approximately 10 minutes showed that main vessels were near saturated, especially closer to the optic nerve. However, main vessels in *db/db mice* were not saturated by 10 minutes, suggesting a difference in sodium fluorescein uptake, which may skew solute flux measurements. These differences were further confirmed by comparing fluorescent intensity profiles for the main vessels. Fluorescent intensity profile for the lean mouse begin to plateau or reach a steady state, as would be expected from previous results in **CHAPTER 5** and discussed in **CHAPTER 2**, but the intensity values themselves were much higher than db/db mice. This seemed to also affect the fluorescent intensity values for the exchange vessels, though notably there did not seem to be a change in the shape of the curve for exchange vessels. This suggest an issue with sodium fluorescein uptake, as main vessels are the first to perfuse with sodium fluorescein. This difference in uptake may be due to the significant differences in fat content between lean and *db/db* mice, as sodium fluorescein was injected i.p. in these mice. In humans, the use of sodium fluorescein angiography imaging is used to determine alterations in retinal vasculature, where a series of static images can be used to pinpoint areas where microaneurysms and other

vascular lesions have occurred (331). Therefore, the rate at which sodium fluorescein is absorbed into the system does not affect the results. In fact, the use of oral administration has been shown to be a safe and effective way to administer sodium fluorescein for angiographies, where signal often does not appear until thirty minutes after ingestion (331). However, because solute flux is a rate measurement, dramatic differences in uptake could have an effect. This might also explain why the use of sodium fluorescein angiographies in the heparinase III studies and the *Ext1*^{CKO} model did not have similar issues, as mice in these groups were similar in weight. A way around this issue would be to inject sodium fluorescein via t.v. injection for diabetic studies, however, the set up for imaging is not conducible to this method. As described in **CHAPTER 2**, mice are on a floating stage that allows for fine adjustments in mouse position to bring the retina into focus, making t.v. injections practically difficult and would require substantial adjustments to the set up. Tail vein injections would also be a more lengthy process, increasing the likelihood of the development of acute anaesthetic induced cataracts, a known side effect of prolonged anaesthesia in mice (332), which would affect imaging of the retina. Additionally, studies performed by our collaborator, Professor David Bates, who originally developed this assay in a STZ rat model, has evidence that a direct intravenous injection does not allow for accurate measurement of solute flux, as vessels saturate too quickly (personal communication). Therefore, the use of *db/db* mice for measurements of solute flux using sodium fluorescein angiography imaging may not be compatible or requires further optimisation before it can be used in this model.

6.4.4 Conclusions and Significance

The work presented in this chapter suggest that a novel HPSE inhibitor OVZ/HS-1638 prevents increased retinal albumin leak in a T2D mouse model of DR at 9 weeks of age. Although protection of eGlx HS was not specifically shown in this study, treatment with HPSE inhibitor significantly increased eGlx coverage, indicating a restorative effect on the eGlx during diabetes. Treatment with OVZ/HS-1638 also significantly reduced the amount of extravascular albumin in *db/db* mice when compared to *db/db* mice treated with vehicle, indicating that break down of the iBRB can be prevented by preventing HS degradation with HPSE inhibitor treatment. This is the first time that protective effects on the eGlx and iBRB by inhibiting HPSE has been shown, demonstrating the potential therapeutic use of HPSE inhibitors in DR to treat microvascular complications.

Chapter 7 Discussion

7.1 *Heparan Sulphate is Functionally Important in the Microvascular Endothelial Glycocalyx in the Kidney and Eye*

7.1.1 Summary of Results for Aim 1

The first aim for this thesis was to demonstrate the importance of HS in the eGlx in the kidney and retinal microvasculature. Microvessels are an essential component in the circulatory system, as they are involved in blood-tissue exchange which is necessary for the delivery of oxygen and nutrients to the tissues in which they are located (1). The appropriate delivery of nutrients is made possible by regulation of microvascular permeability in different vessel beds. Two types of vessels exist in the vascular system, fenestrated and continuous, and as discussed throughout this thesis, the glomerulus in the kidney and retina in the eye serve as two examples of such vessel beds. While the glomerulus and the retina have two very distinct structures to match the need of its respective tissue type, there are similarities as well. Both the glomerular and retinal vessels have endothelial cells which are in direct contact with flowing blood and are the first cell in the permeability barriers that form the glomerular filtration barrier (GFB) and the inner blood retina barrier (iBRB). The presence of the eGlx is common to both of these vessel beds, as well as all other vessel beds in the body. As previously discussed, the eGlx is known to have a role in the maintenance of microvascular permeability in the kidney, and some evidence exists for its role in the retina. However, the role that the various eGlx components have in structure and function has not been fully established and is important to understand, as damage to the eGlx is associated with increased vascular permeability in diseases such as diabetes.

To this end, I have examined the role of HS in the eGlx in the glomerulus and retina in maintaining the integrity of the GFB and the iBRB. Using two different approaches, I have shown that HS is important for maintaining barrier properties in both the glomerulus and retina. I first showed conclusively that HS is indeed present in the eGlx of both the glomerulus and the retina, using immunofluorescence. Although HS is regarded as the most abundant GAG in the eGlx, making up to 90% of the total GAGs in the glycocalyx (12), surprisingly, to my knowledge there is no visual evidence demonstrating its presence in the eGlx in tissue samples in the literature. And so, this is the first time that HS in the eGlx in both the GFB and the retina has been demonstrated.

The first approach used to demonstrate a role for HS in the eGlx was with the use of heparinase III to enzymatically remove HS in the glomerulus and retina in healthy mice. Treatment with an HS shedding enzyme resulted in structural damage to the eGlx, measured by EM in both vessel beds. *In vitro* studies by our group as well as others on GEnCs have indeed shown that treatment with heparinase III results in loss of cell surface HS and increased albumin passage across the cell monolayer (10). While parallel studies for REnC have not been done, REnC in which HPSE is upregulated, do show increase HS cleavage, pointing to potential similarities between the GEnC and REnC eGlx (294). Functional studies presented in this thesis on heparinase III treated mice provided evidence for a role of HS in the eGlx, as mice treated with active enzyme had increased glomerular albumin permeability (Ps'alb) and increased solute flux in the retina, compared to inactive enzyme-treated mice. This is evidence that eGlx HS is functionally important for maintaining GFB and iBRB integrity. Loss of eGlx in these mice did not coincide with any other structural changes in the GFB or iBRB, suggesting that eGlx HS specifically is an important factor in maintaining barrier properties.

As a second approach to investigate the importance of eGlx HS, the $Ext1^{CKO}$ model in which the Ext1 enzyme required for HS chain elongation is conditionally knocked out in endothelial cells, was used. Because this is a whole-body knockout, these mice could be used to study both vessel beds. Analysis of EM images showed that $Ext1^{CKO}$ mice had significant loss of eGlx, in line with heparinase III studies above. Unfortunately, due to time constraints, I was not able to analyse eGlx in the retinas of these mice, though eGlx functional studies were performed, discussed below. Previous work by our group showed that $Ext1^{CKO}$ mice have a significant increase in Ps'alb when compared to litter mate controls (LMC). Although these mice did not have a significant increase in albuminuria under normal conditions, treatment with L-Lysine, a tubular reabsorption inhibitor, revealed a significant increase in albuminuria in $Ext1^{CKO}$ mice, suggesting a masking effect of tubular reabsorption on increased albumin permeability. I also performed vascular integrity studies in the retina and found that as in the glomerulus, $Ext1^{CKO}$ mice had a significant increase in solute flux compared to LMCs. Of note, the assay used to measure solute flux is a novel method of measuring changes in the iBRB in the retina and was developed through the collaboration with Professor David Bates and Dr. Kenton Arkill. Additionally, the software developed by MSc student Kevin Ho in collaboration with our group is a new analysis tool with the potential to be used in clinical settings to detect early changes in the iBRB which may not be visible by eye. This data supports the idea that HS

is an important component in the GFB and iBRB, and removal of it in the eGlx results in loss of barrier integrity and increased permeability. This suggest a possible mechanism in diseases such as diabetic nephropathy (DN) and diabetic retinopathy (DR), in which loss of barrier integrity results in increased permeability associated organ damage.

7.1.1.1 Limitations of This Study and Follow-Up Studies

A major limitation of this study was the availability of suitable antibodies to detect changes in HS in both the heparinase III treated mice and *Ext1*^{CKO} mice, as discussed in **CHAPTER 3** and **CHAPTER 5**. Although heparinase III has been used in a multitude of studies as a method to shed HS *in vivo* and *in vitro* (10,170,333), it would be useful to confirm loss of HS in the eGlx specifically after treatment with heparinase III. However, I did show that treatment with heparinase III resulted in a decrease in eGlx, and heparinase III's specificity for heparan sulphate is well documented (196,334), indicating that the results observed after heparinase III treatment can be attributed to loss of eGlx HS. In *Ext1*^{CKO}, reduction in Ext1 mRNA was confirmed by qPCR in GEnCs, however the HS antibody used could not detect changes in the glomeruli of these mice. As mentioned in **CHAPTER 3**, this may be due to pre-existing HS chains that are present, as Ext1 is involved in HS chain elongation. *In vitro* studies have shown that Ext1 knockout cells can still produce HS, though the chain length is significantly shorter compared to control cells (335). Therefore, the antibody used in this study may detect these shorter chains.

In the future, it will be necessary to find a suitable HS antibody that can be used to detect changes in eGlx HS, and can confirm loss of HS in heparinase III treated animals as well as *Ext1*^{CKO} mice. For heparinase III treatment studies, one possible candidate is the 3G10 antibody, which recognizes the neo-epitopes 3G10 on HS. This epitope is generated when HS is cleaved by heparinase III (336), therefore I would expect to see an increase in signal with the use of this antibody in heparinase III treated animals. For *Ext1*^{CKO} mice, as well as heparinase III treated mice, use of commercially available antibodies such as 10E4 or JM403 may be suitable, as treatment with heparinase III has been shown to almost completely abolish signal using these antibody (210), and would therefore expect to see some decrease in *Ext1*^{CKO} mice as well, which should have shorter HS chains, therefore less available epitopes. Alternatively, isolation of endothelial cells and measurement of HS chain length using anion-exchange HPLC (high-performance liquid chromatography), as was done in the study mentioned above (335), can be used to confirm reduction in HS in *Ext1*^{CKO} mice.

It should also be noted that interpretation of the results obtained with these two different models should be carefully considered, as well as how they relate to diabetic studies in this thesis. While heparinase III treatment tells us something about the effect on HS shedding in the eGlx, as would be expected in the case of upregulated HPSE in diabetes, *Ext1*^{CKO} mouse studies gives information about the effect of reduced HS synthesis in the eGlx. *In vitro* studies on aortic endothelial cells treated with high glucose show a significant reduction in GAG isolated from cells, and a significant increase in GAGs in the media of the cells (337), suggesting increased GAG shedding. Importantly for interpretation of these results, the researchers also performed correlation studies on total HS disaccharides and total GAGs found in cultured endothelial cells, and found that there was a positive correlation between the two (337). The authors suggest that this is evidence that investigation of total GAGs reflect the total HS present in the endothelial cells (337), making these results reflective of changes in HS. There is, however, evidence in glomerular epithelial cells and mesangial cells from T1D rats, that diabetes results in reduced synthesis of HS in these cells (338). It is therefore possible that a combination of both occur in diabetes, and therefore heparinase III and *Ext1*^{CKO} studies may reflect two different aspects of HS loss in diabetes.

7.1.2 Possible Mechanisms for the Contribution of eGlx Heparan Sulphate to Vascular Permeability Barriers

The work presented in this thesis provides evidence that HS is an important component of the eGlx, which contributes to the functional role of the eGlx in the GFB and the iBRB. However, how HS contributes to the barrier properties of eGlx has yet be determined and will require further investigations. The following is a discussion of possible mechanisms for how HS contributes to the eGlx barrier properties in the GFB and iBRB based on the data presented in this thesis and available published literature.

7.1.2.1 Heparan Sulphate's Contribution to the eGlx of the Glomerular Filtration Barrier

In the GFB, the eGlx has an established role in permeability, as numerous studies by our group and others have shown that loss of eGlx coincides with increased albumin permeability in GEnC cell monolayers, and increased albuminuria and glomerular albumin permeability in animal models (33,108,116,155,170). **FIGURE 7-1** shows a schematic of ways in which eGlx HS may contribute to barrier function. One way in which HS likely contributes to the eGlx barrier function, is through its anionic charge. HS as well as other GAGs have a net negative charge due to their carboxylic acid and sulphated groups which become deprotonated at physiological pH (339), making the eGlx a highly negatively

charged layer as mentioned in **CHAPTER 1**. In fact, HS has been shown to have the highest negative charge density of any other known biomolecules (340). Indeed, it has been shown that treatment of rats with heparinase III reduces anionic sites in the GBM, evidence that there is a contribution to the anionic charge by HS in the GFB (184). A study using all-atom molecular dynamic (MD) simulations focused on HSPGs, also provides evidence that HS contributes to the anionic charge of the eGlx (16). In a healthy state in which HS remains abundant, the eGlx is able to repel molecules such as plasma proteins based on charge density alone, acting as a physical barrier to plasma proteins (341) **(FIGURE 7-1 A)**. However, loss of HS and consequently damage to the eGlx may allow for larger molecules such as plasma proteins and albumin, to passively diffuse through the GFB through the endothelial cell fenestrations **(FIGURE 7-1 B)** which are 60-70nm in diameter, and physically large enough to allow the passage of large molecules such as albumin (30).

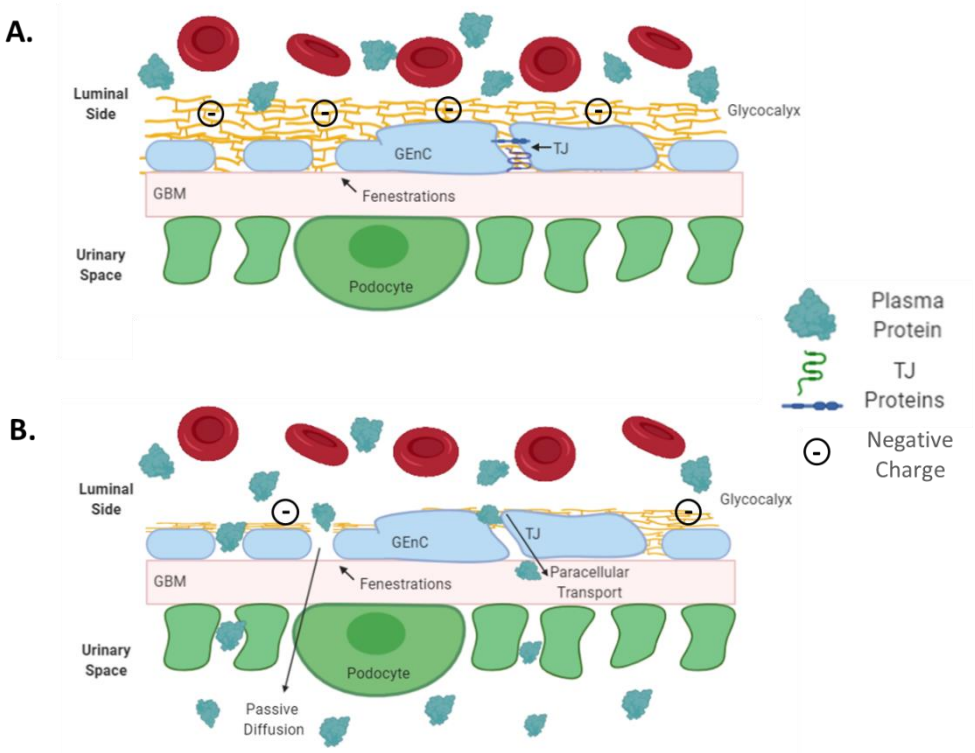

Figure 7-1 Possible Mechanisms for HS Contribution to eGlx Barrier Function in the GFB

A. In healthy conditions, eGlx HS acts as a physical barrier and contributes to net negative charge inhibiting free passage of large molecules through fenestrations. HS may also provide a barrier in junctional complexes like tight junctions (TJ). B. In a disease state, loss of eGlx HS results in increased passage of large molecules through the fenestrations. Loss of eGlx HS may also impact charge and TJ integrity, resulting in an alternate pathway for increased permeability. Image made using Biorender.com

The role of eGlx HS in junctional complexes such as tight junctions or adherens junctions of GEnCs is unclear. *In vitro* studies have shown that removal of HS by heparinase III or HPSE, had no significant impact on transendothelial electrical resistance (TEER), but did result in increased albumin passage as previously mentioned (10). TEER measurements are used to determine the integrity of tight junctions in a cell monolayer, where it is inversely related to the amount of passage of water and small solutes (10). Therefore, an increase in TEER, would be equivalent to a decrease in the passage of water and small solutes. Additionally, removal of HS had no effect on vascular endothelial cadherin (VE-cadherin), a vital protein in the endothelial cell-to-cell barriers which are sealed by cell-cell adhesions molecules(342). However, another study on GEnC showed that treatment with advanced glycated end -products (AGEs), which interestingly are also increased in diabetes, resulted in loss of tight junction proteins occludin and claudin-5 by immunofluorescence, which was accompanied by a decrease in TEER and an increase in 4kDa FITC-dextran passage(343). Treatment with AGEs also induced upregulation of MMP-2 and MMP-9 in these studies (343). Our group has shown that MMP-9 has been shown to mediate eGlx loss by shedding of the HSPG, sydencan 4 (344). It is therefore possible that HS, by way of HSPGs, does have a role in the maintaining tight junction integrity in GEnC, and that loss of HS increases paracellular passage of plasma proteins as shown in **FIGURE 7-1 B.** However, more studies would need to be conducted to make any conclusions as these studies did not directly address this question. It should also be noted that GEnCs do not form clear fenestrations in tissue culture, likely making the role of tight junctions in in these studies much more important in maintaining barrier function than *in vivo*. It is likely that tight junctions play a more crucial role in microvessels which are continuous and lack fenestrations, such as the retina, discussed below.

7.1.2.2 Heparan Sulphates' Contribution to the eGlx of the Inner Blood Retina Barrier

A lot less is known about the eGlx in the iBRB. While previously mentioned studies have shown the presence of eGlx in animal models and eGlx can be measured in human retinal vessels, few studies have shown a functional role. Functional studies that have been done focused on HA, as discussed in **CHAPTER 5**, and showed that treatment of mice with hyaluronidase resulted in reduced eGlx and increased permeability (113). However, HS has not been investigated in the retina eGlx until now. Furthermore, there is currently no published work which has directly addressed how the eGlx and HS contribute to the maintenance of the iBRB. The data presented in this thesis provides strong evidence that HS has a structural and functional role in the eGlx in the iBRB, but how its role is

accomplished is not clear as these microvessels have a much more tightly regulated permeability barrier which is immune privileged and the endothelial cells lack fenestrations (345). As discussed in **CHAPTER 1**, vascular permeability in the retina is regulated by paracellular transport and transcytosis. But how does the HS eGlx contribute to these, as the eGlx is on the surface of vascular endothelial cells?

As in the GFB, HS may act as a physical barrier in tight junctions as demonstrated in **FIGURE 7-2 A**, and loss of eGlx HS can result in an opening in which plasma proteins can escape through already damaged tight junctions **(FIGURE 7-2 B)**. Loss of tight junction proteins such as occludins have in fact been observed in experimental models of diabetes such as T1D rats in the retina (346). However, there is some evidence that HS itself may have a bigger role in the maintenance of junctional complexes. Studies previously described in human retinal endothelial cells (hREC) showed that shedding of HS, likely resulting from the observed upregulated HPSE in high glucose treated cells, coincided with a loss of occludin (294). This suggests that loss of HS may lead to changes which result in loss of tight junction proteins. However, one major pitfall to this study was that protein levels were investigated only by Western blot, therefore localisation of the proteins could not be concluded. On a similar note, cell surface HSPGs are known to act as reservoirs of growth factors such as VEGF (347). In the retina, shedding of HS may result in the release of VEGF, which is well known to increase vascular permeability, and is associated with loss of eGlx (33,123). Interestingly, treatment of bovine retinal endothelial cells (BRECs) with VEGF results in enhanced phosphorylation of occludin and ZO-1 (346). Phosphorylation of these junctional proteins is thought to modulate their cellular localisation, where phosphorylation results in cytoplasmic localisation (348), *i.e*. loss in membrane tight junction localisation. Increased phosphorylation of junctional proteins is also associated with increase permeability both *in vitro* in BRECs as well as *in vivo* in rat models in which VEGF is injected into the vitreous of the eye (348,349). Therefore, it is possible that eGlx HS not only acts as a physical barrier as mentioned above, but also acts to maintain tight junction integrity through its growth factor binding/sequestering capabilities, such as binding of VEGF. When HS is shed, release of growth factors may induce a breakdown in tight junction protein complexes, allowing an increase in paracellular transport of plasma proteins as shown in **FIGURE 7-2 B**. Further adding to this, treatment of rat fat pad endothelial cells (RFPECs) with heparinase III results in decreased expression of Connexin 43 (Cx43), a gap junction protein (333). And loss of Cx43 is associated with increased permeability in the retina in experimental *in vivo* diabetic rat models using FITC-dextran,

and is also reduced in the retinas of DR patients (350,351). This provides further evidence that changes in HS can indirectly impact junctional complexes.

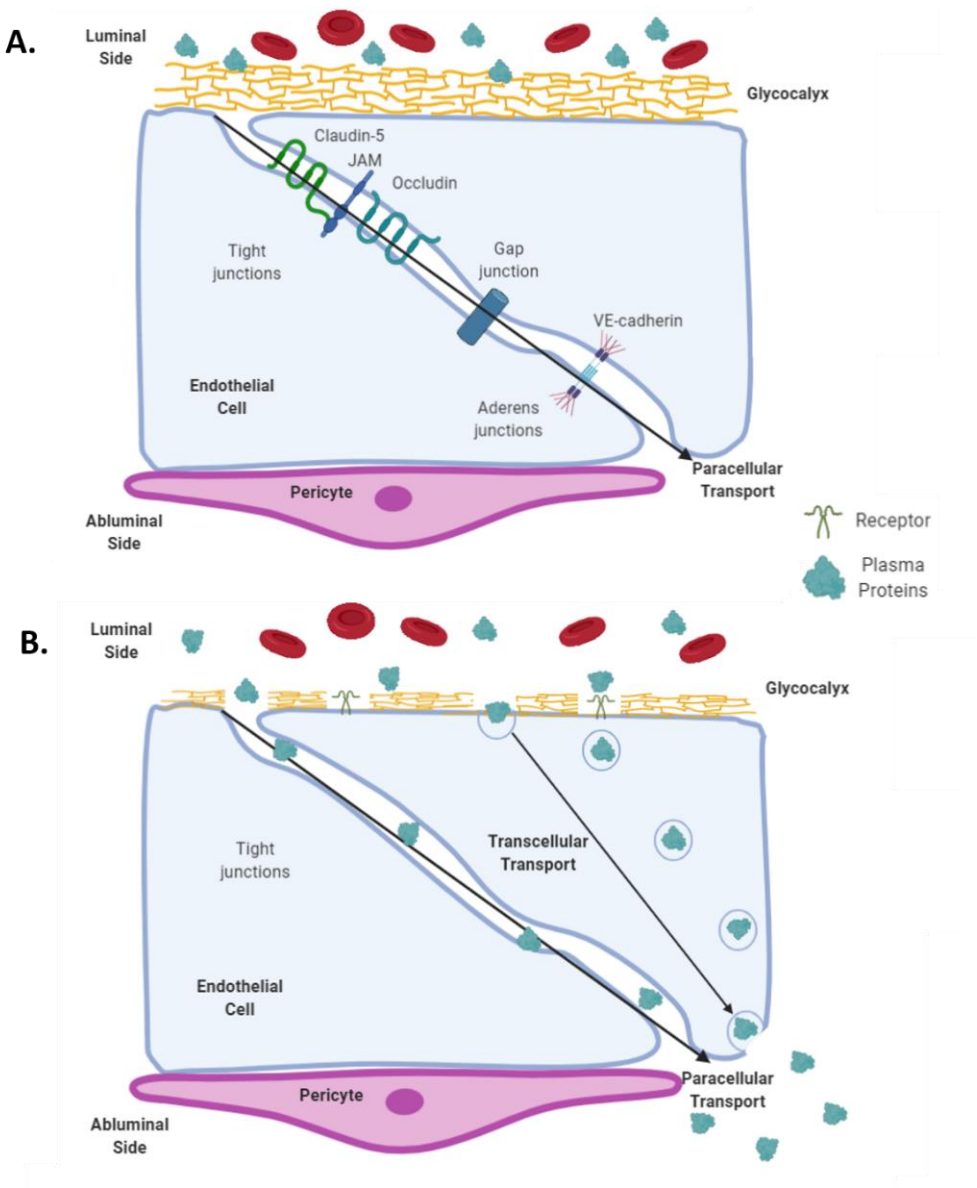

Figure 7-2 Possible Mechanisms for HS Contribution to eGlx Barrier Function in the iBRB

A. In healthy conditions, eGlx HS acts as a physical barrier, inhibiting of passage of molecules through tight junctions (TJ) and may shield receptors that are involved in transcellular transport. B. In a disease state, loss of eGlx HS results in loss of barrier at TJ. Additionally, HS shedding may induce loss of TJ integrity by deregulation of TJ proteins, resulting in increased paracellular transport. Loss of eGlx HS may also increase transcellular transport directly by exposure of receptors or indirectly by downstream signalling resulting in increased vesicle formation. Image made using Biorender.com

Alternatively, HS eGlx may also have a role in regulation of transcellular transport. In addition to the effects of VEGF on permeability mentioned above, VEGF has been shown to induce permeability through an increase in transcytosis *in vivo* in monkeys which received intravitreal injections of VEGF (123). However, it should be noted that this study had a small sample size of four animals, three treated with VEGF and one control, so more work is needed to make any definitive conclusions. These studies do however line up with *in vitro* work on BRECs, which showed that cells treated with VEGF have a significant increase in vesicle related genes such as caveolin-1 and flotillin-1 and -2 (352). Interestingly, caveolae which are named after the structural molecular component of plasmalemma vesicles, cavoline-1 mentioned above, have been shown to contain receptors for albumin (48). It is therefore possible that shedding of HS results in downstream signals that result in increases vesicular transport of plasma proteins such as albumin, as demonstrated in **FIGURE 7-2 B**. In fact, T1D rat models have increased retinal vascular endothelial cell endocytosis, and is perhaps contributed to by loss of eGlx HS via the VEGF effects on vesicle formation mentioned previously. It is also possible that loss of HS exposes receptors that are normally masked by the eGlx. For example, loss of the HSPG syndecan-1 results in increase adhesion of leukocytes in retinal blood vessels after TNF-α stimulation (353), suggesting that loss of HS results in exposure of adhesion molecules as shown in **FIGURE 7-2 B,** that could mediate an increase in receptor mediated vesicular transport. As this was not the focus of this thesis, further experiments will need to be done to determine exactly how HS contributes to iBRB integrity, though the work in this thesis establishes a foundation for further investigation into eGlx HS and vascular permeability in the retina.

7.2 *Preventing Heparan Sulphate Degradation Prevents Damage to the Endothelial Glycocalyx In Diabetic Microvascular Diseases*

7.2.1 Summary of Results for Aim 2 and Aim 3

Completion of the first aim gave strong evidence that HS has a structural and functional role in the eGlx in the GFB and the iBRB, as loss of HS lead to increased glomerular permeability and solute flux in the eye. As vascular diseases such as DN and DR are associated with a break down in the GFB and iBRB resulting in increased vascular permeability, the second aim of this thesis was to determine if the eGlx is damaged in these vessel beds in *db/db* mice, a type 2 diabetic mouse model. Once loss of eGlx was established, the third aim was to demonstrate that treatment with a novel HPSE inhibitor

OVZ/HS-1638 could prevent loss of HS and associated eGlx damage, preventing increased vascular permeability observed in DN and DR. The overarching goal, was to demonstrate that early treatment in the same diabetic animal, could prevent the increased vascular permeability associated with DN and DR.

I began this investigation at an early time point in which *db/db* mice were treated with OVZ/HS-1638 from 7-9 weeks of age, with an endpoint of 9 weeks. In the kidney, *db/db* mice showed an increase in albuminuria and glomerular albumin permeability at end point, however this was not associated with significant loss of eGlx in the GFB. Though unexpected, as discussed in **CHAPTER 4**, it is possible that there were moderate changes in eGlx, but moderate changes likely require a bigger sample size to see significant differences. Furthermore, mice did not have any significant changes in GFB ultrastructure, suggesting this time point may have been too early to investigate robust eGlx changes in DN. Though no significant protective effects were observed in the eGlx with OVZ/HS-1638 treatment or with albuminuria, *db/db* mice treated with OVZ/HS-1638 did not have a significant increase in glomerular albumin permeability contrary to vehicle treated *db/db* mice, suggesting a mild protective effect on GFB function at this time.

In the same mice, a significant reduction in retinal thickness was observed in *db/db* mice, as is commonly observed in early stages of DR. *Db/db* mice did not have a significant loss of eGlx, though there was a strong trend toward a decrease. Unfortunately, no changes were observed in solute flux in these mice, but as discussed in **CHAPTER 6**, this model may not be suitable for the assay used to measure solute flux without further optimisation. However, *db/db* mice had a significant increase in extravascular albumin in their retinas at 9 weeks, measured by immunofluorescence. Presence of extravascular albumin staining likely results from an accumulation of albumin leak over a period, as opposed to solute flux which measures changes at the time of measurement. In DR patients, accumulation of lipid and proteinaceous material such as albumin, results in the formation of hard exudates, indicating a breakdown in the iBRB (354). Treatment with OVZ/HS-1638 resulted in a significant increase in eGlx coverage in the retina, compared to *db/db* mice treated with vehicle, indicating a restorative effect on eGlx HS. Additionally, extravascular albumin was significantly reduced, further confirming that HS is important for barrier function and preventing its degradation in the retina during diabetes prevents breakdown of the iBRB.

Because *db/db* mice at 9 weeks of age did not show measurable changes in eGlx, I used a later time point in which mice were treated from 9-11 weeks of age. *Db/db* mice had changes in GFB ultrastructure, consistent with the development of DN. *Db/db* mice had an increase in albuminuria, which was associated with loss of eGlx, and increase in glomerular albumin permeability. *Db/db* mice treated with OVZ/HS-1638 however did not have a significant increase in albuminuria, contrary *db/db* mice treated with vehicle. This was associated with restoration of eGlx, and a significant decrease in glomerular albumin permeability. These data indicate that HS shedding and loss of eGlx results in increased permeability in the kidney, and therapeutically targeting it by preventing its degradation in diabetes has restorative effects on the GFB. This was further confirmed by PAS staining, in which mice treated with OVZ/HS-1638 had a significant reduction in glomerular fibrosis compared to vehicle treated *db/db* mice. This indicates that treatment with OVZ/HS-1638 in diabetes not only has protective effects on eGlx, but also may prevent progression of DN, as glomerular fibrosis is a characteristic pathological change in DN (355).

Unfortunately, the data obtained for the retina portion of this cohort did not yield any conclusive results. The first issue arose with imaging of the mouse retina *in vivo,* due to use of unsuitable anaesthetics for this mouse model. This resulted in an incomplete set of data of retina images. However, the images that were obtained at 9 weeks in these mice did show a similar trend to the 9-week-old cohort, where *db/db* mice had retinal thinning. This same issue resulted in an incomplete set of solute flux measurements for this cohort, though as mentioned above, the data presented in **CHAPTER 6** suggest that this method of solute flux measurement is not suitable for this mouse model, and will require significant optimisation should this model be chosen for future studies. Another issue that arose was poor fixation of the retinal tissue in these mice, which was evident by collapsed vessels by EM. This resulted in eGlx staining which was suboptimal in all groups. Despite this, eGlx was measured and no apparent changes were observed between groups, though statistics could not be performed due to insufficient sample size resulting from one mouse which did not perfuse. As a result, no conclusions on eGlx changes and protective effects of OVZ/HS-1638 treatment could be made at this time point.

7.2.2 Limitations of This Study and Follow-Up Studies

As with the aim 1, one limitation in the investigation of aims 2 and 3 is the inability to confirm a loss of HS in the eGlx specifically. As discussed in **CHAPTER 1**, HS is linear polysaccharide that ranges in the number of disaccharide units as well as unique

variations in number of acetyl groups and sulfation (14). These variations are functionally important and differ in different tissues types and species. As a result, there is a wide range of epitopes which can be recognized. For example, two commonly used antibody JM403 and 10E4, discussed previously, require an N-unsubstituted glucosamine residue and an N-sulphated glucosamine residue for antibody binding, respectively (356), however both epitopes may not be present in all tissues or cell types. Similarly, the phage display antibodies such as HS3A8V and EV3C3V used in this thesis, were raised against bovine kidney HS and human lung HS, respectively (357). Published studies with these antibodies showed that both had the same binding pattern in rat lung tissue from embryonic days (E) 15.5 of gestation (357). However, the same two antibodies had different binding patterns in E17.5 rat lung tissue (357). This demonstrates how variable HS chains can be even in the same species, making it difficult to find a suitable antibody to detect changes.

While loss of HS in DN has been shown in glomeruli from humans and experimental rodent models (109,282,358), reduced HS is often attributed to loss of GBM HS, and eGlx HS has not been specifically addressed. Of note, a study performed on Wister-Munich rats showed that glomeruli from T1D rats had reduced HS staining using the antibody JM403, after 5 months of diabetes (109). On the other hand, another study also performed on Wister-Munich rats after 5 months of diabetes, showed no changes in glomerular HS, but the researches used the antibodies 3G10, 10E4, and monoclonal antibody (mAb) 865 (359). This nicely demonstrates the difficulty and great importance in finding a suitable antibody to detect changes in eGlx HS, as discussed above. Reduced HS synthesis has been shown in the retinas of diabetic Wistar-Munich rats by assessing the incorporation of radiolabelled ^{35}S-sulphate into HS (297), and may be a suitable way to measure changes in HS. However, this was performed on whole retinas, therefore changes to the eGlx cannot be concluded. Future studies should therefore involve finding a suitable antibody or method to detect changes in the eGlx of the glomerulus and retina, as mentioned in aim 1.

Another limitation in this study involves the mouse model chosen to investigate DN and DR in the same animal. Historically, DR and DN have been shown to be strongly linked, with the likelihood of developing one increasing the chance of developing the other (360,361). However, these associations have primarily been investigated in humans, and to my knowledge, there have not been any published studies investigating the development of permeability changes associated with DN and DR in parallel in the same

diabetic mouse models, as was done in this thesis. As discussed in **CHAPTER 4** and **CHAPTER 6**, the use of *db/db* mice was chosen based on a literature search which upon reviewing, gave evidence that *db/db* mice were a suitable model to study early changes in DN and DR, at the same timepoints of 9 and 11 weeks as end points. *Db/db* mice are hyperglycaemic and become albuminuric by 8 weeks of age and have increased vascular permeability in the retina measured by FITC-dextran by 20 weeks (215,315). In children with T1D, changes in sublingual eGlx has been observed before any clinical signs of vascular complications become apparent in the eye or kidney (362). As I was investigating early changes in the eGlx during DN and DR, the hope was that by 9-11 weeks, mice would have developed changes in eGlx and associated increase in vascular permeability. In retrospect, this model may not have been the best choice, as *db/db* mice at 9 weeks of age did not show significant changes in eGlx in glomeruli or the retina, and so protective effects on eGlx structure by the OVZ/HS-1638 could not be concluded. However, some restorative affects were seen in eGlx coverage in the retinas of 9-week-old mice by OVZ/HS-1638. It is possible that these studies lacked power to detect small but significant changes in the eGlx. However, a breakdown in the GFB and iBRB was evident at this timepoint, by glomerular albumin permeability assays and albuminuria, and extravascular albumin staining in the retina, respectively. These results indicated that mice at 9 weeks of age did have some changes associated with DN and DR, and I therefore reasoned that a later timepoint may yield more robust changes in the eGlx.

As a result, I performed the same studies with an 11-week-old end point and did in fact find that there were significant changes in eGlx and permeability in the glomeruli from *db/db* mice, which were prevented by OVZ/HS-1638 treatment. But studies in the eye were not conclusive, primarily due to technical difficulties mentioned previously. Furthermore, investigation of the solute flux assay used to show functional changes in the eGlx, revealed that this assay may not be suitable for *db/db* mice. As evidence provided in **CHAPTER 6** shows, this is likely due to the large differences in body mass which resulted in differences of sodium fluorescein absorption between non-diabetic and diabetic mice, which appeared to skew solute flux measurements, as described in **CHAPTER 6**.

As a result, I was unable to directly and conclusively address the loss and restoration of eGlx HS in the GFB and iBRB in the same animal, which was the overarching goal for this thesis. It is possible that the 11-week time point would have been suitable to study changes in eGlx in both vessel beds had there been no issues encountered in the retina studies, but the issue with functional studies in the eye would remain, as this appeared to

be primarily a body mass issue. As will be discussed in the **FUTURE STUDIES** section of this chapter, a model in which non-diabetic and diabetic rodents have less of a difference in body fat, would potentially help avoid the issue encountered with *db/db* mice.

7.3 *Clinical Implications of This Work*

The work presented in this thesis is a step toward finding a treatment which helps prevent microvascular complications in diabetes. Currently, the most important goal in T1D and T2D patients is the maintenance of blood glucose levels within a normal range and control of blood pressure(127). As discussed in **CHAPTER 1**, to achieve this, in addition to lifestyle interventions, the use of exogenous insulin, or use of other glucose lowering agents such as SGLT2 inhibitors and metformin are now common practice in in T1D and T2D patients, respectively. Use of ACE inhibitors and RAAS blockers also aid in lowering blood pressure (135). Despite this, DR continues to be the most frequent cause of blindness in 20-74 year olds, and DN is the most common cause of end stage renal disease in the Western world (363,364). As diabetes diagnoses has been on an upward trend for decades, and currently there is no cure for T1D or T2D, the development of therapeutics that can prevent and/or alleviate microvascular complications such as DR and DN remains crucial.

One of the features that links microvascular complication in diabetes is the associated increase in permeability, resulting in damage to the respective organ. In DN, loss of the eGlx in diabetes has been established, and is now known to contribute to increased vascular permeability. Though some studies have looked at the eGlx in the retina, the association of eGlx loss in DR is not as strong, as few studies have investigated its role in the retina microvasculature. The data in this thesis not only provides evidence that eGlx is functionally important in the eye, but also that HS is an important component of the eGlx, which contributes to microvascular barrier function in both the eye and kidney. Importantly, together these data indicate similarities between the eye and kidney microvasculature, despite their anatomical differences, suggesting that a single treatment may be effective in preventing damage to the eGlx in both vessel beds. It is possible that this treatment can be applied more widely to all vessel beds in diabetes, such as the brain, in which diabetics are at increased risk for developing vascular dementia and Alzheimer's disease contributed to by alterations in the blood brain barrier (365).

Currently, there are no treatments that specifically target the glomerulus in DN, and although treatments such as anti-VEGF signalling therapies that target the retina are effective in reducing retinal permeability (117), they are local treatments which do not

have therapeutic effects on the kidney. In fact, there is evidence that treatment with anti-VEGF therapies in retinopathy patients may even lead to proteinuria and glomerular endothelial cell injury (366,367). The data in this thesis suggests that development of a treatments which can therapeutically target eGlx HS systemically, may prevent or diminish the development of microvascular complication in diabetes.

In addition, the diabetic studies conducted in this thesis are further evidence that damage to the eGlx is an important factor in the development of DN and DR. Loss of eGlx in the GFB was associated with increased HPSE and increased glomerular permeability, and inhibiting HPSE with OVZ/HS-1638 restored GFB properties in diabetes. Although loss of eGlx in the eye was not significant in diabetes in the small cohort of mice, eGlx coverage results suggest that eGlx HS can be therapeutically targeted, as treatment with OVZ/HS-1638 significantly increased eGlx coverage in the retina. Furthermore, restoration of the iBRB by OVZ/HS-1638 treatment was evident by reduced extravascular albumin staining in the retina. Together, these data suggest that indeed, treatment with a OVZ/HS-1638 can therapeutically target eGlx HS systemically in DN and DR, as mentioned above. Although other HPSE inhibitors have been used in a handful of diabetic studies showing therapeutic affects in the kidney and eye (114,318,368,369), to my knowledge this is the first study to show that the use of HPSE inhibitors can be used to prevent eGlx damage in diabetes and associated microvascular permeability changes. Of note, this work has the possibility to be translated into clinical use, as HPSE inhibitor clinical trials are already underway for use in various cancers (256,265).

In addition to showing potential for the use of HPSE inhibitors as therapeutic treatments for DN and DR, this thesis provides evidence for efficacy of a novel class of HPSE inhibitors in DN and DR. As discussed in **CHAPTER 4**, currently available HPSE inhibitors are linear polysaccharides, which are costly to produce and have undefined structures, increasing batch-to-batch variation. Additionally, many of the HPSE inhibitors used still possess significant anticoagulant activity. The HPSE inhibitor used in this study is a dendrimer, a new class of structurally unique HPSE inhibitors. Work by our collaborator Dr. Olga Zubkova has shown that this inhibitor has nanomolar potency and has significantly lower anticoagulant activity compared to commercially available HPSE inhibitors PG545 and M410 (271). Additionally, OVZ/HS-1638 had no cytotoxic effects on cell lines tested at 100µg/mL, or 15-32µM, which is 100-1500 times higher than the IC_{50} required for HPSE inhibition (271). This inhibitor therefore has the real potential for clinical use, and our

collaborator is currently evaluating pharmacokinetics, bioavailability, and safety of this HPSE inhibitor class in hopes that it can progress to clinical testing (271).

7.4 *Future Work*

As this thesis provided evidence for a functional role of HS in the eGlx, future studies should be conducted to determine a mechanism for how it contributes to vascular permeability. As discussed earlier in this chapter, potential mechanisms for its contribution may include both physical barrier properties as well as regulation of junctions and transcellular pathways. This has not been actively investigated, and those studies which have been done on HS in the GFB and iBRB primarily focus on its role in the basement membranes of the respective vessel beds. Studies aimed at investigating the loss of eGlx HS and resulting affects should therefore be conducted. To my knowledge, the effect of loss of HS charge specifically in the eGlx in the GFB for example, has not been tested. Experiments in which eGlx HS is enzymatically shed and confirmed by immunofluorescence, could be used to determine what the effects on eGlx charge are, and its associated loss of function, which was demonstrated in **CHAPTER 3** and **CHAPTER 6**. However, the technical difficulty of this should be noted, as traditional investigations into loss of anionic sites after HS removal have focused on the GBM, labelled with cationic molecules such as cuprolinic blue or polyethyleneimine (184,370). But the GBM is a stable structure which does not require special fixation techniques for visualization, whereas the eGlx requires stabilisation with a cationic molecule such as Alcian blue, which would interfere with anionic labelling.

It would also be interesting to determine if treatment with heparinase III in a healthy state results in changes in junctional complex proteins such as ZO-1 and occludins in the iBRB, which are associated with increased HPSE as discussed early in this chapter. This can potentially be accomplished with the use of immunogold labelling, allowing for direct visualisation of eGlx and tight junctions at an ultrastructural level while also assessing potential changes in junctional proteins. Immunogold labelling has been successfully used to stain for tight junction proteins *in vitro* as well as tissue sections (371,372). These studies would provide further insight into how HS contributes to the eGlx, allowing for a better understanding of how HS can be therapeutically targeted in disease.

As discussed in earlier sections, the mouse model chosen for this experiment did not allow for a full investigation into the development and prevention of DN and DR in the same animal. It is possible that later timepoints would yield more robust changes in eGlx,

particularly in the eye, where, based on the literature discussed in **CHAPTERS 4** and **CHAPTER 6**, it appears that development of microvascular changes associated with DR may be slower than DN, although evidence of retina vascular leak was observed at 9 weeks in *db/db* mice. Therefore, future studies could be performed in the same *db/db* mouse model near 20 weeks, in which increased vascular permeability in the retina has been shown through the use of FITC-dextran (315). However, because *db/db* mice develop albuminuria by 8 weeks and this study focuses on early microvascular changes in DN and DR, it is possible that a 20-week timepoint would be too late for DN studies.

Alternatively, rat diabetic models may be a better model to investigate changes in eGlx and HS in the eye and kidney in parallel. T1D Wistar rats have been shown to have increased BSA-fluorescein extravasation in the retina and kidney after 6 weeks of diabetes induction (373). Additionally, increased urine albumin excretion and glomerular sclerosis can be observed in these rats by 5 weeks after induction of diabetes (374,375). In the retina, this model was shown to have reduced visual function of 31%, measured by electroretinography (ERG), after 4 weeks of diabetes (376). Reduced eGlx was also visualised in diabetic Wistar rats just 1 week after diabetes, measured by EM in tissue from cationic colloidal perfused rats (57). In future studies, it would also be useful to perform ERG to measure retinal function. Classical ERG objectively evaluates retinal function by using diffuse flashes of light and measuring the electrical response of the retina. In diabetic patients, reduced retina function is measured with ERG, and has been shown to correlate with retinopathy severity as well as a predictor of developing retinopathy (377,378). Additionally, because the proposed model is a T1D model, differences in body mass should not be an issue in solute flux measurements and would allow for functional measurements of solute flux. In fact, our collaborator, Professor David Bates, has successfully shown increased solute flux in T1D rats compared to non-diabetic rats (unpublished data). Therefore, this model may be a good model in future studies to study the effects of diabetes on eGlx and restoration by HPSE inhibition in DN and DR in parallel.

In addition to the use of a different model, the optimal route of injection for OVZ/HS-1638 will need to be investigated in future studies. The studies conducted in this thesis used i.p. and s.c. While i.p. did have restorative effects in the kidney, the issues that arose in the 11-week-old cohort did not allow for efficacy to be examined in the retina. Use of s.c. as a route of administration in the 9-week-old cohort did appear to yield some protective effects in the retina, evident by reduced albumin staining in treated *db/db* mice. However,

because eGlx was not significantly reduced in the kidney or the retina at this timepoint, protection of the eGlx by i.p. administration could not be concluded. In humans, the use of HPSE inhibitors in clinical trials such as PG545 and PI-88 have been administered i.v. and s.c. (262,266,268,379,380). For PI-88, which has been the most extensively tested HPSE inhibitor, s.c. appeared to be the best route of administration (379). Of course, oral administration would be the most clinically advantageous due to ease of administration, which dendrimers are well suited for due to their tuneable functionality (381,382). Indeed, dendrimers have been successfully used as delivery system to orally administer drugs like propranolol, triclosan, and ketoconazole (382). It is possible that OVZ/HS-1638 can be used orally or modified to be more suitable for oral administration. However, it is evident from published studies that route of administration and efficacy will differ with different HPSE inhibitors and will need to be determined for new dendrimer HPSE inhibitors such as OVZ/HS-1638.

7.5 *Conclusions and Final Remarks*

This thesis has provided evidence which indicates HS is structurally and functionally important in the eGlx in two structurally unique vessel beds, the glomerulus and in the retina microvessels. Using two approaches in mice, enzymatic removal and a transgenic mouse model, I was able to show that loss or reduction of eGlx HS resulted in structural damage and loss of barrier function in the GFB and iBRB. These parameters were measured by EM in both tissue types, and by permeability and solute flux assays in the glomerulus and retina, respectively. Although follow up immunofluorescence studies need to be done to directly confirm loss of HS in the eGlx, results showing damage to the eGlx using two HS targeting approaches is a good indication that the results observed are likely due to HS changes.

Using a T2D mouse model, I was further able to demonstrate diabetes resulted in significant increase in permeability and extravascular albumin accumulation, in the kidney and the eye, respectively. This increase was associated with a significant loss of eGlx in the kidney, and a trend in eGlx loss in the eye, albeit at two different time points for each vessel bed. Furthermore, the data indicated that treatment with a novel HPSE inhibitor OVZ/HS-1638 resulted in restoration of eGlx structure and GFB barrier properties in the kidney. In the eye, a significant increase in eGlx coverage was observed with OVZ/HS-1638 treatment, which coincided with a significant reduction in extravascular albumin accumulation in the retina. These data indicate that HS is therapeutically amendable in

microvascular complications of diabetes such as DN and DR, with the possibility of treatment translating to other diseases which involve similar microvascular changes which result in increased permeability.

References

1. Yuan SY, Rigor RR. Structure and Function of Exchange Microvessels [Internet]. Morgan & Claypool Life Sciences; 2010 [cited 2020 Jan 20]. Available from: https://www.ncbi.nlm.nih.gov/books/NBK54123/

2. Starling EH. On the Absorption of Fluids from the Connective Tissue Spaces. J Physiol. 1896 May 5;19(4):312–26.

3. Landis EM. MICRO-INJECTION STUDIES OF CAPILLARY PERMEABILITY. :22.

4. Levick JR, Michel CC. Microvascular fluid exchange and the revised Starling principle. Cardiovasc Res. 2010 Jul 15;87(2):198–210.

5. Levick JR. An Introduction to Cardiovascular Physiology. Butterworth-Heinemann; 2013. 288 p.

6. Reitsma S, Slaaf DW, Vink H, van Zandvoort MAMJ, oude Egbrink MGA. The endothelial glycocalyx: composition, functions, and visualization. Pflugers Arch. 2007 Jun;454(3):345–59.

7. Curry F-RE. Microvascular solute and water transport. Microcirculation. 2005 Feb;12(1):17–31.

8. Hu X, Adamson RH, Liu B, Curry FE, Weinbaum S. Starling forces that oppose filtration after tissue oncotic pressure is increased. American Journal of Physiology-Heart and Circulatory Physiology. 2000 Oct 1;279(4):H1724–36.

9. Fu B, Curry F-RE, Adamson RH, Weinbaum S. A model for interpreting the tracer labeling of interendothelial clefts. Ann Biomed Eng. 1997 Mar 1;25(2):375–97.

10. Singh A, Satchell SC, Neal CR, McKenzie EA, Tooke JE, Mathieson PW. Glomerular Endothelial Glycocalyx Constitutes a Barrier to Protein Permeability. JASN. 2007 Nov 1;18(11):2885–93.

11. Tarbell JM. Shear stress and the endothelial transport barrier. Cardiovasc Res. 2010 Jul 15;87(2):320–30.

12. Pries AR, Secomb TW, Gaehtgens P. The endothelial surface layer. Pflügers Arch - Eur J Physiol. 2000 Sep 1;440(5):653–66.

13. Kwok JCF, Warren P, Fawcett JW. Chondroitin sulfate: A key molecule in the brain matrix. The International Journal of Biochemistry & Cell Biology. 2012 Apr 1;44(4):582–6.

14. Reitsma S, Slaaf DW, Vink H, van Zandvoort MAMJ, oude Egbrink MGA. The endothelial glycocalyx: composition, functions, and visualization. Pflugers Arch. 2007 Jun;454(3):345–59.

15. Turnbull J, Powell A, Guimond S. Heparan sulfate: decoding a dynamic multifunctional cell regulator. Trends in Cell Biology. 2001 Feb 1;11(2):75–82.

16. Cruz-Chu ER, Malafeev A, Pajarskas T, Pivkin IV, Koumoutsakos P. Structure and Response to Flow of the Glycocalyx Layer. Biophys J. 2014 Jan 7;106(1):232–43.

17. Pappenheimer JR, Renkin EM, Borrero LM. Filtration, Diffusion and Molecular Sieving Through Peripheral Capillary Membranes. American Journal of Physiology-Legacy Content. 1951 Sep 30;167(1):13–46.

18. Stefánsson E, Loftsson T. The Stokes−Einstein equation and the physiological effects of vitreous surgery. Acta Ophthalmologica Scandinavica. 2006;84(6):718–9.

19. Renkin EM. Cellular Aspects of Transvascular Exchange: A 40-Year Perspective. Microcirculation. 1994;1(3):157–67.

20. Michel CC. Starling: the formulation of his hypothesis of microvascular fluid exchange and its significance after 100 years. Experimental Physiology. 1997 Jan 1;82(1):1–30.

21. Oxburgh L. Kidney Nephron Determination. Annual Review of Cell and Developmental Biology. 2018;34(1):427–50.

22. Kokko JP. The role of the collecting duct in urinary concentration. Kidney International. 1987 Feb 1;31(2):606–10.

23. Kitching AR, Hutton HL. The Players: Cells Involved in Glomerular Disease. CJASN. 2016 Sep 7;11(9):1664–74.

24. Schlöndorff D, Banas B. The Mesangial Cell Revisited: No Cell Is an Island. JASN. 2009 Jun 1;20(6):1179–87.

25. Gelberg H, Healy L, Whiteley H, Miller LA, Vimr E. In vivo enzymatic removal of alpha 2-->6-linked sialic acid from the glomerular filtration barrier results in podocyte charge alteration and glomerular injury. Lab Invest. 1996 May;74(5):907–20.

26. Reiser J, Altintas MM. Podocytes. F1000Res [Internet]. 2016 Jan 28 [cited 2019 Dec 23];5. Available from: https://www.ncbi.nlm.nih.gov/pmc/articles/PMC4755401/

27. Miner JH. The Glomerular Basement Membrane. Exp Cell Res. 2012 May 15;318(9):973–8.

28. Lea PJ, Silverman M, Hegele R, Hollenberg MJ. Tridimensional ultrastructure of glomerular capillary endothelium revealed by high-resolution scanning electron microscopy. Microvasc Res. 1989 Nov;38(3):296–308.

29. Rostgaard J, Qvortrup K. Electron microscopic demonstrations of filamentous molecular sieve plugs in capillary fenestrae. Microvasc Res. 1997 Jan;53(1):1–13.

30. Satchell SC, Braet F. Glomerular endothelial cell fenestrations: an integral component of the glomerular filtration barrier. Am J Physiol Renal Physiol. 2009 May;296(5):F947–56.

31. Siddiqi FS, Advani A. Endothelial-Podocyte Crosstalk: The Missing Link Between Endothelial Dysfunction and Albuminuria in Diabetes. Diabetes. 2013 Nov 1;62(11):3647–55.

32. Satchell SC. The glomerular endothelium emerges as a key player in diabetic nephropathy. Kidney International. 2012 Nov 1;82(9):949–51.

33. Foster RR, Armstrong L, Baker S, Wong DWL, Wylie EC, Ramnath R, et al. Glycosaminoglycan Regulation by VEGFA and VEGFC of the Glomerular Microvascular Endothelial Cell Glycocalyx in Vitro. The American Journal of Pathology. 2013 Aug;183(2):604–16.

34. Salmon AHJ, Neal CR, Sage LM, Glass CA, Harper SJ, Bates DO. Angiopoietin-1 alters microvascular permeability coefficients in vivo via modification of endothelial glycocalyx. Cardiovasc Res. 2009 Jul 1;83(1):24–33.

35. Jeansson M, Haraldsson B. Morphological and functional evidence for an important role of the endothelial cell glycocalyx in the glomerular barrier. American Journal of Physiology-Renal Physiology. 2006 Jan 1;290(1):F111–6.

36. Desideri S, Onions KL, Qiu Y, Ramnath RD, Butler MJ, Neal CR, et al. A novel assay provides sensitive measurement of physiologically relevant changes in albumin permeability in isolated human and rodent glomeruli. Kidney Int. 2018 Feb 9;

37. Bevan HS, Slater SC, Clarke H, Cahill PA, Mathieson PW, Welsh GI, et al. Acute laminar shear stress reversibly increases human glomerular endothelial cell permeability via activation of endothelial nitric oxide synthase. Am J Physiol Renal Physiol. 2011 Oct;301(4):F733–42.

38. Singh A, Ramnath RD, Foster RR, Wylie EC, Fridén V, Dasgupta I, et al. Reactive Oxygen Species Modulate the Barrier Function of the Human Glomerular Endothelial Glycocalyx. PLOS ONE. 2013 Feb 14;8(2):e55852.

39. van Golen RF, van Gulik TM, Heger M. Mechanistic overview of reactive species-induced degradation of the endothelial glycocalyx during hepatic ischemia/reperfusion injury. Free Radical Biology and Medicine. 2012 Apr 15;52(8):1382–402.

40. Nieuwdorp M, Haeften TW van, Gouverneur MCLG, Mooij HL, Lieshout MHP van, Levi M, et al. Loss of Endothelial Glycocalyx During Acute Hyperglycemia Coincides With Endothelial Dysfunction and Coagulation Activation In Vivo. Diabetes. 2006 Feb 1;55(2):480–6.

41. Schött U, Solomon C, Fries D, Bentzer P. The endothelial glycocalyx and its disruption, protection and regeneration: a narrative review. Scand J Trauma Resusc Emerg Med [Internet]. 2016 Apr 12 [cited 2019 Dec 23];24. Available from: https://www.ncbi.nlm.nih.gov/pmc/articles/PMC4828893/

42. Rabelink TJ, de Zeeuw D. The glycocalyx—linking albuminuria with renal and cardiovascular disease. Nat Rev Nephrol. 2015 Nov;11(11):667–76.

43. Willoughby CE, Ponzin D, Ferrari S, Lobo A, Landau K, Omidi Y. Anatomy and physiology of the human eye: effects of mucopolysaccharidoses disease on

structure and function – a review. Clinical & Experimental Ophthalmology. 2010;38(s1):2–11.

44. Abràmoff MD, Garvin MK, Sonka M. Retinal Imaging and Image Analysis. IEEE Rev Biomed Eng. 2010 Jan 1;3:169–208.

45. About Retinal Blood Vessels | Retina Doctor Melbourne [Internet]. [cited 2020 Jan 21]. Available from: https://www.retinadoctor.com.au/about-the-eye/the-retinal-blood-vessels/

46. Nickla DL, Wallman J. THE MULTIFUNCTIONAL CHOROID. Prog Retin Eye Res. 2010 Mar;29(2):144–68.

47. Cunha-Vaz J, Bernardes R, Lobo C. Blood-Retinal Barrier. European Journal of Ophthalmology. 2011 Nov 1;21(6_suppl):3–9.

48. Díaz-Coránguez M, Ramos C, Antonetti DA. The inner Blood-Retinal Barrier: Cellular Basis and Development. Vision Res. 2017 Oct;139:123–37.

49. Umeda K, Ikenouchi J, Katahira-Tayama S, Furuse K, Sasaki H, Nakayama M, et al. ZO-1 and ZO-2 independently determine where claudins are polymerized in tight-junction strand formation. Cell. 2006 Aug 25;126(4):741–54.

50. Ooshio T, Kobayashi R, Ikeda W, Miyata M, Fukumoto Y, Matsuzawa N, et al. Involvement of the interaction of afadin with ZO-1 in the formation of tight junctions in Madin-Darby canine kidney cells. J Biol Chem. 2010 Feb 12;285(7):5003–12.

51. Navaratna D, McGuire PG, Menicucci G, Das A. Proteolytic Degradation of VE-Cadherin Alters the Blood-Retinal Barrier in Diabetes. Diabetes. 2007 Sep 1;56(9):2380–7.

52. Klaassen I, Van Noorden CJF, Schlingemann RO. Molecular basis of the inner blood-retinal barrier and its breakdown in diabetic macular edema and other pathological conditions. Progress in Retinal and Eye Research. 2013 May 1;34:19–48.

53. Song JH, Chin HS, Kwon OW, Lim SJ, Kim HK, for the DRESS Research Group. Effect of sulodexide in patients with non-proliferative diabetic retinopathy: diabetic retinopathy sulodexide study (DRESS). Graefes Arch Clin Exp Ophthalmol. 2015 Jun 1;253(6):829–37.

54. Wylie E, Foster R, Salmon A, Satchell S. Role of the endothelial glycocalyx in kidney disease and vascular dysfunction. The Lancet. 2014 Feb 26;383:S112.

55. Yilmaz O, Afsar B, Ortiz A, Kanbay M. The role of endothelial glycocalyx in health and disease. Clin Kidney J. 2019 Apr 23;12(5):611–9.

56. Kim Y-H, Nijst P, Kiefer K, Tang WHW. Endothelial Glycocalyx as Biomarker for Cardiovascular Diseases: Mechanistic and Clinical Implications. Curr Heart Fail Rep. 2017 Apr 1;14(2):117–26.

57. Kumase F, Morizane Y, Mohri S, Takasu I, Ohtsuka A, Ohtsuki H. Glycocalyx degradation in retinal and choroidal capillary endothelium in rats with diabetes and hypertension. Acta Med Okayama. 2010 Oct;64(5):277–83.

58. Broekhuizen LN, Lemkes BA, Mooij HL, Meuwese MC, Verberne H, Holleman F, et al. Effect of sulodexide on endothelial glycocalyx and vascular permeability in patients with type 2 diabetes mellitus. Diabetologia. 2010 Dec 1;53(12):2646–55.

59. Leskova W, Pickett H, Eshaq RS, Shrestha B, Pattillo CB, Harris NR. Effect of diabetes and hyaluronidase on the retinal endothelial glycocalyx in mice. Experimental Eye Research. 2019 Feb 1;179:125–31.

60. Niu T, Zhao M, Jiang Y, Xing X, Shi X, Cheng L, et al. Endomucin restores depleted endothelial glycocalyx in the retinas of streptozotocin-induced diabetic rats. The FASEB Journal. 2019 Sep 21;33(12):13346–57.

61. 3.8 million people in England now have diabetes - GOV.UK [Internet]. [cited 2017 Apr 20]. Available from: https://www.gov.uk/government/news/38-million-people-in-england-now-have-diabetes

62. Belle TLV, Coppieters KT, Herrath MGV. Type 1 Diabetes: Etiology, Immunology, and Therapeutic Strategies. Physiological Reviews. 2011 Jan 1;91(1):79–118.

63. Katsarou A, Gudbjörnsdottir S, Rawshani A, Dabelea D, Bonifacio E, Anderson BJ, et al. Type 1 diabetes mellitus. Nature Reviews Disease Primers. 2017 Mar 30;3:17016.

64. Cerf ME. Beta Cell Dysfunction and Insulin Resistance. Front Endocrinol (Lausanne) [Internet]. 2013 Mar 27 [cited 2017 Apr 20];4. Available from: http://www.ncbi.nlm.nih.gov/pmc/articles/PMC3608918/

65. Stienstra R, Duval C, Müller M, Kersten S. PPARs, Obesity, and Inflammation. PPAR Res [Internet]. 2007 [cited 2017 Apr 21];2007. Available from: http://www.ncbi.nlm.nih.gov/pmc/articles/PMC1783744/

66. Fowler MJ. Microvascular and Macrovascular Complications of Diabetes. Clinical Diabetes. 2008 Apr 1;26(2):77–82.

67. Rader DJ. Effect of Insulin Resistance, Dyslipidemia, and Intra-abdominal Adiposity on the Development of Cardiovascular Disease and Diabetes Mellitus. The American Journal of Medicine. 2007 Mar;120(3, Supplement 1):S12–8.

68. Yun J-S, Ko S-H, Kim J-H, Moon K-W, Park Y-M, Yoo K-D, et al. Diabetic Retinopathy and Endothelial Dysfunction in Patients with Type 2 Diabetes Mellitus. Diabetes Metab J. 2013 Aug;37(4):262–9.

69. Cheng H, Harris RC. Renal Endothelial Dysfunction in Diabetic Nephropathy. Cardiovasc Hematol Disord Drug Targets. 2014;14(1):22–33.

70. Brownlee M. The Pathobiology of Diabetic Complications: A Unifying Mechanism. Diabetes. 2005 Jun 1;54(6):1615–25.

71. Koya D, King GL. Protein kinase C activation and the development of diabetic complications. Diabetes. 1998 Jun;47(6):859–66.

72. Busik JV, Mohr S, Grant MB. Hyperglycemia-Induced Reactive Oxygen Species Toxicity to Endothelial Cells Is Dependent on Paracrine Mediators. Diabetes. 2008 Jul;57(7):1952–65.

73. Kaneto H, Xu G, Song K-H, Suzuma K, Bonner-Weir S, Sharma A, et al. Activation of the Hexosamine Pathway Leads to Deterioration of Pancreatic β-Cell Function through the Induction of Oxidative Stress. J Biol Chem. 2001 Aug 17;276(33):31099–104.

74. Steckelings UM, Rompe F, Kaschina E, Unger T. The evolving story of the RAAS in hypertension, diabetes and CV disease: moving from macrovascular to microvascular targets. Fundam Clin Pharmacol. 2009 Dec;23(6):693–703.

75. Hotamisligil GS. Mechanisms of TNF-alpha-induced insulin resistance. Exp Clin Endocrinol Diabetes. 1999;107(2):119–25.

76. Sawant DA, Tharakan B, Wilson RL, Stagg HW, Hunter FA, Childs EW. Regulation of TNF-α-Induced Microvascular Endothelial Cell Hyperpermeability by Recombinant Bcl-xL. J Surg Res. 2013 Sep;184(1):628–37.

77. Banerjee M, Saxena M. Interleukin-1 (IL-1) family of cytokines: Role in Type 2 Diabetes. Clinica Chimica Acta. 2012 Aug 16;413(15):1163–70.

78. Rehman K, Akash MSH, Liaqat A, Kamal S, Qadir MI, Rasul A. Role of Interleukin-6 in Development of Insulin Resistance and Type 2 Diabetes Mellitus. Crit Rev Eukaryot Gene Expr. 2017;27(3):229–36.

79. Achari AE, Jain SK. Adiponectin, a Therapeutic Target for Obesity, Diabetes, and Endothelial Dysfunction. Int J Mol Sci [Internet]. 2017 Jun 21 [cited 2020 Mar 17];18(6). Available from: https://www.ncbi.nlm.nih.gov/pmc/articles/PMC5486142/

80. Aiello LP, Wong JS. Role of vascular endothelial growth factor in diabetic vascular complications. Kidney Int Suppl. 2000 Sep;77:S113-119.

81. Braga Gomes K, Fontana Rodrigues K, Fernandes AP. The Role of Transforming Growth Factor-Beta in Diabetic Nephropathy [Internet]. International Journal of Medical Genetics. 2014 [cited 2020 Mar 17]. Available from: https://www.hindawi.com/journals/ijmg/2014/180270/

82. Idriss HT, Naismith JH. TNF alpha and the TNF receptor superfamily: structure-function relationship(s). Microsc Res Tech. 2000 Aug 1;50(3):184–95.

83. Wellen KE, Hotamisligil GS. Inflammation, stress, and diabetes. J Clin Invest. 2005 May 2;115(5):1111–9.

84. Qiao Y, Chen Y, Pan Y, Tian F, Xu Y, Zhang X, et al. The change of serum tumor necrosis factor alpha in patients with type 1 diabetes mellitus: A systematic review and meta-analysis. PLoS One [Internet]. 2017 Apr 20 [cited 2020 Mar 16];12(4). Available from: https://www.ncbi.nlm.nih.gov/pmc/articles/PMC5398633/

85. McFarlane SI, Sowers JR. Aldosterone Function in Diabetes Mellitus: Effects on Cardiovascular and Renal Disease. J Clin Endocrinol Metab. 2003 Feb 1;88(2):516–23.

86. Viana LV, Leitão CB, Grillo MF, Rocha EPCC, Brenner JK, Friedman R, et al. Hypertension management algorithm for type 2 diabetic patients applied in primary care. Diabetology & Metabolic Syndrome. 2013;5:52.

87. Lovshin JA, Lytvyn Y, Lovblom LE, Katz A, Boulet G, Bjornstad P, et al. Retinopathy and RAAS Activation: Results From the Canadian Study of Longevity in Type 1 Diabetes. Diabetes Care. 2019;42(2):273–80.

88. Chawla T, Sharma D, Singh A. Role of the renin angiotensin system in diabetic nephropathy. World J Diabetes. 2010 Nov 15;1(5):141–5.

89. Maharaj ASR, D'Amore PA. Roles for VEGF in adult. Microvasc Res. 2007;74(2–3):100–13.

90. Singh A, Satchell SC. Microalbuminuria: causes and implications. Pediatr Nephrol. 2011 Nov;26(11):1957–65.

91. Forman JP, Fisher NDL, Schopick EL, Curhan GC. Higher Levels of Albuminuria within the Normal Range Predict Incident Hypertension. J Am Soc Nephrol. 2008 Oct;19(10):1983–8.

92. Roshan B, Stanton RC. A story of microalbuminuria and diabetic nephropathy. J Nephropathol. 2013 Oct;2(4):234–40.

93. Pagtalunan ME, Miller PL, Jumping-Eagle S, Nelson RG, Myers BD, Rennke HG, et al. Podocyte loss and progressive glomerular injury in type II diabetes. J Clin Invest. 1997 Jan 15;99(2):342–8.

94. Marshall CB. Rethinking glomerular basement membrane thickening in diabetic nephropathy: adaptive or pathogenic? Am J Physiol Renal Physiol. 2016 Nov 1;311(5):F831–43.

95. Arif E, Nihalani D. Glomerular Filtration Barrier Assembly: An insight. Postdoc J. 2013 Apr;1(4):33–45.

96. Pavenstädt H, Kriz W, Kretzler M. Cell Biology of the Glomerular Podocyte. Physiological Reviews. 2003 Jan 1;83(1):253–307.

97. Haraldsson B, Jeansson M. Glomerular filtration barrier. Current Opinion in Nephrology and Hypertension. 2009 Jul;18(4):331–5.

98. Tufro A, Veron D. VEGF AND PODOCYTES IN DIABETIC NEPHROPATHY. Semin Nephrol. 2012 Jul;32(4):385–93.

99. Lemley KV, Blouch K, Abdullah I, Boothroyd DB, Bennett PH, Myers BD, et al. Glomerular Permselectivity at the Onset of Nephropathy in Type 2 Diabetes Mellitus. JASN. 2000 Nov 1;11(11):2095–105.

100. Fioretto P, Stehouwer CDA, Mauer M, Chiesura-Corona M, Brocco E, Carraro A, et al. Heterogeneous nature of microalbuminuria in NIDDM: studies of endothelial function and renal structure. Diabetologia. 1998 Jan 1;41(2):233–6.

101. Satchell SC, Tooke JE. What is the mechanism of microalbuminuria in diabetes: a role for the glomerular endothelium? Diabetologia. 2008 May;51(5):714–25.

102. Weil EJ, Lemley KV, Mason CC, Yee B, Jones LI, Blouch K, et al. Podocyte detachment and reduced glomerular capillary endothelial fenestration promote kidney disease in type 2 diabetic nephropathy. Kidney Int. 2012 Nov;82(9):1010–7.

103. Toyoda M, Najafian B, Kim Y, Caramori ML, Mauer M. Podocyte Detachment and Reduced Glomerular Capillary Endothelial Fenestration in Human Type 1 Diabetic Nephropathy. Diabetes. 2007 Aug 1;56(8):2155–60.

104. Dogné S, Flamion B, Caron N. Endothelial Glycocalyx as a Shield Against Diabetic Vascular Complications. Arterioscler Thromb Vasc Biol. 2018 Jul;38(7):1427–39.

105. Nieuwdorp M, Holleman F, de Groot E, Vink H, Gort J, Kontush A, et al. Perturbation of hyaluronan metabolism predisposes patients with type 1 diabetes mellitus to atherosclerosis. Diabetologia. 2007 Jun;50(6):1288–93.

106. Lewandowski KC, Banach E, Bieńkiewicz M, Lewiński A. Matrix metalloproteinases in type 2 diabetes and non-diabetic controls: effects of short-term and chronic hyperglycaemia. Arch Med Sci. 2011 Apr;7(2):294–303.

107. Chung Ada W.Y., Hsiang York N., Matzke Lise A., McManus Bruce M., van Breemen Cornelis, Okon Elena B. Reduced Expression of Vascular Endothelial Growth Factor Paralleled With the Increased Angiostatin Expression Resulting From the Upregulated Activities of Matrix Metalloproteinase-2 and -9 in Human Type 2 Diabetic Arterial Vasculature. Circulation Research. 2006 Jul 21;99(2):140–8.

108. Ramnath RD, Butler MJ, Newman G, Desideri S, Russell A, Lay AC, et al. Blocking matrix metalloproteinase-mediated syndecan-4 shedding restores the endothelial glycocalyx and glomerular filtration barrier function in early diabetic kidney disease. Kidney International [Internet]. 2019 Nov 2 [cited 2020 Jan 15];0(0). Available from: https://www.kidney-international.org/article/S0085-2538(19)31110-X/abstract

109. van den Hoven MJ, Rops AL, Bakker MA, Aten J, Rutjes N, Roestenberg P, et al. Increased expression of heparanase in overt diabetic nephropathy. Kidney International. 2006 Dec 2;70(12):2100–8.

110. Rops ALWMM, Hoven VD, J M, Veldman BA, Salemink S, Vervoort G, et al. Urinary heparanase activity in patients with Type 1 and Type 2 diabetes. Nephrol Dial Transplant. 2012 Jul 1;27(7):2853–61.

111. Svennevig K, Kolset SO, Bangstad H-J. Increased syndecan-1 in serum is related to early nephropathy in type 1 diabetes mellitus patients. Diabetologia. 2006 Sep 1;49(9):2214–6.

112. Koźma EM, Olczyk K, Głowacki A, Komosińska K, Sonecki P, Najmiec T, et al. Glycosaminoglycans of human serum and their alterations in diabetes mellitus. Acta Biochim Pol. 1996;43(3):567–74.

113. Dogné S, Rath G, Jouret F, Caron N, Dessy C, Flamion B. Hyaluronidase 1 Deficiency Preserves Endothelial Function and Glycocalyx Integrity in Early Streptozotocin-Induced Diabetes. Diabetes. 2016;65(9):2742–53.

114. Gil N, Goldberg R, Neuman T, Garsen M, Zcharia E, Rubinstein AM, et al. Heparanase Is Essential for the Development of Diabetic Nephropathy in Mice. Diabetes. 2012 Jan 1;61(1):208–16.

115. Xu X, Xiao L, Xiao P, Yang S, Chen G, Liu F, et al. A Glimpse of Matrix Metalloproteinases in Diabetic Nephropathy. Curr Med Chem. 2014;21(28):3244–60.

116. Onions KL, Gamez M, Buckner NR, Baker SL, Betteridge KB, Desideri S, et al. VEGFC Reduces Glomerular Albumin Permeability and Protects Against Alterations in VEGF Receptor Expression in Diabetic Nephropathy. Diabetes. 2019 Jan 1;68(1):172–87.

117. Duh EJ, Sun JK, Stitt AW. Diabetic retinopathy: current understanding, mechanisms, and treatment strategies. JCI Insight [Internet]. [cited 2020 Jan 16];2(14). Available from: https://www.ncbi.nlm.nih.gov/pmc/articles/PMC5518557/

118. Frey T, Antonetti DA. Alterations to the blood-retinal barrier in diabetes: cytokines and reactive oxygen species. Antioxid Redox Signal. 2011 Sep 1;15(5):1271–84.

119. Stitt AW, Curtis TM, Chen M, Medina RJ, McKay GJ, Jenkins A, et al. The progress in understanding and treatment of diabetic retinopathy. Prog Retin Eye Res. 2016 Mar;51:156–86.

120. Mizutani M, Kern TS, Lorenzi M. Accelerated death of retinal microvascular cells in human and experimental diabetic retinopathy. J Clin Invest. 1996 Jun 15;97(12):2883–90.

121. Ljubimov AV, Burgeson RE, Butkowski RJ, Couchman JR, Zardi L, Ninomiya Y, et al. Basement membrane abnormalities in human eyes with diabetic retinopathy. J Histochem Cytochem. 1996 Dec;44(12):1469–79.

122. Gardiner TA, Stitt AW, Archer DB. Retinal vascular endothelial cell endocytosis increases in early diabetes. Lab Invest. 1995 Apr;72(4):439–44.

123. Hofman P, Blaauwgeers HG, Tolentino MJ, Adamis AP, Nunes Cardozo BJ, Vrensen GF, et al. VEGF-A induced hyperpermeability of blood-retinal barrier endothelium in vivo is predominantly associated with pinocytotic vesicular transport and not with formation of fenestrations. Vascular endothelial growth factor-A. Curr Eye Res. 2000 Aug;21(2):637–45.

124. Kuiper EJ, Hughes JM, Geest RJV, Vogels IMC, Goldschmeding R, Noorden CJFV, et al. Effect of VEGF-A on Expression of Profibrotic Growth Factor and Extracellular Matrix Genes in the Retina. Invest Ophthalmol Vis Sci. 2007 Sep 1;48(9):4267–76.

125. El-Asrar AMA, Alam K, Nawaz MI, Mohammad G, Eynde KV den, Siddiquei MM, et al. Upregulated Expression of Heparanase in the Vitreous of Patients With Proliferative Diabetic Retinopathy Originates From Activated Endothelial Cells and Leukocytes. Invest Ophthalmol Vis Sci. 2015 Dec 1;56(13):8239–47.

126. Ma P, Luo Y, Zhu X, Li T, Hu J, Tang S. Retinal heparanase expression in streptozotocin-induced diabetic rats. Canadian Journal of Ophthalmology / Journal Canadien d'Ophtalmologie. 2010 Feb 1;45(1):46–51.

127. Fadini GP, Bonora BM, Avogaro A. SGLT2 inhibitors and diabetic ketoacidosis: data from the FDA Adverse Event Reporting System. Diabetologia. 2017 May 12;

128. DeFronzo RA. Overview of Newer Agents: Where Treatment Is Going. The American Journal of Medicine. 2010 Mar;123(3, Supplement):S38–48.

129. Gastaldelli A, Miyazaki Y, Mahankali A, Berria R, Pettiti M, Buzzigoli E, et al. The Effect of Pioglitazone on the Liver. Diabetes Care. 2006 Oct 1;29(10):2275–81.

130. Hundal RS, Krssak M, Dufour S, Laurent D, Lebon V, Chandramouli V, et al. Mechanism by Which Metformin Reduces Glucose Production in Type 2 Diabetes. Diabetes. 2000 Dec;49(12):2063–9.

131. Chi C, Snaith J, Gunton JE. Diabetes Medications and Cardiovascular Outcomes in Type 2 Diabetes. Heart, Lung and Circulation [Internet]. [cited 2017 May 15]; Available from: http://www.sciencedirect.com/science/article/pii/S1443950617302913

132. King P, Peacock I, Donnelly R. The UK Prospective Diabetes Study (UKPDS): clinical and therapeutic implications for type 2 diabetes. Br J Clin Pharmacol. 1999 Nov;48(5):643–8.

133. Gastaldelli A, Miyazaki Y, Pettiti M, Santini E, Ciociaro D, DeFronzo RA, et al. The Effect of Rosiglitazone on the Liver: Decreased Gluconeogenesis in Patients with Type 2 Diabetes. J Clin Endocrinol Metab. 2006 Mar 1;91(3):806–12.

134. Gastaldelli A, Ferrannini E, Miyazaki Y, Matsuda M, Mari A, DeFronzo RA. Thiazolidinediones improve β-cell function in type 2 diabetic patients. American Journal of Physiology - Endocrinology and Metabolism. 2007 Mar 1;292(3):E871–83.

135. Grossman A, Grossman E. Blood pressure control in type 2 diabetic patients. Cardiovascular Diabetology. 2017;16:3.

136. Aghazadeh Y, Nostro MC. Cell Therapy for Type 1 Diabetes: Current and Future Strategies. Curr Diab Rep. 2017 Jun 1;17(6):37.

137. Aye MM, Atkin SL. Patient safety and minimizing risk with insulin administration – role of insulin degludec. Drug Healthc Patient Saf. 2014 Apr 30;6:55–67.

138. Staeva TP, Chatenoud L, Insel R, Atkinson MA. Recent Lessons Learned From Prevention and Recent-Onset Type 1 Diabetes Immunotherapy Trials. Diabetes. 2013 Jan;62(1):9–17.

139. MacCraith E, Davis NF, Browne C, Mohan P, Hickey D. Simultaneous pancreas and kidney transplantation: Incidence and risk factors for amputation after 10-year follow-up. Clin Transplant. :n/a-n/a.

140. Jacobsen P, Andersen S, Rossing K, Jensen BR, Parving H-H. Dual blockade of the renin-angiotensin system versus maximal recommended dose of ACE inhibition in diabetic nephropathy. Kidney Int. 2003 May;63(5):1874–80.

141. Mogensen CE, Neldam S, Tikkanen I, Oren S, Viskoper R, Watts RW, et al. Randomised controlled trial of dual blockade of renin-angiotensin system in patients with hypertension, microalbuminuria, and non-insulin dependent diabetes: the candesartan and lisinopril microalbuminuria (CALM) study. BMJ. 2000 Dec 9;321(7274):1440–4.

142. Rossing K, Schjoedt KJ, Smidt UM, Boomsma F, Parving H-H. Beneficial effects of adding spironolactone to recommended antihypertensive treatment in diabetic nephropathy: a randomized, double-masked, cross-over study. Diabetes Care. 2005 Sep;28(9):2106–12.

143. Schjoedt KJ, Rossing K, Juhl TR, Boomsma F, Rossing P, Tarnow L, et al. Beneficial impact of spironolactone in diabetic nephropathy. Kidney Int. 2005 Dec;68(6):2829–36.

144. Bakris GL, Copley JB, Vicknair N, Sadler R, Leurgans S. Calcium channel blockers versus other antihypertensive therapies on progression of NIDDM associated nephropathy. Kidney Int. 1996 Nov;50(5):1641–50.

145. Kelly MS, Lewis J, Huntsberry AM, Dea L, Portillo I. Efficacy and renal outcomes of SGLT2 inhibitors in patients with type 2 diabetes and chronic kidney disease. Postgrad Med. 2019 Jan;131(1):31–42.

146. Greco EV, Russo G, Giandalia A, Viazzi F, Pontremoli R, De Cosmo S. GLP-1 Receptor Agonists and Kidney Protection. Medicina (Kaunas) [Internet]. 2019 May 31 [cited 2020 Jan 29];55(6). Available from: https://www.ncbi.nlm.nih.gov/pmc/articles/PMC6630923/

147. Loon NR. Diabetic Kidney Disease: Preventing Dialysis and Transplantation. Clinical Diabetes. 2003 Apr 1;21(2):55–62.

148. Simó R, Sundstrom JM, Antonetti DA. Ocular Anti-VEGF Therapy for Diabetic Retinopathy: The Role of VEGF in the Pathogenesis of Diabetic Retinopathy. Diabetes Care. 2014 Apr 1;37(4):893–9.

149. Wang W, Lo ACY. Diabetic Retinopathy: Pathophysiology and Treatments. Int J Mol Sci [Internet]. 2018 Jun 20 [cited 2020 Jan 16];19(6). Available from: https://www.ncbi.nlm.nih.gov/pmc/articles/PMC6032159/

150. Diabetic Retinopathy Clinical Research Network, Elman MJ, Aiello LP, Beck RW, Bressler NM, Bressler SB, et al. Randomized trial evaluating ranibizumab plus prompt or deferred laser or triamcinolone plus prompt laser for diabetic macular edema. Ophthalmology. 2010 Jun;117(6):1064-1077.e35.

151. Pearson PA, Comstock TL, Ip M, Callanan D, Morse LS, Ashton P, et al. Fluocinolone acetonide intravitreal implant for diabetic macular edema: a 3-year multicenter, randomized, controlled clinical trial. Ophthalmology. 2011 Aug;118(8):1580–7.

152. Reddy SV, Husain D. Panretinal Photocoagulation: A Review of Complications. Seminars in Ophthalmology. 2018 Jan 2;33(1):83–8.

153. Lee SN, Chhablani J, Chan CK, Wang H, Barteselli G, El-Emam S, et al. Characterization of microaneurysm closure after focal laser photocoagulation in diabetic macular edema. Am J Ophthalmol. 2013 May;155(5):905-912.e2.

154. Fong DS, Girach A, Boney A. Visual side effects of successful scatter laser photocoagulation surgery for proliferative diabetic retinopathy: a literature review. Retina (Philadelphia, Pa). 2007 Sep;27(7):816–24.

155. Oltean S, Qiu Y, Ferguson JK, Stevens M, Neal C, Russell A, et al. Vascular Endothelial Growth Factor-A165b Is Protective and Restores Endothelial Glycocalyx in Diabetic Nephropathy. J Am Soc Nephrol. 2015 Aug;26(8):1889–904.

156. Drumond MC, Deen WM. Structural determinants of glomerular hydraulic permeability. American Journal of Physiology-Renal Physiology. 1994 Jan 1;266(1):F1–12.

157. Li R, Xing J, Mu X, Wang H, Zhang L, Zhao Y, et al. Sulodexide therapy for the treatment of diabetic nephropathy, a meta-analysis and literature review. Drug Des Devel Ther. 2015;9:6275–83.

158. Achour A, Kacem M, Dibej K, Skhiri H, Bouraoui S, El May M. One year course of oral sulodexide in the management of diabetic nephropathy. J Nephrol. 2005 Oct;18(5):568–74.

159. Packham DK, Wolfe R, Reutens AT, Berl T, Heerspink HL, Rohde R, et al. Sulodexide Fails to Demonstrate Renoprotection in Overt Type 2 Diabetic Nephropathy. J Am Soc Nephrol. 2012 Jan;23(1):123–30.

160. Sosińska-Zawierucha P, Maćkowiak B, Staniszewski R, Sumińska-Jasińska K, Maj M, Krasiński Z, et al. Sulodexide Slows Down the Senescence of Aortic Endothelial Cells Exposed to Serum from Patients with Peripheral Artery Diseases. Cell Physiol Biochem. 2018;45(6):2225–32.

161. Zilişteanu D-S, Atasie T, Voiculescu M. Efficacy of long-term low-dose sulodexide in diabetic and non-diabetic nephropathies. Rom J Intern Med. 2015 Jun;53(2):161–9.

162. Masola V, Onisto M, Zaza G, Lupo A, Gambaro G. A new mechanism of action of sulodexide in diabetic nephropathy: inhibits heparanase-1 and prevents FGF-2-induced renal epithelial-mesenchymal transition. J Transl Med. 2012 Oct 24;10:213.

163. Levy-Adam F, Feld S, Cohen-Kaplan V, Shteingauz A, Gross M, Arvatz G, et al. Heparanase 2 Interacts with Heparan Sulfate with High Affinity and Inhibits Heparanase Activity. J Biol Chem. 2010 Sep 3;285(36):28010–9.

164. Masola V, Bellin G, Gambaro G, Onisto M. Heparanase: A Multitasking Protein Involved in Extracellular Matrix (ECM) Remodeling and Intracellular Events. Cells [Internet]. 2018 Nov 28 [cited 2020 Jan 17];7(12). Available from: https://www.ncbi.nlm.nih.gov/pmc/articles/PMC6316874/

165. Roy M, Marchetti D. Cell Surface Heparan Sulfate Released by Heparanase Promotes Melanoma Cell Migration and Angiogenesis. J Cell Biochem. 2009 Feb 1;106(2):200–9.

166. Goodall KJ, Poon IKH, Phipps S, Hulett MD. Soluble Heparan Sulfate Fragments Generated by Heparanase Trigger the Release of Pro-Inflammatory Cytokines through TLR-4. PLOS ONE. 2014 Oct 8;9(10):e109596.

167. Rehm Markus, Bruegger Dirk, Christ Frank, Conzen Peter, Thiel Manfred, Jacob Matthias, et al. Shedding of the Endothelial Glycocalyx in Patients Undergoing Major Vascular Surgery With Global and Regional Ischemia. Circulation. 2007 Oct 23;116(17):1896–906.

168. Rivara S, Milazzo FM, Giannini G. Heparanase: a rainbow pharmacological target associated to multiple pathologies including rare diseases. Future Medicinal Chemistry. 2016 Apr 1;8(6):647–80.

169. Garsen M, Rops ALWMM, Rabelink TJ, Berden JHM, van der Vlag J. The role of heparanase and the endothelial glycocalyx in the development of proteinuria. Nephrol Dial Transplant. 2014 Jan 1;29(1):49–55.

170. Jeansson M, Haraldsson B. Glomerular Size and Charge Selectivity in the Mouse after Exposure to Glucosaminoglycan-Degrading Enzymes. JASN. 2003 Jul 1;14(7):1756–65.

171. Pahakis MY, Kosky JR, Dull RO, Tarbell JM. The role of endothelial glycocalyx components in mechanotransduction of fluid shear stress. Biochemical and Biophysical Research Communications. 2007 Mar 30;355(1):228–33.

172. Solari V, Rudd TR, Guimond SE, Powell AK, Turnbull JE, Yates EA. Heparan sulfate phage display antibodies recognise epitopes defined by a combination of sugar sequence and cation binding. Org Biomol Chem. 2015 May 19;13(21):6066–72.

173. Thompson SM, Fernig DG, Jesudason EC, Losty PD, van de Westerlo EMA, van Kuppevelt TH, et al. Heparan Sulfate Phage Display Antibodies Identify Distinct Epitopes with Complex Binding Characteristics. J Biol Chem. 2009 Dec 18;284(51):35621–31.

174. Schindelin J, Arganda-Carreras I, Frise E, Kaynig V, Longair M, Pietzsch T, et al. Fiji: an open-source platform for biological-image analysis. Nature Methods. 2012 Jul;9(7):676–82.

175. Betteridge KB, Arkill KP, Neal CR, Harper SJ, Foster RR, Satchell SC, et al. Sialic acids regulate microvessel permeability, revealed by novel in vivo studies of endothelial glycocalyx structure and function. J Physiol. 2017 Aug 1;595(15):5015–35.

176. Ho Ho K. Retinopathy [Thesis]. The Univeristy of Bristol; 2019.

177. GraphPad Statistics Guide [Internet]. [cited 2018 Apr 23]. Available from: https://www.graphpad.com/guides/prism/7/statistics/index.htm?stat_the_methods_of_tukey_and_dunne.htm

178. Stringer SE, Gallagher JT. Heparan sulphate. The International Journal of Biochemistry & Cell Biology. 1997 May 1;29(5):709–14.

179. Laremore TN, Zhang F, Dordick JS, Liu J, Linhardt RJ. Recent progress and applications in glycosaminoglycan and heparin research. Curr Opin Chem Biol. 2009 Dec;13(5–6):633–40.

180. Sarrazin S, Lamanna WC, Esko JD. Heparan Sulfate Proteoglycans. Cold Spring Harb Perspect Biol [Internet]. 2011 Jul [cited 2020 Jan 23];3(7). Available from: https://www.ncbi.nlm.nih.gov/pmc/articles/PMC3119907/

181. Chen S, Wassenhove-McCarthy D, Yamaguchi Y, Holzman L, van Kuppevelt TH, Orr AW, et al. Podocytes require the engagement of cell surface heparan sulfate proteoglycans for adhesion to extracellular matrices. Kidney Int. 2010 Dec;78(11):1088–99.

182. Chen S, Wassenhove-McCarthy DJ, Yamaguchi Y, Holzman LB, van Kuppevelt TH, Jenniskens GJ, et al. Loss of heparan sulfate glycosaminoglycan assembly in podocytes does not lead to proteinuria. Kidney International. 2008 Aug 1;74(3):289–99.

183. Morita H, Yoshimura A, Kimata K. The role of heparan sulfate in the glomerular basement membrane. Kidney International. 2008 Feb 1;73(3):247–8.

184. van den Hoven MJ, Wijnhoven TJ, Li J-P, Zcharia E, Dijkman HB, Wismans RG, et al. Reduction of anionic sites in the glomerular basement membrane by heparanase does not lead to proteinuria. Kidney International. 2008 Feb 1;73(3):278–87.

185. Goldberg S, Harvey SJ, Cunningham J, Tryggvason K, Miner JH. Glomerular filtration is normal in the absence of both agrin and perlecan–heparan sulfate from the glomerular basement membrane. Nephrol Dial Transplant. 2009 Jul;24(7):2044–51.

186. Harvey SJ, Jarad G, Cunningham J, Rops AL, van der Vlag J, Berden JH, et al. Disruption of Glomerular Basement Membrane Charge through Podocyte-Specific Mutation of Agrin Does Not Alter Glomerular Permselectivity. Am J Pathol. 2007 Jul;171(1):139–52.

187. Borza D-B. Glomerular basement membrane heparan sulfate in health and disease: a regulator of local complement activation. Matrix Biol. 2017 Jan;57–58:299–310.

188. Savery MD, Jiang JX, Park PW, Damiano ER. The Endothelial Glycocalyx in Syndecan-1 Deficient Mice. Microvasc Res. 2013 May;87:83–91.

189. Rops AL, Loeven MA, Gemst JJ van, Eversen I, Wijk XMV, Dijkman HB, et al. Modulation of heparan sulfate in the glomerular endothelial glycocalyx decreases leukocyte influx during experimental glomerulonephritis. Kidney International. 2014 Nov 1;86(5):932–42.

190. Florian Jeffry A., Kosky Jason R., Ainslie Kristy, Pang Zhengyu, Dull Randal O., Tarbell John M. Heparan Sulfate Proteoglycan Is a Mechanosensor on Endothelial Cells. Circulation Research. 2003 Nov 14;93(10):e136–42.

191. Forsberg E, Pejler G, Ringvall M, Lunderius C, Tomasini-Johansson B, Kusche-Gullberg M, et al. Abnormal mast cells in mice deficient in a heparin-synthesizing enzyme. Nature. 1999 Aug;400(6746):773–6.

192. Sasisekharan R, Venkataraman G. Heparin and heparan sulfate: biosynthesis, structure and function. Current Opinion in Chemical Biology. 2000 Dec 1;4(6):626–31.

193. Rosenberg RD, Shworak NW, Liu J, Schwartz JJ, Zhang L. Heparan sulfate proteoglycans of the cardiovascular system. Specific structures emerge but how is synthesis regulated? J Clin Invest. 1997 May 1;99(9):2062–70.

194. McCormick C, Duncan G, Goutsos KT, Tufaro F. The putative tumor suppressors EXT1 and EXT2 form a stable complex that accumulates in the Golgi apparatus and catalyzes the synthesis of heparan sulfate. Proc Natl Acad Sci U S A. 2000 Jan 18;97(2):668–73.

195. Wicklund CL, Pauli RM, Johnston D, Hecht JT. Natural history study of hereditary multiple exostoses. Am J Med Genet. 1995 Jan 2;55(1):43–6.

196. Wei Z, Lyon M, Gallagher JT. Distinct substrate specificities of bacterial heparinases against N-unsubstituted glucosamine residues in heparan sulfate. J Biol Chem. 2005 Apr 22;280(16):15742–8.

197. Linhardt RJ, Turnbull JE, Wang HM, Loganathan D, Gallagher JT. Examination of the substrate specificity of heparin and heparan sulfate lyases. Biochemistry. 1990 Mar 1;29(10):2611–7.

198. Sasisekharan R, Raman R, Prabhakar V. Glycomics Approach to Structure-Function Relationships of Glycosaminoglycans. Annual Review of Biomedical Engineering. 2006;8(1):181–231.

199. Häcker U, Nybakken K, Perrimon N. Heparan sulphate proteoglycans: the sweet side of development. Nat Rev Mol Cell Biol. 2005 Jul;6(7):530–41.

200. Elhegni HEH. The glomerular endothelial glycocalyx: focus on shear stress, HMMR and EXT1 [Thesis]. [Bristol]: The Univeristy of Bristol; 2017.

201. Kisanuki YY, Hammer RE, Miyazaki J, Williams SC, Richardson JA, Yanagisawa M. Tie2-Cre transgenic mice: a new model for endothelial cell-lineage analysis in vivo. Dev Biol. 2001 Feb 15;230(2):230–42.

202. Kobayashi H, Yoo TM, Kim IS, Kim MK, Le N, Webber KO, et al. L-lysine effectively blocks renal uptake of 125I- or 99mTc-labeled anti-Tac disulfide-stabilized Fv fragment. Cancer Res. 1996 Aug 15;56(16):3788–95.

203. Lazzara MJ, Deen WM. Model of albumin reabsorption in the proximal tubule. American Journal of Physiology-Renal Physiology. 2007 Jan 1;292(1):F430–9.

204. Mogensen CE, Vittinghus E, Sølling K. Abnormal albumin excretion after two provocative renal tests in diabetes: Physical exercise and lysine injection. Kidney International. 1979 Sep 1;16(3):385–93.

205. Rehm M, Zahler S, Lötsch M, Welsch U, Conzen P, Jacob M, et al. Endothelial glycocalyx as an additional barrier determining extravasation of 6% hydroxyethyl starch or 5% albumin solutions in the coronary vascular bed. Anesthesiology. 2004 May;100(5):1211–23.

206. Jacob M, Bruegger D, Rehm M, Welsch U, Conzen P, Becker BF. Contrasting effects of colloid and crystalloid resuscitation fluids on cardiac vascular permeability. Anesthesiology. 2006 Jun;104(6):1223–31.

207. Yokoi H, Kasahara M, Mukoyama M, Mori K, Kuwahara K, Fujikura J, et al. Podocyte-specific expression of tamoxifen-inducible Cre recombinase in mice. Nephrol Dial Transplant. 2010 Jul 1;25(7):2120–4.

208. Busse M, Feta A, Presto J, Wilén M, Grønning M, Kjellén L, et al. Contribution of EXT1, EXT2, and EXTL3 to Heparan Sulfate Chain Elongation. J Biol Chem. 2007 Nov 9;282(45):32802–10.

209. van den Born J, van den Heuvel LP, Bakker MA, Veerkamp JH, Assmann KJ, Berden JH. Monoclonal antibodies against the protein core and glycosaminoglycan side chain of glomerular basement membrane heparan sulfate proteoglycan: characterization and immunohistological application in human tissues. J Histochem Cytochem. 1994 Jan 1;42(1):89–102.

210. Born J van den, Salmivirta K, Henttinen T, Östman N, Ishimaru T, Miyaura S, et al. Novel Heparan Sulfate Structures Revealed by Monoclonal Antibodies. J Biol Chem. 2005 May 27;280(21):20516–23.

211. Thelle K, Christensen EI, Vorum H, ørskov H, Birn H. Characterization of proteinuria and tubular protein uptake in a new model of oral L-lysine administration in rats. Kidney International. 2006 Apr 2;69(8):1333–40.

212. Winterborn MH, Bradwell AR, Chesner IM, Jones GT. The origin of proteinuria at high altitude. Postgrad Med J. 1987 Mar;63(737):179–81.

213. Mogensen CE, Sølling K. Studies on renal tubular protein reabsorption: Partial and near complete inhibition by certain amino acids. Scandinavian Journal of Clinical and Laboratory Investigation. 1977 Jan 1;37(6):477–86.

214. Qi Z, Fujita H, Jin J, Davis LS, Wang Y, Fogo AB, et al. Characterization of susceptibility of inbred mouse strains to diabetic nephropathy. Diabetes. 2005 Sep;54(9):2628–37.

215. Kitada M, Ogura Y, Koya D. Rodent models of diabetic nephropathy: their utility and limitations. Int J Nephrol Renovasc Dis. 2016 Nov 14;9:279–90.

216. Sugimoto H, Grahovac G, Zeisberg M, Kalluri R. Renal fibrosis and glomerulosclerosis in a new mouse model of diabetic nephropathy and its regression by bone morphogenic protein-7 and advanced glycation end product inhibitors. Diabetes. 2007 Jul;56(7):1825–33.

217. Breyer MD, Böttinger E, Brosius FC, Coffman TM, Harris RC, Heilig CW, et al. Mouse Models of Diabetic Nephropathy. JASN. 2005 Jan 1;16(1):27–45.

218. Leiter EH. Multiple low-dose streptozotocin-induced hyperglycemia and insulitis in C57BL mice: Influence of inbred background, sex, and thymus. PNAS. 1982 Jan 1;79(2):630–4.

219. Rossini AA, Appel MC, Williams RM, Like AA. Genetic Influence of the Streptozotocin-induced Insulitis and Hyperglycemia. Diabetes. 1977 Oct 1;26(10):916–20.

220. Ron D. Proteotoxicity in the endoplasmic reticulum: lessons from the Akita diabetic mouse. J Clin Invest. 2002 Feb;109(4):443–5.

221. Gurley SB, Clare SE, Snow KP, Hu A, Meyer TW, Coffman TM. Impact of genetic background on nephropathy in diabetic mice. Am J Physiol Renal Physiol. 2006 Jan;290(1):F214-222.

222. Chang J-H, Gurley SB. Assessment of Diabetic Nephropathy in the Akita Mouse. In: Joost H-G, Al-Hasani H, Schürmann A, editors. Animal Models in Diabetes Research [Internet]. Totowa, NJ: Humana Press; 2012 [cited 2020 Feb 4]. p. 17–29. (Methods in Molecular Biology). Available from: https://doi.org/10.1007/978-1-62703-068-7_2

223. King A, Austin A. Chapter 10 - Animal Models of Type 1 and Type 2 Diabetes Mellitus. In: Conn PM, editor. Animal Models for the Study of Human Disease (Second Edition) [Internet]. Academic Press; 2017 [cited 2020 Feb 4]. p. 245–65. Available from: http://www.sciencedirect.com/science/article/pii/B9780128094686000103

224. Alpers CE, Hudkins KL. Mouse Models of Diabetic Nephropathy. Curr Opin Nephrol Hypertens. 2011 May;20(3):278–84.

225. Mauvais-Jarvis F, Clegg DJ, Hevener AL. The Role of Estrogens in Control of Energy Balance and Glucose Homeostasis. Endocr Rev. 2013 Jun;34(3):309–38.

226. Betz B, Conway BR. An Update on the Use of Animal Models in Diabetic Nephropathy Research. Curr Diab Rep [Internet]. 2016 [cited 2018 Apr 8];16. Available from: https://www.ncbi.nlm.nih.gov/pmc/articles/PMC4729785/

227. Koya D, Haneda M, Nakagawa H, Isshiki K, Sato H, Maeda S, et al. Amelioration of accelerated diabetic mesangial expansion by treatment with a PKC β inhibitor in diabetic db/db mice, a rodent model for type 2 diabetes. The FASEB Journal. 2000 Mar 1;14(3):439–47.

228. Cohen MP, Lautenslager GT, Shearman CW. Increased urinary type IV collagen marks the development of glomerular pathology in diabetic d/db mice. Metab Clin Exp. 2001 Dec;50(12):1435–40.

229. Gärtner K. Glomerular hyperfiltration during the onset of diabetes mellitus in two strains of diabetic mice (c57bl/6j db/db and c57bl/ksj db/db). Diabetologia. 1978 Jul;15(1):59–63.

230. Susztak K, Raff AC, Schiffer M, Böttinger EP. Glucose-induced reactive oxygen species cause apoptosis of podocytes and podocyte depletion at the onset of diabetic nephropathy. Diabetes. 2006 Jan;55(1):225–33.

231. Sung SH, Ziyadeh FN, Wang A, Pyagay PE, Kanwar YS, Chen S. Blockade of Vascular Endothelial Growth Factor Signaling Ameliorates Diabetic Albuminuria in Mice. JASN. 2006 Nov 1;17(11):3093–104.

232. Unnikrishnan R, Pradeepa R, Joshi SR, Mohan V. Type 2 Diabetes: Demystifying the Global Epidemic. Diabetes. 2017 Jun 1;66(6):1432–42.

233. Fairbanks MB, Mildner AM, Leone JW, Cavey GS, Mathews WR, Drong RF, et al. Processing of the human heparanase precursor and evidence that the active enzyme is a heterodimer. J Biol Chem. 1999 Oct 15;274(42):29587–90.

234. Shteingauz A, Ilan N, Vlodavsky I. Processing of heparanase is mediated by syndecan-1 cytoplasmic domain and involves syntenin and α-actinin. Cell Mol Life Sci. 2014 Nov;71(22):4457–70.

235. Abboud-Jarrous G, Atzmon R, Peretz T, Palermo C, Gadea BB, Joyce JA, et al. Cathepsin L Is Responsible for Processing and Activation of Proheparanase through Multiple Cleavages of a Linker Segment. J Biol Chem. 2008 Jun 27;283(26):18167–76.

236. Levy-Adam F, Miao H-Q, Heinrikson RL, Vlodavsky I, Ilan N. Heterodimer formation is essential for heparanase enzymatic activity. Biochem Biophys Res Commun. 2003 Sep 5;308(4):885–91.

237. Fux L, Ilan N, Sanderson RD, Vlodavsky I. Heparanase: busy at the cell surface. Trends Biochem Sci. 2009 Oct;34(10):511–9.

238. Bernard D, Méhul B, Delattre C, Simonetti L, Thomas-Collignon A, Schmidt R. Purification and characterization of the endoglycosidase heparanase 1 from human plantar stratum corneum: a key enzyme in epidermal physiology? J Invest Dermatol. 2001 Nov;117(5):1266–73.

239. D'Souza SS, Daikoku T, Farach-Carson MC, Carson DD. Heparanase expression and function during early pregnancy in mice. Biol Reprod. 2007 Sep;77(3):433–41.

240. Gingis-Velitski S, Zetser A, Kaplan V, Ben-Zaken O, Cohen E, Levy-Adam F, et al. Heparanase Uptake Is Mediated by Cell Membrane Heparan Sulfate Proteoglycans. J Biol Chem. 2004 Oct 15;279(42):44084–92.

241. Vaday GG, Lider O. Extracellular matrix moieties, cytokines, and enzymes: dynamic effects on immune cell behavior and inflammation. J Leukoc Biol. 2000 Feb;67(2):149–59.

242. Rabelink TJ, van den Berg BM, Garsen M, Wang G, Elkin M, van der Vlag J. Heparanase: roles in cell survival, extracellular matrix remodelling and the development of kidney disease. Nat Rev Nephrol. 2017;13(4):201–12.

243. Shu J, Santulli G. Heparanase in health and disease: The neglected housekeeper of the cell? Atherosclerosis. 2019 Apr;283:124–6.

244. Meirovitz A, Goldberg R, Binder A, Rubinstein AM, Hermano E, Elkin M. Heparanase enzyme in inflammation and inflammation-associated cancer. FEBS J. 2013 May;280(10):2307–19.

245. Shafat I, Ilan N, Zoabi S, Vlodavsky I, Nakhoul F. Heparanase Levels Are Elevated in the Urine and Plasma of Type 2 Diabetes Patients and Associate with Blood Glucose Levels. PLOS ONE. 2011 Feb 22;6(2):e17312.

246. Zhao Y, Liu J, Ten S, Zhang J, Yuan Y, Yu J, et al. Plasma heparanase is associated with blood glucose levels but not urinary microalbumin excretion in type 2 diabetic nephropathy at the early stage. Renal Failure. 2017 Jan 1;39(1):698–701.

247. Katz A, Van-Dijk DJ, Aingorn H, Erman A, Davies M, Darmon D, et al. Involvement of human heparanase in the pathogenesis of diabetic nephropathy. Isr Med Assoc J. 2002 Nov;4(11):996–1002.

248. Sonoda E, Hochegger H, Saberi A, Taniguchi Y, Takeda S. Differential usage of non-homologous end-joining and homologous recombination in double strand break repair. DNA Repair. 2006 Sep 8;5(9–10):1021–9.

249. An X, Zhang L, Yuan Y, Wang B, Yao Q, Li L, et al. Hyperoside pre-treatment prevents glomerular basement membrane damage in diabetic nephropathy by inhibiting podocyte heparanase expression. Scientific Reports. 2017 Jul 25;7(1):1–12.

250. Kramer A, Hoven M van den, Rops A, Wijnhoven T, Heuvel L van den, Lensen J, et al. Induction of Glomerular Heparanase Expression in Rats with Adriamycin Nephropathy Is Regulated by Reactive Oxygen Species and the Renin-Angiotensin System. JASN. 2006 Sep 1;17(9):2513–20.

251. Vlodavsky I, Friedmann Y. Molecular properties and involvement of heparanase in cancer metastasis and angiogenesis. J Clin Invest. 2001 Aug 1;108(3):341–7.

252. Kundu S, Xiong A, Spyrou A, Wicher G, Marinescu VD, Edqvist P-HD, et al. Heparanase Promotes Glioma Progression and Is Inversely Correlated with Patient Survival. Mol Cancer Res. 2016;14(12):1243–53.

253. Li J, Pan Q, Rowan PD, Trotter TN, Peker D, Regal KM, et al. Heparanase promotes myeloma progression by inducing mesenchymal features and motility of myeloma cells. Oncotarget. 2016 Feb 3;7(10):11299–309.

254. Sun X, Zhang G, Nian J, Yu M, Chen S, Zhang Y, et al. Elevated heparanase expression is associated with poor prognosis in breast cancer: a study based on systematic review and TCGA data. Oncotarget. 2017 Mar 26;8(26):43521–35.

255. Vlodavsky I, Friedmann Y, Elkin M, Aingorn H, Atzmon R, Ishai-Michaeli R, et al. Mammalian heparanase: gene cloning, expression and function in tumor progression and metastasis. Nat Med. 1999 Jul;5(7):793–802.

256. Heyman B, Yang Y. Mechanisms of Heparanase Inhibitors in Cancer Therapy. Exp Hematol. 2016 Nov;44(11):1002–12.

257. Zcharia E, Jia J, Zhang X, Baraz L, Lindahl U, Peretz T, et al. Newly Generated Heparanase Knock-Out Mice Unravel Co-Regulation of Heparanase and Matrix Metalloproteinases. PLoS One [Internet]. 2009 Apr 10 [cited 2020 Feb 17];4(4). Available from: https://www.ncbi.nlm.nih.gov/pmc/articles/PMC2664924/

258. Ritchie JP, Ramani VC, Ren Y, Naggi A, Torri G, Casu B, et al. SST0001, a chemically modified heparin, inhibits myeloma growth and angiogenesis via disruption of the heparanase/syndecan-1 axis. Clin Cancer Res. 2011 Mar 15;17(6):1382–93.

259. Cassinelli G, Lanzi C, Tortoreto M, Cominetti D, Petrangolini G, Favini E, et al. Antitumor efficacy of the heparanase inhibitor SST0001 alone and in combination with antiangiogenic agents in the treatment of human pediatric sarcoma models. Biochem Pharmacol. 2013 May 15;85(10):1424–32.

260. Galcheva-Gargova Z, Chu CL, Long A, Duffner J, Holte K, Schultes BC. Role of M402, a novel heparan sulfate mimetic, in pancreatic cancer cell invasion and metastasis: Inhibition of the Sonic Hedgehog pathway and heparanase activity. JCO. 2012 Oct 20;30(30_suppl):25–25.

261. Ostapoff KT, Awasthi N, Cenik BK, Hinz S, Dredge K, Schwarz RE, et al. PG545, an Angiogenesis and Heparanase Inhibitor, Reduces Primary Tumor Growth and Metastasis in Experimental Pancreatic Cancer. Mol Cancer Ther. 2013 Jul 1;12(7):1190–201.

262. Liu C-J, Lee P-H, Lin D-Y, Wu C-C, Jeng L-B, Lin P-W, et al. Heparanase inhibitor PI-88 as adjuvant therapy for hepatocellular carcinoma after curative resection: a randomized phase II trial for safety and optimal dosage. J Hepatol. 2009 May;50(5):958–68.

263. Simeonovic CJ, Ziolkowski AF, Wu Z, Choong FJ, Freeman C, Parish CR. Heparanase and Autoimmune Diabetes. Front Immunol [Internet]. 2013 Dec 26 [cited 2018 Feb 22];4. Available from: https://www.ncbi.nlm.nih.gov/pmc/articles/PMC3872651/

264. Roshan-Milani S, Khalilpour J, Fard AA. The Heparanase Inhibitor (Sulodexide) Decreases Urine Glycosaminoglycan Excretion and Mitigates Functional and Histological Renal Damages in Diabetic Rats. Acta Medica Bulgarica. 2019 May 1;46(2):41–6.

265. Coombe DR, Gandhi NS. Heparanase: A Challenging Cancer Drug Target. Front Oncol [Internet]. 2019 [cited 2020 Feb 10];9. Available from: https://www.frontiersin.org/articles/10.3389/fonc.2019.01316/full

266. Lewis KD, Robinson WA, Millward MJ, Powell A, Price TJ, Thomson DB, et al. A phase II study of the heparanase inhibitor PI-88 in patients with advanced melanoma. Invest New Drugs. 2008 Feb 1;26(1):89–94.

267. Liu C-J, Chang J, Lee P-H, Lin D-Y, Wu C-C, Jeng L-B, et al. Adjuvant heparanase inhibitor PI-88 therapy for hepatocellular carcinoma recurrence. World J Gastroenterol. 2014 Aug 28;20(32):11384–93.

268. Hammond E, Handley P, Dredge K, Bytheway I. Mechanisms of heparanase inhibition by the heparan sulfate mimetic PG545 and three structural analogues. FEBS Open Bio. 2013 Jan 1;3:346–51.

269. Ornitz DM, Yayon A, Flanagan JG, Svahn CM, Levi E, Leder P. Heparin is required for cell-free binding of basic fibroblast growth factor to a soluble receptor and for mitogenesis in whole cells. Mol Cell Biol. 1992 Jan;12(1):240–7.

270. Zhou H, Roy S, Cochran E, Zouaoui R, Chu CL, Duffner J, et al. M402, a Novel Heparan Sulfate Mimetic, Targets Multiple Pathways Implicated in Tumor Progression and Metastasis. PLoS One [Internet]. 2011 Jun 16 [cited 2020 Feb 10];6(6). Available from: https://www.ncbi.nlm.nih.gov/pmc/articles/PMC3116871/

271. Zubkova OV, Ahmed YA, Guimond SE, Noble S-L, Miller JH, Alfred Smith RA, et al. Dendrimer Heparan Sulfate Glycomimetics: Potent Heparanase Inhibitors for Anticancer Therapy. ACS Chemical Biology. 2018 Dec 21;13(12):3236–42.

272. Madaan K, Kumar S, Poonia N, Lather V, Pandita D. Dendrimers in drug delivery and targeting: Drug-dendrimer interactions and toxicity issues. J Pharm Bioallied Sci. 2014;6(3):139–50.

273. Zheng Y, Li S, Weng Z, Gao C. Hyperbranched polymers: advances from synthesis to applications. Chem Soc Rev. 2015 Jun 8;44(12):4091–130.

274. Kalomiraki M, Thermos K, Chaniotakis NA. Dendrimers as tunable vectors of drug delivery systems and biomedical and ocular applications. Int J Nanomedicine. 2015 Dec 22;11:1–12.

275. Mcmanus JFA. Histological Demonstration of Mucin after Periodic Acid. Nature. 1946 Aug;158(4006):202–202.

276. Ziolkowski AF, Popp SK, Freeman C, Parish CR, Simeonovic CJ. Heparan sulfate and heparanase play key roles in mouse β cell survival and autoimmune diabetes. J Clin Invest. 2012 Jan;122(1):132–41.

277. Tsilibary EC. Microvascular basement membranes in diabetes mellitus. The Journal of Pathology. 2003;200(4):537–46.

278. Ditzel J, Brøchner-Mortensen J. Tubular Reabsorption Rates as Related to Elevated Glomerular Filtration in Diabetic Children. Diabetes. 1983 Jun 1;32(Supplement 2):28–33.

279. Tojo A, Onozato M, Ha H, Kurihara H, Sakai T, Goto A, et al. Reduced albumin reabsorption in the proximal tubule of early-stage diabetic rats. Histochem Cell Biol. 2001 Sep;116(3):269–76.

280. Witte EC, Lambers Heerspink HJ, de Zeeuw D, Bakker SJL, de Jong PE, Gansevoort R. First Morning Voids Are More Reliable Than Spot Urine Samples to Assess Microalbuminuria. J Am Soc Nephrol. 2009 Feb;20(2):436–43.

281. Goldberg R, Meirovitz A, Hirshoren N, Bulvik R, Binder A, Rubinstein AM, et al. Versatile role of heparanase in inflammation. Matrix Biology. 2013 Jun 24;32(5):234–40.

282. Wijnhoven TJM, van den Hoven MJW, Ding H, van Kuppevelt TH, van der Vlag J, Berden JHM, et al. Heparanase induces a differential loss of heparan sulphate domains in overt diabetic nephropathy. Diabetologia. 2008 Feb 1;51(2):372–82.

283. Hewitson TD. Fibrosis in the kidney: is a problem shared a problem halved? Fibrogenesis & Tissue Repair. 2012 Jun 6;5(1):S14.

284. Brosius FC. New insights into the mechanisms of fibrosis and sclerosis in diabetic nephropathy. Rev Endocr Metab Disord. 2008 Aug 23;9(4):245.

285. Park PJ, Shukla D. Role of Heparan Sulfate in Ocular Diseases. Exp Eye Res. 2013 May;110:1–9.

286. Inatani M, Honjo M, Oohira A, Kido N, Otori Y, Tano Y, et al. Spatiotemporal Expression Patterns of N-Syndecan, a Transmembrane Heparan Sulfate Proteoglycan, in Developing Retina. Invest Ophthalmol Vis Sci. 2002 May 1;43(5):1616–21.

287. Liu I-H, Zhang C, Kim MJ, Cole GJ. Retina development in zebrafish requires the heparan sulfate proteoglycan agrin. Developmental Neurobiology. 2008;68(7):877–98.

288. Biroc SL, Payan DG, Fisher JM. Isoforms of agrin are widely expressed in the developing rat and may function as protease inhibitors. Developmental Brain Research. 1993 Sep 17;75(1):119–29.

289. Halfter W, Schurer B, Yip J, Yip L, Tsen G, Lee JA, et al. Distribution and substrate properties of agrin, a heparan sulfate proteoglycan of developing axonal pathways. J Comp Neurol. 1997 Jun 23;383(1):1–17.

290. Amini R, Rocha-Martins M, Norden C. Neuronal Migration and Lamination in the Vertebrate Retina. Front Neurosci [Internet]. 2018 Jan 9 [cited 2020 Feb 12];11. Available from: https://www.ncbi.nlm.nih.gov/pmc/articles/PMC5767219/

291. Tao C, Zhang X. Retinal Proteoglycans Act as Cellular Receptors for Basement Membrane Assembly to Control Astrocyte Migration and Angiogenesis. Cell Rep. 2016 Nov 8;17(7):1832–44.

292. Wen Y, Li J, Wang L, Tie K, Magdalou J, Chen L, et al. UDP-glucose dehydrogenase modulates proteoglycan synthesis in articular chondrocytes: its possible involvement and regulation in osteoarthritis. Arthritis Res Ther [Internet]. 2014 [cited 2020 Feb 17];16(6). Available from: https://www.ncbi.nlm.nih.gov/pmc/articles/PMC4298080/

293. Clark SJ, Keenan TDL, Fielder HL, Collinson LJ, Holley RJ, Merry CLR, et al. Mapping the Differential Distribution of Glycosaminoglycans in the Adult Human Retina, Choroid, and Sclera. Invest Ophthalmol Vis Sci. 2011 Aug 1;52(9):6511–21.

294. Bhattacharjee PS, Huq TS, Potter V, Young A, Davenport IR, Graves R, et al. High-Glucose-Induced Endothelial Cell Injury Is Inhibited by a Peptide Derived from Human Apolipoprotein E. PLOS ONE. 2012 Dec 19;7(12):e52152.

295. Eshaq RS, Aldalati AMZ, Alexander JS, Harris NR. Diabetic retinopathy: Breaking the barrier. Pathophysiology [Internet]. 2017 Jul 12 [cited 2017 Aug 31]; Available from: http://www.sciencedirect.com/science/article/pii/S0928468016300827

296. Becker BF, Chappell D, Bruegger D, Annecke T, Jacob M. Therapeutic strategies targeting the endothelial glycocalyx: acute deficits, but great potential. Cardiovasc Res. 2010 Jul 15;87(2):300–10.

297. Bollineni JS, Alluru I, Reddi AS. Heparan sulfate proteoglycan synthesis and its expression are decreased in the retina of diabetic rats. Current Eye Research. 1997 Jan 1;16(2):127–30.

298. Lensen JFM, Rops ALWMM, Wijnhoven TJM, Hafmans T, Feitz WFJ, Oosterwijk E, et al. Localization and Functional Characterization of Glycosaminoglycan Domains in the Normal Human Kidney as Revealed by Phage Display-Derived Single Chain Antibodies. JASN. 2005 May 1;16(5):1279–88.

299. Jiang X, Yang L, Luo Y. Animal Models of Diabetic Retinopathy. Current Eye Research. 2015 Aug 3;40(8):761–71.

300. Olivares AM, Althoff K, Chen GF, Wu S, Morrisson MA, DeAngelis MM, et al. Animal Models of Diabetic Retinopathy. Curr Diab Rep [Internet]. 2017 [cited 2018 Mar 21];17(10). Available from: https://www.ncbi.nlm.nih.gov/pmc/articles/PMC5569142/

301. Kumar S, Zhuo L. Longitudinal in vivo imaging of retinal gliosis in a diabetic mouse model. Experimental Eye Research. 2010 Oct 1;91(4):530–6.

302. Mizutani M, Gerhardinger C, Lorenzi M. Müller cell changes in human diabetic retinopathy. Diabetes. 1998 Mar 1;47(3):445–9.

303. Ramos D, Carretero A, Navarro M, Mendes-Jorge L, Rodriguez-Baeza A, Nacher V, et al. Mouse models of diabetic retinopathy. Drug Discovery Today: Disease Models. 2013;10(4):e195–206.

304. Ng DS, Chiang PP, Tan G, Cheung CG, Cheng C-Y, Cheung CY, et al. Retinal ganglion cell neuronal damage in diabetes and diabetic retinopathy. Clin Experiment Ophthalmol. 2016 May;44(4):243–50.

305. Pincelli Netto M, Lima VC, Pacheco MA, Unonius N, Gracitelli CPB, Prata TS. Macular Inner Retinal Layer Thinning in Diabetic Patients without Retinopathy Measured by Spectral Domain Optical Coherence Tomography. Med Hypothesis Discov Innov Ophthalmol. 2018;7(3):133–9.

306. Huang SS, Marcantonio C. The Role of Optical Coherence Tomography in Managing Diabetic Maculopathy and Retinopathy. The Asia-Pacific Journal of Ophthalmology. 2016 Oct;5(5):317.

307. Feit-Leichman RA, Kinouchi R, Takeda M, Fan Z, Mohr S, Kern TS, et al. Vascular Damage in a Mouse Model of Diabetic Retinopathy: Relation to Neuronal and Glial Changes. Invest Ophthalmol Vis Sci. 2005 Nov 1;46(11):4281–7.

308. Kim YH, Park SY, Park J, Kim YS, Hwang EM, Park JY, et al. Reduction of experimental diabetic vascular leakage and pericyte apoptosis in mice by delivery of αA-crystallin with a recombinant adenovirus. Diabetologia. 2012 Oct 1;55(10):2835–44.

309. Barber AJ, Antonetti DA, Kern TS, Reiter CEN, Soans RS, Krady JK, et al. The Ins2Akita Mouse as a Model of Early Retinal Complications in Diabetes. Invest Ophthalmol Vis Sci. 2005 Jun 1;46(6):2210–8.

310. Lai AKW, Lo ACY. Animal Models of Diabetic Retinopathy: Summary and Comparison. J Diabetes Res [Internet]. 2013 [cited 2020 Feb 18];2013. Available from: https://www.ncbi.nlm.nih.gov/pmc/articles/PMC3826427/

311. Bogdanov P, Corraliza L, Villena JA, Carvalho AR, Garcia-Arumí J, Ramos D, et al. The db/db Mouse: A Useful Model for the Study of Diabetic Retinal Neurodegeneration. PLOS ONE. 2014 May 16;9(5):e97302.

312. van Dijk HW, Verbraak FD, Kok PHB, Stehouwer M, Garvin MK, Sonka M, et al. Early Neurodegeneration in the Retina of Type 2 Diabetic Patients. Invest Ophthalmol Vis Sci. 2012 May;53(6):2715–9.

313. Barber AJ, Gardner TW, Abcouwer SF. The Significance of Vascular and Neural Apoptosis to the Pathology of Diabetic Retinopathy. Invest Ophthalmol Vis Sci. 2011 Feb 1;52(2):1156–63.

314. Park DY, Lee J, Kim J, Kim K, Hong S, Han S, et al. Plastic roles of pericytes in the blood–retinal barrier. Nature Communications. 2017 May 16;8:15296.

315. Jung E, Kim J, Kim C-S, Kim S-H, Cho M-H. Gemigliptin, a dipeptidyl peptidase-4 inhibitor, inhibits retinal pericyte injury in db/db mice and retinal neovascularization in mice with ischemic retinopathy. Biochimica et Biophysica Acta (BBA) - Molecular Basis of Disease. 2015 Dec 1;1852(12):2618–29.

316. Clements RS, Robison WG, Cohen MP. Anti-glycated albumin therapy ameliorates early retinal microvascular pathology in db/db mice. J Diabetes Complicat. 1998 Feb;12(1):28–33.

317. Zhao Y, Liu J, Ten S, Zhang J, Yuan Y, Yu J, et al. Plasma heparanase is associated with blood glucose levels but not urinary microalbumin excretion in type 2 diabetic nephropathy at the early stage. Renal Failure. 2017 Jan 1;39(1):698–701.

318. Hamoud S, Shekh Muhammad R, Abu-Saleh N, Hassan A, Zohar Y, Hayek T. Heparanase Inhibition Reduces Glucose Levels, Blood Pressure, and Oxidative Stress in Apolipoprotein E Knockout Mice [Internet]. BioMed Research International. 2017 [cited 2020 Feb 18]. Available from: https://www.hindawi.com/journals/bmri/2017/7357495/

319. Mayfosh AJ, Baschuk N, Hulett MD. Leukocyte Heparanase: A Double-Edged Sword in Tumor Progression. Front Oncol [Internet]. 2019 [cited 2020 Feb 18];9. Available from: https://www.frontiersin.org/articles/10.3389/fonc.2019.00331/full

320. Roy S, Ha J, Trudeau K, Beglova E. Vascular Basement Membrane Thickening in Diabetic Retinopathy. Current Eye Research. 2010 Dec 1;35(12):1045–56.

321. Remington LA. Chapter 11 - Orbital Blood Supply. In: Remington LA, editor. Clinical Anatomy and Physiology of the Visual System (Third Edition) [Internet]. Saint Louis: Butterworth-Heinemann; 2012 [cited 2020 Feb 20]. p. 202–17. Available from: http://www.sciencedirect.com/science/article/pii/B9781437719260100116

322. Ferreira JT, Alves M, Dias-Santos A, Costa L, Santos BO, Cunha JP, et al. Retinal Neurodegeneration in Diabetic Patients Without Diabetic Retinopathy. Invest Ophthalmol Vis Sci. 2016 Nov 1;57(14):6455–60.

323. Barber AJ, Lieth E, Khin SA, Antonetti DA, Buchanan AG, Gardner TW. Neural apoptosis in the retina during experimental and human diabetes. Early onset and effect of insulin. J Clin Invest. 1998 Aug 15;102(4):783–91.

324. Enea NA, Hollis TM, Kern JA, Gardner TW. Histamine H1 receptors mediate increased blood-retinal barrier permeability in experimental diabetes. Arch Ophthalmol. 1989 Feb;107(2):270–4.

325. Simó R, Stitt AW, Gardner TW. Neurodegeneration in diabetic retinopathy: does it really matter? Diabetologia. 2018;61(9):1902–12.

326. Lawrence T. The Nuclear Factor NF-κB Pathway in Inflammation. Cold Spring Harb Perspect Biol [Internet]. 2009 Dec [cited 2020 Feb 19];1(6). Available from: https://www.ncbi.nlm.nih.gov/pmc/articles/PMC2882124/

327. Riaz A, Ilan N, Vlodavsky I, Li J-P, Johansson S. Characterization of Heparanase-induced Phosphatidylinositol 3-Kinase-AKT Activation and Its Integrin Dependence. J Biol Chem. 2013 Apr 26;288(17):12366–75.

328. Ikeguchi M, Hirooka Y, Kaibara N. Heparanase gene expression and its correlation with spontaneous apoptosis in hepatocytes of cirrhotic liver and carcinoma. European Journal of Cancer. 2003 Jan 1;39(1):86–90.

329. Roy S, Sato T, Paryani G, Kao R. Downregulation of Fibronectin Overexpression Reduces Basement Membrane Thickening and Vascular Lesions in Retinas of Galactose-Fed Rats. Diabetes. 2003 May 1;52(5):1229–34.

330. Ingrande J, Lemmens HJ. Anesthetic Pharmacology and the Morbidly Obese Patient. Curr Anesthesiol Rep. 2013 Mar 1;3(1):10–7.

331. Hara T, Inami M, Hara T. Efficacy and safety of fluorescein angiography with orally administered sodium fluorescein. American Journal of Ophthalmology. 1998 Oct 1;126(4):560–4.

332. Li X-T, Qin Y, Zhao J-Y, Zhang J-S. Acute lens opacity induced by different kinds of anesthetic drugs in mice. Int J Ophthalmol. 2019 Jun 18;12(6):904–8.

333. Mensah SA, Cheng MJ, Homayoni H, Plouffe BD, Coury AJ, Ebong EE. Regeneration of glycocalyx by heparan sulfate and sphingosine 1-phosphate restores inter-endothelial communication. PLoS One [Internet]. 2017 Oct 12 [cited 2018 Apr 4];12(10). Available from: https://www.ncbi.nlm.nih.gov/pmc/articles/PMC5638341/

334. Dong W, Lu W, McKeehan WL, Luo Y, Ye S. Structural basis of heparan sulfate-specific degradation by heparinase III. Protein Cell. 2012 Dec;3(12):950–61.

335. Okada M, Nadanaka S, Shoji N, Tamura J, Kitagawa H. Biosynthesis of heparan sulfate in EXT1-deficient cells. Biochem J. 2010 Jun 15;428(3):463–71.

336. Keenan TDL, Toso M, Pappas C, Nichols L, Bishop PN, Hageman GS. Assessment of Proteins Associated With Complement Activation and Inflammation in Maculae of Human Donors Homozygous Risk at Chromosome 1 CFH-to-F13B. Invest Ophthalmol Vis Sci. 2015 Jul 1;56(8):4870–9.

337. Han J, Zhang F, Xie J, Linhardt RJ, Hiebert LM. Changes in cultured endothelial cell glycosaminoglycans under hyperglycemic conditions and the effect of insulin and heparin. Cardiovasc Diabetol. 2009 Aug 20;8(1):46.

338. van Det NF, van den Born J, Tamsma JT, Verhagen NAM, Berden JHM, Bruijn JA, et al. Effects of high glucose on the production of heparan sulfate proteoglycan by mesangial and epithelial cells. Kidney International. 1996 Apr 1;49(4):1079–89.

339. Gandhi NS, Mancera RL. The Structure of Glycosaminoglycans and their Interactions with Proteins. Chemical Biology & Drug Design. 2008;72(6):455–82.

340. Capila I, Linhardt RJ. Heparin–Protein Interactions. Angewandte Chemie International Edition. 2002;41(3):390–412.

341. Spiess BD. Heparin: Effects upon the Glycocalyx and Endothelial Cells. J Extra Corpor Technol. 2017;49(3):192–7.

342. Gavard J. Endothelial permeability and VE-cadherin. Cell Adh Migr. 2014 Mar 1;8(2):158–64.

343. Luo P, Peng H, Li C, Ye Z, Tang H, Tang Y, et al. Advanced glycation end products induce glomerular endothelial cell hyperpermeability by upregulating matrix metalloproteinase activity. Molecular Medicine Reports. 2015 Jun 1;11(6):4447–53.

344. Ramnath R, Foster RR, Qiu Y, Cope G, Butler MJ, Salmon AH, et al. Matrix metalloproteinase 9-mediated shedding of syndecan 4 in response to tumor necrosis factor α: a contributor to endothelial cell glycocalyx dysfunction. FASEB J. 2014 Nov;28(11):4686–99.

345. Taylor AW. Ocular Immune Privilege and Transplantation. Front Immunol [Internet]. 2016 Feb 8 [cited 2020 Mar 10];7. Available from: https://www.ncbi.nlm.nih.gov/pmc/articles/PMC4744940/

346. Antonetti DA, Barber AJ, Khin S, Lieth E, Tarbell JM, Gardner TW. Vascular permeability in experimental diabetes is associated with reduced endothelial occludin content: vascular endothelial growth factor decreases occludin in retinal endothelial cells. Penn State Retina Research Group. Diabetes. 1998 Dec 1;47(12):1953–9.

347. Iozzo RV, San Antonio JD. Heparan sulfate proteoglycans: heavy hitters in the angiogenesis arena. J Clin Invest. 2001 Aug 1;108(3):349–55.

348. Antonetti DA, Barber AJ, Hollinger LA, Wolpert EB, Gardner TW. Vascular Endothelial Growth Factor Induces Rapid Phosphorylation of Tight Junction Proteins Occludin and Zonula Occluden 1 A POTENTIAL MECHANISM FOR VASCULAR PERMEABILITY IN DIABETIC RETINOPATHY AND TUMORS. J Biol Chem. 1999 Aug 13;274(33):23463–7.

349. Aiello LP, Bursell S-E, Clermont A, Duh E, Ishii H, Takagi C, et al. Vascular Endothelial Growth Factor–Induced Retinal Permeability Is Mediated by Protein Kinase C In Vivo and Suppressed by an Orally Effective β-Isoform–Selective Inhibitor. Diabetes. 1997 Sep 1;46(9):1473–80.

350. Tien T, Muto T, Barrette K, Challyandra L, Roy S. Downregulation of Connexin 43 promotes vascular cell loss and excess permeability associated with the development of vascular lesions in the diabetic retina. Mol Vis. 2014 Jun 2;20:732–41.

351. Tien T, Muto T, Zhang J, Sohn EH, Mullins RF, Roy S. Association of reduced Connexin 43 expression with retinal vascular lesions in human diabetic retinopathy. Exp Eye Res. 2016;146:103–6.

352. Klaassen I, Hughes JM, Vogels IMC, Schalkwijk CG, Van Noorden CJF, Schlingemann RO. Altered expression of genes related to blood-retina barrier disruption in streptozotocin-induced diabetes. Exp Eye Res. 2009 Jun 15;89(1):4–15.

353. Götte M, Joussen AM, Klein C, Andre P, Wagner DD, Hinkes MT, et al. Role of Syndecan-1 in Leukocyte–Endothelial Interactions in the Ocular Vasculature. Invest Ophthalmol Vis Sci. 2002 Apr 1;43(4):1135–41.

354. Davoudi S, Papavasileiou E, Roohipoor R, Cho H, Kudrimoti S, Hancock H, et al. Optical coherence tomography characteristics of macular edema and hard exudates and their association with lipid serum levels in type 2 diabetes. Retina. 2016 Sep;36(9):1622–9.

355. Gilbert RE, Cox A, Dziadek M, Cooper ME, Jerums G. Extracellular matrix and its interactions in the diabetic kidney: a molecular biological approach. J Diabetes Complicat. 1995 Dec;9(4):252–4.

356. Heparan Sulfate Antibodies | amsbio [Internet]. [cited 2020 Feb 3]. Available from: http://www.amsbio.com/heparan-sulfate-antibodies.aspx

357. Thompson SM, Fernig DG, Jesudason EC, Losty PD, van de Westerlo EMA, van Kuppevelt TH, et al. Heparan Sulfate Phage Display Antibodies Identify Distinct Epitopes with Complex Binding Characteristics. J Biol Chem. 2009 Dec 18;284(51):35621–31.

358. Tamsma JT, van den Born J, Bruijn JA, Assmann KJ, Weening JJ, Berden JH, et al. Expression of glomerular extracellular matrix components in human diabetic nephropathy: decrease of heparan sulphate in the glomerular basement membrane. Diabetologia. 1994 Mar;37(3):313–20.

359. Born J van den, Pisa B, Bakker MAH, Celie JWAM, Straatman C, Thomas S, et al. No Change in Glomerular Heparan Sulfate Structure in Early Human and Experimental Diabetic Nephropathy. J Biol Chem. 2006 Oct 6;281(40):29606–13.

360. Lee WJ, Sobrin L, Lee MJ, Kang MH, Seong M, Cho H. The relationship between diabetic retinopathy and diabetic nephropathy in a population-based study in Korea (KNHANES V-2, 3). Invest Ophthalmol Vis Sci. 2014 Sep 9;55(10):6547–53.

361. Klein R, Zinman B, Gardiner R, Suissa S, Donnelly SM, Sinaiko AR, et al. The Relationship of Diabetic Retinopathy to Preclinical Diabetic Glomerulopathy Lesions in Type 1 Diabetic Patients: The Renin-Angiotensin System Study. Diabetes. 2005 Feb 1;54(2):527–33.

362. Nussbaum C, Cavalcanti Fernandes Heringa A, Mormanova Z, Puchwein-Schwepcke AF, Bechtold-Dalla Pozza S, Genzel-Boroviczény O. Early Microvascular Changes with Loss of the Glycocalyx in Children with Type 1 Diabetes. The Journal of Pediatrics. 2014 Mar 1;164(3):584-589.e1.

363. Solomon SD, Chew E, Duh EJ, Sobrin L, Sun JK, VanderBeek BL, et al. Diabetic Retinopathy: A Position Statement by the American Diabetes Association. Diabetes Care. 2017 Mar;40(3):412–8.

364. Gnudi L, Coward RJM, Long DA. Diabetic Nephropathy: Perspective on Novel Molecular Mechanisms. Trends in Endocrinology & Metabolism. 2016 Nov 1;27(11):820–30.

365. Miyakawa T. Vascular pathology in Alzheimer's disease. Psychogeriatrics. 2010 Mar;10(1):39–44.

366. Hanna RM, Lopez EA, Hasnain H, Selamet U, Wilson J, Youssef PN, et al. Three patients with injection of intravitreal vascular endothelial growth factor inhibitors and subsequent exacerbation of chronic proteinuria and hypertension. Clin Kidney J. 2019 Feb 1;12(1):92–100.

367. Touzani F, Geers C, Pozdzik A. Intravitreal Injection of Anti-VEGF Antibody Induces Glomerular Endothelial Cells Injury [Internet]. Case Reports in Nephrology. 2019 [cited 2020 Mar 10]. Available from: https://www.hindawi.com/journals/crin/2019/2919080/

368. Hu J, Song X, He YQ, Freeman C, Parish CR, Yuan L, et al. Heparanase and vascular endothelial growth factor expression is increased in hypoxia-induced retinal neovascularization. Invest Ophthalmol Vis Sci. 2012 Oct 3;53(11):6810–7.

369. Liang X-J, Yuan L, Hu J, Yu H-H, Li T, Lin S-F, et al. Phosphomannopentaose sulfate (PI-88) suppresses angiogenesis by downregulating heparanase and vascular endothelial growth factor in an oxygen-induced retinal neovascularization animal model. Mol Vis. 2012 Jun 20;18:1649–57.

370. Vernier RL, Klein DJ, Sisson SP, Mahan JD, Oegema TR, Brown DM. Heparan Sulfate–Rich Anionic Sites in the Human Glomerular Basement Membrane. New England Journal of Medicine. 1983 Oct 27;309(17):1001–9.

371. Schneeberger EE. Chapter 2 - Morphological Studies of Claudins in the Tight Junction. In: L. Yu AS, editor. Current Topics in Membranes [Internet]. Academic Press; 2010 [cited 2020 Mar 5]. p. 21–37. Available from: http://www.sciencedirect.com/science/article/pii/S1063582310650028

372. Nasdala I, Wolburg-Buchholz K, Wolburg H, Kuhn A, Ebnet K, Brachtendorf G, et al. A Transmembrane Tight Junction Protein Selectively Expressed on Endothelial Cells and Platelets. J Biol Chem. 2002 May 3;277(18):16294–303.

373. Doczi-Keresztesi Z, Jung J, Kiss I, Mezei T, Szabo L, Ember I. Retinal and Renal Vascular Permeability Changes Caused by Stem Cell Stimulation in Alloxan-induced Diabetic Rats, Measured by Extravasation of Fluorescein. In Vivo. 2012 May 1;26(3):427–35.

374. Abouzed TK, Contreras M del M, Sadek KM, Shukry M, H. Abdelhady D, Gouda WM, et al. Red onion scales ameliorated streptozotocin-induced diabetes and diabetic nephropathy in Wistar rats in relation to their metabolite fingerprint. Diabetes Research and Clinical Practice. 2018 Jun 1;140:253–64.

375. Bardoux P, Bruneval P, Heudes D, Bouby N, Bankir L. Diabetes-induced albuminuria: role of antidiuretic hormone as revealed by chronic V2 receptor antagonism in rats. Nephrol Dial Transplant. 2003 Sep 1;18(9):1755–63.

376. Naderi A, Zahed R, Aghajanpour L, Amoli FA, Lashay A. Long term features of diabetic retinopathy in streptozotocin-induced diabetic Wistar rats. Experimental Eye Research. 2019 Jul 1;184:213–20.

377. Han Y, Bearse MA, Schneck ME, Barez S, Jacobsen CH, Adams AJ. Multifocal electroretinogram delays predict sites of subsequent diabetic retinopathy. Invest Ophthalmol Vis Sci. 2004 Mar;45(3):948–54.

378. Fortune B, Schneck ME, Adams AJ. Multifocal electroretinogram delays reveal local retinal dysfunction in early diabetic retinopathy. Invest Ophthalmol Vis Sci. 1999 Oct;40(11):2638–51.

379. Basche M, Gustafson DL, Holden SN, O'Bryant CL, Gore L, Witta S, et al. A Phase I Biological and Pharmacologic Study of the Heparanase Inhibitor PI-88 in Patients with Advanced Solid Tumors. Clin Cancer Res. 2006 Sep 15;12(18):5471–80.

380. Dredge K, Brennan TV, Hammond E, Lickliter JD, Lin L, Bampton D, et al. A Phase I study of the novel immunomodulatory agent PG545 (pixatimod) in subjects with advanced solid tumours. British Journal of Cancer. 2018 Apr;118(8):1035–41.

381. Liu Y, Tee JK, Chiu GNC. Dendrimers in oral drug delivery application: current explorations, toxicity issues and strategies for improvement. Curr Pharm Des. 2015;21(19):2629–42.

382. Singh AK, Sharma AK, Khan I, Gothwal A, Gupta L, Gupta U. Chapter 9 - Oral drug delivery potential of dendrimers. In: Andronescu E, Grumezescu AM, editors. Nanostructures for Oral Medicine [Internet]. Elsevier; 2017 [cited 2020 Mar 10]. p. 231–61. (Micro and Nano Technologies). Available from: http://www.sciencedirect.com/science/article/pii/B9780323477208000109

Appendix I: Publications and Awards

First Author Publications Arising from This Work

Gamez M, Hussien HE, Fawaz S, Butler MJ, Wasson EJ, Crompton M, Ramnath RD, Qui Y, Turnbull JE, Zubkova OV, Yamaguchi Y, Welsh GI, Satchell SC, Foster RR. Endothelial glycocalyx heparan sulphate plays a key role in glomerular filtration barrier function in health and is amenable to therapeutic targeting in diabetes.

Submitted to Journal of the American Society of Nephrology, Rapid Communications on March 12, 2020.

First Author Abstracts Presented on This Work

Gamez M, Wasson EJ, Welsh GI, Zubkova OV, Satchell SC, Foster RR (2018) A Novel Heparanase Inhibitor Protects Glomerular Endothelial Glycocalyx During Diabetes Mellitus. *British Microcirculation Society*, Nottingham, England.

Gamez M, Wasson EJ, Welsh GI, Zubkova OV, Satchell SC, Foster RR (2018) A Novel Heparanase Inhibitor Protects Glomerular Endothelial Glycocalyx During Diabetes Mellitus. *Bristol Heart Institute 2nd Annual Specialist Research Institute Meeting*, Bristol, England.

Gamez M, Copland DA, Butler MJ, Bates DO, Atan D, Welsh GI, Satchell SC, Foster RR (2019) Heparan sulfate contributes to maintenance of vascular permeability in the retina**.** *British Microcirculation Society*, Exeter, England.

Gamez M, Wasson EJ, Welsh GI, Zubkova OV, Satchell SC, Foster RR (2019) A Novel Heparanase Inhibitor Protects Glomerular Endothelial Glycocalyx During Diabetes Mellitus. *European Diabetic Nephropathy Study Group*, Paris, France.

Gamez M, Wasson EJ, Welsh GI, Zubkova OV, Satchell SC, Foster RR (2019) A Novel Heparanase Inhibitor Protects Glomerular Endothelial Glycocalyx During Diabetes Mellitus. *Renal Association, UK Kidney Week*, Brighton, England.

Gamez M, Wasson EJ, Welsh GI, Zubkova OV, Satchell SC, Foster RR (2019) A Novel Heparanase Inhibitor Protects Glomerular Endothelial Glycocalyx During Diabetes

Mellitus. *Bristol Heart Institute 3rd Annual Specialist Research Institute Meeting*, Bristol, England.

Gamez M, Wasson EJ, Welsh GI, Zubkova OV, Satchell SC, Foster RR (2019) A Novel Heparanase Inhibitor Protects Glomerular Endothelial Glycocalyx During Diabetes Mellitus. *Bristol Endothelial Meeting*, Bristol, England.

Awards Arising from This Work

Best poster award. *British Microcirculation Society* (2018), Nottingham, England.

Best poster award. *European Diabetic Nephropathy Study Group* (2019), Paris, France.

Best poster award. *Bristol Endothelial Meeting* (2019), Bristol, England.

Student assistant scheme travel award, *British Microcirculation Society* (2018), Nottingham, England.

Travel grant. *European Diabetic Nephropathy Study Group* (2019), Paris, France.

Student assistant scheme travel award, *British Microcirculation Society* (2019), Exeter, England.

Non-First Author Publications Contributed to During PhD Course

Onions KL, Gamez M, Buckner NR, Baker SL, Betteridge KB, Desideri S, Dallyn BP, Ramnath RD, Neal CR, Farmer LK, Mathieson PW, Gnudi L, Alitalo K, Bates DO, Salmon AHJ, Welsh GI, Satchell SC, Foster RR. (2019). VEGFC reduces glomerular albumin permeability and protects against alterations in VEGF receptor expression in diabetic nephropathy. *Diabetes* **68** (1): 172-187

Ramnath RD, Butler MJ, Newman G, Desideri S, Russell A, Lay AC, Neal CR, Qiu Y, Fawaz S, Onions KL, Gamez M, Crompton M, Michie C, Finch N, Coward RJ, Welsh GI, Foster RR, Satchell SC. (2019). Blocking matrix metalloproteinase-mediated syndecan-4 shedding restores the endothelial glycocalyx and glomerular filtration barrier function in early diabetic kidney disease. *Kidney Int* doi: 10.1016/j.kint.2019.09.035

Desideri S, Onions KL, Baker SL, Gamez M, El Hegni E Hussien H, Russel A, Satchell SC, Foster RR. (2019) Endothelial Glycocalyx Restoration by Growth Factors in Diabetic Nephropathy. *Biorheology*. PMID:31156139

Non-First Author Publications Contributed to in Past Labs

Bishop LR, Davis AS, Bradshaw K, Gamez M, et al. (2018) Characterization of p57, a Stage-Specific Antigen Pneumocystis Murina. *Journal of Infectious Diseases*. 218(2):282-290. PMID:29471356

Murthy V, Dacus D, Gamez M, et al. (2018) Characterizing DNA Repair Processes at Transient and Long-lasting Double-strand DNA Breaks by Immunofluorescence Microscopy. *Journal of Visualized Experiments*. (136). PMID:29939192

Kolawole AO, Li M, Xia C, Foscher AE, Giacobbi NS, Rippinger CM, Proescher JB, Wu SK, Bessling SL, Gamez M, et al. (2014) Flexibility in Surface-Exposed Loops in a Virus Capsid Mediates Escape From Antibody Neutralization. *Journal of Virology*. 88 (8):4543-4557. PMID: 24501415

Kolawole AO, Xia C, Li M, Gamez M, et al. (2014) Newly Isolated mAbs Broaden the Neutralizing Epitope in Murine Norovirus. *Journal of General Virology*. 95(Pt 9): 19581968. PMID: 24899153

Jiang M, Zhao L, Gamez M, Imperiale MJ (2012) Roles of ATM and ATR-Mediated DNA Damage Responses during Lytic BK Polyomavirus Infection. *PLoS Pathogens*. 8(8):e1002898. PMID: 22952448

Jiang M, Entezami P, Gamez M, Stamminger T, Imperiale MJ. (2011) Functional reorganization of promyelocytic leukemia nuclear bodies during BK virus infection. *mBio*. 2(1):e00281-10. PMID: 21304169